RADC-TR-65-43

OUT OF BAND PERFORMANCE OF ANTENNAS

W. R. Lind
Univ. of Penna.

TECHNICAL REPORT NO. RADC-TR- 65-43
May 1965

Vulnerability Reduction Branch
Rome Air Development Center
Research and Technology Division
Air Force Systems Command
Griffiss Air Force Base, New York

BLANK PAGES
IN THIS
DOCUMENT
WERE NOT
FILMED

DISCLAIMER NOTICE

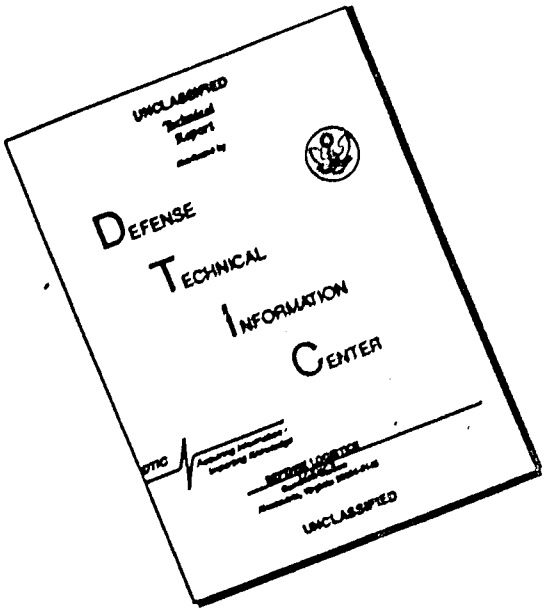

THIS DOCUMENT IS BEST QUALITY AVAILABLE. THE COPY FURNISHED TO DTIC CONTAINED A SIGNIFICANT NUMBER OF PAGES WHICH DO NOT REPRODUCE LEGIBLY.

When US Government drawings, specifications, or other data are used for any purpose other than a definitely related government procurement operation, the government thereby incurs no responsibility nor any obligation whatsoever; and the fact that the government may have formulated, furnished, or in any way supplied the said drawings, specifications, or other data is not to be regarded by implication or otherwise, as in any manner licensing the holder or any other person or corporation, or conveying any rights or permission to manufacture, use, or sell any patented invention that may in any way be related thereto

OUT OF BAND PERFORMANCE OF ANTENNAS

W. R. Lind

AIR FORCE, Cato Show Prtg. Co. 5/28/65 - 112 -

FOREWORD

The work on this contract was initiated by the Vulnerability Reduction Branch at Rome Air Development Center under Contract AF30(602)-3290, Project 4540, Task 454002. Project direction at RADC was obtained from the Interference Research Section (EMCVR) with Mr. John H. Edwards, Project Engineer. The guidance and many research reports supplied are gratefully acknowledged.

It is impossible to properly acknowledge all of the people who, directly or indirectly, have contributed to this report. The author is indebted to Dr. O. M. Salati, whose assistance and encouragement were invaluable to the completion of this report. All calculations were carried out by Mrs. Ping Yao Tsao and Mr. Richard Kalagher. The experimental work was accomplished by Messrs. Robert Dresp, Kuo-Chun Lang, and Shun-Jen Houng.

Secondary Report Number : Moore School Report 65-18.

This report has been reviewed and is approved.

Approved: JOHN H. EDWARDS
EMCVR
Interference Research Section

Approved: T. B. SWANSON
Colonel, USAF
Chief, Communications Division

ABSTRACT

This report concerns the out of band performance of antennas. The types covered are cylindrical, biconical, horn and parabolic antennas.

Both measured and theoretical data are presented. The antenna parameters covered are radiation and input impedances, gain, and radiation patterns.

The work presented in this report comprises a small sample of the work done at the University of Pennsylvania and elsewhere in the past and the results of recent experiments at the University of Pennsylvania.

TABLE OF CONTENTS

TABLE OF CONTENTS (continued)

LIST OF ILLUSTRATIONS

LIST OF ILLUSTRATIONS

LIST OF ILLUSTRATIONS

LIST OF ILLUSTRATIONS

LIST OF ILLUSTRATIONS

LIST OF ILLUSTRATIONS

LIST OF ILLUSTRATIONS

LIST OF TABLES

INTRODUCTION

An antenna is a device that is designed to transfer energy from a closed guiding structure to free space over a limited frequency range. Over this frequency range the performance of the antenna in terms of impedance and radiation characteristics are specified and controlled.

Outside of this design band it is very unusual to find the antenna characteristics specified and in general they are not known. The mathematics that are necessary to solve an antenna problem, even in its design band, are formidable. If the antenna aperture amplitude and phase distribution were known, its performance could be calculated. It is most unfortunate that the aperture distribution outside of the design band depends critically on higher order modes of transmission surface irregularities and mechanical tolerances. The higher order modes being set up by the various components in the transmission system and the method of excitation of the transmission line by the generator. These are not controlled since they usually do not affect performance in the design band. For these reasons very few problems of antennas operating outside of their design band have been solved analytically.

If one is interested in antenna performance outside of the design band, the data must be acquired by experimental measurements. One should expect considerable variability in such data since they result, as shown above, from aperture distributions which are not controlled. These data would not be required if generators were free of all out of band energy and receivers were free of all out of band responses. Until generators and receivers are free of out of band energy and responses, some information on out of band antenna performance must be available, even if of considerable variability, in order to make reasonable predictions of interference in

systems.

This paper is essentially a summary of the available information on the performance of antennas outside of their design band. The material was gathered from scattered references and from the results of research in our laboratories (several hundred patterns were measured by us during this report period to supplement previously available data). The references were obtained from an intensive literature search. Over 1000 references were obtained from ASTIA and all pertinent references were ordered and scanned. An effort was made in this report to reference the technical literature as much as possible since it is assumed that access to this is usually easier and quicker than access to government publications.

In many cases it was found that published material did not contain enough information about the manner in which the data were obtained or the equipment used in the experiment. That is, details of the antenna feed system, transmission lines, transducers, etc. were not usually given. These data are, therefore, not very useful. The largest fault was found with the literature dealing with aperture antennas. As pointed out above and in detail in this report the performance of these antennas is very sensitive to the feed structure and all known information on the feed structure should be included in the report of an aperture antenna.

There seems to be some confusion in the literature as to what the radiation pattern is. In this report the term "far field pattern" is used to indicate a plot proportional to field strength and the term "power pattern" to indicate a plot proportional to the square of field strength. If a square law detector is used in the measuring equipment,

it is the latter that is measured on an antenna pattern range. This is the usual case.

Section I is concerned with cylindrical antennas. The majority of the discussion is centered about monopole and dipole structures. Values of radiation resistance and reactance are presented over a 20:1 frequency range. This is an extension of the results found in the literature and was accomplished using the IBM 7090 computer. Radiation power patterns, calculated with the RPC-4000 computer, are also presented over a 20:1 frequency range. Input resistance and reactance are presented and compared with data obtained experimentally during the course of this contract in our laboratories.

Section II is concerned with the performance of circular aperture antennas and presents the results of research conducted in our laboratories during the past two years. This work has not been reported on before. The first is an experimental study of the performance of a six foot diameter parabolic reflector with a double-dipole feed over an 8:1 frequency range. The second consists of an experimental study of all possible combinations of two, two foot diameter parabolic reflectors and two double-dipole feed antennas. The purpose of this study, besides providing out of band performance on this type of antenna, was to determine the variation in performance of "identical" reflectors with the same feed structure.

Section III is concerned with the biconical antenna. For small cone angles this antenna behaves like a dipole antenna. Patterns and radiation resistance and reactance are presented. For large cone angles (i.e. cone semi-angle greater than 30°) patterns and impedance data are presented. It is pointed out that the increase in complexity of the first order impedance solution over the zeroth order solution yields little

additional accuracy. VSWR data from our laboratories for several related antenna types which show excellent agreement between theoretical and experimental values is also presented.

Section IV is concerned with the performance of horn antennas. Gain measurements were repeated to corroborate earlier findings. It is shown, from experimental data, that the performance of the horn antenna is very sensitive to the modes that are excited in the feed structure. Radiation patterns of an exponential horn when excited by various modes, which were measured in our laboratories during 1964, are presented. It is pointed out that the gain of horn antennas at harmonic frequencies is essentially constant with frequency as was predicted by researchers at our laboratories several years ago.

Section V is concerned with elliptical aperture antennas. Experimental data is presented which indicates that this type of aperture antenna has out of band characteristics similar to those of circular and rectangular aperture antennas.

I. Cylindrical Antennas

A. Introduction

The dipole antenna and related structures will be discussed in this section. The majority of the discussion will be on monopole and dipole structures. These will be assumed to be thin enough so that any variation in current density over the cross-sectional area may be neglected.

Antenna structures related to the dipole are the monopole, whip, blade, thin biconical structures, etc.

Neglecting problems introduced by the feed structure (coaxial, two wire line, etc.) the properties of the monopole and dipole are closely related. The coordinate system used in this section is shown in Figure 2.15 where the dipole is located along the z axis with the terminals at the origin. The radiation fields of the monopole and dipole lie in the regions $0 \leq \theta \leq \pi/2$ and $0 \leq \theta \leq \pi$ respectively. The fields of the dipole are symmetrical about the $\theta = \pi/2$ plane, and they are equal to those of the monopole in the $0 \leq \theta \leq \pi/2$ region. Other antenna properties are related in the following manner:

$$Z_i \text{ (monopole)} = \frac{1}{2} \; Z_i \text{ (dipole)}$$

$$\text{GAIN (monopole)} = 2 \text{ GAIN (dipole)}$$

An extensive work on the dipole antenna has been completed by King[18] which includes an extensive bibliography. The various theories of the dipole have recently been examined by Shin[8] and Bohn.[6]

B. Current Distribution on a Transmitting Antenna

The instantaneous complex current on the antenna is

$$i_z = I_z e^{j\omega t} \tag{1-1}$$

where I_z is a complex function of the length, L, diameter, D, and conductivity of the antenna.

Since $D \ll L$ it has been assumed that there is no current variation throughout the cross-section of the antenna and that the effect of the end faces at $z = \pm \frac{L}{2}$ can be neglected. The coordinate z is measured along the antenna which is fed (connected to transmission line whose effect is neglected) at z = 0. Positive values of z are in the upward direction and negative values in the downward direction, Figure 2.15.

$$I_z = I_z'' + j I_z' \tag{1-2}$$

$$I_o = I_o'' + j I_o' \tag{1-3}$$

I_o is the complex input current flowing through the antenna terminals and I_o' and I_o'' are functions of the length, diameter, and conductivity of the antenna. The simple current distribution with $I_z'' = 0$ and I_z' a sinusoidal function of the distance z along the antenna is a good approximation in most cases. Using this approximation we obtain

$$I_z = I_o \frac{\sin \beta \left(\frac{L}{2} - |z| \right)}{\sin \beta \frac{L}{2}} \tag{1-4}$$

and

$$I_o = I_{max} \sin \beta \frac{L}{2} \tag{1-5}$$

where I_{max} occurs at $z = \pm (\frac{L}{2} - \frac{\lambda}{4})$ and $\beta = \frac{2\pi}{\lambda}$. I_{max} is always a fictitious current for antennas with $L < \frac{\lambda}{4}$.

Using this approximation will cause errors between computed and measured antenna parameters that will increase as $\frac{L}{D}$ increases.

For antenna lengths that are less than or equal to $\frac{\lambda}{2}$ the formula

$$I_z = I_o \sin \beta \left(\frac{L}{2} - |z|\right) \tag{1-6}$$

is a reasonably good approximation even for moderately thick antennas if I_o is the complex input current flowing through the antenna terminals.

It is usual to show the current distribution on an antenna at the instant when it has its maximum value in time. A few typical distributions are shown in Figure 1.1. Using (1-5) we may rewrite (1-4) as

$$I_z = I_{max} \sin \beta \left(\frac{L}{2} - |z|\right) \tag{1-7}$$

C. Radiation Resistance and Input Resistance

The total power, P, supplied to an antenna is used partly in heating the conductors ($P^L = I^2R$ loss) of the antenna and partly in heating the universe (P^r = radiated power). Thus,

$$P = P^L + P^r \tag{1-8}$$

If the current flowing through the antenna terminals is I_o and an input impedance $Z_o = R_o + j X_o$ is defined, then

$$P = \frac{1}{2} \quad I_o^2 \quad R_o \tag{1-9}$$

Now combining (1) and (2) we obtain

$$R_o^L = \frac{2P^L}{I_o^2} \qquad R_o^2 = \frac{2P^2}{I_o^2} \tag{1-10}$$

where

$$R_o = R_o^L + R_o^r \tag{1-11}$$

Here R_o^L is the internal input resistance and R_o^r is the radiation input resistance. Both of these quantities are defined by (1-10). Analytically, R_o is not easily separated into R_o^L and R_o^r since both of these quantities are complicated functions of conductivity and the current distribution. In antennas constructed of highly conducting materials P^L is negligible compared with P^r so that

$$P \approx P^r \qquad P^L \ll P^r \tag{1-12}$$

$$R_o \approx R_o^r \qquad R_o^L \ll R^r \tag{1-13}$$

the data computed in this report are subject this approximation so that the input impedance should properly be called the input radiation impedance.

It is frequently attempted to define the input radiation resistance of a centerfed antenna using (1-10) under the assumption that

$$I_o = I_{max} \sin \beta \frac{L}{2} \tag{1-10}$$

If this value is substituted into (1-10) we obtain

$$R_o^r = \frac{2P}{\left|I_{max}\right|^2 \sin^2 \beta \frac{L}{2}} \tag{1-14}$$

Since P is always finite in any antenna that has a nonvanishing radius, (1-14) requires that R_o^r become extremely large as $\frac{\beta L}{2}$ approaches π, 2π, etc. and in fact to become infinite at these values. This is a physical absurdity that is the result of assuming a physically impossible current distribution in an antenna of finite radius. This difficulty is overcome by multiplying both sides of (1-14) by $\sin^2\beta \frac{L}{2}$ to obtain

$$R_m^r \equiv R_o^r \sin^2\beta \frac{L}{2} = \frac{2P}{\left|I_{max}\right|^2} \tag{1-15}$$

R_m^r has the dimensions of ohms but it is not a resistance in the ordinary sense that it is the real part of an impedance that can be measured between two terminals of a circuit. R_m^r is the power supplied to the antenna divided not by the square of the magnitude of the current flowing through the terminals but by the square of the magnitude of a current at another point on the antenna (i.e. $z = \pm \frac{L}{2} - \frac{\lambda}{4}$). As noted before for $L < \frac{\lambda}{2}$ I_{max} is a fictitious current that exists nowhere on the antenna. The advantage of R_m^r over R_o^r is that the former remains finite when the current distribution (1-14) is assumed.

R_m^2 will be called the radiation resistance since this is the usual useage although the term radiation resistance referred to a maximum sinusoidal current is more accurate and is preferred by some writers.[17,18]

Using (1-7) the far field terms for a infinitesimally thin dipole are[19]

$$H_\phi = j \frac{I_{max}}{2\pi r} E \tag{1-16a}$$

$$E_\theta = j \frac{60 I_{max}}{r} E \tag{1-16b}$$

where E is the radiation pattern factor given by

$$E = \left[\cos\left(\frac{m\pi}{2}\cos\theta\right) - \cos\frac{m\pi}{2}\right]\frac{1}{\sin\theta} \tag{1-17}$$

where m, called the harmonic order, is given by $m = \frac{\beta L}{\pi}$. The coordinate system (r, θ, ϕ) is shown in Figure 2.15.

The radiation resistance is given by

$$R_m^r = \frac{2P}{|I_{max}|^2} = 60\int_0^\pi E^2 \sin\theta\, d\theta \tag{1-18}$$

By a series of transformations (1-18) can be rewritten as[46]

$$R_m^r = 30 - \cos\beta L\, \mathrm{Cin}\, 2\beta L + 2(1 + \cos\beta L)\, \mathrm{Cin}\, \beta L + \sin\beta L\,(\mathrm{Si}\, 2\beta L - 2\,\mathrm{Si}\,\beta L) \tag{1-19}$$

where

$$\mathrm{Cin}(x) = \ell n\, \gamma\, x - \mathrm{Ci}(x)$$

$$\mathrm{Ci}(x) = \int_\infty^x \frac{\cos v}{v}\, dv$$

$$\mathrm{Si}(x) = \int_0^x \frac{\sin v}{v}\, dv$$

$\gamma = 1.781$, Euler's constant

Ci(x) and Si(x) are the cosine and sine integrals respectively and tabulated values are available. This can be reduced to

$$R_m^r = 30\left[\ell n\, 2m\pi\gamma - \mathrm{Ci}\, 2m\pi\right] \tag{1-20}$$

for m a negative integer and to

$$R_m^r = 30 \left[4 \text{ Cin } \beta L - \text{Cin } 2\beta L \right] \qquad (1\text{-}21)$$

if m is a positive integer. For non-integer values of m (1-19) must be used. This work was first done by Labus[20] and may be partially found in Kraus[19] and King.[17,18] The radiation resistance is shown in Figure 1.2. Labus' work was extended using the IBM 7040. The program is presented in Appendix B.

Using a similar development which takes into account the near fields of the dipole radiation reactance is found to be[19]

$$X_m^r = 30 \int_0^L \left[\frac{\cos \beta z}{z} + \frac{\cos (L-z)}{L-z} \right] \sin \beta z \, dz \qquad (1\text{-}22)$$

This equation is plotted in Figure 1.3 from the data obtained using the IBM 7090. The program is presented in Appendix B.

The properties of the center-driven dipole have recently been examined for the case of long dipoles.[3,50,51]

The impedance of a center-driven dipole for various ratios of radius to wavelength (a/x) are shown in Figure 1.4 for dipoles operating up to the nineteenth harmonic.

This work has been extended by Harrison[12] who calculated impedance in steps of $\beta \frac{L}{2} = 0.1$ for various length to diameter ratios (L/D) over the ranges of $\beta \frac{L}{2}$ shown in Table 1.1.

Ω	ℓ_{min}	$\leq \beta \frac{L}{2} \leq$	ℓ_{max}
7	1.0		1.6
8	1.0		2.7
9	1.0		4.5
10	1.0		7.4
11	1.0		12.2
12.5	1.0		25.9
15	1.0		90.4
16	1.0		149.0
17.5	1.0		300.9
20.0	1.0		999.99

Table 1.1 Range of $\beta \frac{L}{2}$ Over Which Harrison Computed Impedance

In Table 1.1 Ω is called the shape parameter and is defined by

$$\Omega = 2 \ln \frac{2L}{D} \qquad (1\text{-}23)$$

D. Radiation Patterns

The Far field radiation patterns can be calculated using (1-17). Since the radiation power patterns are usually the quantities we measure, they were calculated from

$$E^2 = \left[\cos\left(\frac{m\pi}{2}\cos\theta\right) - \cos\frac{m\pi}{2}\right]^2 \frac{1}{\sin^2\theta} \qquad (1\text{-}24)$$

using the RPC 4000 computer. The program is presented in Appendix B. The normalized radiation power patterns are plotted for $0 \leq \theta \leq \pi/2$ in Figures 1.5a through 1.5d for antennas operating up to the twentieth harmonic.

The radiation power patterns for harmonic operation have many lobes. The location of the maxima and minima are shown in Figure 1.6. The relationship of the strength of these lobes is shown in Figure 1.7 where the lobes are numbered from $\theta = 0^{\circ}$ in the direction of increasing θ.

Figure 1.8 shows the direction of maximum radiation. The directivity of the antenna in this direction and in the $\theta = \pi/2$ direction are shown in Figure 1.9.

The effect of the conductivity of the antenna is to reduce the magnitude of the radiation power pattern for increasing conductivity.

For increasing length to diameter ratios the magnitude of the radiation power pattern is also reduced.

A comparison of measured and calculated radiation power patterns shows that the theoretical patterns based on sinusoidal current distribution (our assumption) do not contain the following information.

1. The nulls between the lobes except the "natural null" in the $\theta = 0^{\circ}$ direction are not directions of zero radiation.
2. The phase of the field varies continuously from lobe to lobe instead of having a sudden 180° jump between lobes.

E. Experimental Study of Wide-Band Monopole Impedance

An experimental study of monopole impedance was begun. The monopole was located in the center of a ten foot diameter copper ground screen. A UG-58A/U connector was mounted in the center of the ground plane and its center conductor was continued for 6 inches above the ground plane to form the monopole. The measured input resistance, reactance, and VSWR of a dipole with a length to diameter ratio, L/D, of 48 is shown in Figures 1.10-1.12 along with theoretical data from Harrison[12] who used Wu's[50] equations to compute extensive tables of data. It is seen that Wu's formulation, which includes the finite thickness of the antenna, gives too large a value for the resistance. This is probably due to the finite conductivity of the antenna which has been neglected. Our model was made of 0.125 inch diameter brass rod. The magnitude of the input reactance is less than the data from Harrison[12] and approaches zero as the frequency of operation is increased. This is identical to the behaviour of the biconical antenna as discussed in Section III-F. The ground plane was ten feet in diameter which is large enough to simulate an infinite ground plane.[45]

II Circular Aperture, Parabolic Reflector with a Double-Dipole Feed

A. Introduction

This section describes two experiments conducted at the University of Pennsylvania during 1963 and 1964.

The first is an experimental study of the performance of a six foot diameter parabolic reflector with a double-dipole feed over a 8:1 frequency range.

The second consists of an experimental study of all possible combinations of two, two foot diameter parabolic reflectors and two double dipole feed antennas. The purpose of this study, besides providing out of band performance data on this type of antenna, was to determine the variation in performance of "identical" reflectors with the same feed antenna.

The identifying antenna nomenclature, which will be used throughout this section, and antenna dimensions are shown in Tables 2.1 and 2.2. The double-dipole feed and mounting dimensions are shown in Figure 2.1 and are based on a design in reference 42.

REFLECTOR SYMBOL	DIAMETER (FEET)
0	6
A	2
B	2

TABLE 2.1 REFLECTOR DEFINITIONS

FEED SYMBOL	T (inches)	s (inches)	ℓ (inches)
a	0.518		
b	1.038	1. 00	2.28
c	1.139		
d	2.250		
e	1.98		
f	4.365	2.26	4.57
g	4.950	3.03	5.79
h	0.341	0.345	0.37
i		0.87	0.87
DESIGN FREQUENCY REFLECTOR USED WITH	1.3GC S	A and B	A and B

TABLE 2.2 FEED DEFINITIONS

At frequencies outside of the design band, the radiation pattern of the reflector feed (horn, dipole, etc.) vary drastically thus causing drastic changes in the secondary radiation pattern. At frequencies outside of the design band the field distribution across the aperture certainly changes and the phase center of the feed may shift from the focus of the parabola. In fact, it is possible that the phase center can not be assigned to a "point" in space and therefore the point source approximation for the feed is not valid.

An attempt was made to analytically determine the far field radiation patterns at harmonic frequencies from simple models of aperture distributions for the six foot diameter parabolic reflector. These attempts were unsuccessful, mainly due to our inability to "guess" the proper phase distribution. If facilities had been available to measure phase patterns, then we would have had some orientation for our analytical work and

possibly obtained a model for this antenna. An analytic solution for a related problem, the field of a dipole in a parabolic reflector, has been obtained.[41] Some work on the effect of reasonable displacements of the phase center has been done.[9,15]

The maximum gain of an aperture is obtained when it is illuminated with a constant phase, constant amplitude field. This gain is given by

$$G_M = 10 \text{ LOG}_{10}\left[\frac{\pi D}{\lambda}\right]^2 \text{ (db)} \qquad (2\text{-}1)$$

where D is the diameter of the reflector and λ is the operating wavelength.

The gain of a reflector is always less than G_M. There are two reasons for this. First, it is physically impossible with conventional feeds to produce an illumination at the center that is equal to that at the edge. Second, some energy from the feed spills over the reflector. The best mathematical work to date predicts a gain loss of 26 per cent while the highest measured gain, G_0, is 65 per cent of G_M.[15] The equation

$$G_0 = 10 \text{ LOG}_{10}\left[6.4 \frac{D^2}{\lambda^2}\right] \qquad (2\text{-}2)$$

is plotted on all gain figures to give another indication of antenna performance.

B. Six Foot Diameter Parabolic Reflector[10]

The dimensions of the feed and reflector are described in Section III-A. The phase center of the feed, as shown in Figure 2.1a, was positioned at the reflector focus. The focal length to diameter ratio is f/D = 0.387.

The VSWR of the double-dipole feed and the complete antenna are shown in Figure 2.2.

For radiation power pattern and gain measurements the parabolic reflector and the various standard gain horns used were mounted on two towers six meters high. The tower separation was 14.5 meters.

Typical radiation power patterns are shown in Figures 2.3 to 2.10. Figures 2.3 to 2.6 are primary patterns of the double-dipole feed. Figures 2.7 to 2.10 are secondary patterns. Both E and H-plane patterns are shown. Note that the H-plane patterns are symmetrical about the antenna axis and that the radiation shifts toward 90° as the frequency increases. This direction corresponds to the opening in the outer conductor of the coaxial line through which the radiating element of the innerconductor emerges. Figure 2.11 shows the side-lobe level and beamwidth of the measured radiation power patterns. Note that in general, the beamwidth decreases with increasing frequency as would be expected. The sidelobe level is relatively constant for the frequency range investigated. In this section a sidelobe is defined as the lobe largest and closest to the main lobe, but separated from it by at least a 3 db null.

The gain of the antenna in the direction of maximum radiation is shown in Figure 2.12. The direction of maximum is not necessarily in the direction of boresight, but inspection of the measured patterns shows that the deviation is only a few degrees. As would be expected at higher frequencies the gain decreases due to the illumination departing farther from uniform illumination.

Several H-plane secondary power patterns measured at 5.2 GC at various distances are plotted in Figure 2.13. The far field distance at this frequency is

$$R = \frac{2D^2}{\lambda} = 116.12 \text{ meters} \qquad (2\text{-}3)$$

The patterns at 14.5 and 22.0 meters have main lobes which do not differ by any great amount. The side and back lobe differences are generally less than 5 db. According to the above criterion, these patterns were taken

in the near field; however, there is some doubt if this criterion is applicable. This criterion is derived for the direction of boresight based on uniform illumination. A theoretical study in this area would prove extremely useful.

Eq. (2-3) is shown in Figure 2.14.

C. Two Foot Diameter Parabolic Reflector

The dimensions of the double-dipole feed antennas and reflectors are described in Section III-A. The position of the feed in the reflector is shown in Figure 2.1b. The focal length to diameter ratio if $^{f}/_{D} = 0.382$.

All radiation power patterns and gain data in this section were measured with an antenna separation of 19.2 meters. The far field distance equation

$$R = \frac{2\,D^2}{\lambda} \qquad (2\text{-}3)$$

where D is the diameter of the parabola and λ is the operating wavelength is plotted in Figure 2.12. A conversion nomograph for converting from meters to feet is also shown.

Figure 2.15 shows the coordinate system used and the placement of the antenna in the coordinate system. The opening in the outerconductor of the coaxial line of the double-dipole antenna through which the radiating element connected to the innerconductor emerges is located at $\theta = 90^{\circ}$, $\phi = 90^{\circ}$.

Photographs of the double-dipole antennas and reflectors are shown in Figure 2.16.

VSWR and impedance data are shown in Figures 2.17 through 2.20. Inspection of these Figures shows that, in general, the performance of the feed and reflector is independent of which "identical" reflector is used. Note however, that occasionally there is a radical change in the performance of the "identical" reflectors.

Figures 2.21 through 2.28 are typical measured secondary radiation power patterns. These are only a small sample of the approximately one-hundred-eighty measured patterns. The angle θ is the angle in which the radiating element of the double-dipole feed points. Vertical polarization denotes that the electric field component parallel to the z-axis of Figures 2.15 was measured. The $\theta = 90^{\circ}$ patterns are cross-polarization patterns. The effect of changing "identical" reflectors was usually not very noticeable; however, occasionally this would cause a pattern to "break-up" into many lobes or a large change in side-lobe level.

Figures 2.29 through 2.36 show beamwidth and beam-tilt. Beam-tilt is the angular variation of the main lobe maximum from boresight.

The front to back ratio and first side-lobe level are shown in Figures 2.37 through 2.44. Front to back ratio is the difference, in db, of the power radiated in the $\phi = 0^{\circ}$ and $\phi = 180^{\circ}$ directions.

Antenna gain is shown in Figures 2.45 through 2.52. The most interesting information contained in these Figures is that the antenna appears to be elliptically polarized with a power axial ratio of less than 10 db. The minimum energy was received in the $\theta = 90^{\circ}$ plane as would be expected since this represents cross-polarization gain. The polarization of the receiving horn was vertical for all gain measurements.

The gain data should be interperted in light of the polarization discrimination ability of the exponential horn. This can be obtained from the cross-polarization gain data, at design frequency, from Section IV.

III The Biconical Antenna

A. Introduction

The biconical antenna and various structures derived from it will be discussed in this section. We will use the term biconical antenna to denote the structure shown in Figure 3.1a where the length of the cones is finite. When the cone length becomes infinite, we will use the term biconical transmission line. The structure shown in Figure 3.1b will be called a disc-cone antenna when the length of the cone is finite.

The space around a biconical antenna can be divided into three regions. These regions, the terminal, antenna, and free space regions, are shown in Figure 3.2.

Neglecting problems introduced by the feed structure (coaxial, two wire line, etc.) the properties of the biconical and disc-cone antennas are closely related. The radiation fields of the disc-cone and biconical antennas lie in the regions $0 \leq \theta \leq \pi/2$ and $0 \leq \theta \leq \pi$ respectively. The fields of the biconical antenna are symmetrical about the $\theta = \frac{\pi}{2}$ plane, and they are equal to those of the disc-cone in the $0 \leq \theta \leq \frac{\pi}{2}$ region. Other antenna properties are related in the following manner:

$$Z_i(\text{disc-cone}) = \frac{1}{2} \; Z_i \; (\text{Biconical})$$

$$\text{Gain (disc-cone)} = 2 \; \text{Gain (Biconical)}$$

Due to the relationship between these antenna types, the data in this section will be presented in detail for one, but not usually both antenna types.

B. The Lossless Biconical Transmission Line [19,26]

For the biconical transmission line shown in Figure 3.1a, the characteristic impedance is easily computed. Assuming that only the TEM mode can propagate we obtain

$$Z_{02} = 60 \ln \text{ TAN } \frac{\theta_o}{2} \text{ COT } \frac{\psi}{2} \qquad (3\text{-}1)$$

For the case of cones with equal semiangles ($\psi = \pi - \theta_o$) (3-1) becomes

$$Z_{01} = 120 \ln \text{ COT } \frac{\theta_o}{2} \qquad (3\text{-}2)$$

The impedance of a single cone above an infinite ground plane is given by

$$Z_o = 60 \ln \text{ COT } \frac{\theta_o}{2} \qquad (3\text{-}3)$$

Eqs. (3-2) and (3-3) are plotted in Figure 3.3.

C. Input Impedance of the Biconical Antenna

We shall consider a biconical antenna with both cones of equal length ($r = \ell$), and terminated by spherical end caps. This antenna is analogous to a terminated transmission line as shown schematically in Figure 3.4. A spherical TEM wave is launched in the terminal region and travels outward a distance $r = \ell$ to the boundary sphere. At the boundary sphere it is partially reflected and partially radiated (absorbed in Z_L). The TEM mode can not exist in free space; therefore, to satisfy the boundary conditions at $r = \ell$ it is necessary that the reflected wave be a superposition of TEM and higher order modes. We shall assume that these higher order modes are attenuated rapidly so that the reflected wave that reaches the terminal region is composed of only the TEM mode.

Under this assumption the input impedance of the antenna is given by

$$Z_i = Z_{02} \quad \frac{Z_L + j\, Z_{02} \ \text{TAN}\ \beta\ell}{Z_{02} + j\, Z_L \ \text{TAN}\ \beta\ell} \tag{3-4}$$

The problem has now been reduced to finding an expression for Z_L. The load admittance is given by[26]

$$Z_{02}\ Y_L = 60 \sum_k \frac{\rho_k}{k(k+1)} \left[P_k\ (\cos \psi) - P_k\ (\cos \theta_o) \right] \tag{3-5}$$

where $P_k\ (x)$ are Legendre polynomials of the 1st kind and ρ_k is the ratio of the reflected to the outward travelling waves in the antenna region. Various expressions for ρ_k and $Z_{02}\ Y_L$ are given in the literature.[19,36,47,49] Except for the limiting cases of large and small cone angles the mathematics are prohibitive[21,26,38] since they involve an infinite set of simultaneous equations and no numerical values based on theoretical considerations are available. Experimental values obtained by Brown and Woodward[5] for disc-cone antennas for $0 \leq \theta_o \leq \pi/2$ are discussed in Section E.

1. The Small Cone Angle Solution

For a biconical antenna with equal cone angles ($\psi = \pi - \theta_o$) and equal cone lengths an exact solution for the load admittance is[35,47,49]

$$Y_L = \frac{30}{\pi^2\ Z_{01}^2} \sum_{k\ \text{odd}} \rho_k \ \frac{1}{k(k+1)} \tag{3-6}$$

where

$$\rho_k = 2\beta\ell\ \pi^2\ (2k+1)\ J_k + \frac{1}{2}\ (\beta\ell)\ H_k^{(2)} + \frac{1}{2}\ (\beta\ell) \tag{3-7}$$

$J_n(x)$ and $H_n^{(2)}(x)$ are Bessel and Hankel functions of the first and second kind respectively.

There are many approximations to (3-6).[47,49] For cone semiangles less than about three degrees, Schelkunoff[19,36] has obtained the following expressions. Let us define an inverse radiation impedance by

$$Z_a = Z_i \Big|_{\beta\ell = \frac{\pi}{2}} = Z_{01}^2 Y_L = R_a + j X_a \tag{3-8}$$

$$R_a = 60 \text{ Cin } 2\beta\ell + 30(\ell n\gamma + \ell n\beta\ell - 2 \text{ Ci } 2\beta\ell + \text{Ci } 4\beta\ell) \cos 2\beta\ell$$

$$+ 30 (\text{Si } 4\beta\ell - 2 \text{ Si } 2\beta\ell) \text{ Sin } 2\beta\ell \tag{3-9}$$

$$X_a = 60 \text{ Si } 2\beta\ell + 30 (\text{Ci } 4\beta\ell - \ell n \beta\ell - \gamma) \text{ Sin } 2\beta\ell - 30 \text{ Si } 4\beta\ell \cos 2\beta\ell \tag{3-10}$$

where Ci, Cin, and Si are defined in Appendix A and γ is Euler's constant ($\ell n \gamma \approx 0.577$). Note that R_a is identical to the expression for R_m^r for a thin dipole (1-19). Substitution of (3-8), (3-9) and (3-10) into (3-4) yields the input impedance. Equations (3-9) and (3-10) are plotted in Fig. 3.5. An interesting comparison of the various approximations is given by Tai.[47,49]

2. The Wide Cone Angle Solution

By use of a variational technique Tai[49] has obtained two approximate solutions for the wide angle biconical antenna which are more accurate than the early work by Smith.[43,44] The zeroth-order solution is:

$$Y_{LO} = \frac{-j\ 120}{Z_{01}^2} \sum_{k \text{ odd}} \frac{2(k+1)}{k(k+1)} \left[P_k(\cos\theta_o)\right]^{-2} \frac{R_k(\beta\ell)}{R_k'(\beta\ell)} \tag{3-11}$$

where $R_k(x) = x^{\frac{1}{2}} H^{(2)}_{k+\frac{1}{2}}(x)$

$$R_k'(x) = \frac{d}{dx} R_k(x)$$

The first-order solution is given by

$$Y_{LI} = Y_{LO} - \frac{\alpha_m^2}{\beta_m + \gamma_m} \qquad (3\text{-}12)$$

where

$$\alpha_m = \frac{-j120}{Z_{01}^2} \sum_{k \text{ odd}} \frac{(2k+1)\, P_k(\cos\theta_o)\, I_{mk}}{2\, M_k}$$

$$\beta_m = \frac{-j120}{Z_{01}^2} \frac{m(m+1)\, I_{mm}}{2N_m}$$

$$\gamma_{mm} = \frac{-j120}{Z_{01}^2} \sum_{k \text{ odd}} \frac{k(k+1)(2k+1)\, I_{mk}^2}{4\, M_k}$$

$$I_{mk} = \frac{2n_1 P_k(\cos\theta_o) P_{m-1}(\cos\theta_o)}{k^2 + k - m^2 - m} \qquad k \neq m^*$$

$$I_{mm} = \frac{4}{2m+1} \frac{P_{m-1}(\cos\theta_o) P_{m-2}(\cos\theta_o)}{(2m-1)(2m-3)}$$

$$+ \frac{P_{m-2}(\cos\theta_o) P_{m-3}(\cos\theta)}{(2m-3)(2m-5)} + \ldots .$$

$$\ldots . + \frac{P_1(\cos\theta_o) P_0(\cos\theta_o)}{3 \cdot 1} \quad *$$

The relationship between m and $\cos\theta_o$ is given in Figure 3.6.

*when m is an odd integer these two equations are available in the literature.[14]

If (3-11) and (3-12) are multiplied by Z_{01}^2 the zeroth and first-order solutions for the Inverse Radiation Impedance result. These results are plotted in Figure 3.7 for m = 3,5,7. The zeroth-order solution assumes that only the TEM wave exists in the terminal region. The first-order solution assumes that the next higher order mode also exists.

As can be seen from Figure 3.7, the zeroth and first order solutions are in fairly good agreement (i.e. within10%).

Experiment has shown that the results stated above are valid for cone semiangles greater than 30°.

D. Far Field Radiation Patterns of the Biconical Antenna

The far field patterns of a thin biconical antenna are very close to those of a thin dipole. This is shown in Figure 3.8. It should be emphasized that these are field and not power patterns. They are plots of $\frac{E_\theta(r,\theta)}{F_\theta(r,\frac{\pi}{2})}$ versus θ for various values of antenna height, A, measured in electrical degrees. The relationship between A and ℓ, antenna length, is

$$A = \ell \cos \theta_o$$

The antennas used in this experiment did not have spherical end caps and the relationship between antennas with and without spherical end caps is shown in Figure 3.8 a.

Since the antenna radiation pattern is symmetrical about all major axis of the coordinate system, only one quadrant is given.

For thin biconical antennas of greater length than those shown in Figure 3.8 the reader is referred to the patterns of thin dipoles discussed in Section I .

The patterns of thick biconical antennas can be obtained from those of thick disc-cones in Section E.

E. Impedance of The Disc-Cone Antenna

The analytic solution of the impedance of the disc-cone antenna feed by a coaxial line has been obtained.[23] As in the case of the biconical antenna an infinite set of simultaneous equations results which are quite unmanageable. However, for large cone semiangles all modes except the TEM in the terminal region can be neglected and a manageable equation results.

1. The Small Cone Angle Solutic

Brown and Woodward[5] have conducted an experimental study of the impedance of the disc-cone antenna over a four wavelength diameter ground plane for $0 \leq \theta_o \leq \frac{\pi}{2}$. These results are shown in Figures 3.10 and 3.11. When θ_o is zero a cylindrical dipole with a diameter of 2.5 electrical degrees is obtained. This is the diameter of the innerconductor of the coaxial feed line.

For analytic results one half of the impedance values obtained in Section III-C.1 should be used.

2. The Wide Cone Angle Solution

The input impedance of a disc-cone antenna of length ℓ and semiangle θ_o fed by a coaxial line is[24]

$$Z_i = Z_o \frac{1 - \rho}{1 + \rho} \qquad (3\text{-}13)$$

where

$$\rho = \frac{1 + Q}{-1 + Q}$$

$$Q = j \frac{60}{Z_o} \sum_{k \text{ odd}} \frac{2k+1}{k(k+1)} \left[P_k(\cos\theta) \right]^2 \zeta_k(\beta\ell)$$

$$\zeta_k(\beta\ell) = \frac{h_k^{(2)}(\beta\ell)}{h_{k-1}(\beta\ell) - \frac{k}{\beta\ell} h_k^{(2)}(\beta\ell)}$$

$$\zeta_k(\beta\ell) = g_k(\beta\ell) + j\, b_k(\beta\ell)$$

$h_k^{(2)}(x)$ is the spherical Hankel function of the second kind of order k, ρ is the ratio of the amplitudes of the reflected and outwardly propagating TEM waves in the antenna region, and the zeta function is plotted in Figures 3.12 and 3.13.

Measured[5] data for a disc-cone with a 30° semiangle with an uncapped cone end shown in Figures 3.14 and 3.15. Note that the different definitions of antenna length in these figures does not cause a large impedance variation. Measured and theoretical data for a disc-cone with a spherical cap are shown in Figure 3.16. Various other theoretical values are shown in figures 3.14, 3.18, and 3.19. Using the theory presented above, Harrison[13] has calculated the input impedance for the range of $0.1 \leq \beta\ell \leq 200.1$ in 0.1 increments for θ_o equal to 30°, 35°, 40°, 45°, 46.982°, 50°, 55°, 60°, 65°, 70°. Inspection of his work and Figures 3.17 to 3.19 indicate that the resistive and reactive components of Z_i oscillate about Z_o and zero respectively. VSWR data for various disc-cone antennas is shown in Figure 3.20.[26]

F. Far Field Radiation Patterns of the Disc-Cone Antenna

For small cone angles see Section D. For cone semiangles greater than 30° the normalized far field radiation distribution is[25]

$$R(\theta) = \frac{E_\theta(r,\theta)}{E_\theta(r,\frac{\pi}{2})} \qquad (3\text{-}14)$$

where

$$E_\theta(r,\theta) = \frac{\sum_{k \text{ odd}} P_k (\cos\theta_o) P_k' (\cos\theta) \frac{2k+1}{k(k+1)} j^k}{h_{k-1}^{(2)}(\beta\ell) - \frac{k}{\beta\ell} h_k^{(2)}(\beta\ell)} \qquad (3\text{-}15)$$

The magnitude of (3-14) is shown in Figure 3.21 for $\theta_o = 30^\circ$, for various values of $\beta\ell$. For $\beta\ell \leq 1$

$$R(\theta) \approx \text{Sin } \theta \qquad (3\text{-}16)$$

G. Related Antenna Types

There are many antenna types related to the biconical antenna. They range from the prolate spheriodial antenna to the thin dipole.

The triangular antenna which is a two dimensional structure feed at one apex has been extensively investigated.[5]

The effects of varing the distance from the cone apex to the disc (ground plane) and of cutting slots in the cone of a disc-cone antenna has been investigated. Variation of these parameters can modify the radiation pattern while retaining the same broadband impedance variations.[7]

A theoretical study of a conical antenna fed by a monopole (i.e. a monopole over a conical ground plane) has been completed.[27] Experimental results are available from 4.0-12.4 Gc for the relationships between cone length, cone semiangle and the direction of maximum radiation. A closely related problem[22] has also been experimently investigated.

The disc-cone over a hemispherical ground plane has been investigated for wide angle cones.[26]

IV The Horn Antenna

A. Introduction

One of the most thoroughly investigated antenna types is the horn antenna. This antenna is of particular interest because it represents a variety of radiators often used in large, high powered antenna reflector systems. It is an aperture antenna whose main beam and first side lobes can be computed with excellent accuracy. The analysis of this class of electromagnetic radiators is complicated by the many variations of basic horn design which are encountered in practice. This report will only discuss the horn antennas with rectangular apertures. Except for one section, all antennas discussed will be linearly polarized. The effect of the waveguide to coaxial line transducer (if used) on the radiation pattern will be discussed.

B. Higher Order Modes

As the operating frequency of a rectangular waveguide system is increased, the number of propagating modes in which energy can exist increases. Figure 4.1 shows the number of modes that can exist at various harmonic frequencies. For purposes of illustration in this figure, it is assumed the relationship between the operating frequency, f_o, and the cutoff frequency, $f_{c_{10}}$, of the TE_{10} mode is

$$f_o = 1.6\, f_{c_{10}} \qquad (4\text{-}1)$$

Consider a waveguide supporting several modes of propagation simultaneously. If one could stop the propagation at a particular cross section of the waveguide, each of the existing modes would combine vectorially to give a particular energy distribution across that section of waveguide.

If the propagation were stopped and the combined field measured at another section of the same waveguide, the distribution would be entirely different than that measured across the first section. The reason for the dependence of energy distribution on the position of measurements is that each mode has a different velocity of propagation.

Consider the simple case[32] of the TE_{10} and TE_{20} modes propagating together (in the + z direction) in a single waveguide. Their electric fields components are[16]

$$TE_{10}: \quad E_{Y1} = A \, \text{SIN} \frac{\pi x}{d} \quad e^{j(\omega t + \beta_1 z)} \tag{4-2}$$

$$TE_{20}: \quad E_{Y2} = B \, \text{SIN} \frac{2\pi x}{d} \quad e^{j(\omega t + \beta_2 z)} \tag{4-3}$$

The total electric field in the waveguide is

$$E_t = E_{Y1} + E_{Y2}$$

$$= E \, e^{j\omega t} \, e^{j(\beta_1 + \beta_2) z} \, e^{j\eta} \tag{4-4}$$

where d is the transverse dimension of the waveguide and

$$E = \left[A^2 \, \text{SIN}^2 \frac{\pi x}{d} + B^2 \, \text{SIN}^2 \frac{2\pi x}{d} + 2 \, AB \, \text{SIN} \frac{\pi x}{d} \, \text{SIN} \frac{2\pi x}{d} \, \text{COS} \, (\beta_1 - \beta_2) \, z \right]^{1/2} \tag{4-5}$$

$$\eta = \text{TAN}^{-1} \frac{(a-b) \, \text{SIN} \left(\frac{\beta_1 - \beta_2}{2} z \right)}{(a+b) \, \text{COS} \left(\frac{\beta_1 - \beta_2}{2} z \right)} \tag{4-6}$$

$$a = A \sin \frac{\pi x}{d}$$

$$b = B \sin \frac{2\pi x}{d}$$

The last term in (4-5) exhibits a variation in the field in the direction of propagation which is similar to a standing wave in a mismatched line; however, it appears here in a perfectly matched line.

The square of E is shown in Figure 4.2 for three values of $(\beta_1 - \beta_2)z$. It is interesting to note that for $(\beta_1 - \beta_2)z = 0$ the symmetrical TE_{10} mode and the unsymmetrical TE_{20} mode combine to yield a symmetric field. It should be remembered that E_t is the sum of two phasor quantities. Note also that the phase of E_t varies continuously in the transverse plane (i.e. $\eta = \eta(x)$).

Since a multimode electromagnetic field in a rectangular waveguide has various amplitude and phase distributions depending on the distance from the source. The aperture distribution of a horn antenna, and hence its radiation pattern, is a function of the distance between the source and the aperture. The analysis is even more complicated than one would think at first since a theoretical study[52] has shown that the first few non-propagating modes must also be considered.

C. The Effect of the Waveguide to Coaxial Line Transducer on the Radiation Pattern

An experimental study[28] of the effect of the parameters (1) coupling probe length, D, (2) distance between the coupling probe and the end of the waveguide (short circuit), C, and (3) distance between the probe and the horn terminals, S has been made. Some typical results are shown in Figure 4.3 where the shaded area of the patterns represents the envelopes of several

measured patterns for the parameter changes mentioned. Notice that the patterns measured in the design band represented by 1000 Mc show very little variation as the parameter is varied. However, at 7900 Mc which is almost the eighth harmonic, the total pattern variation is greater for the same degree of parameter variation.

Figures 4.4 and 4.5 represent the maximum variation of major and minor lobes over a 10:1 frequency range. A major lobe is any lobe whose maximum is less than 10 db below the highest peak of the radiation pattern. Except at a few frequencies, major lobe variations are less than 4 db. There exists a slight tendency for an increase in pattern distortion as frequency is increased. This tendency would be expected since at higher frequencies a given parameter variation represents an increasing portion of a wavelength. The minor lobe variations are much greater and much more erratic. The general shape of the beam usually remained the same throughout the series of parameter variations.

Transducers which have identical characteristics in their design range do not necessarily have the same characteristics outside of this range. Figure 4.6 shows radiation power patterns of the AN/FPS-8 feed horn at about the seventh harmonic. The difference in the patterns is due entirely to the difference in the waveguide to coaxial transducers used. The one has a ball-ended probe and the other a straight probe held in place by a cylinder of dielectric material. The differences are even more pronounced at higher frequencies.

D. Wide Band Performance of Various Antennas

1. S-Band Sectorial Horn [28]

An S-band sectorial horn designed to produce a 100 degree 10 db beam width in both E and H planes was measured over a 7:1 frequency range. The radiation power patterns were measured with pure TE_{10} mode excitation and then with multimode excitation produced by a waveguide to coaxial line probe type adaptor (exact design unknown). Typical patterns and results are shown in Figures 4.7 to 4.12.

One trend which is apparent is the symmetry consistently found in the H-plane patterns.

Gain measured with and without multimode propagation is shown in Figures 4.10 to 4.12. The TE_{10} gain curve increases with frequency as would be expected due to the increasing antenna aperture measured in wavelengths. Gain with multimode propagation increases very little past 4500 Mc and varies erratically about the +14db level. These variations from the TE_{10} gain are caused by a combination of higher order modes at the horn aperture and resonances in the feed structure.

It is evident from Figures 4.11 and 4.12 that radiation patterns dominated by multimode propagation do not necessarily have maximum gain on axis (i.e. $\phi=0^{\circ}$, $\theta = \frac{\pi}{2}$). In the E-plane the on axis gain is consistently lower than the peak gain while in the H-plane they are approximately equal.

2. Circularly Polarized Horn [28]

The circularly polarized horn used for this experiment is of standard design. A twist transition section transforms the 45 degree oriented rectangular waveguide at the flange into a square section with a slight flare. A plexiglass

"quarter-wave plate" extends the entire length of the square section and approximately one inch into the twist section. Unfortunately, no exact dimensions on this antenna are given.

Radiation patterns were measured with pure TE_{10} and multimode excitation as described in the last section. These are shown in Figures 4.13 and 4.14. Due to the conditions imposed by the "quarter-wave plate" higher order modes must exist in the square section even with pure TE_{10} mode excitation.

Axial ratio, which is the ratio of the major to minor axis of the polarization ellipse is shown in Figure 4.15.

3. AT-316 Exponential Horn

A theoretical solution[52] of the radiation pattern of the AT-316 horn operating at harmonic frequencies has been obtained. The design of these antennas and their design band radiation patterns are well known.[15,19,30] Out of band information first became available as the result of experimental work designed to aid in predicting the behaviour of aperture antennas at harmonic frequencies.[31] Further work by Anne[2] and Salati and Lewis[34] showed that multimode propagation in the feed system influenced antenna gain values. The latter reference contains a systematic measurement program of the radiation patterns, gain, and impedance of the antenna over a 10:1 frequency range. Typical radiation power patterns are shown in Figures 4.19 and 4.20.[33] VSWR and gain data for both normal and cross-field components are shown in Figure 4.21.[32,33] Figure 4.22 shows AT-316 gain data from reference 28. This data which averages about 5 db higher than the data from reference 33, was measured with an unknown type of waveguide to coaxial line transducer.

4. AN/FPS-8 Feed Horn [28]

This antenna has a more complicated feed structure than any other horn antenna considered in this report. Radiation power patterns, gain, and 10 db beam width data are shown in Figures 4.16 to 4.18. The entire AN/FPS-8 antenna is discussed in Section V. The data presented in this section was obtained with the antenna fed by a Narda model 616 waveguide to coaxial line transducer which had a ball ended coupling probe.

5. S-Band Exponential Horn

Radiation power patterns of a Narda model 644 exponential horn fed by a Hewlett-Packard S281A waveguide to coaxial line transducer were measured at 2.8 and 5.6 Gc. Table 5.1 shows the various modes that may have existed at 5.6 Gc in the radiating system and those which were used to excite the system for radiation power pattern measurements.

Mode	propagating		power pattern measurement	
	yes	no	yes	no
TE_{10}	X		X	
TE_{20}	X		X	
TE_{01}	X		X	
TE_{11}	X		X	
TM_{11}	X			X
TE_{21}		X		X
TM_{21}		X		X

TABLE 4.1 Modes in S-Band Waveguide at 5.6 GC

The TE_{21} and TM_{21} modes are included in Table 5.1 since, as indicated in Section IV-B, the first few nonpropagating modes also contribute to the radiation pattern.[52]

The measured radiation patterns of the modes indicated in Table 5.1, are shown in Figures 4.24 to 4.29. Unfortunately to determine exactly which modes contribute to the second harmonic pattern (i.e. Figure 4.25), the phase patterns and gain data are necessary. The necessary gain data is unavailable at the present time, and the Moore School does not have the equipment to measure phase patterns.

V. Elliptical Aperture, AN/FPS-8 Antenna

The AN/FPS-8 antenna system is composed of a reflector and feed horn. The reflector is of the "banana peel" variety. The feed horn and its characteristics are discussed in Section IV-D4. For the data presented in this section the feed horn was again fed directly with the NARDA model 616 waveguide to coaxial line transducer with a ball ended coupling probe. The rotary joint and all other waveguide components in the transmission system were omitted from the test setup. The antenna which was investigated over a 10:1 frequency range was designed to operate at 1315 Mc and give a 3° half power beamwidth in the azimuth plane and a cosecant squared pattern in the elevation plane.

Gain and beamwidth data is presented in Figures 4.18a and 4.18b. Typical radiation power patterns are shown in Figures 5.1 and 5.2. More complete data may be found in reference 53.

Recommendations

The usual far field criterion, $R = \frac{2D^2}{\lambda}$, was used in performing the antenna measurements described in this report whenever possible. For a six foot parabolic reflector operating at 10.0 Gc, R is 7200 feet. It is impossible to approach this distance on our antenna range or on a large number of antenna ranges. The trend in present day antenna design is toward larger apertures and it is becoming increasingly impossible to measure antenna patterns in the far field at their design frequencies. Measurements in the far field at harmonic frequencies are already quite difficult if not impossible for the aperture antennas in use today.

The above comments show the necessity of developing a simple technique of measuring antenna patterns in the near field and then extending the measured results to obtain the far field radiation pattern. The maximum amount of information necessary to obtain the far field pattern from near field data is the magnitude and phase of the electric field tangent to a sphere with the antenna under test at the center. The minimum amount of information necessary to perform this task is unknown. It is therefore recommended that the following investigations be undertaken:

1. A theoretical investigation to determine the minimum amount of information necessary to specify the far field radiation pattern from data measured near field data within a specified error limit.

2. A theoretical and experimental investigation to determine a practical method of making near field antenna pattern measurements and extrapolating them to determine far field patterns. It should be recognized that both magnitude and phase patterns will be necessary.

The far field criterion, $R = \frac{2D^2}{\lambda}$, was derived on the basis of uniform phase across the aperture which is certainly not true for antennas operating outside of their design band. It is in fact only a good approximation for aperture antennas that operate in their design band. A further deficiency is that the criterion was derived in the direction of boresight and although it is usually assumed to hold in all azumuthal directions there is no theoretical justification for this assumption. There is no far field criterion for antennas operating at harmonic frequencies. It is therefore, further recommended that:

3. A theoretical and experimental investigation be undertaken to determine a far field criterion that is valid at the fundamental and harmonic frequencies for all azumuthal directions.

The experimental study of wide-band monopole impedance begun in our laboratories under this contract showed that while the manner in which the impedance varied agreed with theoretical predictions the magnitude did not. This work indicates that the following studies should be undertaken:

4. An extension of the wide-band impedance measurement program to other antenna types such as biconical and aperture structures.

5. An investigation of the effects of conductivity and finite size of the ground plane on antenna radiation patterns, impedance, and gain.

It can easily be seen from the size of this report that a large amount of data can be measured and/or computed in a relatively short time. To reduce data to useable form for interference prediction, it is recommended that:

6. All information relating to the gain, impedance and radiation patterns of antennas both in and outside of their design band be reduced to statistical form.

CONCLUSIONS

Section I considers the properties of the dipole antenna. The radiation resistance and reactance, R_m^r and X_m^r, of thin dipoles were computed over a 20:1 frequency range using the IBM 7040 computer. This was an extension of Labus' work originally done in 1933. These quantities when divided by $\sin \beta \frac{L}{2}$, where L is the length of the dipole and β has its usual meaning, determine bounds on the quantities we would actually measure at the antenna terminals. In the case of radiation input impedance, R_o^r, it is an upper bound. This can be seen as follows.

$$R_o^r = \frac{R_m^r}{\sin \beta \frac{L}{2}}$$

It is easily seen that at $\beta \frac{L}{2} = n\pi$, where n is any integer, that R_o^r is infinite. The value of R_o^r as calculated by Wu using a refined technique which considers the finite thickness of the antenna is shown in Fig. 1.4. It is noticed in this figure that input resistance is always finite. In fact the curve labeled A in the figure is always less in magnitude than R_o^r. Thus R_o^r is an upper bound. The measured input resistance, reactance, and VSWR of a dipole with a length to diameter ratio, L/D, of 48 is shown in Figs. 1.10 - 1.12 along with theoretical data from Harrison who used Wu's equations to compute extension tables of data. It is seen that even Wu's formulation gives too large a value for the resistance. This is probably due to the finite conductivity of the antenna which has been neglected. Our model was made of 0.125 inch diameter brass rod. The radiation input reactance defined by

$$X_o^r = \frac{X_o^m}{\sin \beta \frac{L}{2}}$$

can be computed from Fig. 1.3. This reactance will be an upper bound (in magnitude) for Wu's data shown in Fig. 1.4. The measured data shown in Fig. 1.12 is even less in magnitude and approaches zero at the frequency of operation is increased. This is identical to the behavior of the biconical antenna. The antenna feed system was designed to support only the TEM mode over the frequency range used in the measurements.

Radiation power patterns (as opposed to field patterns which have been presented under previous contracts[33] and in the literature[19]) have been computed using the RPC-4000 computer. These patterns were computed using a current distribution of the form.

$$I_z = I_{max} \sin \beta \left(\frac{L}{2} - |z|\right)$$

This is not the current distribution used in the literature in all cases[46], but it is the only physically realizable one. Comparison measured and theoretical data in Fig. 1.5 show that the above current distribution corresponds to the correct radiation pattern. The effect of increasing the thickness or the conductivity of the antenna is the same.

The former is shown in Fig. 1.5e while the latter is illustrated in Stratton. The following conclusions can be drawn:

1. The radiation input impedance, $R_o^r + j X_o^r$, can be computed from the radiation impedance $R_m^r + j X_m^r$ using

$$Z_o^r = \frac{Z_m^r}{\sin \beta \frac{L}{2}}$$

where L is the length of the dipole.

2. The infinities in the radiation input resistance are never obtained in practice due to the conductivity and finite thickness of the antenna.

3. The radiation input impedance and the input impedance obtained by Wu and Harrison are upper bounds. Measured data is always smaller in magnitude due to the finite thickness of the antenna and the conductivity of the antenna and ground plane (if used).

4. Theoretical and experimental data are in agreement that the magnitude and phase of the input impedance tend toward zero as the frequency of operation is increased.

5. The only physically realizable current distribution is

$$I_z = I_{max} \sin \beta \left(\frac{L}{2} - |z|\right)$$

and this distribution should be used to compute radiation power patterns and radiation input impedance of center feed cylindrical antennas.

6. The effects of the finite thickness and conductivity are identical and are listed below (7. to 10.).

7. The nulls between the lobes except the "natural null" along the antenna element are not directions of zero radiation.

8. The phase of the fields vary continuously from lobe to lobe instead of having a sudden 180° jump between lobes.

9. The small lobes disappear.

10. The magnitude of the main lobe is decreased.

11. The H-plane radiation patterns are symmetrical about the antenna axis.

Section II describes two experiments which were conducted at the University of Pennsylvania. The first is an experimental study of the performance of a six foot diameter parabolic reflector with a double-dipole feed over an 8:1 frequency range. The second consists of an experimental study of all possible combinations of two, two foot diameter parabolic reflectors and two double-dipole feed antennas. The purpose of this study, besides providing out of band performance data on this type of antenna, was to determine the variation in performance of "identical"reflectors with the same feed antenna. The only mode other than the TEM mode that could exist in the coaxial double-dipole feed is the TE_{11} mode. If this mode existed and its effect if it did are unknown. In general the properties of these antennas can be summarized as follows:

1. Out of band gain tends to remain constant.
2. Out of band beam width is relatively constant with a tendency to decrease with increasing frequency.
3. Beam tilt (the deviation from bore sight of the main lobe) is not a function of frequency.
4. Front to back ratio tends to remain constant.
5. Side lobe level tends to remain constant.
6. VSWR is generally below 5:1.
7. The H-plane radiation patterns are symmetrical about the antenna axis.

The tendency for gain of an aperture antenna to remain constant at harmonic frequencies was pointed out by investigators in our laboratories several years ago.[31] The effect of the minor physical variations between two "identical" parabolic reflectors is in general minor variations in

antenna impedance, gain, beamwidth and side lobe structure. Occasionally these minor reflector variations will cause major changes such as a 10 db increase in side lobe level or the break up of the main beam into many lobes. The effect of these minor variations has been noticed lately by other investigators.[8]

Section III is a summary of the work done in our laboratories and elsewhere on the biconical antenna. The biconical antenna problem has been solved analytically for small and large cone angles. As the cone angle decreases the properties of the biconical antenna become asymptotic to those of the thin dipole. For small cone angles the radiation resistance, eq. (3-9), is identical to the expression for R_m^r for the thin dipole. Zeroth and a first order solutions for the impedance of biconical antennas is presented.

The complexity of the first order solution, eq. (3-12), is much greater than that of the zeroth order solution, eq. (3-11). Both solutions are plotted in Fig. 3.7 and it can easily be seen that the small increase in accuracy obtained with the first order solution is not worth the labor necessary to use it. The accuracy of these calculations is indicated by the close agreement between measured and theoretical data shown in Figs. 3.14 to 3.16. Excellent agreement between theory and experiment has also been obtained in our laboratories for related antenna types. Data for the disc-cone antenna over a hemisphere and a circular ground plane is presented in Fig. 3.20. Measured radiation patterns for biconical antennas operating up to the third harmonic are presented in Fig. 3.8 for a wide range of cone angles and for a cone semiangle of 30° calculated data is presented in Fig. 3.21. The properties of these antennas may be summarized as follows:

1. Thin biconical antennas behave like dipole antennas.

2. The input resistance of biconical antennas oscillates about and approaches the characteristic resistance of a biconical transmission line of same dimensions.

3. The input reactance of a biconical antenna oscillates about and approaches zero.

4. The zeroth order input impedance solution has sufficient accuracy and is not mathematically complex.

5. The theoretical impedance is an upper bound. In practice measured impedance data is smaller in magnitude.

6. Due to the finite conductivity of the antenna the magnitude of the radiation pattern is decreased. Small lobes may disappear and the pattern nulls will be filled in.

7. The radiation patterns are symmetrical about the antenna axis.

Section IV presents data on the out of band performance of the horn antenna. This is a continuation of work first performed in our laboratories several years ago.[31] and which has been continued to date. The radiation pattern is the Fourier integral of the fields at the aperture of the horn. Therefore both propagating and non-propagating modes will effect the radiation pattern. The modes in the horn and feed system are produced by the feed structure (waveguide to coaxial line transducer, rotary joint, magnetron, etc.) and discontinuities in the horn and feed system. It was shown, Figure 4.6 that waveguide to coaxial line transducer with identical characteristics in their design band will not necessarily have identical characteristics out of the design band. Radiation patterns of an exponential horn, Figs. 4.24 to 4.29, when excited with various modes at the second harmonic are presented. These data were obtained at our laboratories during the fall of 1964. In general we may say:

1. The gain of horn antennas remains relatively constant at harmonic frequencies.

2. The beamwidth decreases with increasing frequency.

3. The radiation pattern is a function of all modes, both propagating and non-propagating that exist at the horn aperture.

4. The components of the feed system (waveguide to coaxial line transducer, rotary joint, transmitter tube, etc.) determine to a large extent the radiation pattern at harmonic frequencies by the modes that they generate.

5. The H-plane radiation patterns are symmetrical about the antenna axis.

Section V discusses an elliptical aperture antenna; the AN/FPS-8 antenna. The following conclusions may be drawn.

1. The gain tends to remain constant above the third harmonic except for a peak at the seventh harmonic.

2. The beamwidth remains constant up to the tenth harmonic.

3. The radiation pattern breaks up into many lobes above the fourth harmonic.

REFERENCES

1. S. Adachi, R.G. Kouyoumjian, and R.G. Van Seckel, "The Finite Conical Antenna" Report 662-30, Ohio State Research Foundation, 30 May 1959, AD-26994.

2. A. Anne, "Study of the Fresnel-Zone Field of a Horn Antenna," Masters Thesis, University of Pennsylvania, 1960.

3. J.G. Beaton and T.T. Wu, "Input Impedances of Center-Driven Dipole Antennas," Technical Report No. 327, Cruft Lab., Harvard University, 25 August 1960, AD 248-029.

4. Bergmann, Ann.Physik, Vol. 82, 1927.

5. G.H. Brown and O.M. Woodward, "Experimentally Determined Radiation Characteristics of Conical and Triangular Antennas," RCA Rev., Vol. 13, December 1952, p. 425.

6. E.V. Bohn, "A Critical Discussion of the Input Impedance of Idealized Mathematical Antenna Models," IEE (Brit.), Monograph No. 458E, July 1961.

7. T.H. Crowley, W. Marsh, "Discone Type Antennas", Contract No. DA-36-039sc-15554, The Ohio State University Research Foundation, 30 June 1954, AD 43-486.

8. A.R. Dion, "Investigation of Effects of Surface Deviations on Haystack Antenna Radiation Patterns," Tech. Report No. 324, Lincoln Lab., MIT, 29 July 1963, AD 418-740.

9. H.T. Friis and W.D. Lewis, "Radar Systems and Components," D.Van Nostrand Co., Inc., 1949.

10. A.J. Grammaticos, "The Performance of the Parabolic Antenna at Frequencies Outside of its Design Band," Masters Thesis, Moore School of Electrical Engineering, University of Pennsylvania, 1963.

11. C.W. Harrison, "On the Impedance of a Base Driven Vertical Antenna with a Radial Ground System," IRE Trans., Vol. AP-10, Sept. 1962.

12. C.W. Harrison, "Tables of Impedance and Radian Effective Half-Length of Electrically Long Cylindrical Antennas of Fixed Length to Diameter Ratio," SCR-576, Sandia Corp. Monograph, Nov. 1962.

13. C.W. Harrison, "Tables of Impedance and Radian Effective Length of Wide-Angle Conical Antennas", Sandia Corporation Monograph, SCR-662, June 1963.

14. E.W. Hobson, "Spherical and Elliptical Harmonics," Cambridge Univ. Press, 1931, p. 35, note that the eq. for I_{mn} in Hobson has a misprint.

15. H. Jasik, "Antenna Engineering Handbook," McGraw-Hill Book Co., Inc.1961.

16. E.C. Jordan, "Electromagnetic Waves and Radiating Systems," Prentice-Hall, Inc., 1950.

17. R.W.P. King, H.R. Mimno, and A.H. Wing, "Transmission Lines and Wave-Guides", McGraw-Hill Book Co., 1945.

18. R.W.P. King, "The Theory of Linear Antennas," Harvard Univ. Press, 1956.

19. J.D. Kraus, "Antennas," McGraw-Hill Book Company, Inc. 1950.

20. J. Labus, "Rechnerische Ermittlung der Impedanz von Antennen," Hochfrequenz-Technik und Elektroakustik, Vol. 41, 1933.

21. J.A. Meier and A. Leitner, "Biconical Antenna," Interim Technical Report No. 6, Contract No. DA-20-018-ORD-13354, Dept. of Math. and Phys., Michigan State University, 1957.

22. C.W. Miley, "Effects Associated with Varying the Length of an Asymmetrical Dipole Antenna when One Side is Comprised of a Conical Counterpoise Attached to a Cylinder", APGC-TDR-64-16, Air Proving Ground Center, Eglin AFB, March 1964, AD-435 546.

23. C.H. Papas and R. King, "Input Impedance of Wide Angle Conical Antennas," Technical Report No. 52, Cruft Laboratory, Harvard University.

24. C. H. Papas and R. King, "Input Impedance of Wide-angle Conical Antennas Fed by a Coaxial Line," Proc. IRE, Vol. 37, Nov. 1949,

25. C.H. Papas and R. King, "Radiation of Wide-Angle Conical Antennas Fed by a Coaxial Line," Proc. IRE, Vol. 39, Nov. 1951.

26. C. Polk, "Analytical and Experimental Investigation of Wide Angle, Finite Length, Biconical Electromagnetic Radiators", Master's Thesis, Univ. of Penna. 1953.

27. P.D. Potter, "Radiation Properties of the Unicone Antenna", Technical Release No. 34-102, J.P.L., Calif. Institute of Tech. Aug.15, 1960, AD 242-291.

28. J.C. Pullara, "Model Techniques for Interference Measurements", Final Report, Contract No. AF 30(602)2295, RADC TR-61-191A(Vol. 1), Melpar, Inc., July 1961.

29. J.C. Pullara, and J.P. Jones, "Radiation Characteristics of Antennas at other than Design Frequencies," IRE Convention Record, Pt. 8, 20-23 March 1961.

30. H.J. Reich, "Very-High Frequency Techniques", Vol. I, McGraw-Hill Book Co., Inc., 1947.

31. O.M. Salati, and E. Jacobs, "The Gain of Aperature Antennas at Spurious Frequencies," Proc. 5th Conference on Radio Interference Reduction, Chicago, Illinois, 6,7,8, Oct. 1959.

32. O.M. Salati and D.J. Lewis, "Interference Studies", Contract No. AF 30(602)1785, RADC TR-61-11, Institute for Cooperative Research, University of Pennsylvania, 7 January 1961, AL 259-533.

33. O.M. Salati, H. Kritikos, W.R. Lind, I. Shin, R.C. Harper, and M.R. Dresp, "Final Report, Interference Studies," Contract No. AF 30(602)1785, RADC TDR-63-359. The Institute for Cooperative Research and The Moore School of Electrical Engineering, University of Penna. July 1963, AD 438-722.

34. O. M. Salati, and D.J. Lewis, "Fresnel Region and Far Field Patterns of a Horn Antenna at Fundamental and Harmonic Frequencies," 7th Conference on Radio Interference Reduction, Chicago, Illinois, 7,8,9 Nov. 1961; also Electronics Vol. 35, 19 January 1962.

35. S.A. Schelkunoff, "Theory of Antennas of Arbitrary Size and Shape," Proc. IRE, Vol. 29, Sept. 1941.

36. S.A. Schelkunoff, "Electromagnetic Waves," D. Van Nostrand Co., Inc. 1943.

37. S.A. Schelkunoff, "Principle and Complementary Waves in Antennas," Proc. IRE, Vol. 34, Jan. 1946.

38. S.A. Schelkunoff, "General Theory of Symmetrical Biconical Antennas," J. Appl. Phys. Vol. 22, Nov. 1951.

39. S.A. Schelkunoff, "Advanced Antenna Theory,"John Wiley and Sons, 1952.

40. S.A. Schelkunoff and H.T. Friis, "Antennas, Theory and Practice," John Wiley and Sons, 1952.

41. I.P. Skal'skaia, "The Electromagnetic Field of a Dipole Radiator which is Located Inside a Parabolic Reflector," Journal of Technical Physics (USSR), Vol. 25, 1955, AD 127-698 (English Translation).

42. S. Silver, "Microwave Antenna Theory and Design", Vol. 12, MIT Radiation Laboratory Series, McGraw-Hill Book Co., Inc., 1949.

43. P.D.P. Smith, "The Conical Dipole of Wide Angle", J. Appl. Phys., Vol. 19, January 1948.

44. P.D.P. Smith, Comments on Biconical Antennas", J. Appl. Phys. Vol. 20, June 1949.

45. J. E. Storer, "The Impedance of an Antenna over a Large Ground Screen," Journal of Applied Phys., Vol. 22, Aug. 1951.

46. J.A. Stratton, "Electromagnetic Theory," McGraw-Hill Book Co., Inc., 1941.

47. C.T. Tai, "On the Theory of Biconical Antennas," J. Appl. Phys. Vol. 19, December 1948.

48. C.T. Tai, "A Study of the e.m.f. Method," J. Appl. Phys., Vol. 20, July 1949.

49. C.T. Tai, "Application of a Variational Principle to Biconical Antennas," J. Appl. Phys., Vol. 20, Nov. 1949.

50. T. T. Wu, "Theory of the Dipole Antenna and the Two-Wire Transmission Line," Technical Report No. 318, Cruft Lab., Harvard Univ., 10 March 1960, AD 237-670.

51. T. T. Wu, "Theory of the Dipole Antenna and the Two-Wire Transmission Line," Journal of Math. Physics, Vol. 2, 1961, (This is a condensation of references 9 and 10)

52. , "Appendix C, Calculation of Free-Space Radiation Characteristics of Horn Antennas at Spurious Frequencies," Final Report, Contract No. AF 30(602)2295, RADC TR-61-191B (vol. 2), Melpar, Inc., May 1961.

53. , "Interference Analysis Study" RADC-TDR-61-312, Contract No. AF 30(602)1934, Jansky and Bailey, January 1962.

APPENDIX A, Mathematical Formulas

Bessel Function of the first kind

$$J_n(x) = \sum_{k=0}^{\infty} \frac{x^{n+2k}}{2^{n+2k}\, k!\, (k+n)!}$$

for n an interger.

Bessel function of the second kind

$$Y_n(x) = \frac{\left[\cos n\pi + (-1)^{n+1}\right] J_n(x)}{\sin n\pi}$$

for n an interger.

Hankel function of the first kind

$$H_n^{(1)}(x) = J_n(x) + j\, Y_n(x)$$

Hankel function of the second kind

$$H_n^{(2)}(x) = J_n(x) - j\, Y_n(x)$$

Spherical Hankel function of the first kind

$$h_n^{(1)}(x) = \sqrt{\frac{\pi}{2x}}\; H_{n+\frac{1}{2}}^{(1)}(x)$$

Spherical Hankel function of the second kind

$$h_n^{(2)}(x) = \sqrt{\frac{\pi}{2x}}\; H_{n+\frac{1}{2}}^{(2)}(x)$$

Other spherical harmonics

$$R_k(x) = x \sqrt{\frac{\pi}{2}}\ h_n^{(1)}(x)$$

Legendre Polynomial of the first kind

$$P_n(x) = \frac{1}{2^n n!} \frac{d^n}{dx^n} (x^2 - 1)^n$$

Associated Legendre Polynomial of the first kind

$$P_n^m(x) = (1 - x^2)^{\frac{m}{2}} \frac{d^m}{dx^m} P_n(x)$$

Sine integral

$$Si(x) = \int_0^x \frac{\text{Sin } v}{v}\ dv$$

Cosine integral

$$Ci(x) = \int_\infty^x \frac{\cos v}{v}\ dv$$

A related integral

$$Cin(x) = \ln \gamma x - Ci(x)$$

$$\gamma = 1,781$$

APPENDIX B Computer Programs

643245F 002 PYCT FORTRAN SOURCE LIST PYCT

```
ISN          SOURCE STATEMENT

    C        RADIATION  RESISTANCE OF DIPOLE ANTENNAS
  1       10 FORMAT (10X, F20.7)
  2        2 W = 0.125
  3          W1 = 0.125
  4          STA1 = 3.14159/36.
  5          DO 200 J = 1, 80
  6          SUM = 0
  7          STA = 0
 10          K = 1
 11          DO 100 I = 1, 37
 12          IF (I.EQ.1.OR.I.EQ.37) GO TO 110
 15          W2 - W*3.14159
 16          F1 = COS(W2*COS(STA))-COS(W2)
 17          F2 = F1*F1
 20          F = F2/SIN(STA)
 21          IF (K.GT.0) GO TO 3
 24          F = F*4.0
 25          GO TO 5
 26        3 F = F*2.0
 27        5 SUM = SUM+F
 30      110 STA = STA+STA1
 31      100 K = -K
 33          SUM = SUM*STA1*60./3.0
 34          PRINT 10, SUM
 35      200 W = W+W1
 37          STOP
 40          END
```

In statement 2, W stands for βL
Fortran III coding was used.

643245F C15 PYCT FORTRAN SOURCE LIST PYCT

```
ISN        SOURCE STATEMENT
    C      RADIATION  REACTANCE OF DIPOLE ANTENNAS
  1     10 FORMAT (10X, F20.7, 10X, F10.5)
  2      2 W = 0.125
  3        W1 = 0.125
  4        X1 = 0.125/36.
  5        DO 200 J = 1, 80
  6        N = W/X1
  7        N1 = N+1
 10        SUM = 0
 11        X = 0
 12        K = 1
 13        DO 100 I = 1, N1
 14        IF (I.EQ.1.OR.I.EQ.N1) GO TO 110
 17        F1 - COS (6.28318*X)
 20        F1 = F1/X
 21        F2 = COS(6.28318*(W-X))
 22        F2 = F2/(W-X)
 23        F = F1+F2
 24        F = F*SIN(6.28318*X)
 25        IF (K.GT.0) GO TO 3
 30        F = F*4.0
 31        GO TO 5
 32      3 F = F*2.0
 33      5 SUM = SUM+F
 34    110 X = X+X1
 35    100 K = -K
 37        SUM = SUM*X1*30./3.0
 40        PRINT 10, SUM, W
 41    200 W = W+W1
 43        STOP
 44        END
```

In statement 2, W stands for βL
Fortran III coding was used.

```
S1.. .5 = M
S2.. CR CR
DAPRITTHEATA          E          E  SQUARED
1. = TH
S3.. COS  TH / 57.2958  = C
SIN   TH/57.2958  = S
 M X 3.14159  /2. = Q
Q X C = R
COS R = L
COS Q = J
  L -J   / S = E
E X E = E2
CR
1000 DPRT TH
1604 DPRT E
1604 DPRT E2
TH + 1. = TH
IF    88. - TH   NEG S10
USE S3
S10..M + .5 = M
CR
DAPRTM=
1002 DPRT M
IF   20. - M   NEG S11
USE S2
S11..QUIT
BEGIN S10
```

Appendix C

MEASUREMENT OF ANTENNA POWER PATTERNS AND GAIN

C.1 Equipment and Definitions

The equipment used to measure antenna power patterns and gain is listed in Tables C-1 through C-4. The antenna range is located on the roof of the Moore School. A fixed tower, 18 feet high, is located at one end of a track 80 feet long. A movable tower carries the antenna positioner and signal generator. Fifteen feet of RG-9B/U coaxial cable was used to connect the transmitting antenna (the antenna under test) located on the movable tower to the signal generator at the base of the tower. The receiver, which was located in the building at the base of the fixed tower, was connected through 30 feet of RG-212/U coaxial cable to the receiving antenna at the top of the tower. As indicated in the block diagrams of Figures C-2 and C-3 the crystal mixer and matching network are located at the antenna terminals. The RG-212/U coaxial cable, therefore, carries only a 65 Mc signal and not the RF signal from the antenna to the receiver.

A surveyor's level was used to bore sight the antenna under test.

Table C-1

Hewlett-Packard Signal Generators

Frequency	Model No./Serial No.
1.0 - 2.0 Gc	HP614A/#420
2.0 - 4.0 Gc	HP616A/#885
4.0 - 7.0 Gc	HP618B/#16
7.0 - 11.0 Gc	HP620A/#1237

Table C-2

Exponential Horn Antennas*

Frequency Range	Band	Model No./Serial No.
1.12 - 1.70 Gc	L	AT316
1.70 - 2.60 Gc	LS	645/01008
2.60 - 3.95 Gc	S	644/165
3.95 - 5.85 Gc	C	643/165
5.85 - 8.20 Gc	XN	642/123
7.05 - 10.00 Gc	XB	641/154

A photograph of these horns is shown in Fig. C-1.

Table C-3

Waveguide to Coaxial Line Transducers

Frequency Range	Band	Model No./Serial No.	Manufacturer
1.12 - 1.70	L	FSN-5985-090-0110/35	King Electronics
1.70 - 2.60	LS	105-LS/	Aircom Microwave
2.60 - 3.95	S	HPS281A/	Hewlett-Packard
3.95 - 5.85	C	HPS281A/	Hewlett-Packard
5.85 - 8.20	XN	HPJ281A/	Hewlett-Packard
7.05 - 10.00	XB	HPH281A/	Hewlett-Packard

* All antennas except AT316 are manufactured by the Narda Microwave Corp.

Table C-4

Other Equipment

Frequency Range	Description	Model No./Serial No.	Manufacturer
400/1000 cps	Square Wave Generator	5226/	American Electronic Labs.
20 Mc - 100 Gc	Receiver	1640/APZ	Scientific Atlanta
2.0 - 16.0 Gc	Crystal Mixer	14-2/159	Scientific Atlanta
1.9 - 100 Gc	Matching Network	1628/79	Scientific Atlanta
0 - 11.0 Gc	SPDT Switch	11300/	Transco
1000 cps	Antenna Pattern Recorder	121B/338	Scientific Atlanta

The polarization of an antenna is defined as the direction of the electric field vector of its radiation field when it is used as a transmitting antenna. The plane of this vector is termed the E-plane. If the antenna was placed in a spherical coordinate system as shown in Fig. 2.15 then the $\theta = 90^{\circ}$ plane is the E-plane. The plane $\varphi = 0^{\circ}$ is the H-plane in this figure and is oriented 90° with respect to the E-plane.

Figure 3 is a photograph of the antenna range showing the 6 foot diameter parabolic reflector with a double-dipole feed being tested.

C.2 Far Field Antenna Power Pattern Measurements

The following procedure was used in measuring far field radiation power patterns.

1. The equipment is connected as in Fig. C-3. Note that the antenna separation distance, R, must be greater than $2D^2/\lambda$ where D is the largest aperture dimension of either antenna.

2. The polarization of the transmitting antenna (test antenna) is adjusted to the desired plane.

3. The receiving antenna is polarized in the same plane as the transmitting antenna.

4. The receiver, signal generator, square wave generator, and antenna pattern recorder are turned on and after the proper warm up period are calibrated according to their instruction manuals.

5. The transmitting antenna is rotated in azimuth to the position of maximum received signal.

6. The square wave generator is adjusted to obtain maximum indication on the antenna pattern recorder.

7. Adjust the signal generator output or receiver gain to obtain zero db on the antenna pattern recorder scale.

8. Check the signal displayed on the receiver oscilloscope to insure that the receiver is not being over driven.

9. Move the transmitting antenna toward and away from the receiving antenna over a distance of approximately two wavelengths and observe the receiver power variation. Large, erratic, or oscillatory variations indicate that energy is arriving at the receiving antenna via more than one path. This is caused by reflections from the ground and objects adjacent to the antenna range. Correct this multipath effect before proceeding further in the antenna measurements. The power should vary smoothly and proportionally to $1/R^2$ as the transmitting antenna is moved.

10. Rotate the receiving antenna in polarization if it is desired to measure the power in a plane other than the plane of polarization of the transmitting antenna. For example, if the antenna under test is a double-dipole feed in a parabolic reflector and in step 2 above the dipole was orientated parallel to the ground (H-plane) and it is desired to measure the power in the cross polarized field then the receiving antenna is oriented to receive an EM field with a vertical E field.

11. The transmitting antenna is rotated in azimuth and the desired antenna pattern is automatically plotted by the antenna pattern recorder.

C.3 Near Field Antenna Power Pattern Measurements

Near field measurements are performed in a manner identical to the far field measurements described in Section C.2 except for step one of that

section. Replace step one by the following step 1a.

1a. The equipment is connected in Fig. C-2 except that the antenna separation distance, R, is less than $2D^2/\lambda$.

Figure 2-13 shows near field power patterns recorded at various separation distances R.

C.4 Gain Measurements

This section describes the measurement of the insertion gain of an antenna. Insertion gain is defined as the gain of an antenna that is measured when the antenna is inserted in a 50 ohm matched system. No correction is made for the VSWR of the antenna under test. Figure C-4 shows the equipment block diagram for gain measurements. In the actual test set-up the antenna under test and the standard gain horn antenna are mounted "back to back".

The various factors that affect the gain measurement are the proximity and irregularity of the ground, reflecting objects near the pattern range and drift in the equipment. These effects and methods of overcoming them are described by the National Bureau of Standards.[54]

In performing a gain measurement the following steps are followed.

a. Connect the equipment as shown in Fig. C-4.

b. Perform steps 2 through 10 of Section C.2.

Step 5 should overcome equipment drift by allowing proper warm up time and step 10 should correct for reflections from the ground or objects near the antenna range.

c. Transmit with the standard gain horn and rotate it in azimuth to obtain maximum received power.

d. Set the signal generator output to a given level, say P_a, and note the magnitude of received power.

e. Check as in step b to make sure that the receiver is not being overloaded.

f. Transmit with the antenna under test and rotate it azimuth to obtain maximum received power.

g. Adjust the signal generator output to obtain the same received power as in step d. Call the new signal generator output P_b.

h. Compute the gain of the antenna under test as follows.

From Silver[42]

$$\frac{P_r}{P_t} = \frac{G_t\, G_r\, \lambda^2}{(4\pi R)^2} \qquad \text{(C-1)}$$

where

P = power

G = gain

λ = wavelength

R = antenna separation

and the subscripts denote

r = received

t = transmitted

Consider transmission between the two standard gain horns as in steps d and e. Let G_o and P_o be the gain of the standard gain horn the power received respectively. Then

$$\frac{P_o}{P_a} = \left[\frac{G_o\, \lambda}{4\pi R}\right]^2 \qquad \text{(C-2)}$$

Now consider transmission between the antenna under test with gain G and the standard gain horn as in steps f and g. Equation (C-1) now becomes

$$\frac{P_o}{P_b} = G_o\, G \left[\frac{\lambda}{4\pi R}\right]^2 \qquad \text{(C-3)}$$

Combination of eqs. (C-2) and (C-3) yield

$$G = \frac{P_a}{P_b} \qquad \text{(C-4)}$$

or in decibels

$$G(db) = 10\ \mathrm{Log}_{10}\ \frac{P_a}{P_b} \qquad \text{(C-5)}$$

Since duplicates of all of the standard gain antennas are on hand, their gains have been checked using the Cottony method (ref. 54). These checks agree within 0.5 db with the calibration curve of the manufacturer.

C.5 Accuracy

The accuracy of the gain, impedance, and radiation power pattern measurements is limited by the accuracy of the equipment used. The accuracy of frequency and power primarily determined by the least count of the signal generator dials. Frequency accuracy is $\pm$ 1%. All power measurements are accurate within $\pm$ 0.5 db. The main lobe structure of the antenna power patterns is repeatable within $\pm$ 0.2 db while the minor lobe structure is repeatable within $\pm$ 0.5 db.

The dynamic range of the recording system was 60 db and care was taken to prevent receiver overload. System noise level was greater than -87 dbm.

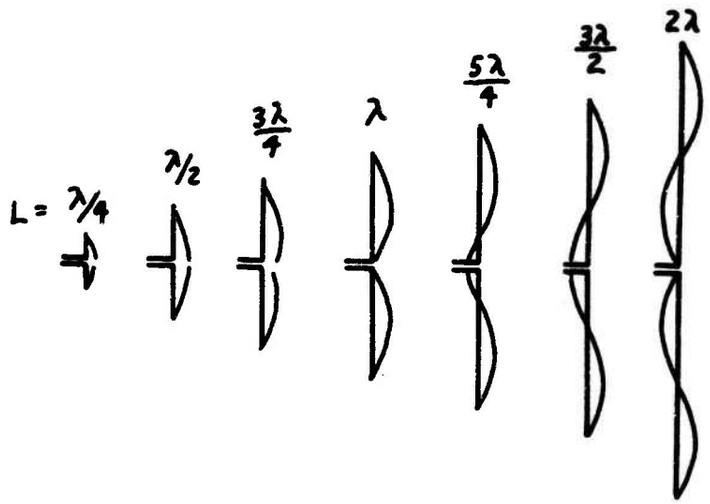

Figure 1.1 Sinusoidal distribution of maximum current on infinitely thin center-driven antennas of different lengths L.

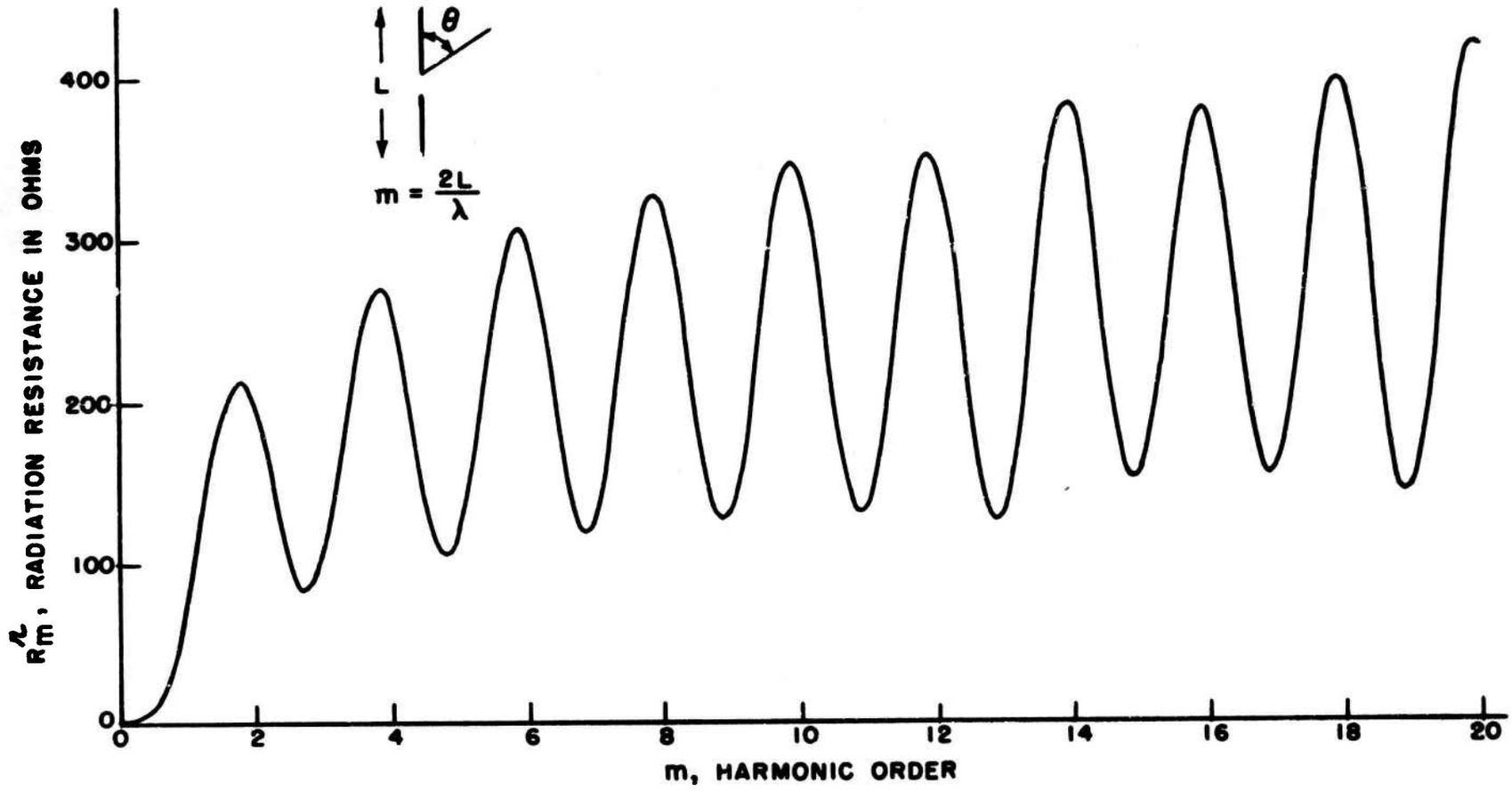

FIGURE 1.2 RADIATION RESISTANCE VS. HARMONIC ORDER FOR A THIN DIPOLE.

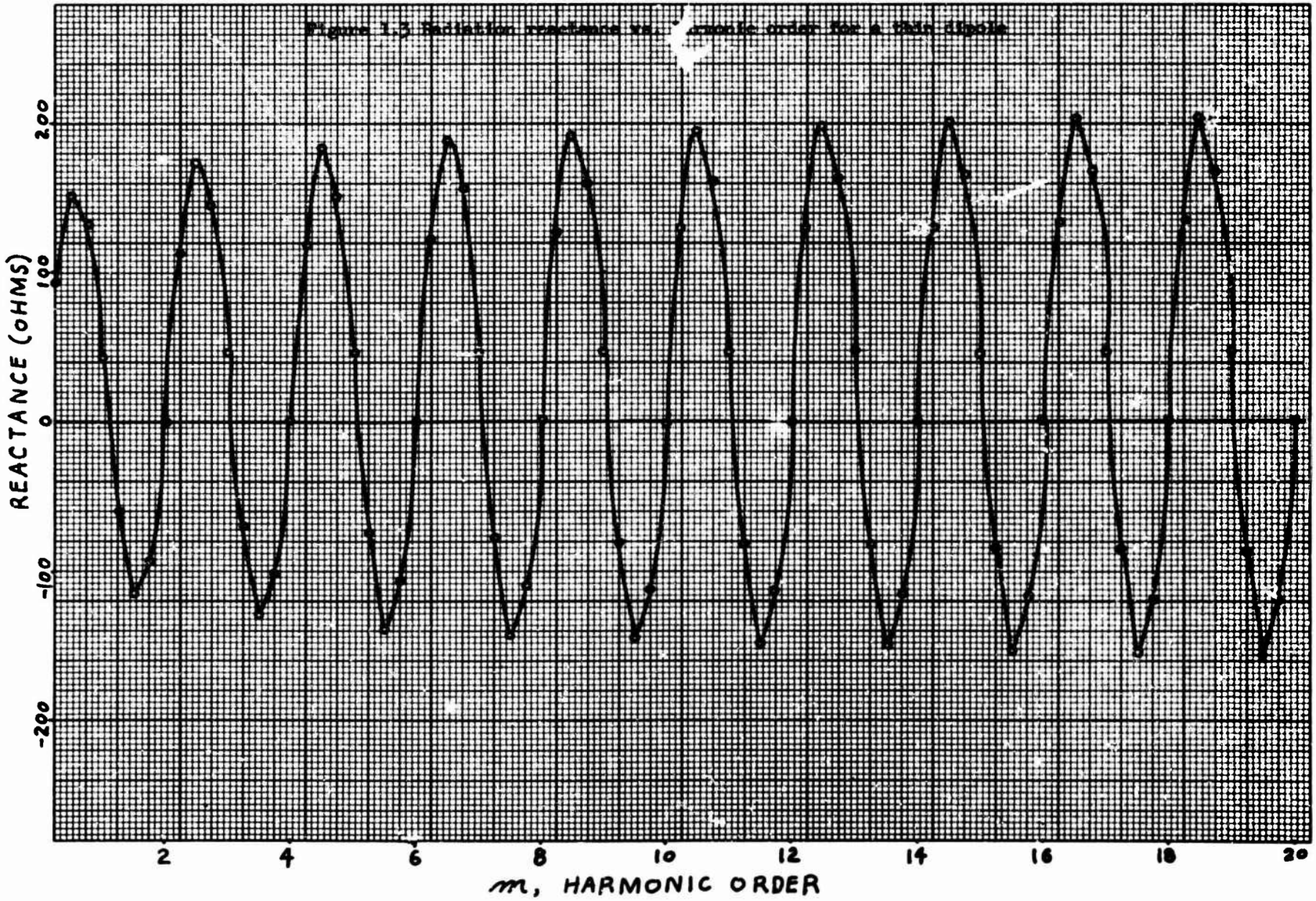

Figure 1.3 Radiation reactance vs. harmonic order for a thin dipole

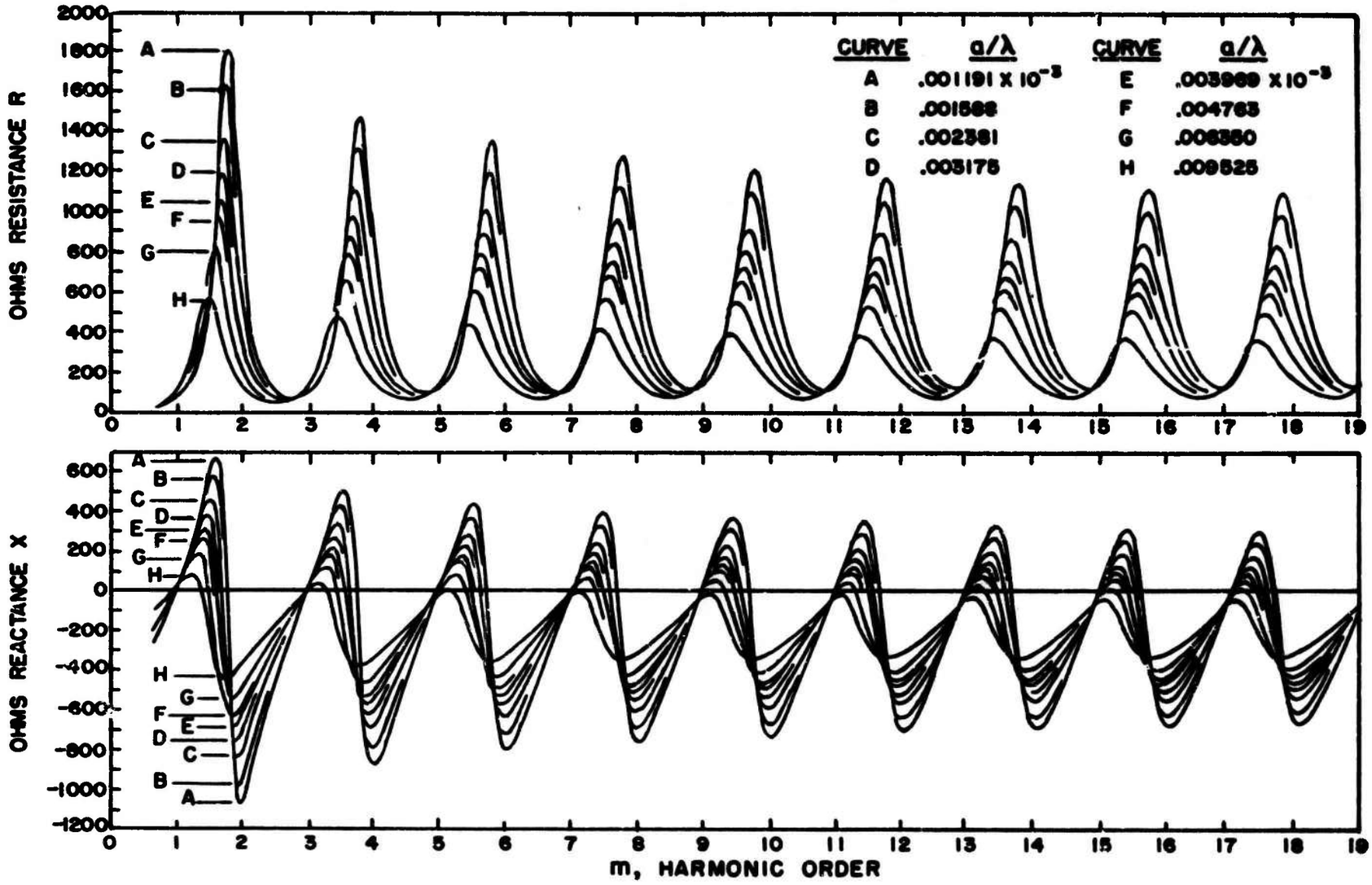

FIGURE 1.4 RESISTANCE AND REACTANCE OF CYLINDRICAL ANTENNA. (WU)

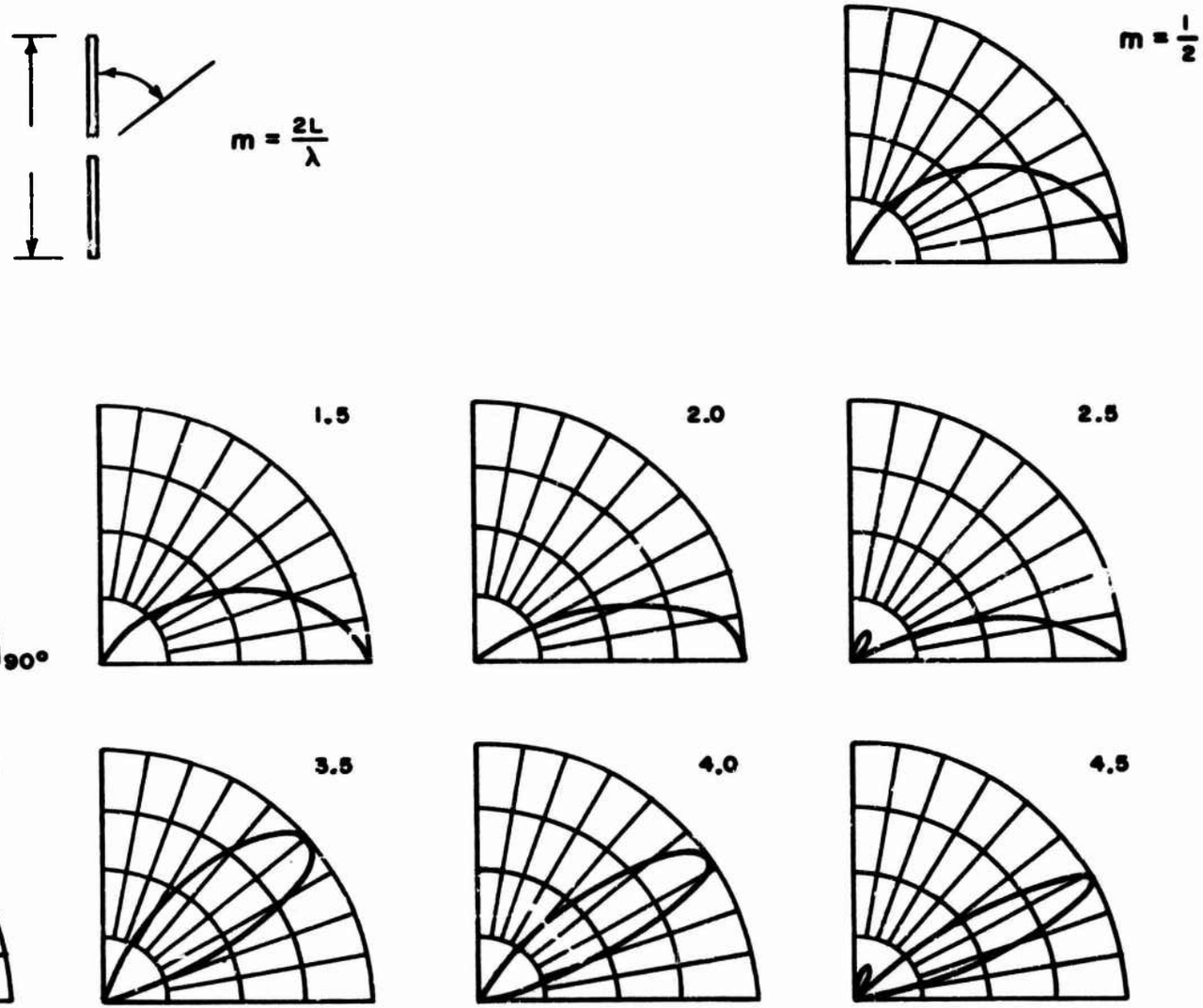

Figure 1.5a Radiation power patterns of thin dipoles

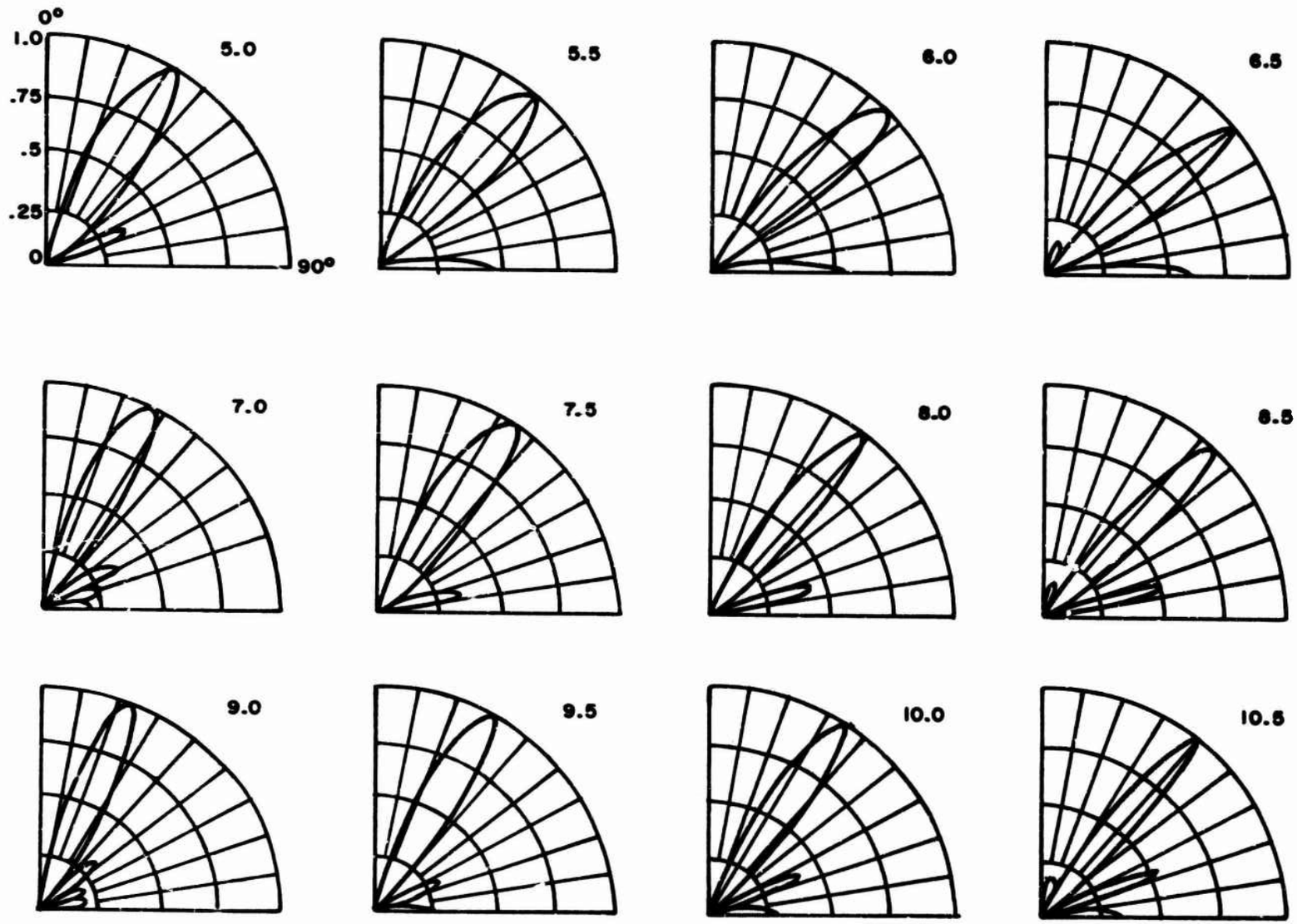

Figure 1.5b Radiation power patterns of thin dipoles

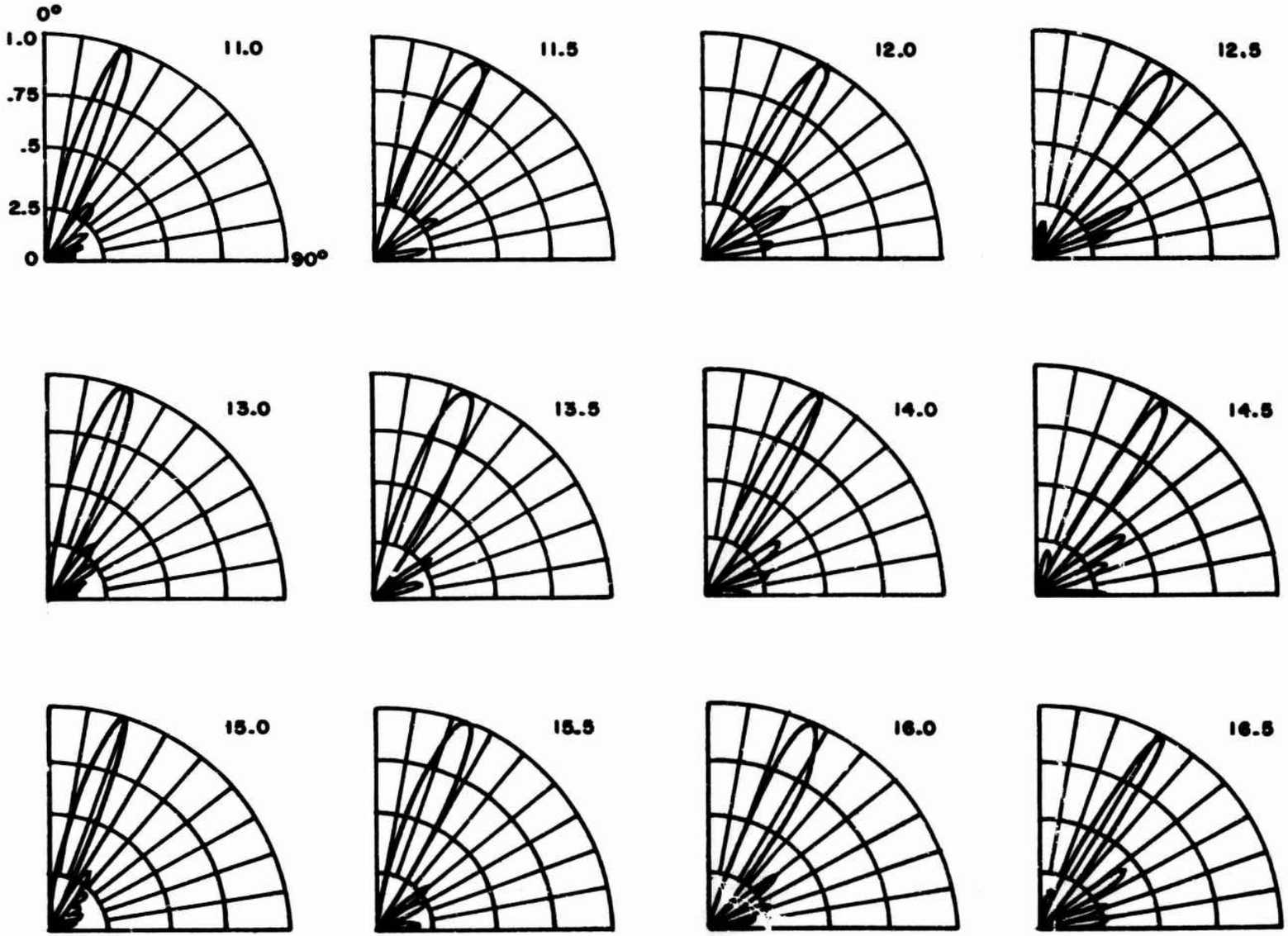

Figure 1.5c Radiation power patterns of thin dipoles

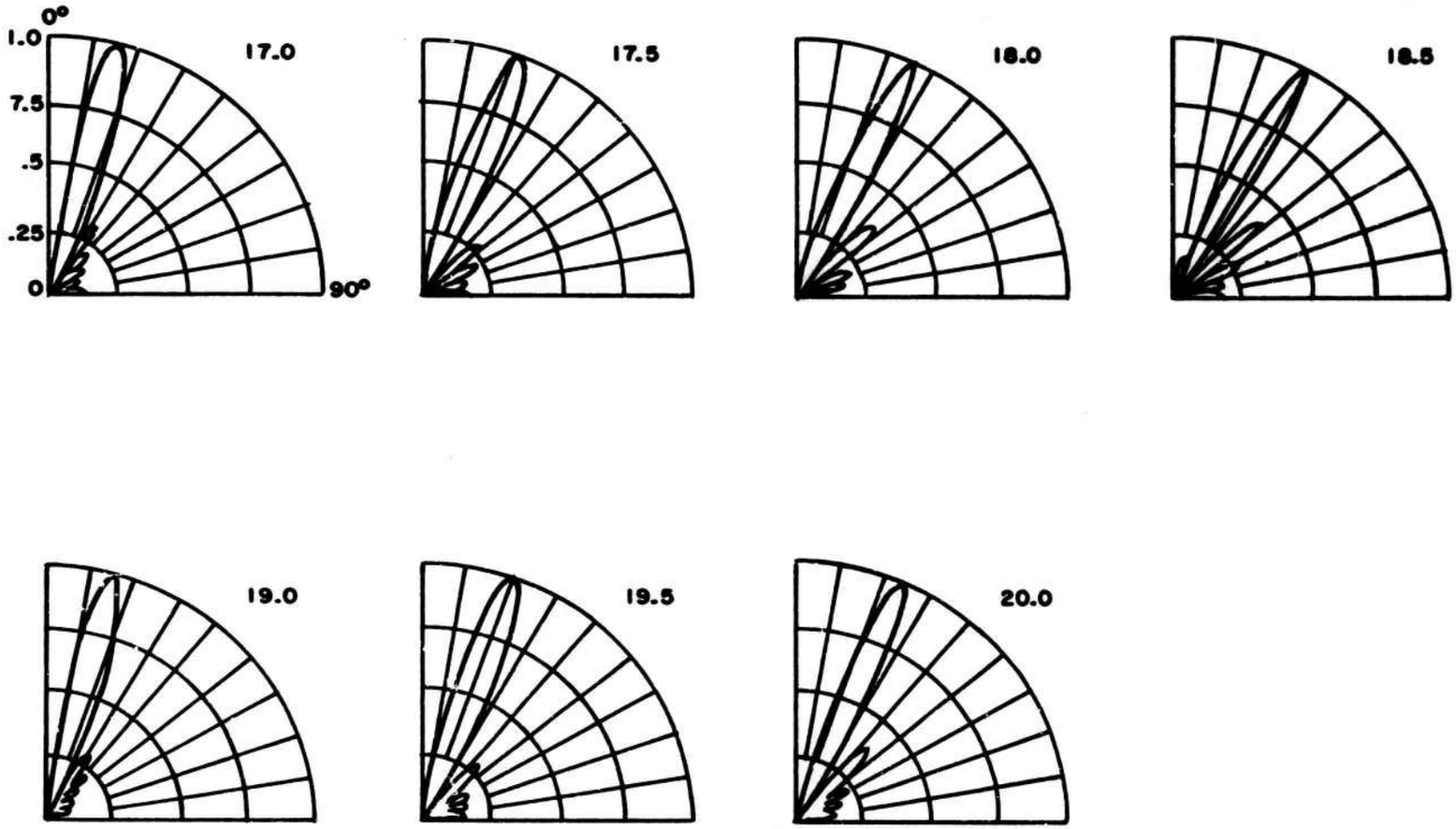

Figure 1.5d Radiation power patterns of thin dipoles

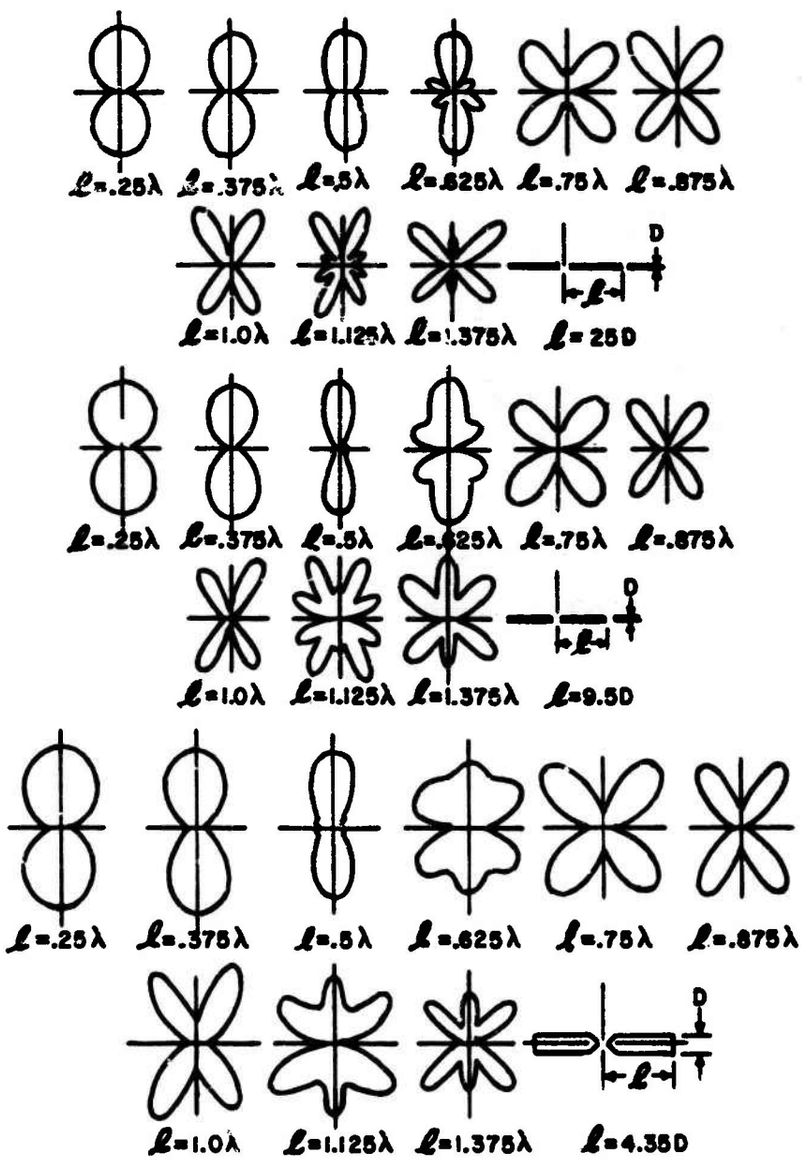

FIG. 1.5e MEASURED RADIATION PATTERNS OF DIPOLES.[18]

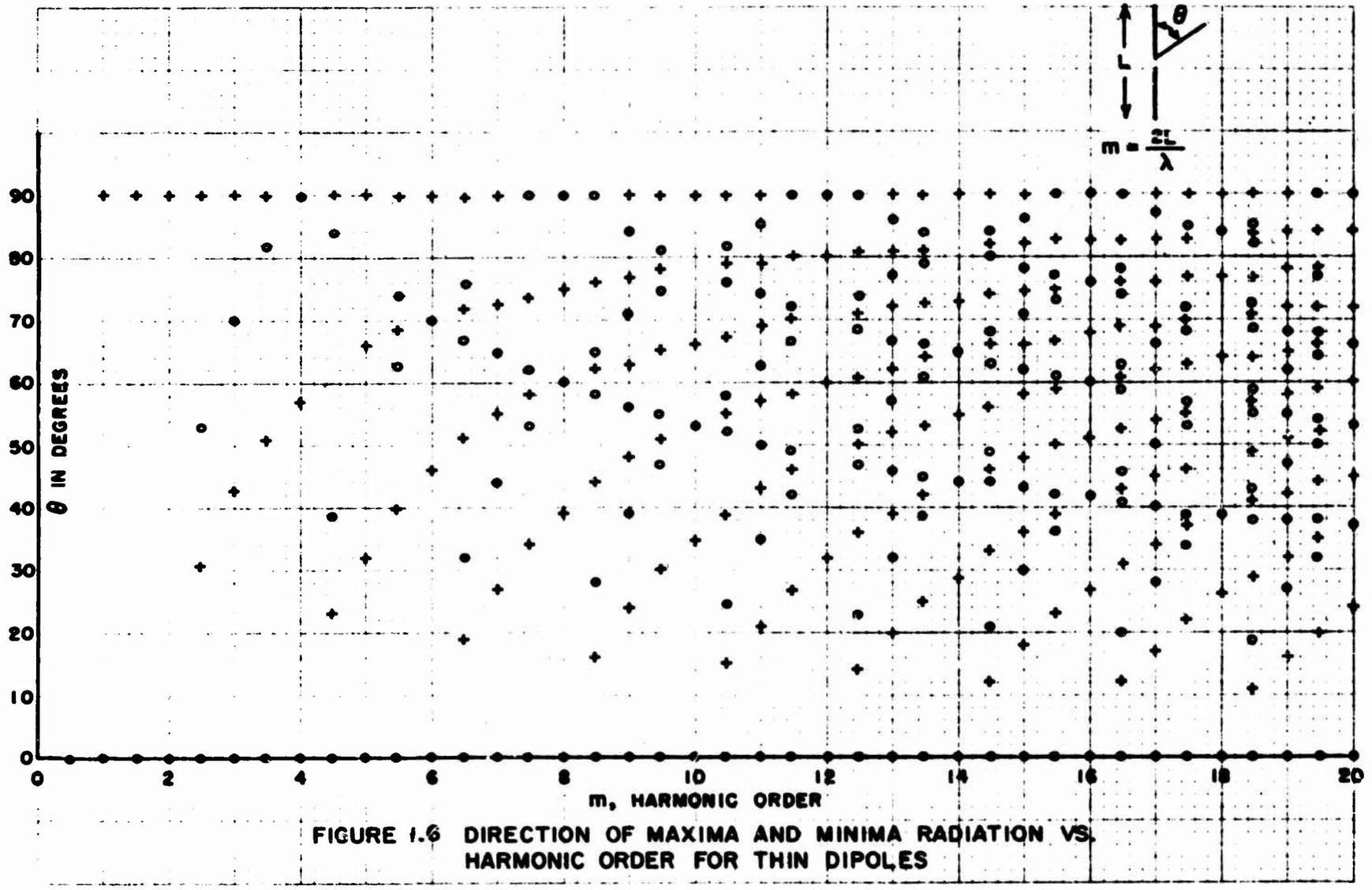

FIGURE 1.6 DIRECTION OF MAXIMA AND MINIMA RADIATION VS. HARMONIC ORDER FOR THIN DIPOLES

m \ SL	1	2	3	4	5	6	7	8	9	10
1	0									
1.5	0									
2	0									
2.5	10.33	0								
3	0	3.02								
3.5	0	17.24								
4	0									
4.5	8.82	0	10.631							
5	0	4.1	4.88							
5.5	0	18.2	3.56							
6	0	2.72								
6.5	8.51	0	17.04	2.14						

FIGURE 1.7 a - Relative Amplitude of the Lobes in the Radiation Power Patterns of Thin Dipoles in db.

M \ SL	1	2	3	4	5	6	7	8	9	10
7	0	4.5	5.89	6.24						
7.5	0	18.65	4.44	20.06						
8	0	3.495								
8.5	8.32	0	17.3	2.83						
9	0	4.7	6.36	7.055	7.27					
9.5	0	18.835	4.84	20.034	5.7					
10	0	3.88	4.64							
10.5	8.2	0	17.445	3.2	19.02	3.85				
11	0	4.81	6.57	7.56	8.02	8.1				
11.5	0	18.935	5.08	21.41	6.66					
12	0	4.1	5.21							
12.5	8.15	0	17.57	3.39	19.54	4.44				

FIGURE 1.7 b - Relative Amplitude of the Lobes in the Radiation Power Patterns of Thin Dipoles in db.

FIGURE 1.7 b - Relative Amplitude of the Lobes in the Radiation Power Patterns of Thin Dipoles in db.

M \ SL	1	2	3	4	5	6	7	8	9	10
13	0	4.9	6.765	7.85	8.38	8.7	8.81			
13.5	0	18.99	5.27	21.78	6.76	22.8	7.135			
14	0	4.21	5.62	5.97						
14.5	8.1	0	17.76	3.57	20.04	4.77	20.33	5.12		
15	0	4.99	6.86	8.01	8.76	9.265	9.4	5.12		
15.5	0	19.065	5.385	22.345	7	27.2	7.72	23		
16	0	4.34	5.85	6.46						
16.5	8.04	0	17.78	3.715	19.77	5.08	20.69	5.57		
17	0	4.99	6.96	8.07	8.87	9.44	9.84	9.94	9.95	
17.5	0	19.12	5.5	22.62	7	22.76	7.775	24.12	8.2	
18	0	4.435	6.14	6.78	7					
18.5	8	0	17.795	3.76	20.08	5.23	20.93	6.03	21.51	6.1

FIGURE 1.7 c - Relative Amplitude of the Lobes in the Radiation Power Patterns of Thin Dipoles in db.

M \ SL	1	2	3	4	5	6	7	8	9	10
19	0	5.05	7.1	8.26	9.04	9.58	10.16	10.27	10.38	10.42
19.5	0	19.16	5.28	21.87	7.32	8.22	23.88	8.6	23.96	
20	0	4.51	6.17	7.15	7.4					

FIGURE 1.7 d - Relative Amplitude of the Lobes in the Radiation Power Patterns of Thin Dipoles in db.

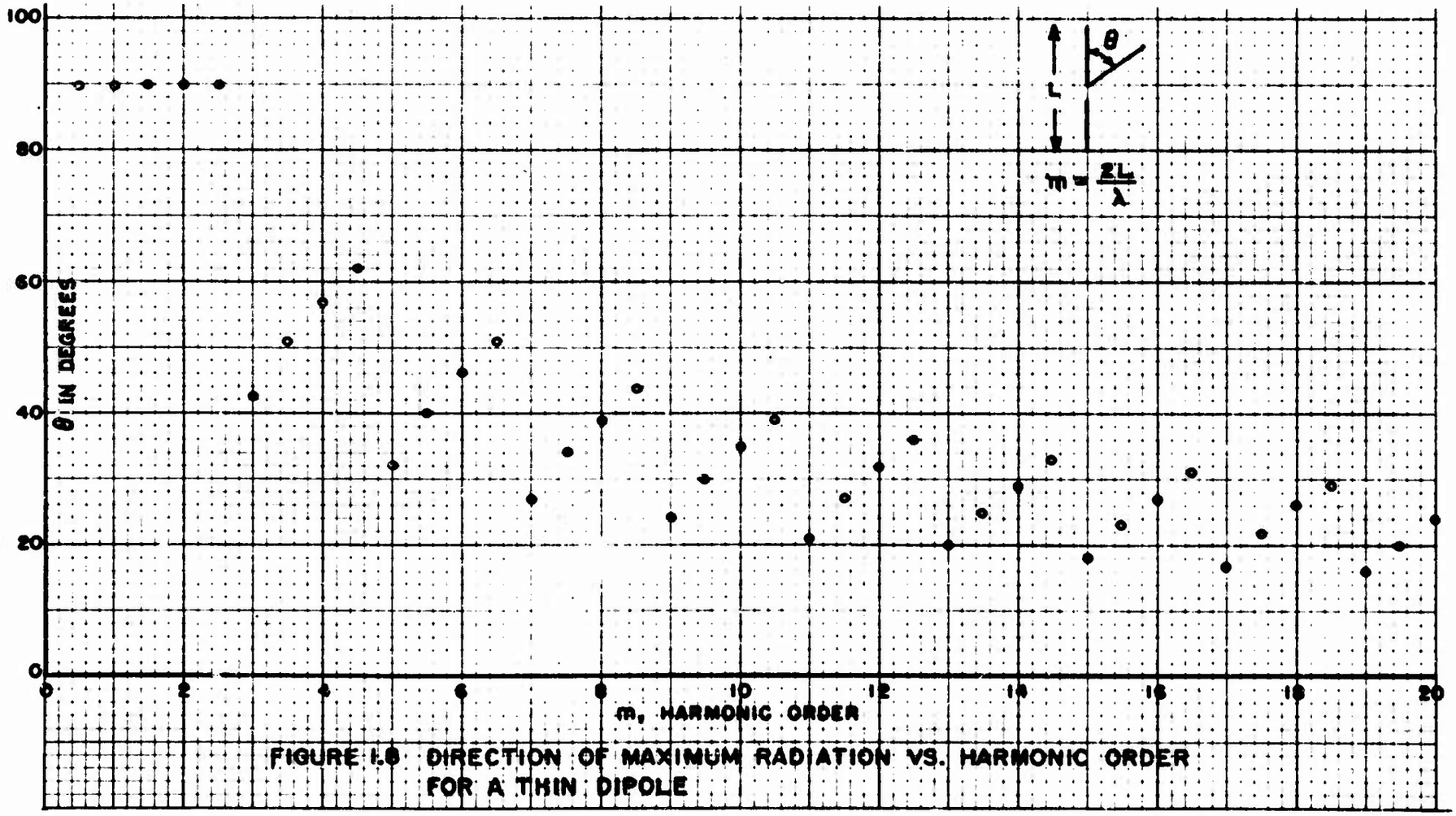

FIGURE 1.8 DIRECTION OF MAXIMUM RADIATION VS. HARMONIC ORDER FOR A THIN DIPOLE

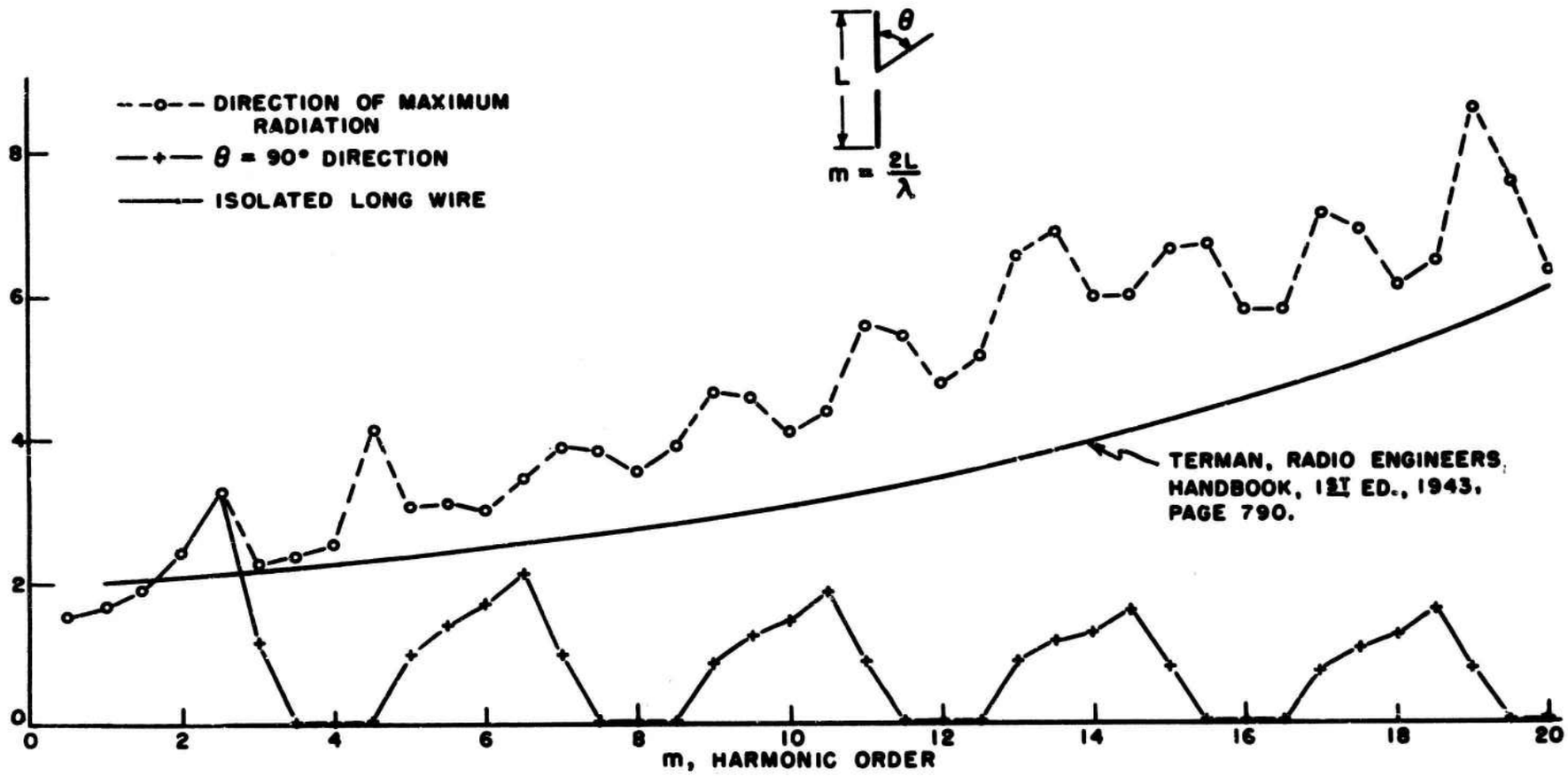

FIG. 1.9 — DIRECTIVITY VS. HARMONIC ORDER FOR A THIN DIPOLE
(LINES CONNECTING DATA POINTS HAVE NO SIGNIFICANCE)

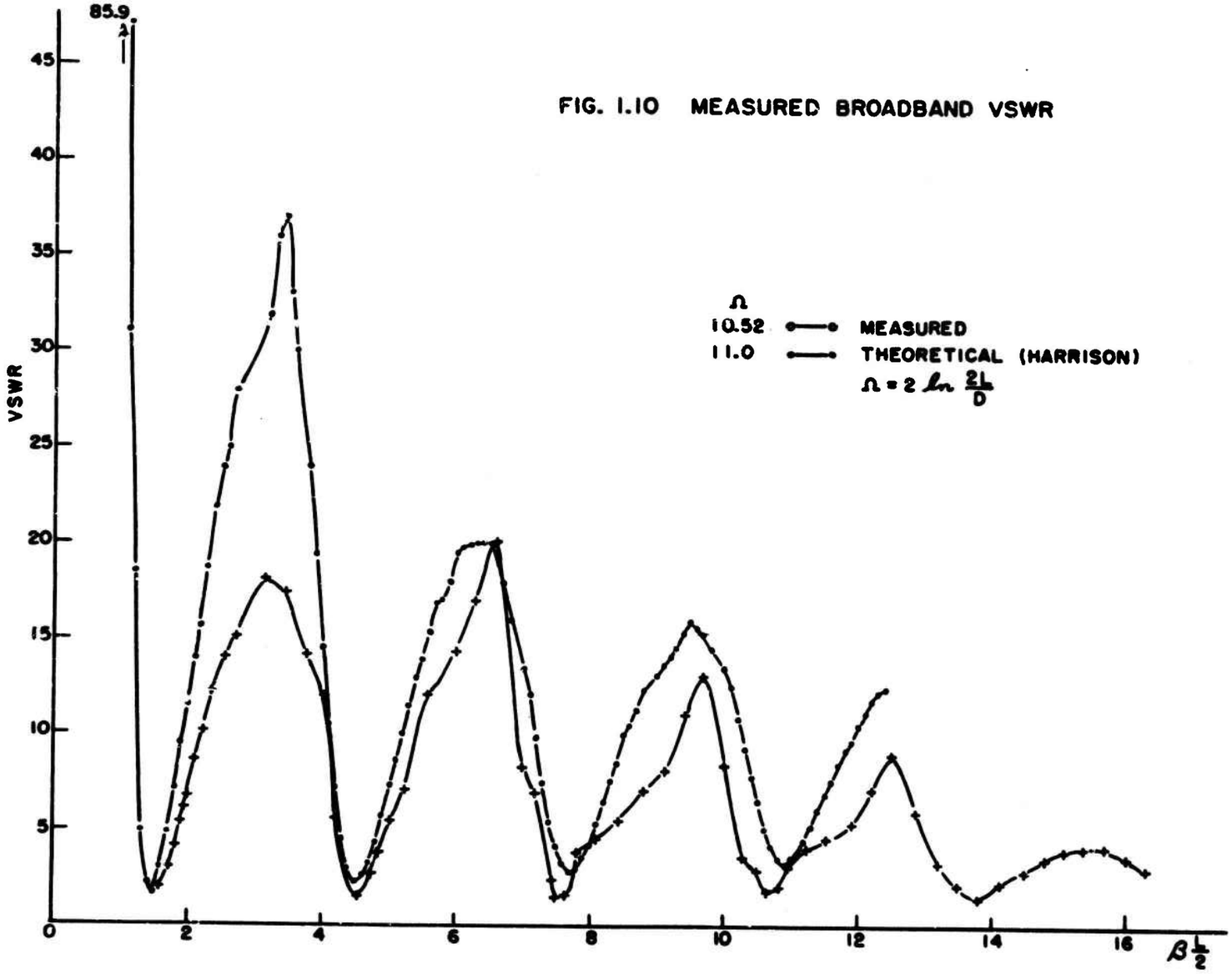

FIG. 1.10 MEASURED BROADBAND VSWR

FIG. 1.11 MEASURED BROADBAND RESISTANCE

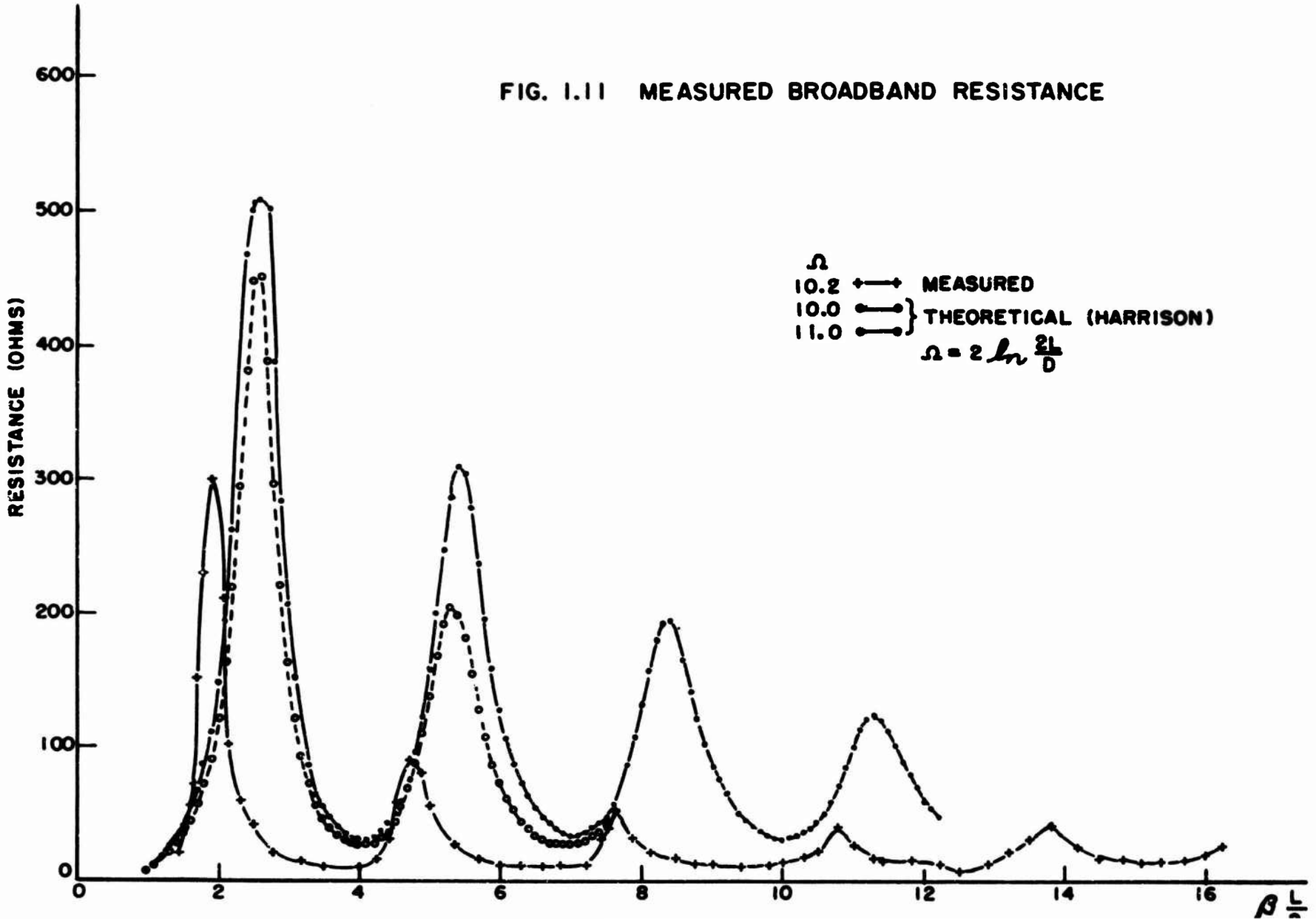

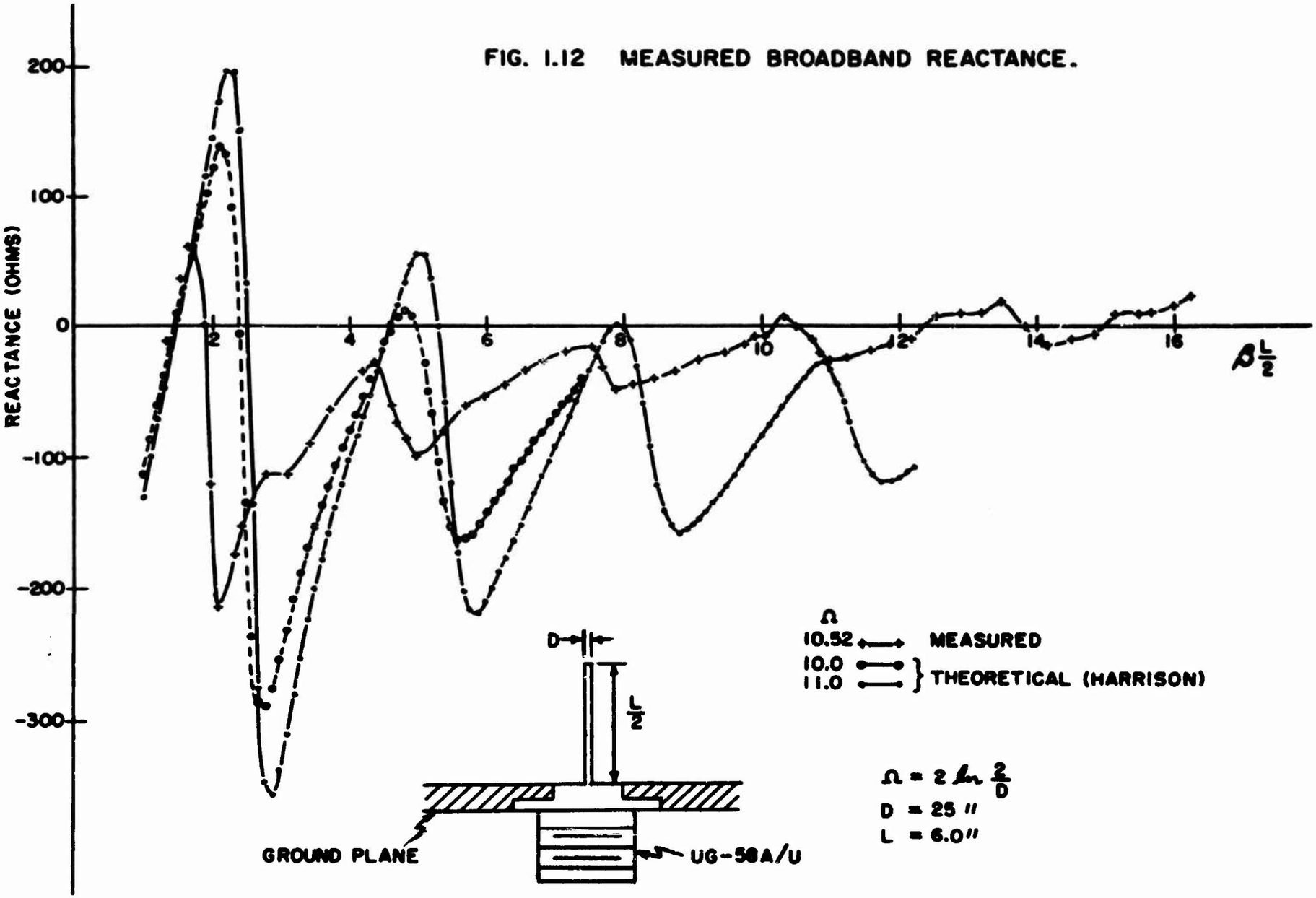

FIG. 1.12 MEASURED BROADBAND REACTANCE.

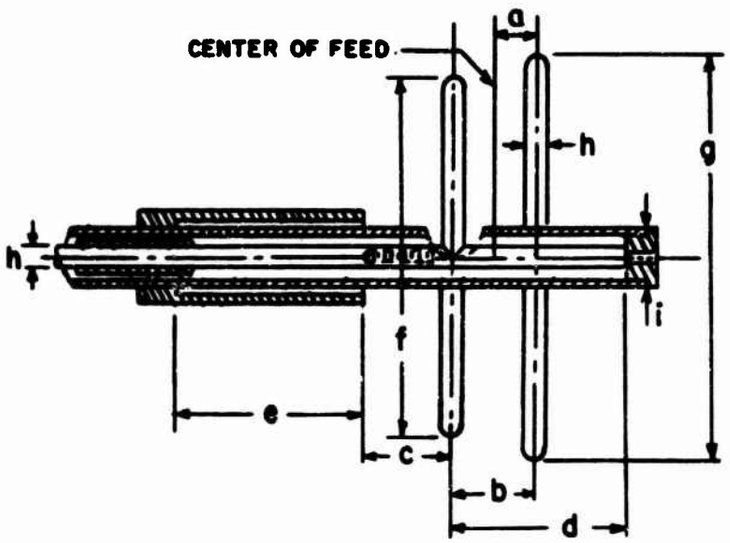

FIG. 2.1a

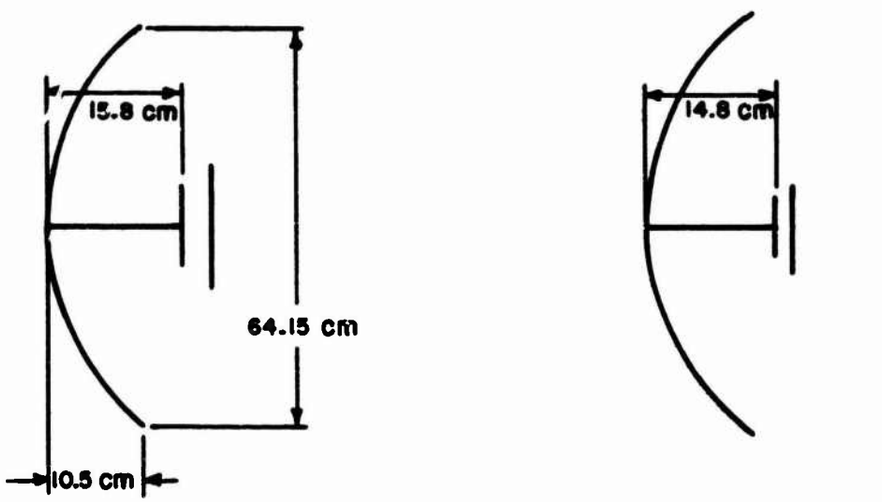

LARGE DOUBLE-DIPOLE

SMALL DOUBLE-DIPOLE

FIG. 2.1b

FIG. 2.1 TWO FOOT PARABOLIC REFLECTOR AND DOUBLE-DIPOLE ANTENNA DIMENSIONS.

Figure 2.2 VSWR vs. Frequency, 6 ft. dia. parabolic reflector and feed.

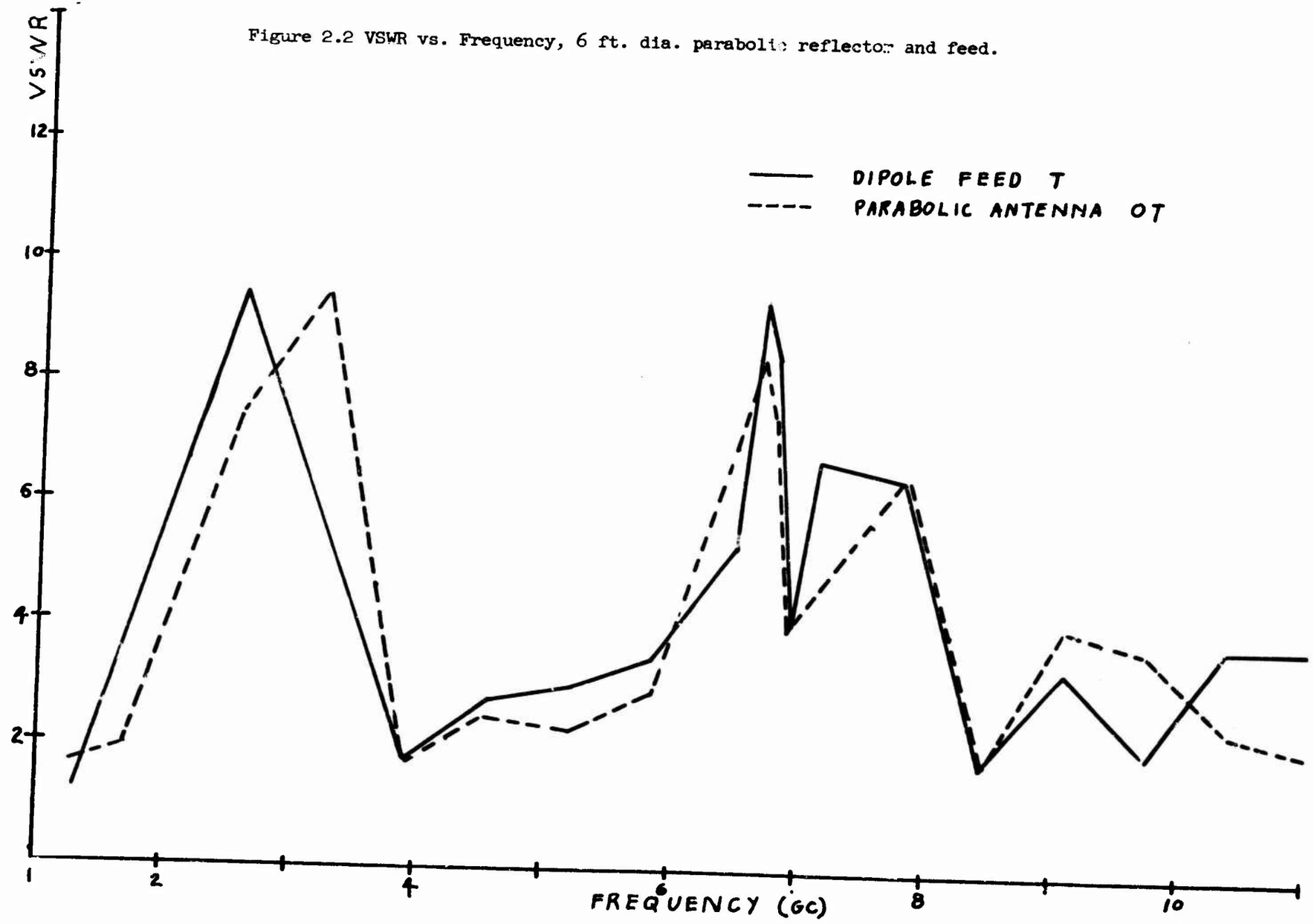

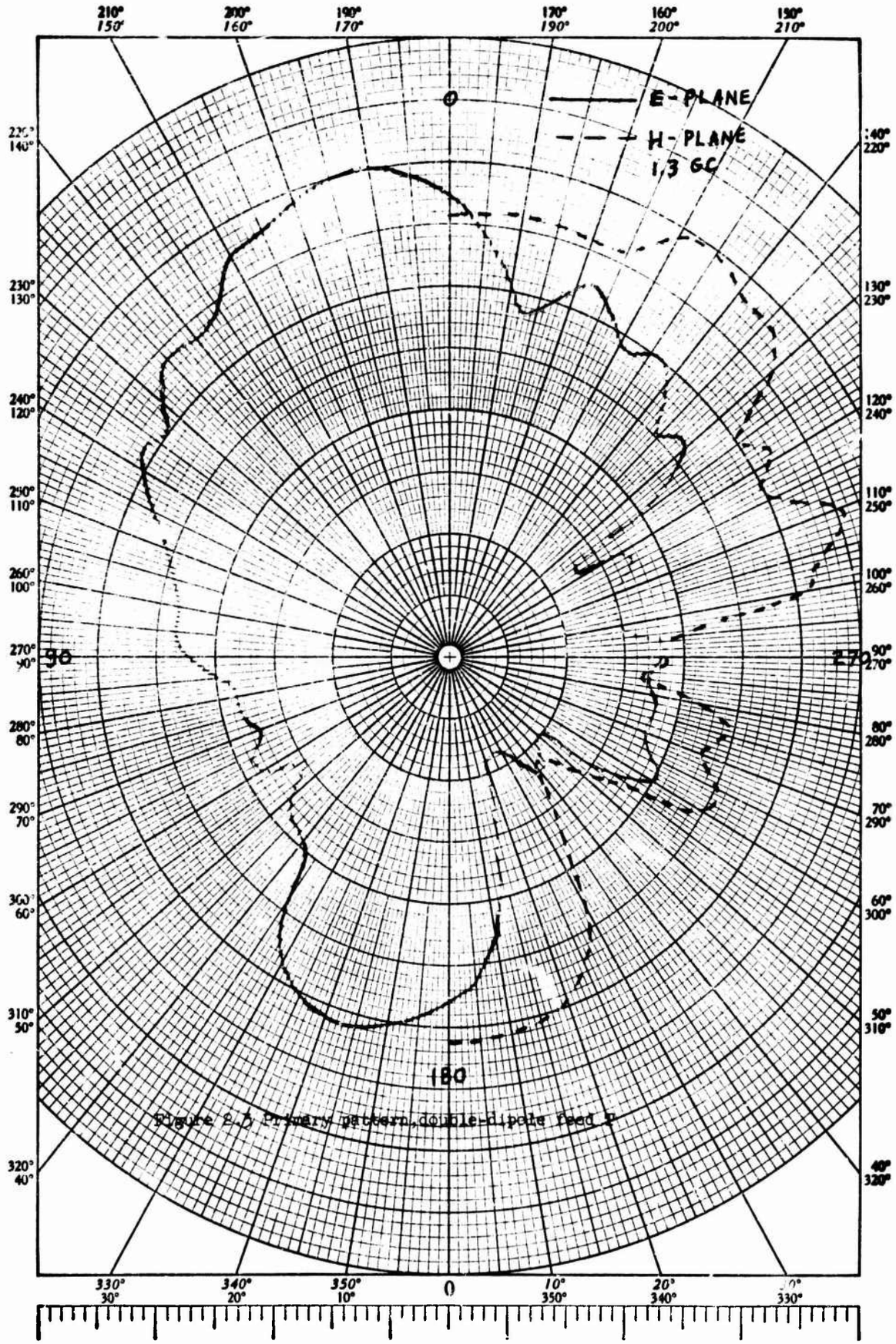

Figure 2.5 Primary pattern, double-dipole feed 2

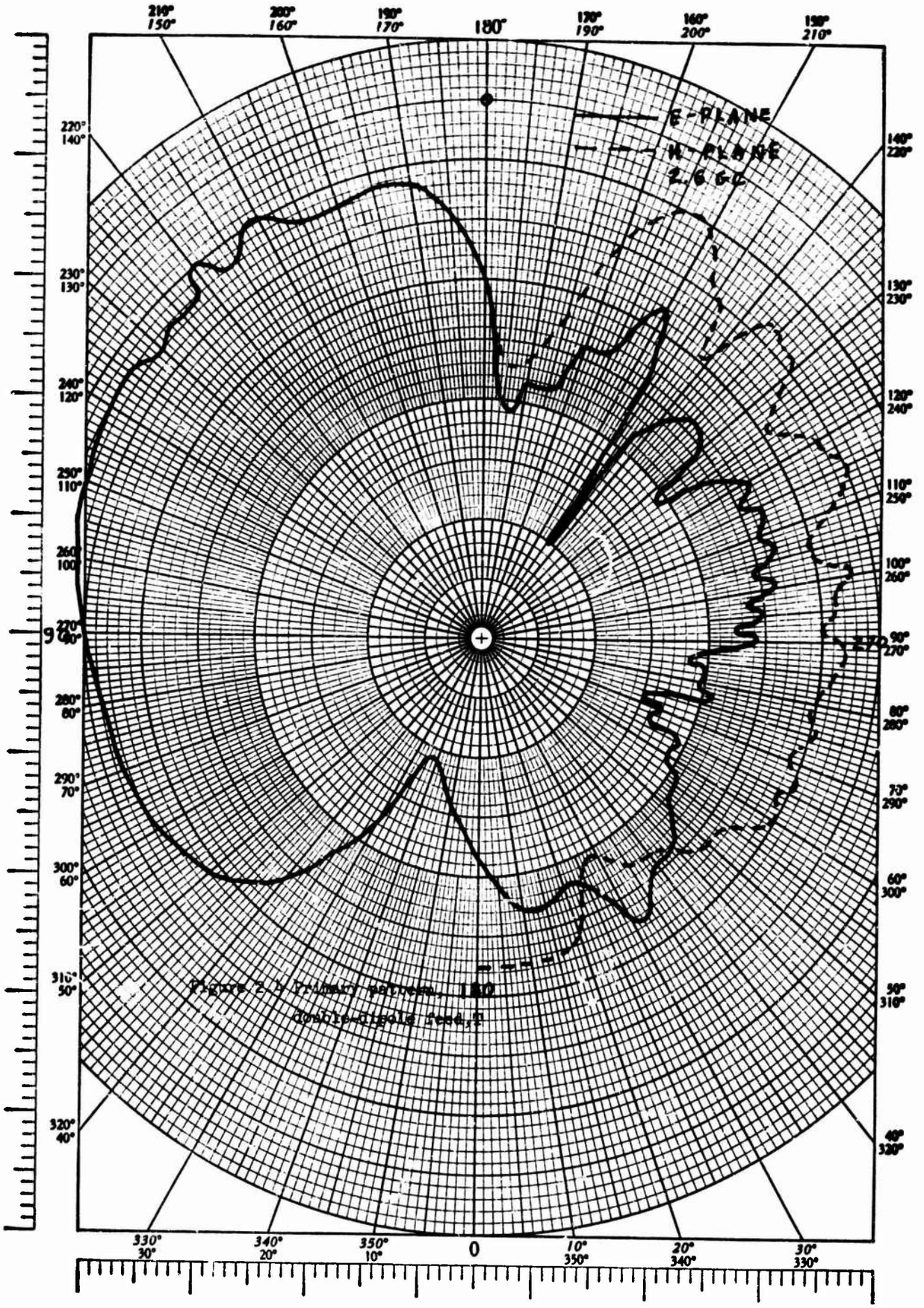

Figure 2.5 Primary pattern, 180° double-dipole feed.

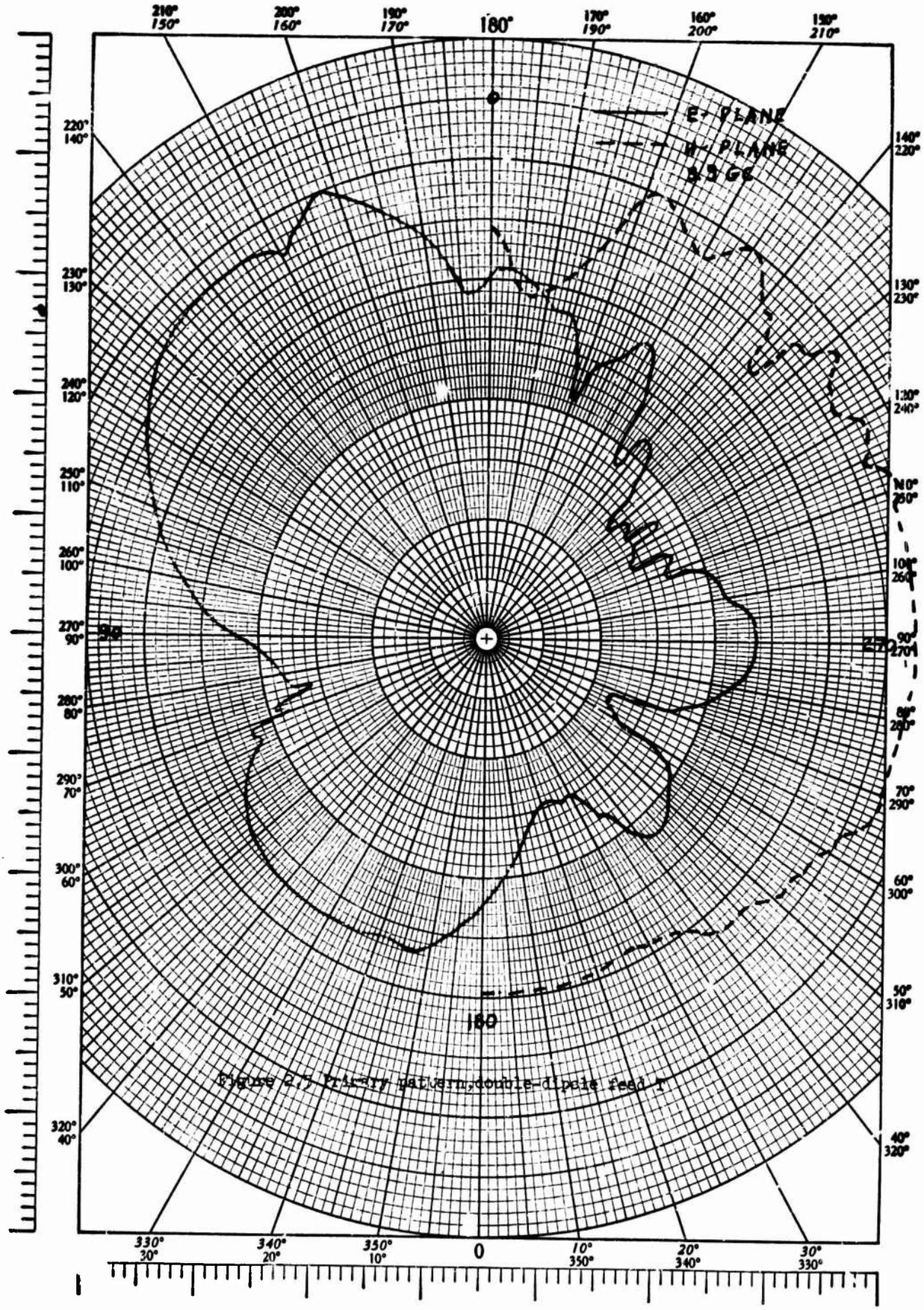

Figure 2.7 Primary pattern, double-dipole feed 1

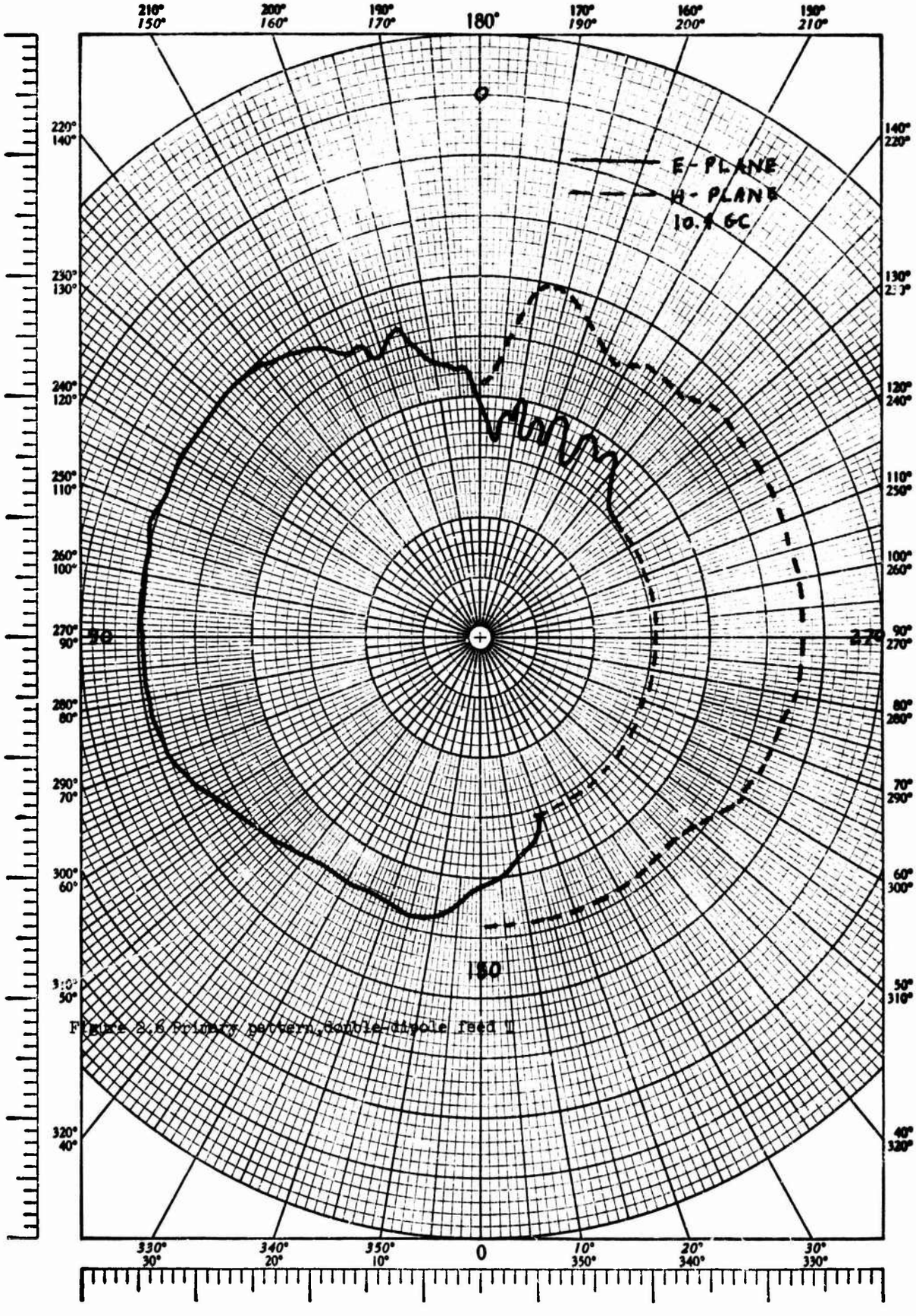

Figure 2.8 Primary pattern, double-dipole feed II

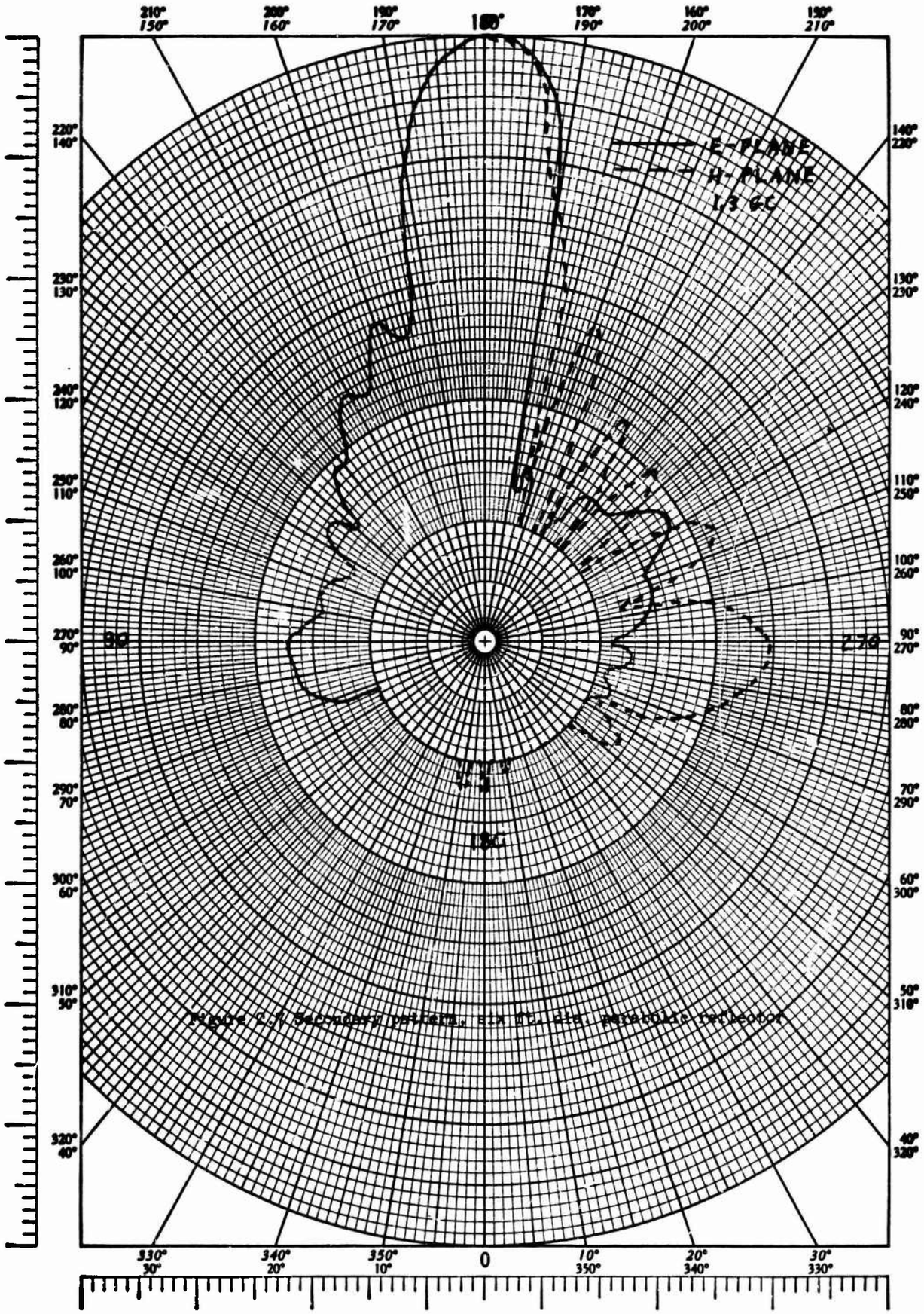

Figure 2.7 Secondary pattern, six ft. dia. paraboloid reflector

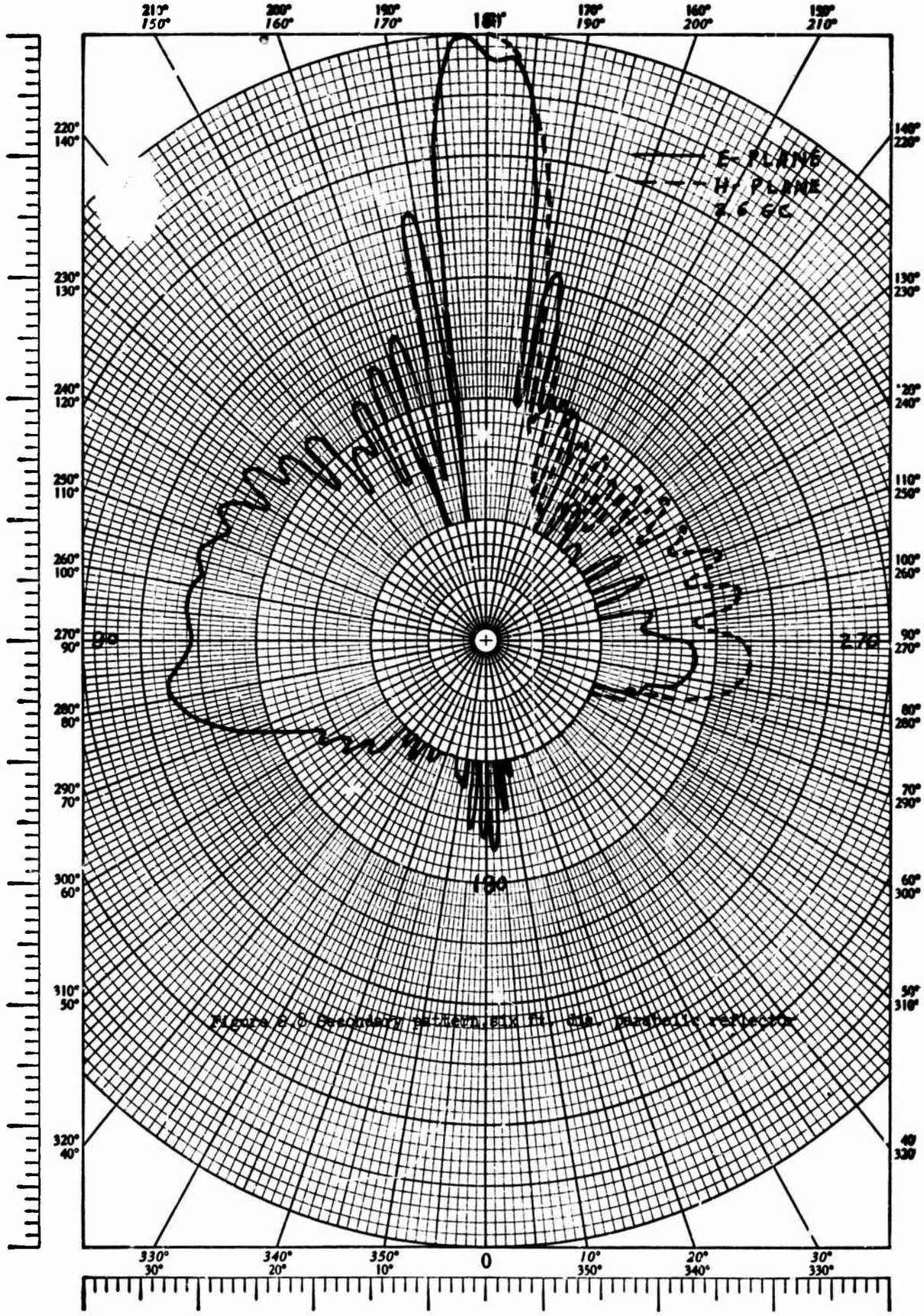

Figure 2.6 Geometry of Cassegrain Fig. dia. parabolic reflector

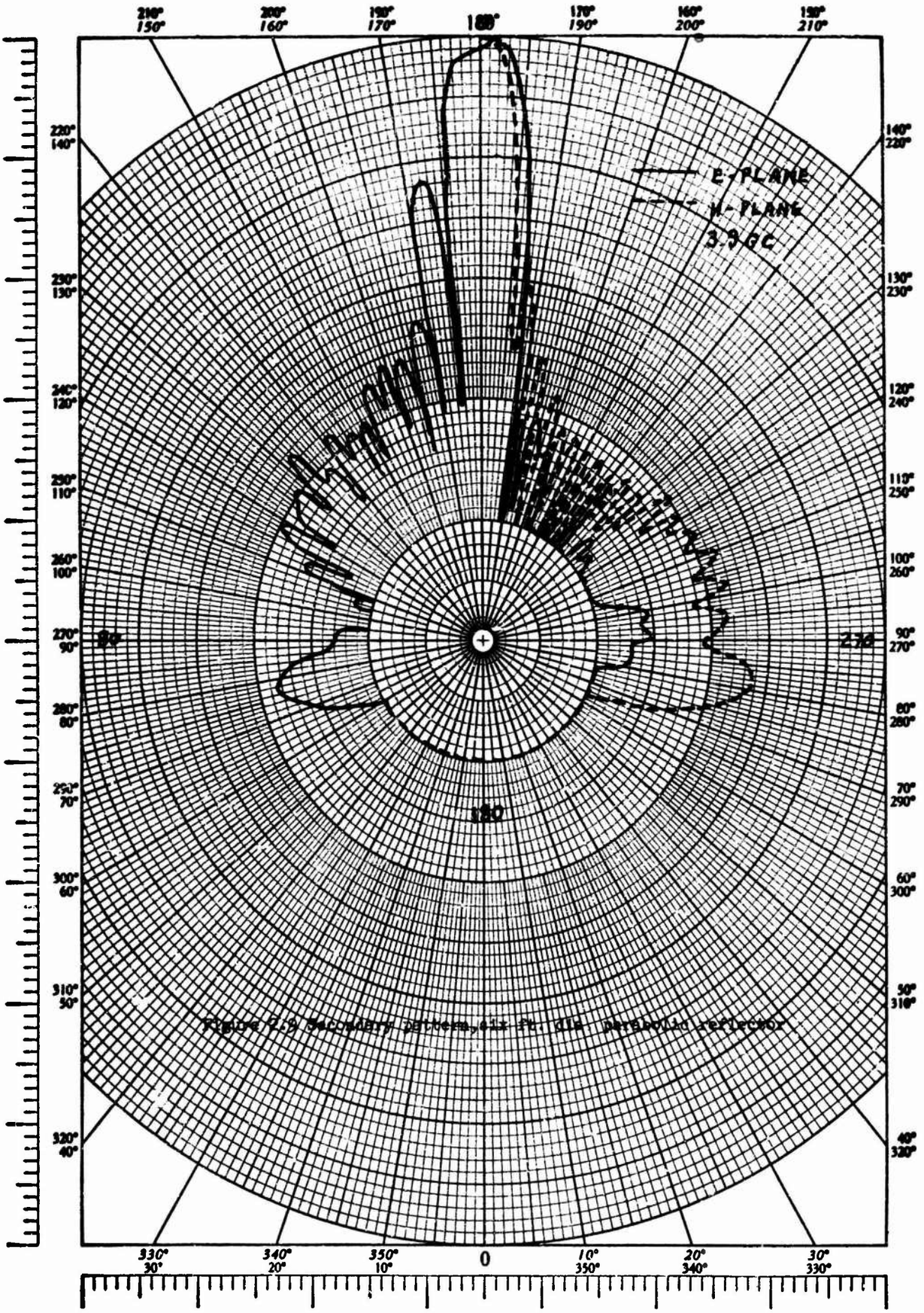

Figure 2.9 Secondary pattern, 6½ ft. dia. paraboloid reflector.

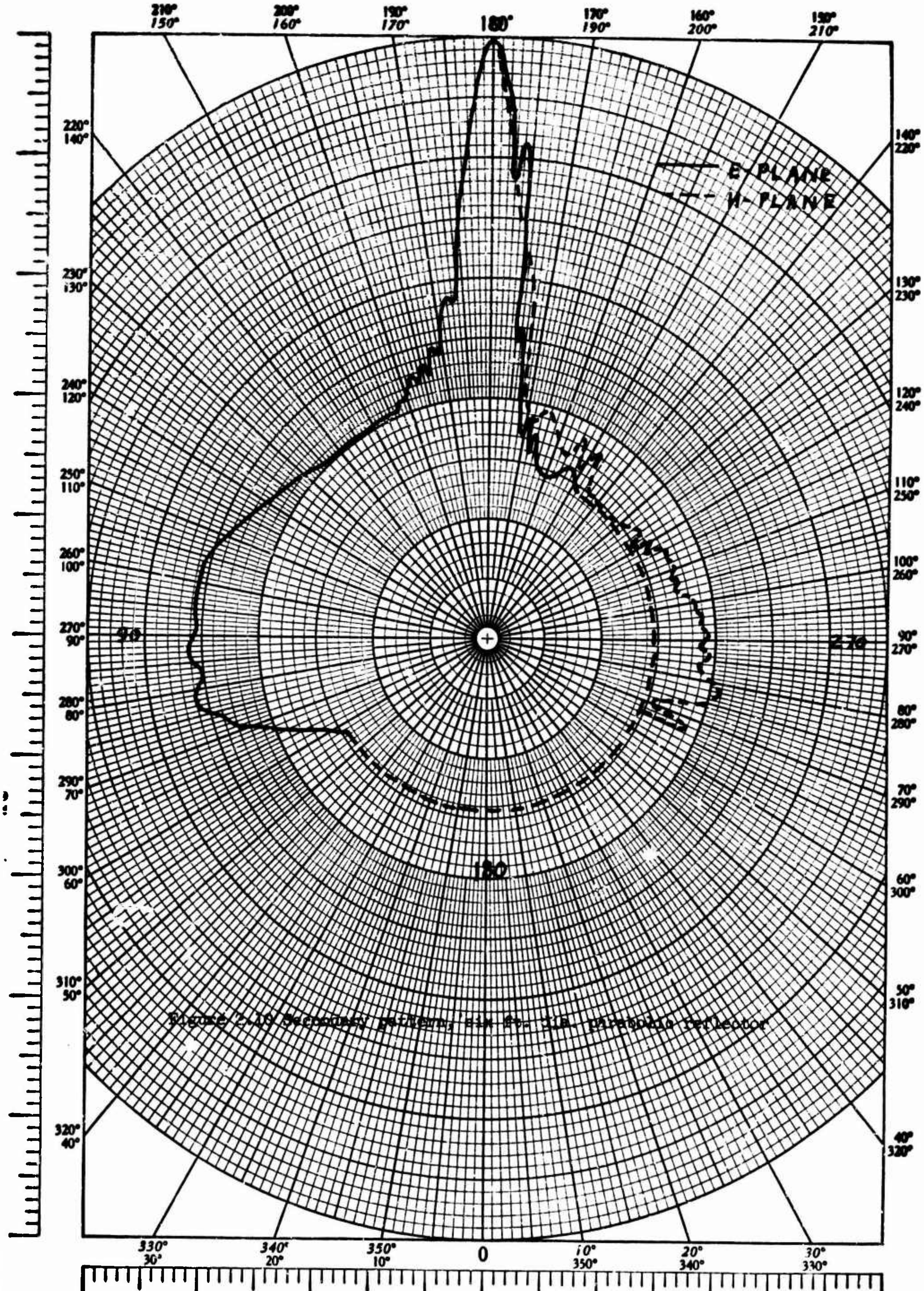

Figure 2-10 Secondary pattern, six ft. dia. parabolic reflector

Figure 2.11 Beamwidth and side lobe level, six foot diameter parabolic dish with double-dipole feed

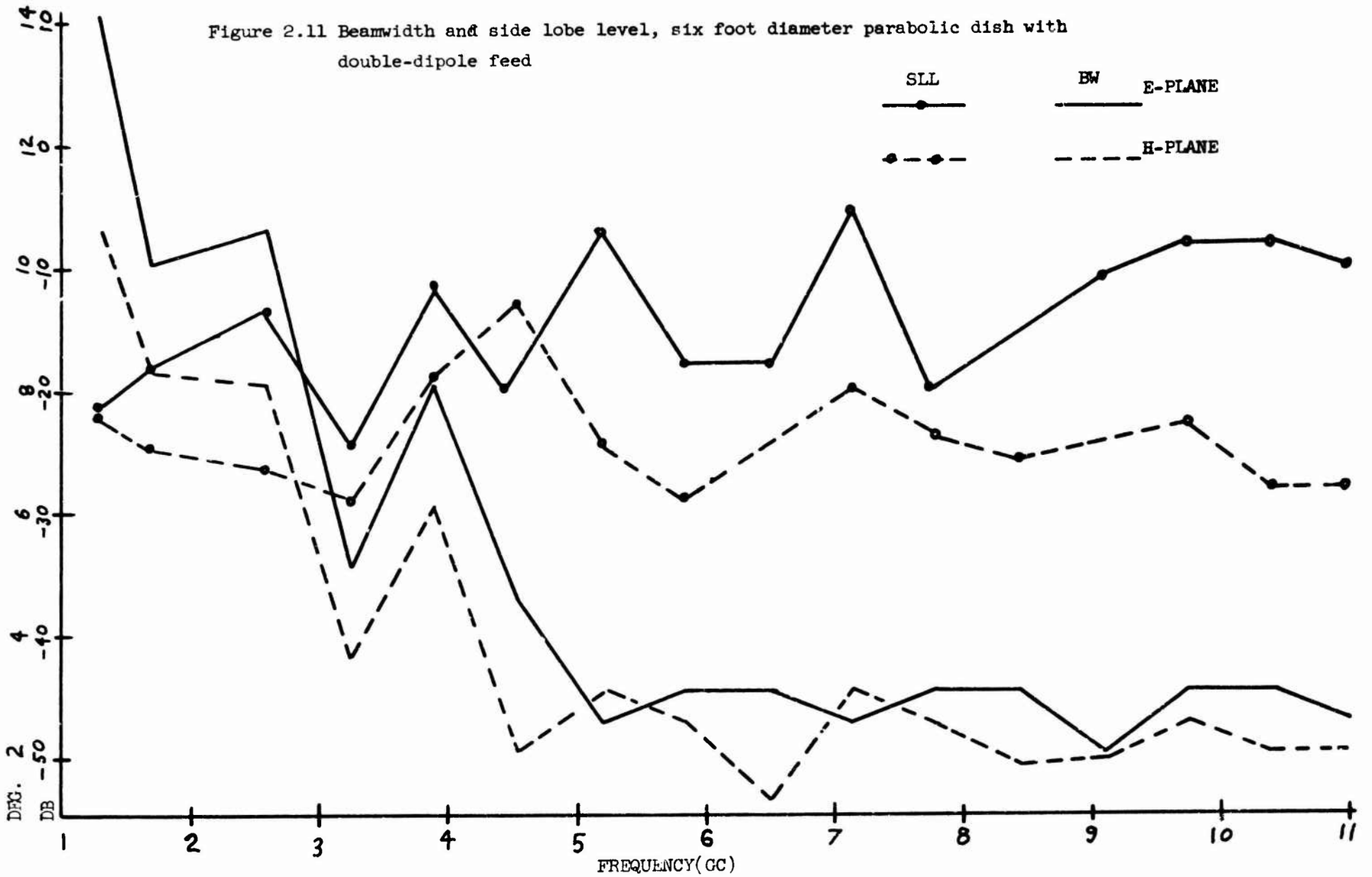

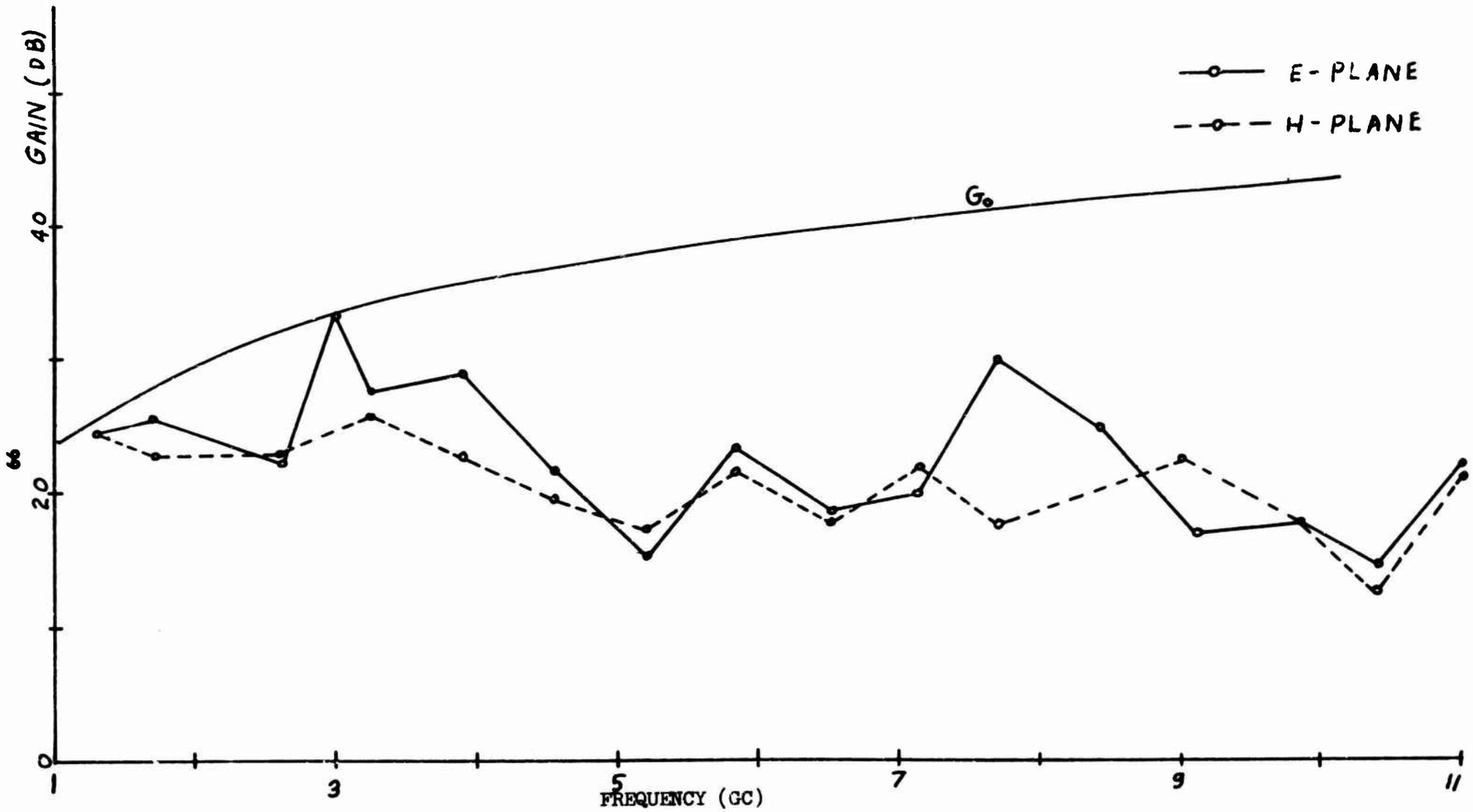

Figure 2.12 Gain in the direction of maximum radiation for 6 ft. dia. parabolic dish with a double-dipole feed

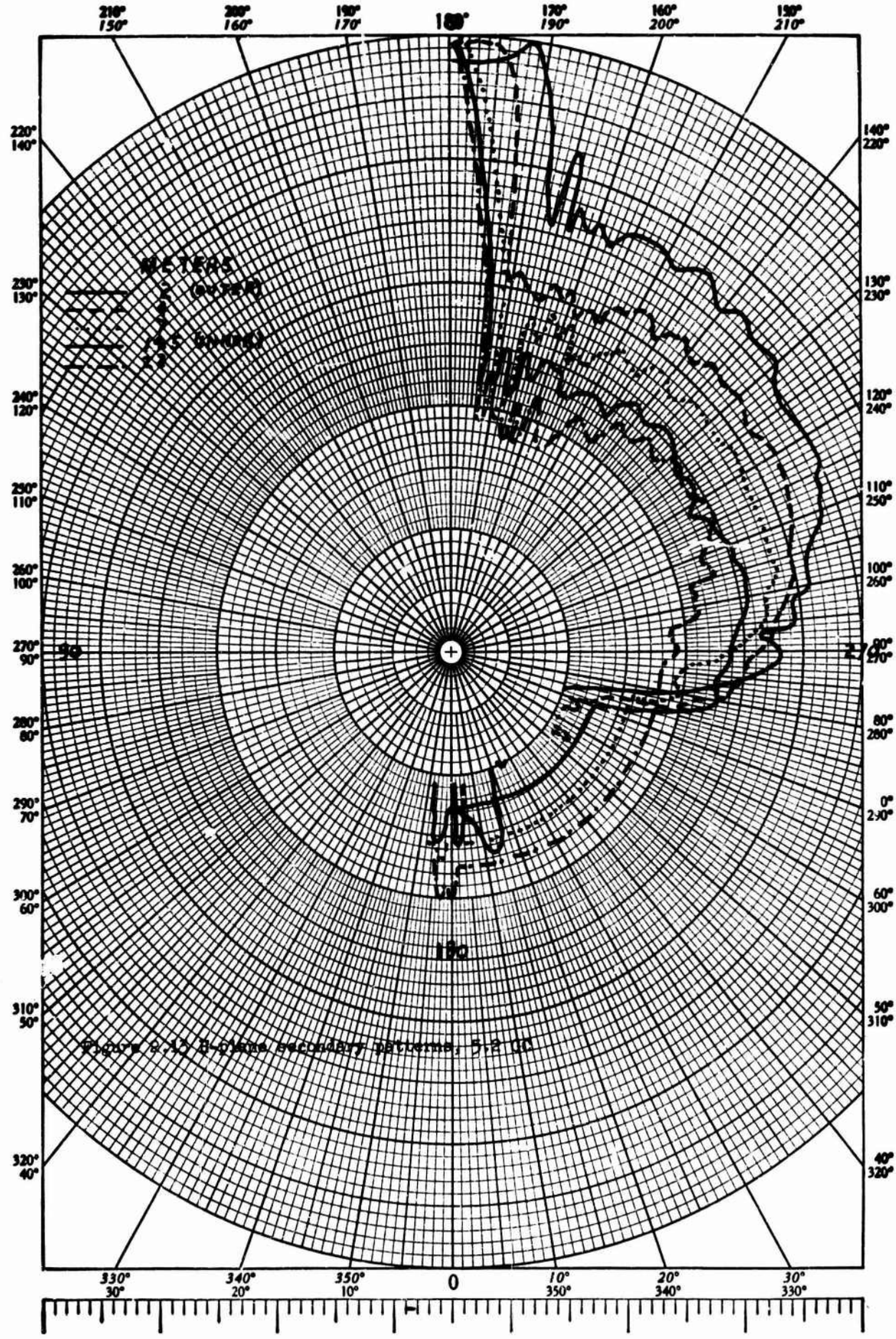

Figure 2.15 H-plane secondary patterns, 5.2 GC

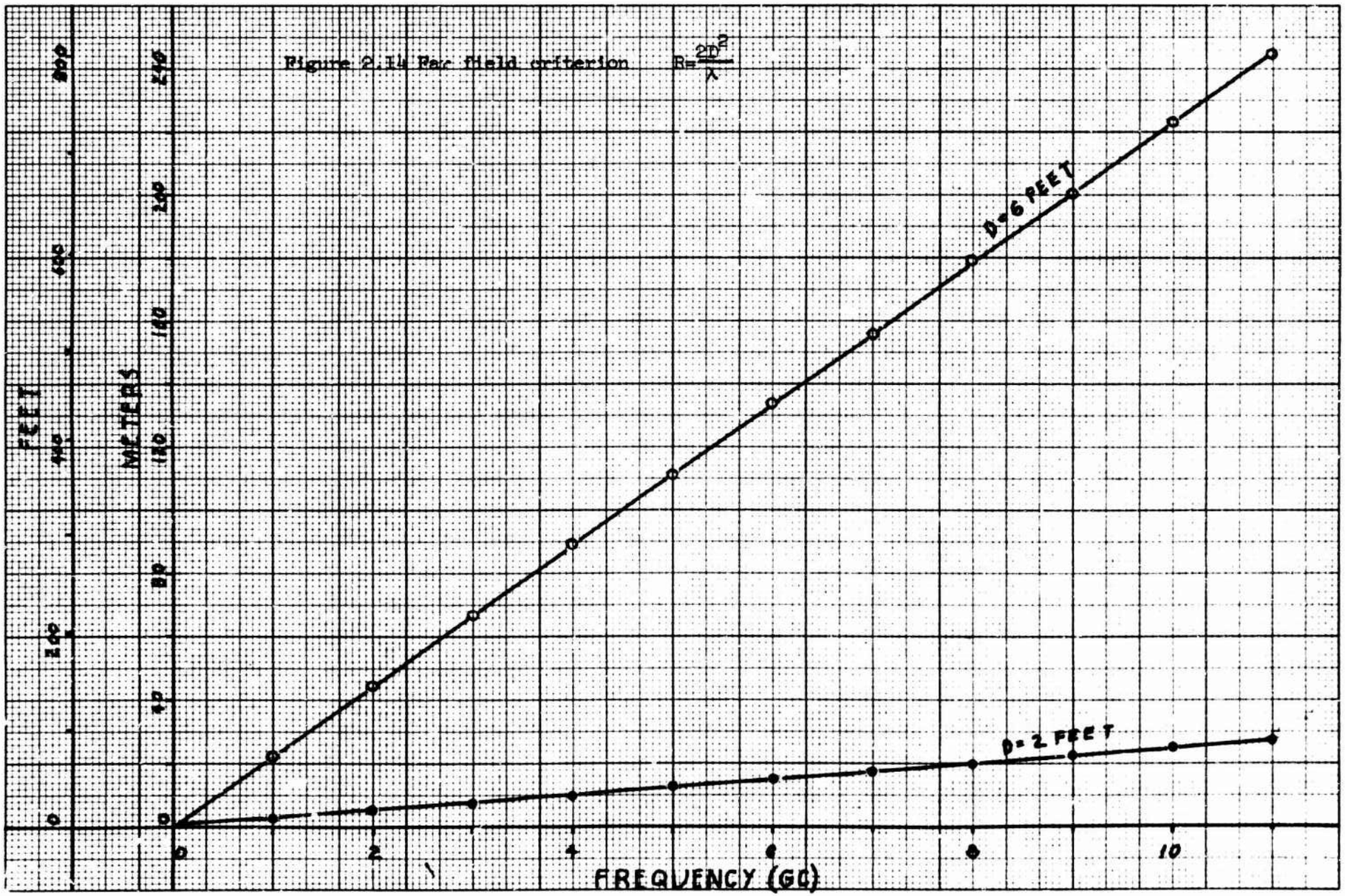

Figure 2.14 Far field criterion $R=\frac{2D^2}{\lambda}$

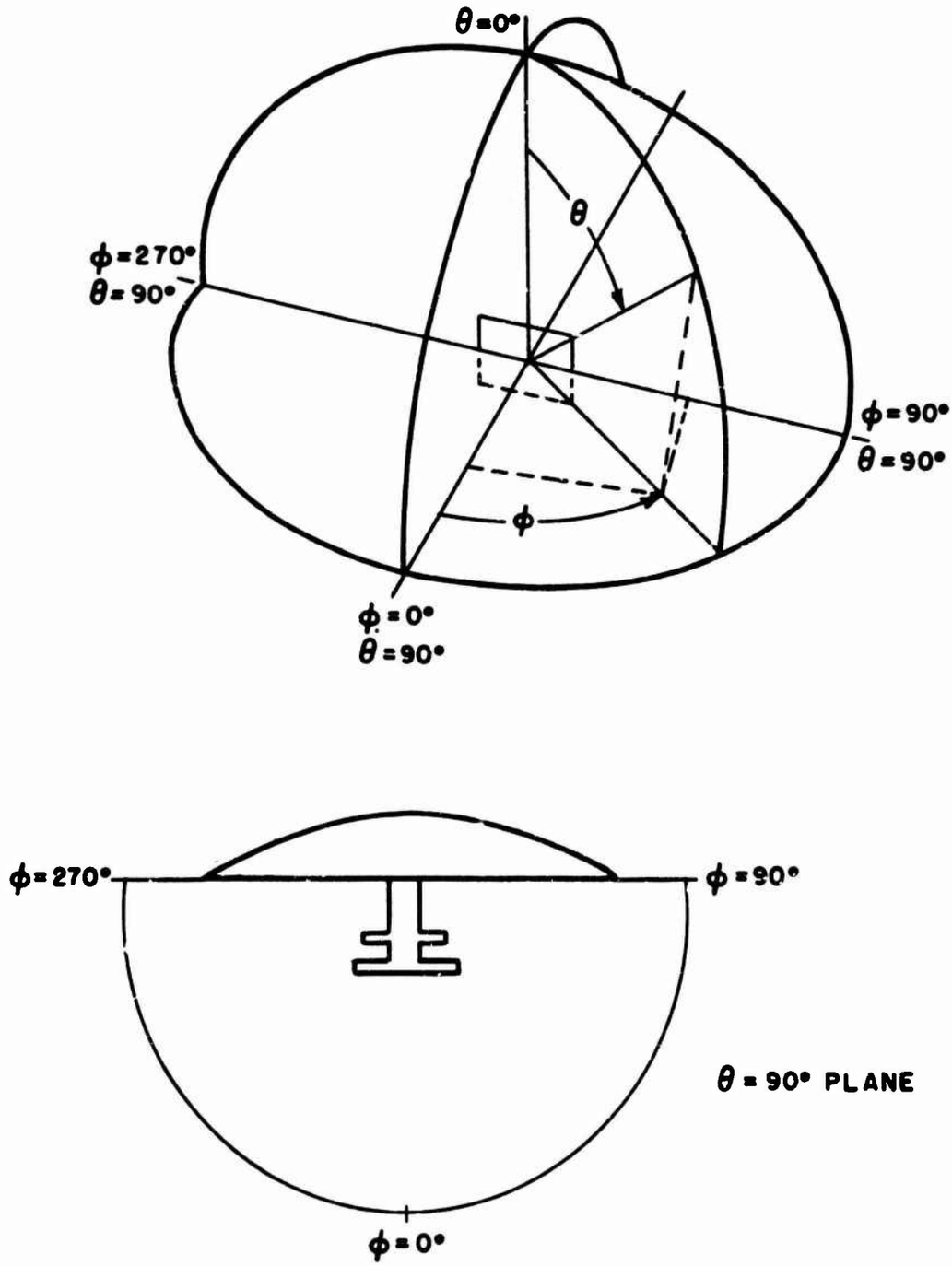

FIGURE 2.15 SPHERICAL COORDINATE SYSTEM USED IN RADIATION POWER PATTERN MEASUREMENTS

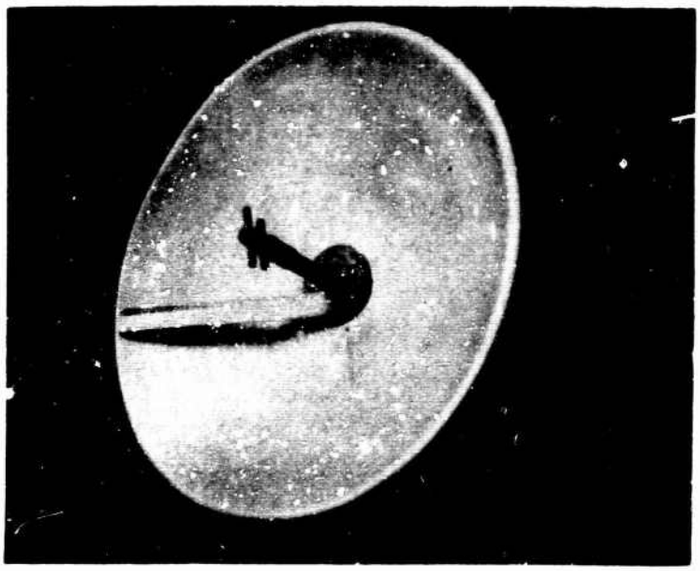

a. Small double-dipole antenna (s) in a parabolic reflector

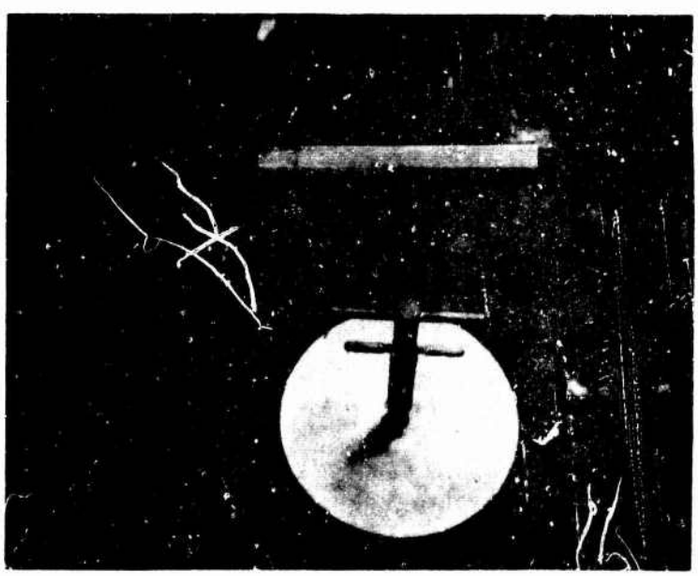

b. Large double-dipole antenna (ℓ) without reflector

Figure 2.16 Photographs, double-dipole feed antennas and parabolic reflector

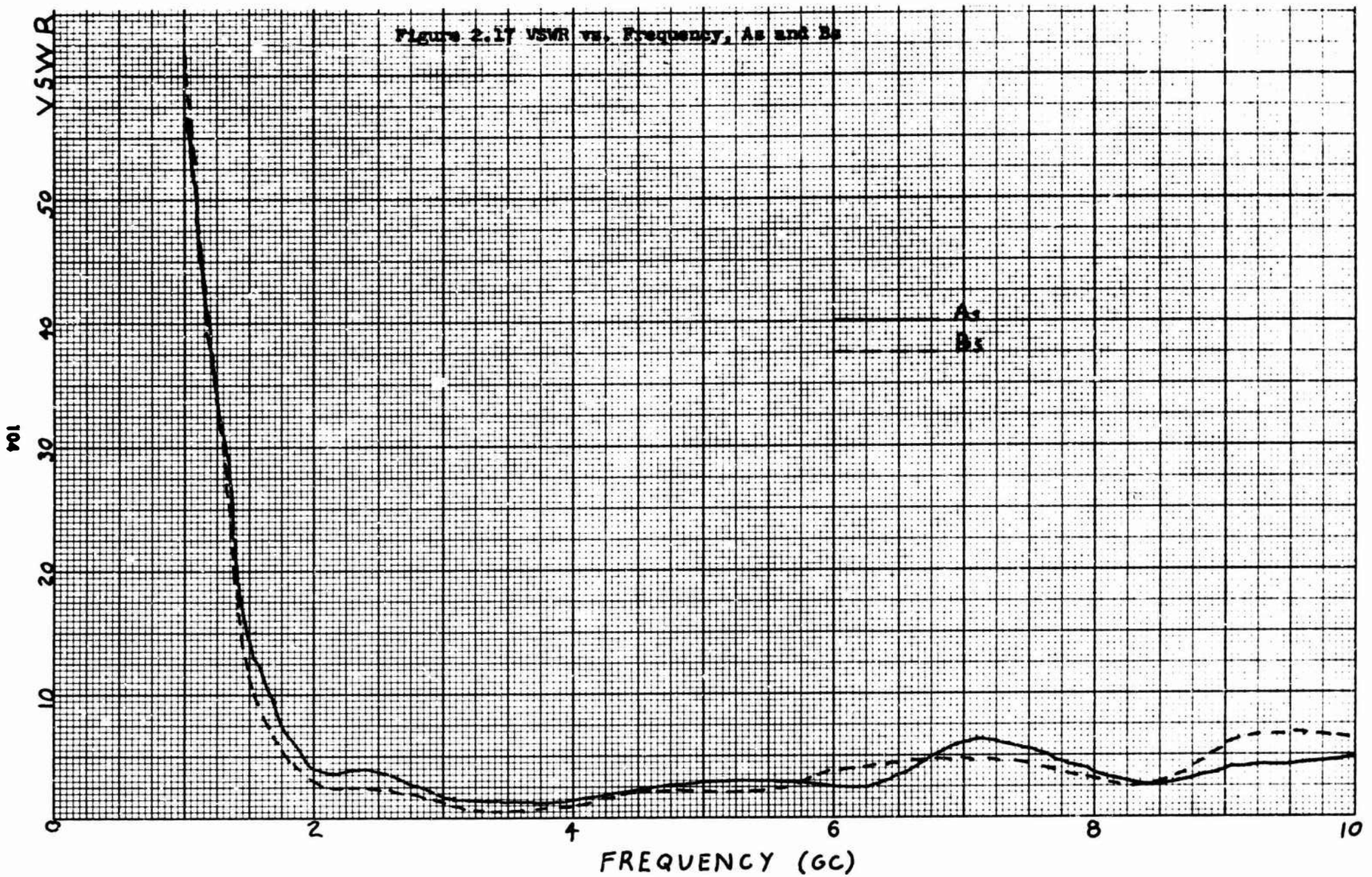

Figure 2.17 VSWR vs. Frequency, As and Bs

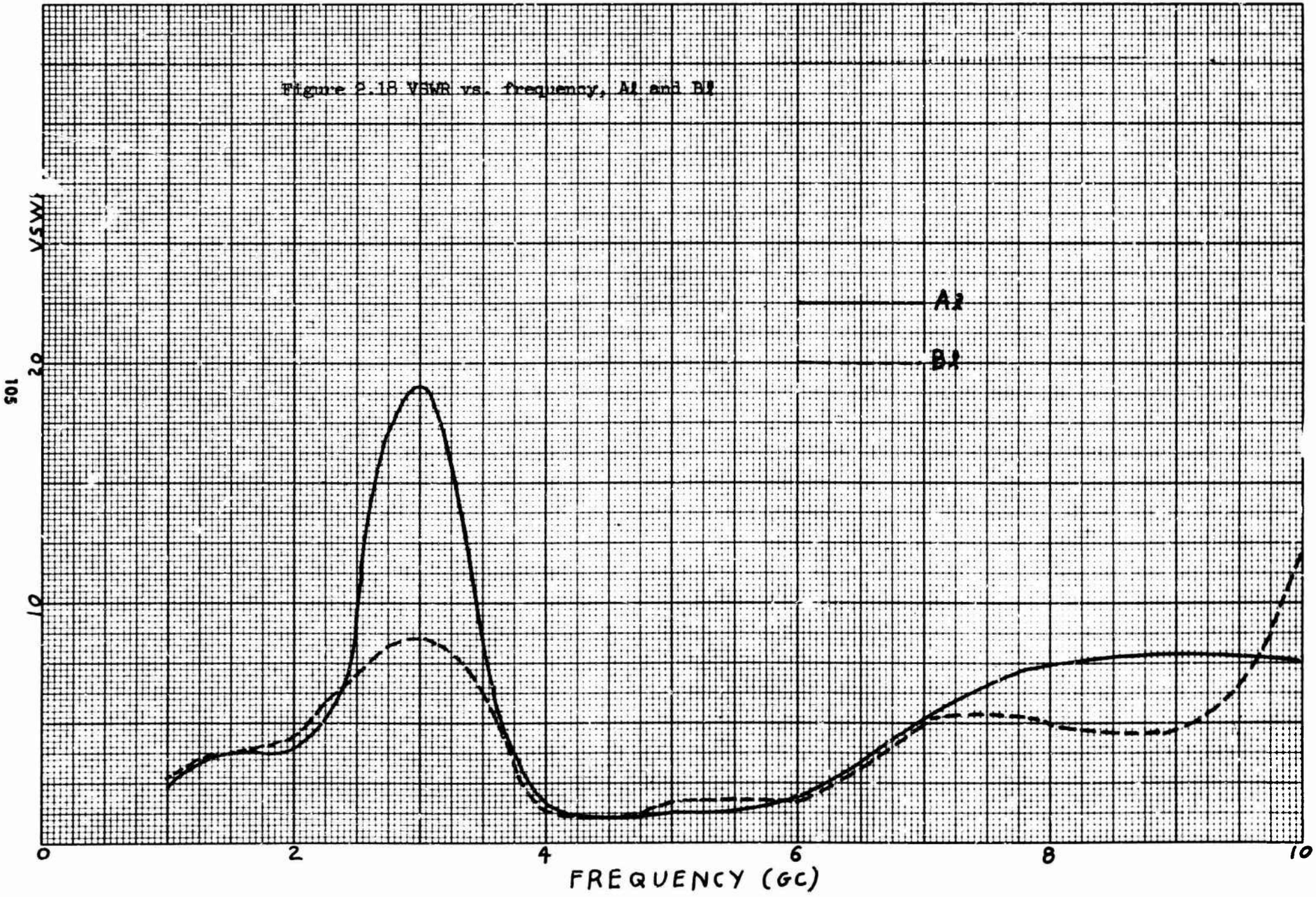
Figure 2.18 VSWR vs. frequency, A1 and B1
VSWR
10
20
A1
B1
0
2
4
6
8
10
FREQUENCY (GC)

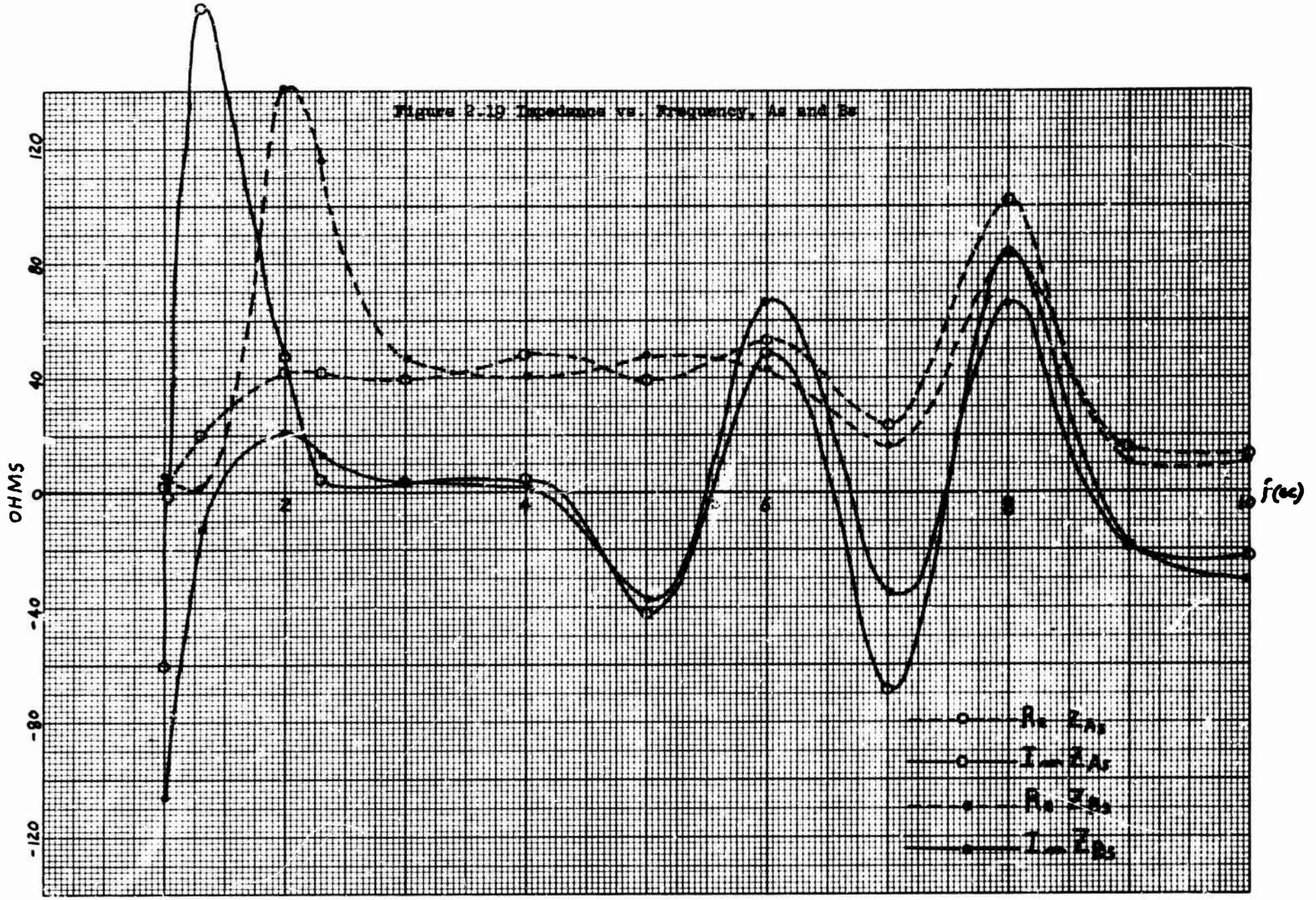

Figure 2-19 Impedance vs. Frequency, As and Bs

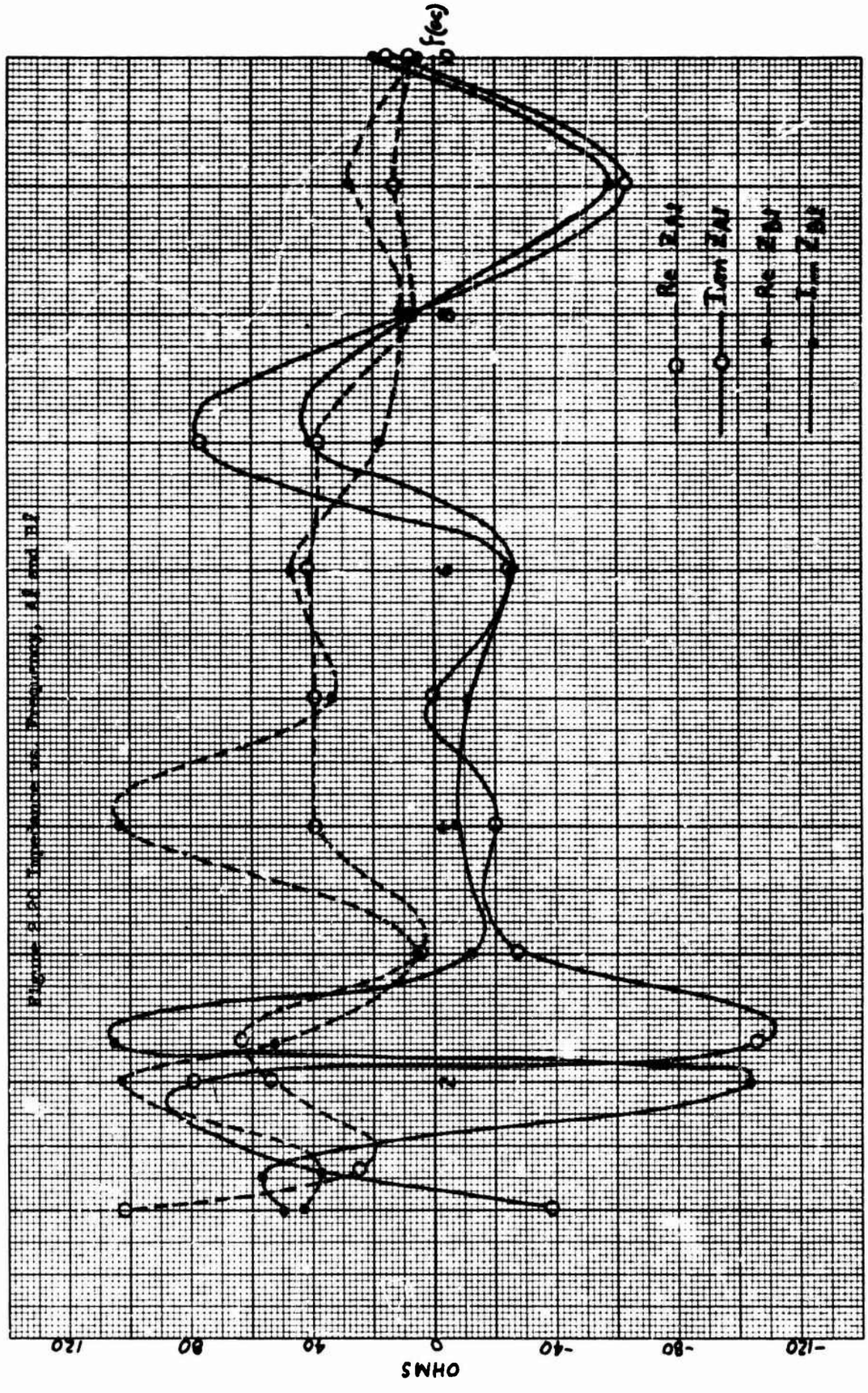

Figure 6-D Impedance vs. Frequency, AB and EF

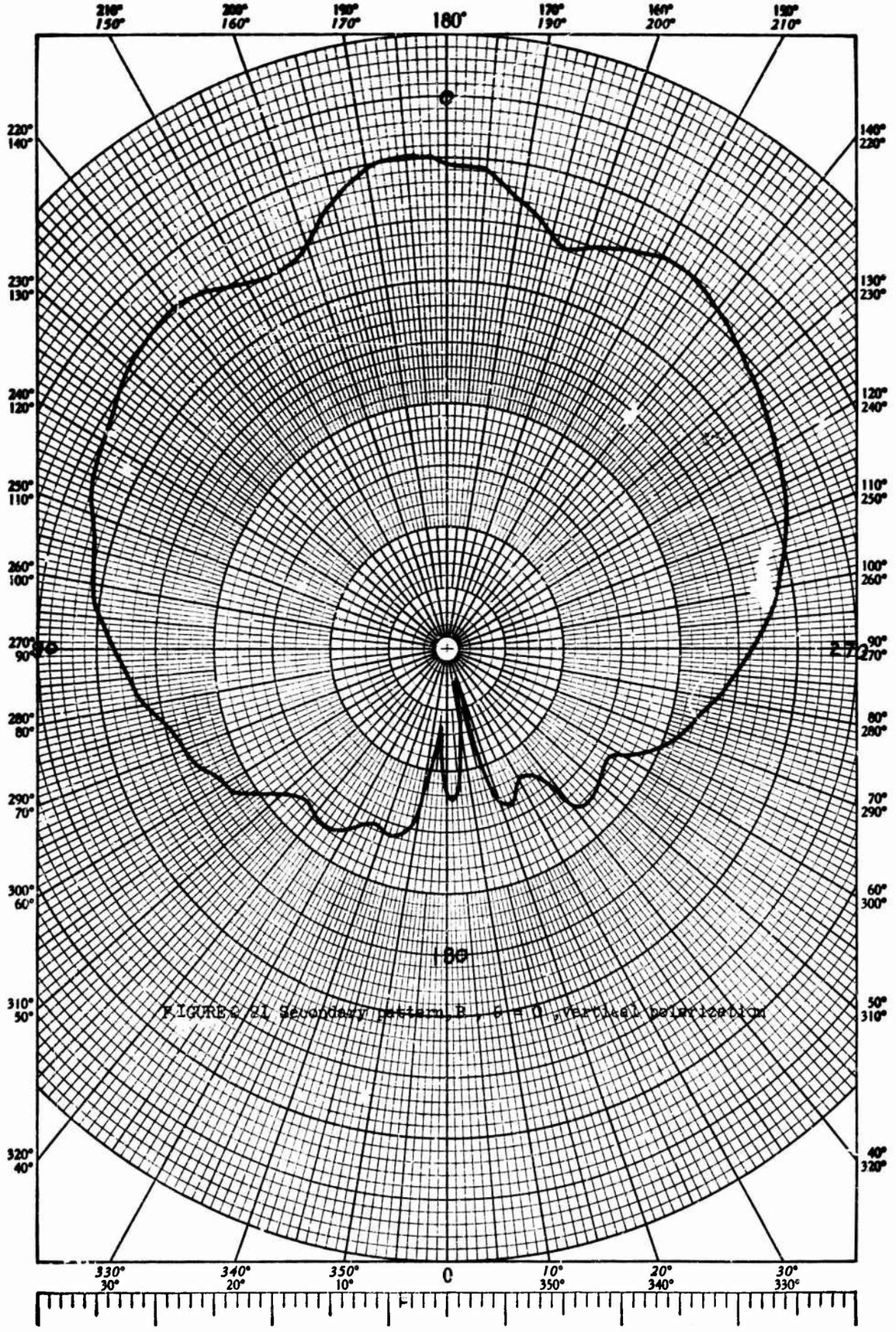

FIGURE 6.21 Secondary pattern, B_{θ}, $\phi = 0$, vertical polarization

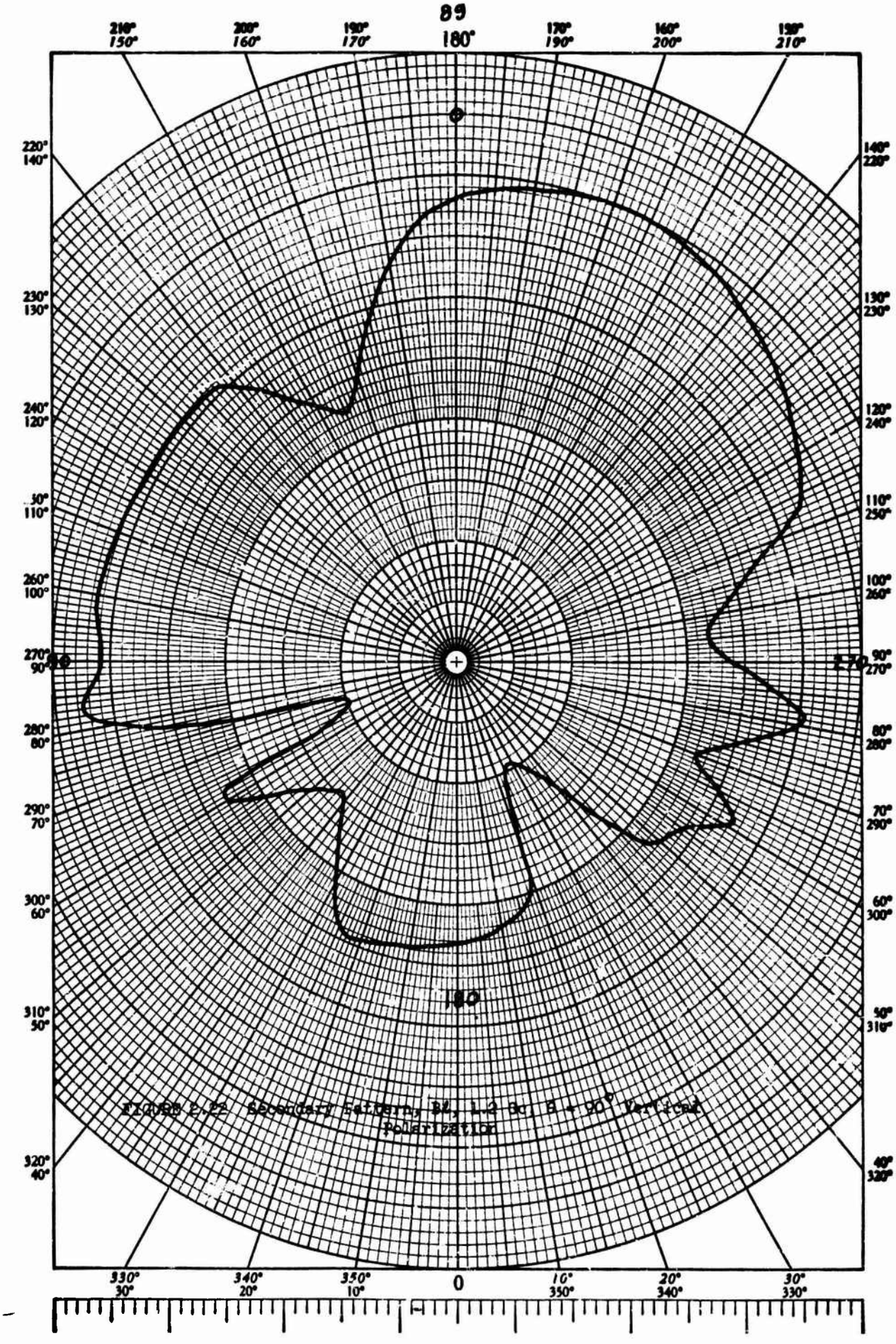

FIGURE 2.22 Secondary Pattern, B_1, L-2 Sc, $\theta = 90°$ Vertical Polarization

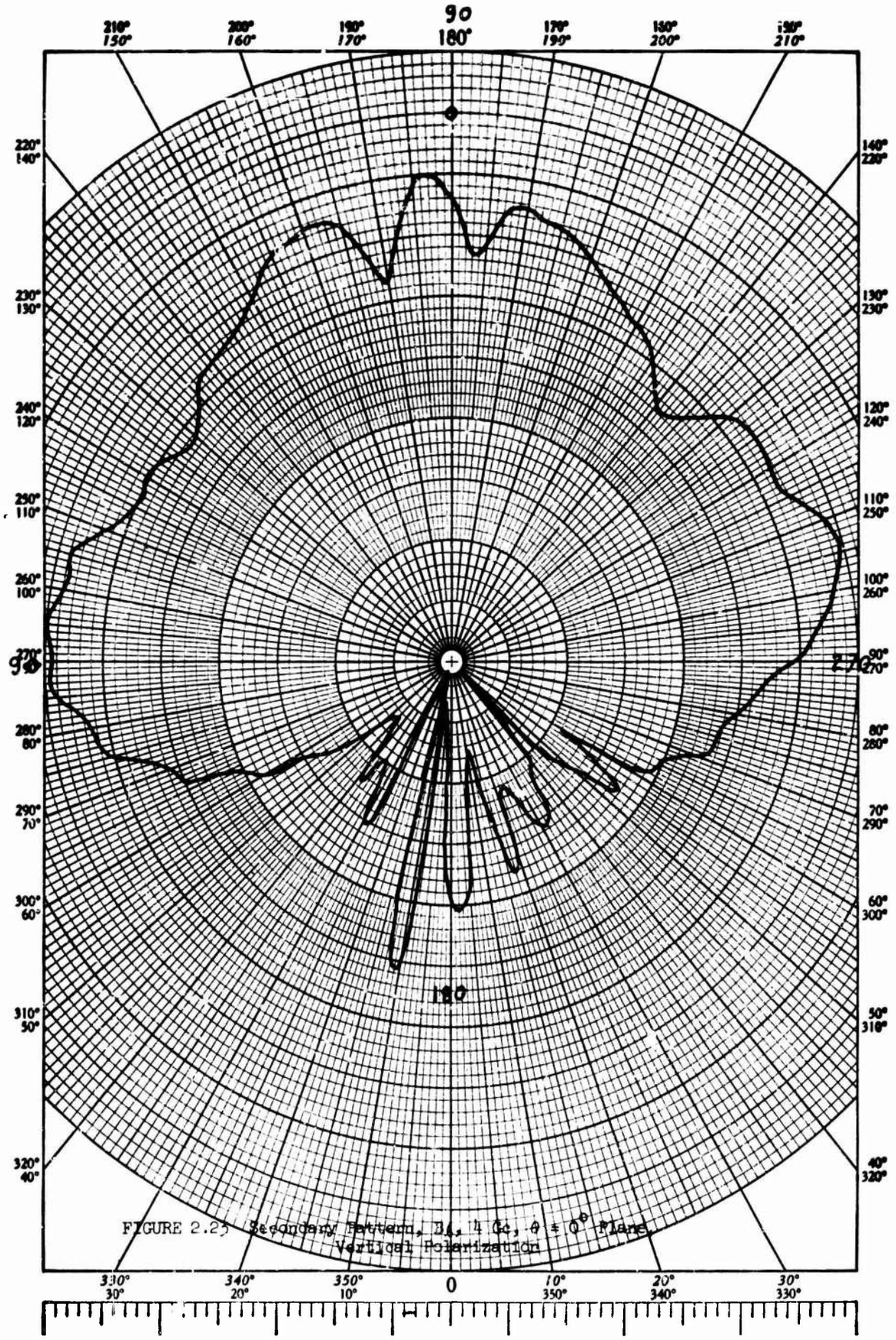

FIGURE 2.23 Secondary Pattern, D4, 4 Ge, $\theta = 0^{\circ}$ Plane, Vertical Polarization

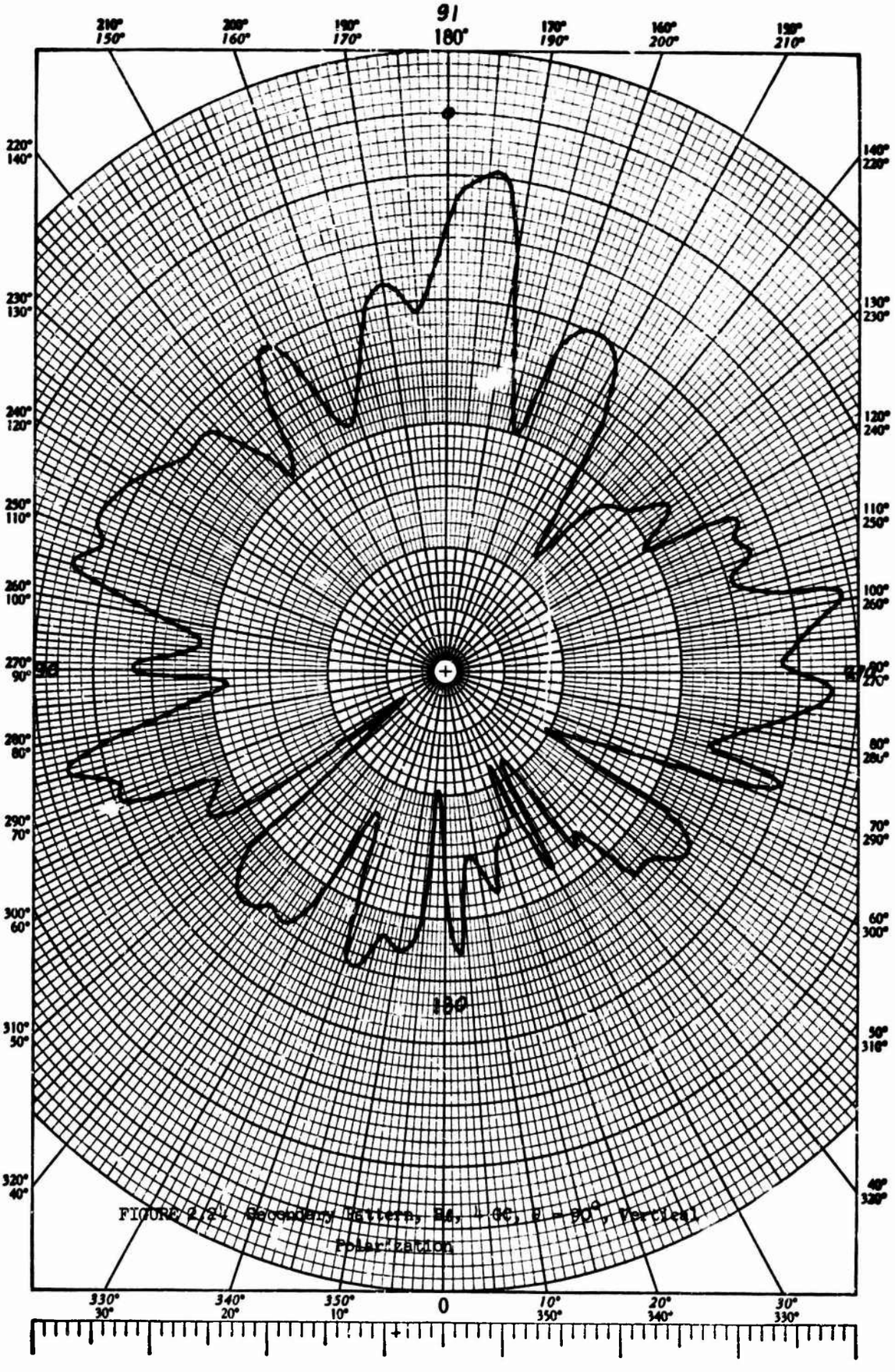

FIGURE 2(2). Secondary Pattern, E_{θ}, $\phi = 0°$, $\theta = 90°$, Vertical Polarization

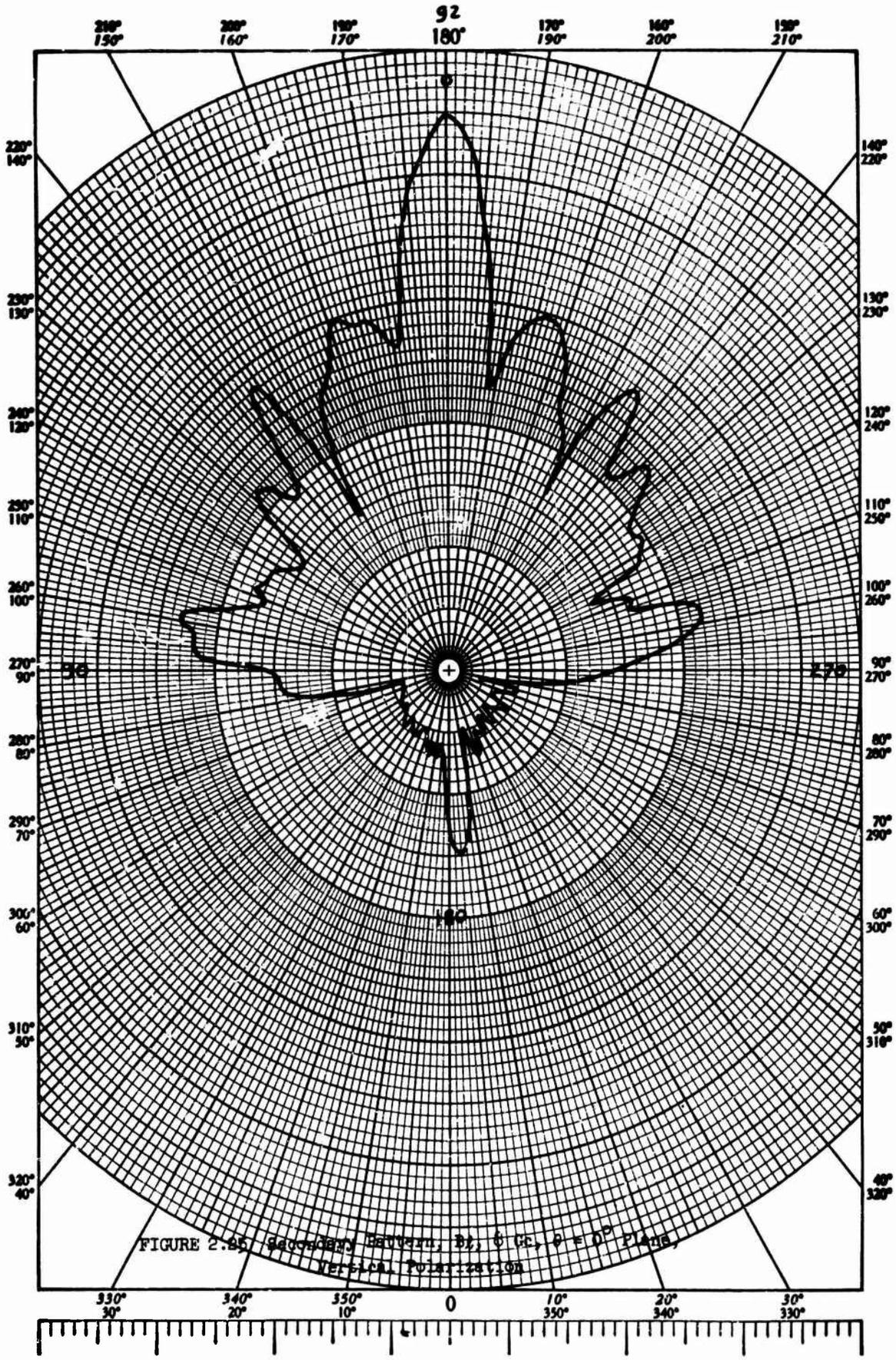

FIGURE 2.85 Secondary Pattern, E_{θ} @ Gc, $\phi = 0^{\circ}$ Plane, Vertical Polarization

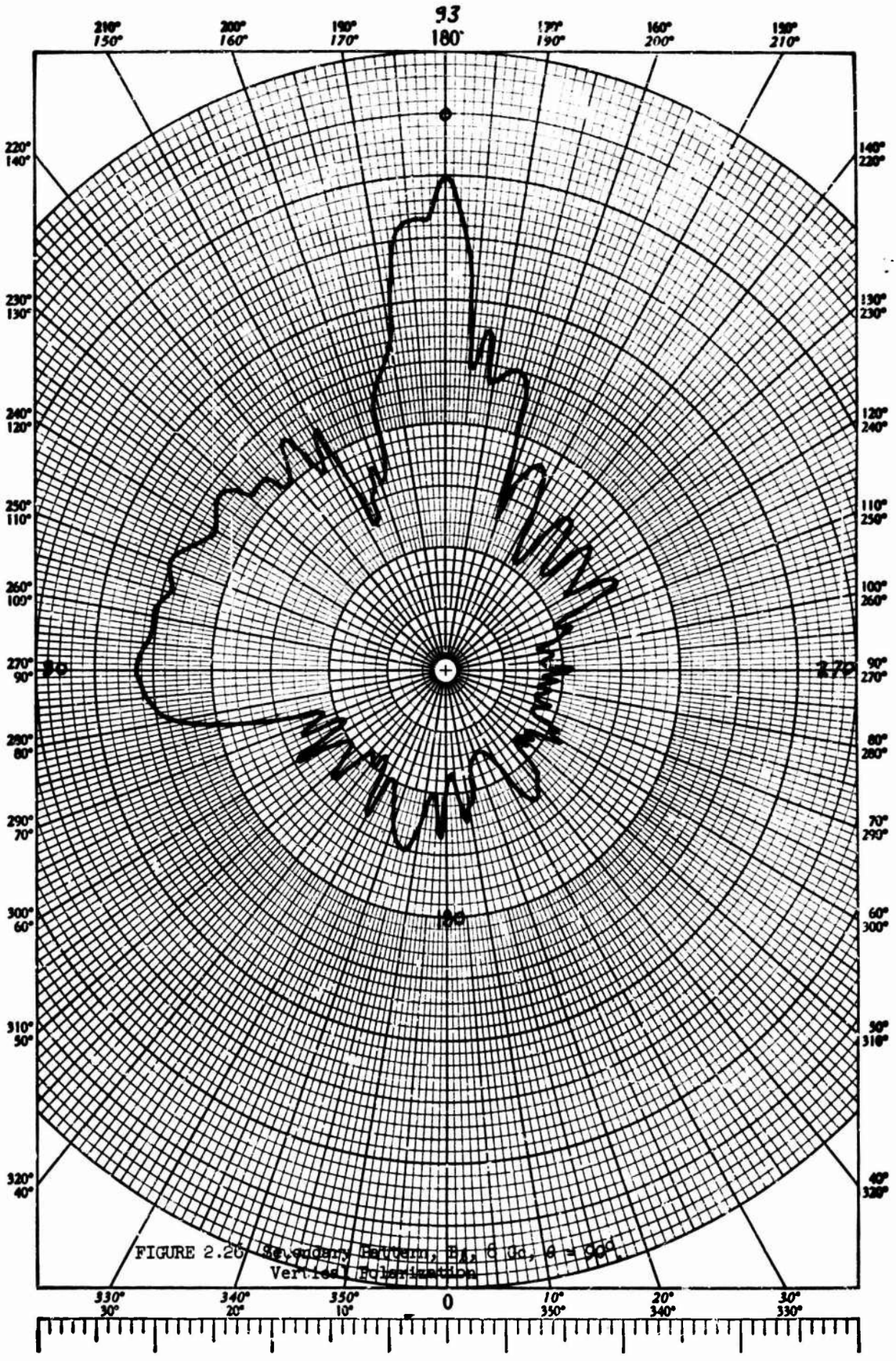

FIGURE 2.20 Secondary Pattern, E_{ϕ}, θ Cut, $\theta = 90°$, Vertical Polarization

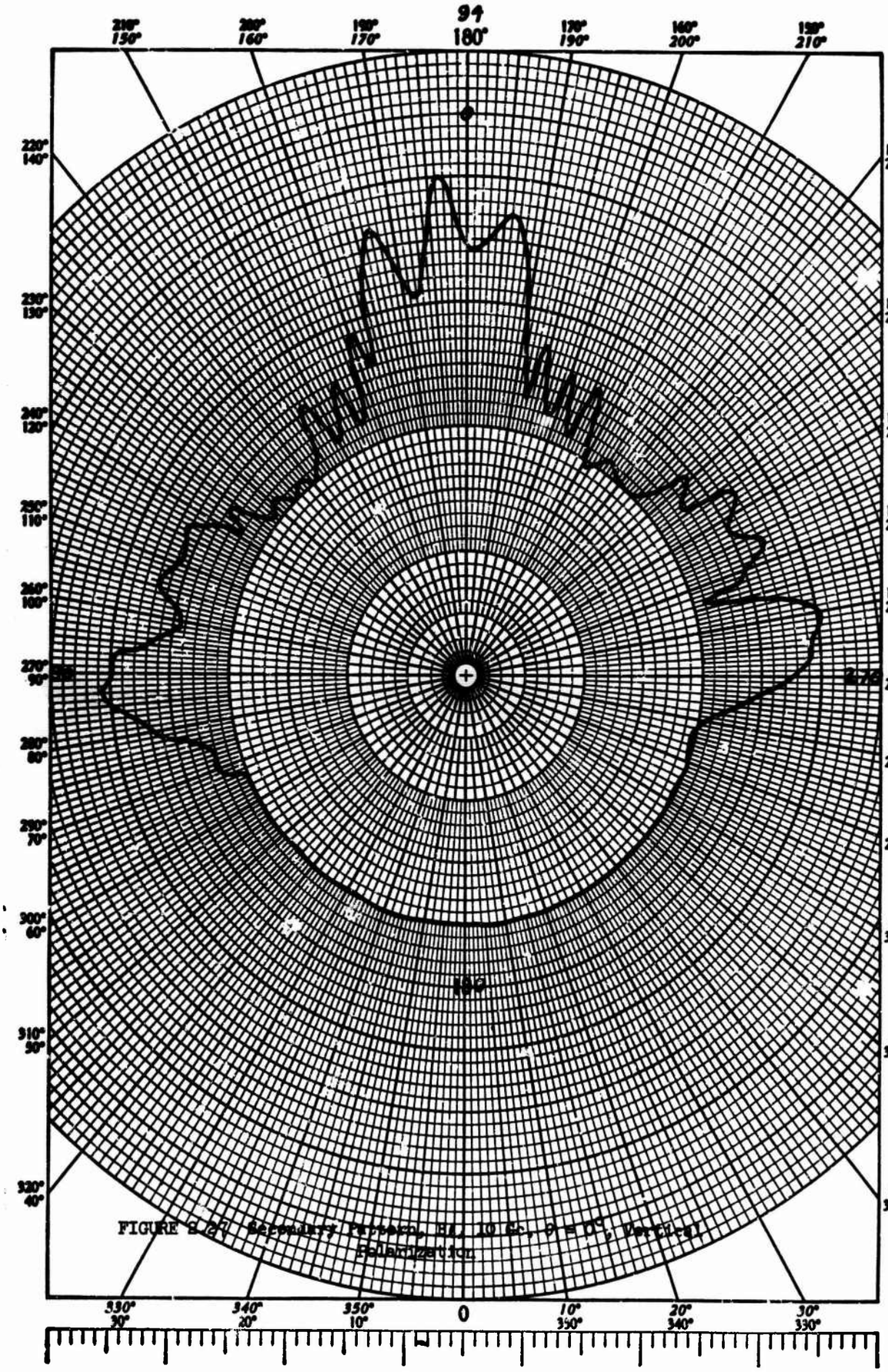

FIGURE 5.27 Secondary Pattern, E4, 10 GHz, $\theta = 0°$, Vertical Polarization

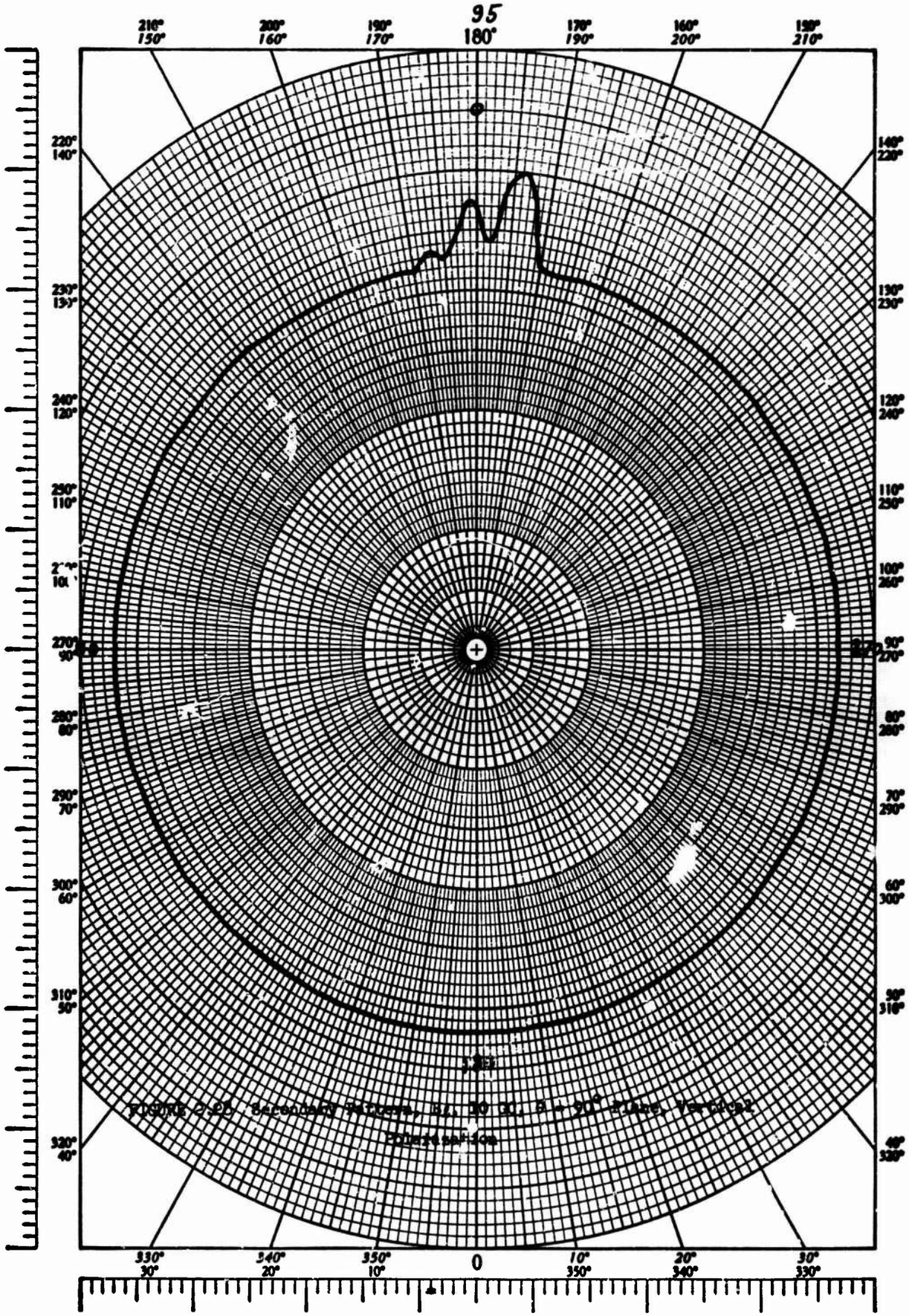

FIGURE 2-22 Secondary Pattern, θ_1 = 30, θ_2 = 90° (Plane, Vertical Polarization)

BEAM TILT (DEG)
FREQUENCY (GC)
BEAM WIDTH (DEG)

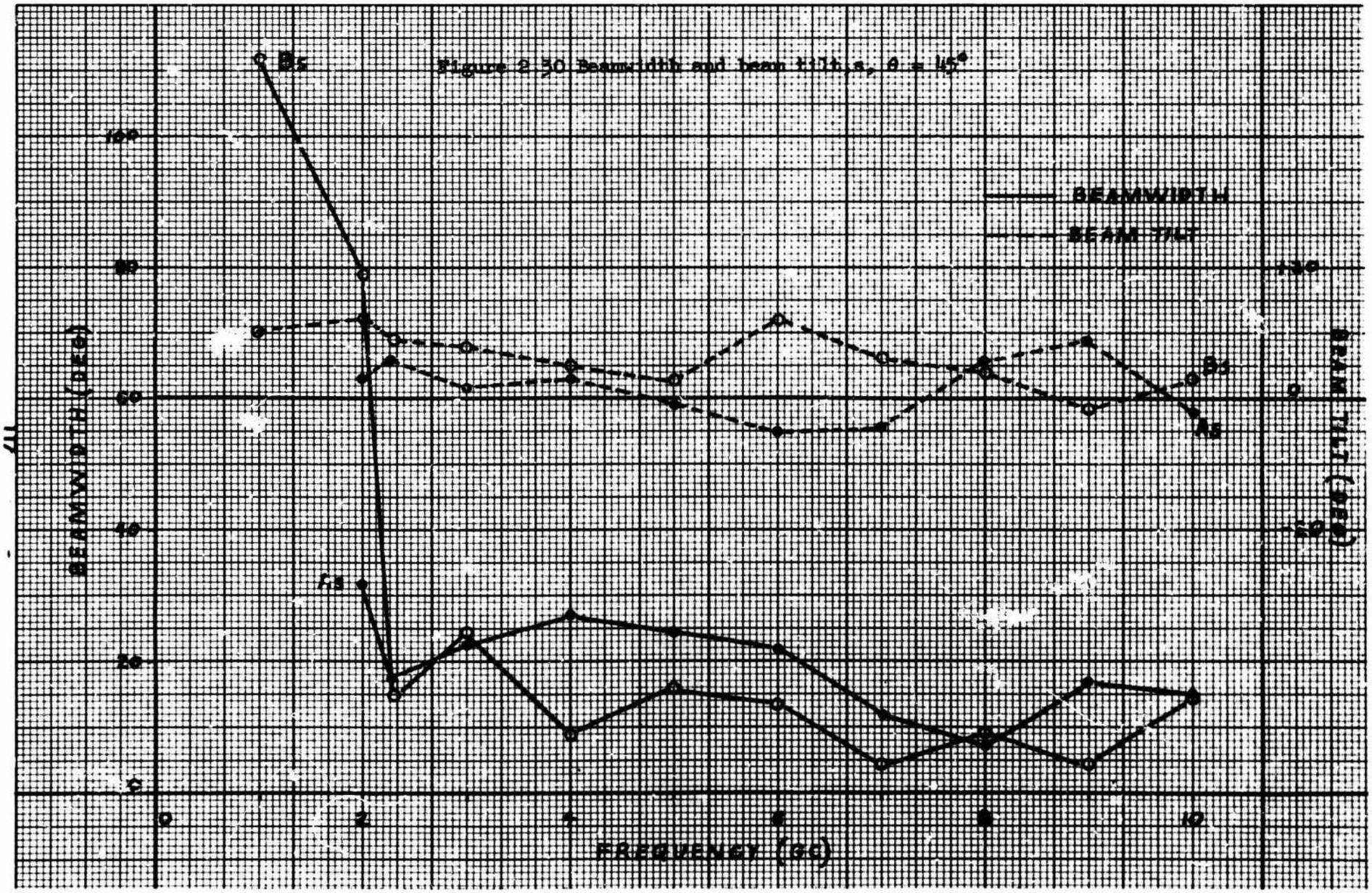
Figure 2.30 Beamwidth and beam tilt, s, θ = 45°
BEAMWIDTH
BEAM TILT
BEAMWIDTH (DEG)
BEAM TILT (DEG)
FREQUENCY (GC)
100
80
60
40
20
0
+30
0
-30
0
2
4
6
8
10
Bs
As
fs

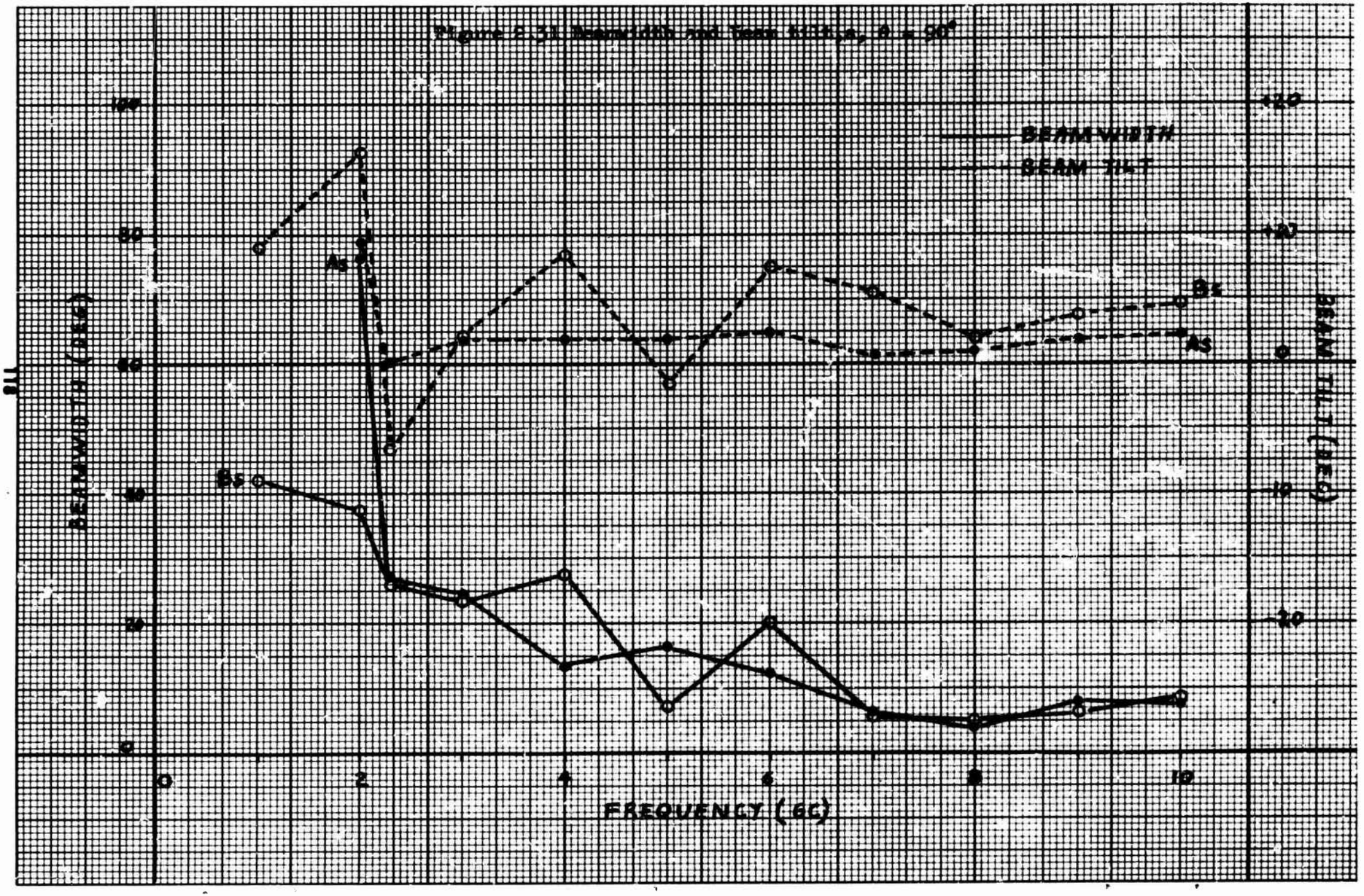
Figure 2.31 Beamwidth and Beam tilt vs f, θ = 90°
BEAMWIDTH
BEAM TILT
BEAMWIDTH (DEG)
BEAM TILT (DEG)
FREQUENCY (GC)
100
80
60
40
20
0
+20
+10
0
-10
-20
0
2
4
6
8
10
A5
B5
A5
B5

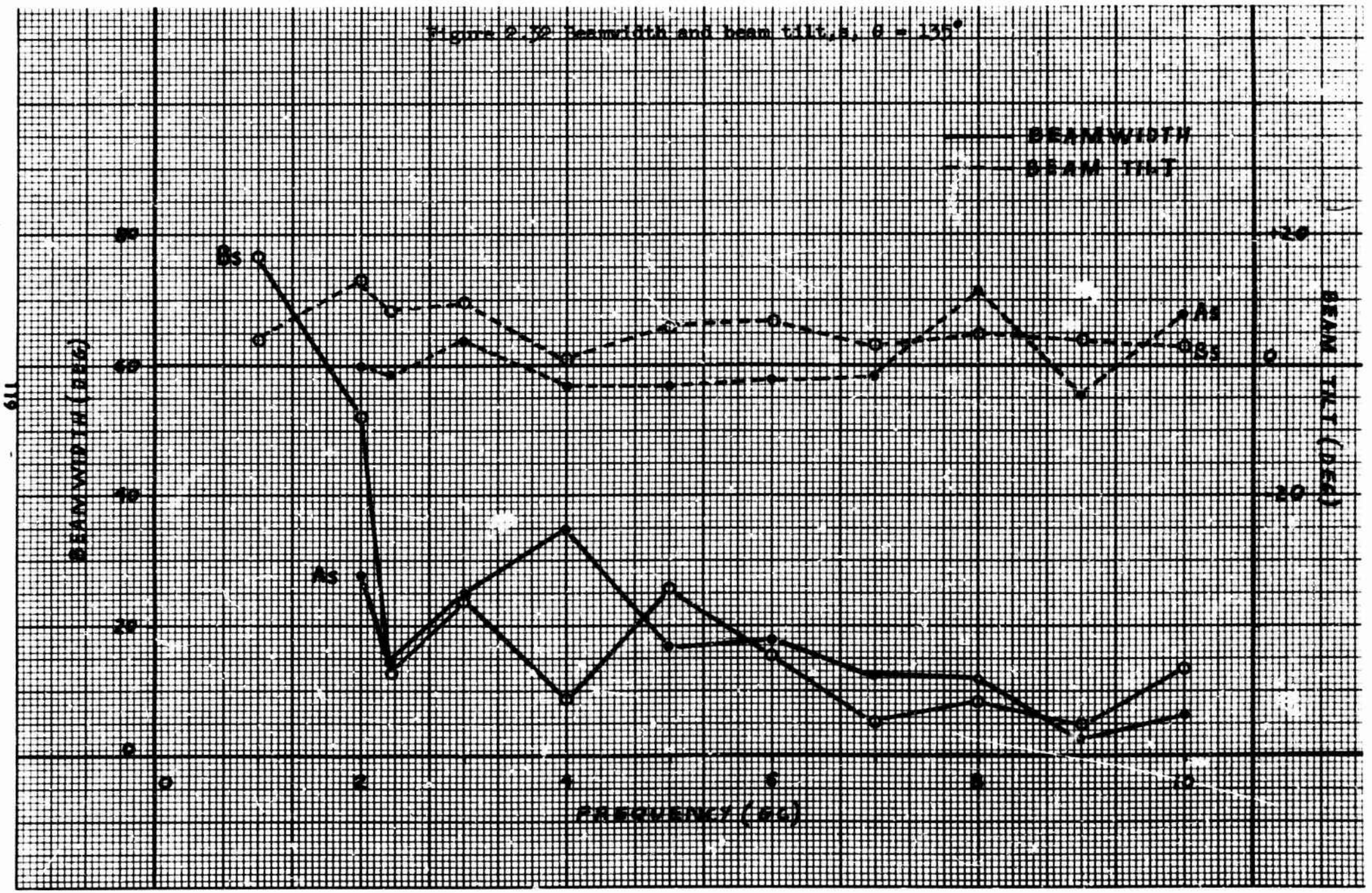

Figure 2.32 Beamwidth and beam tilt, s, $\theta = 135^\circ$

BEAM TILT (RAD)
FREQUENCY (GHz)
BEAMWIDTH (DEG)

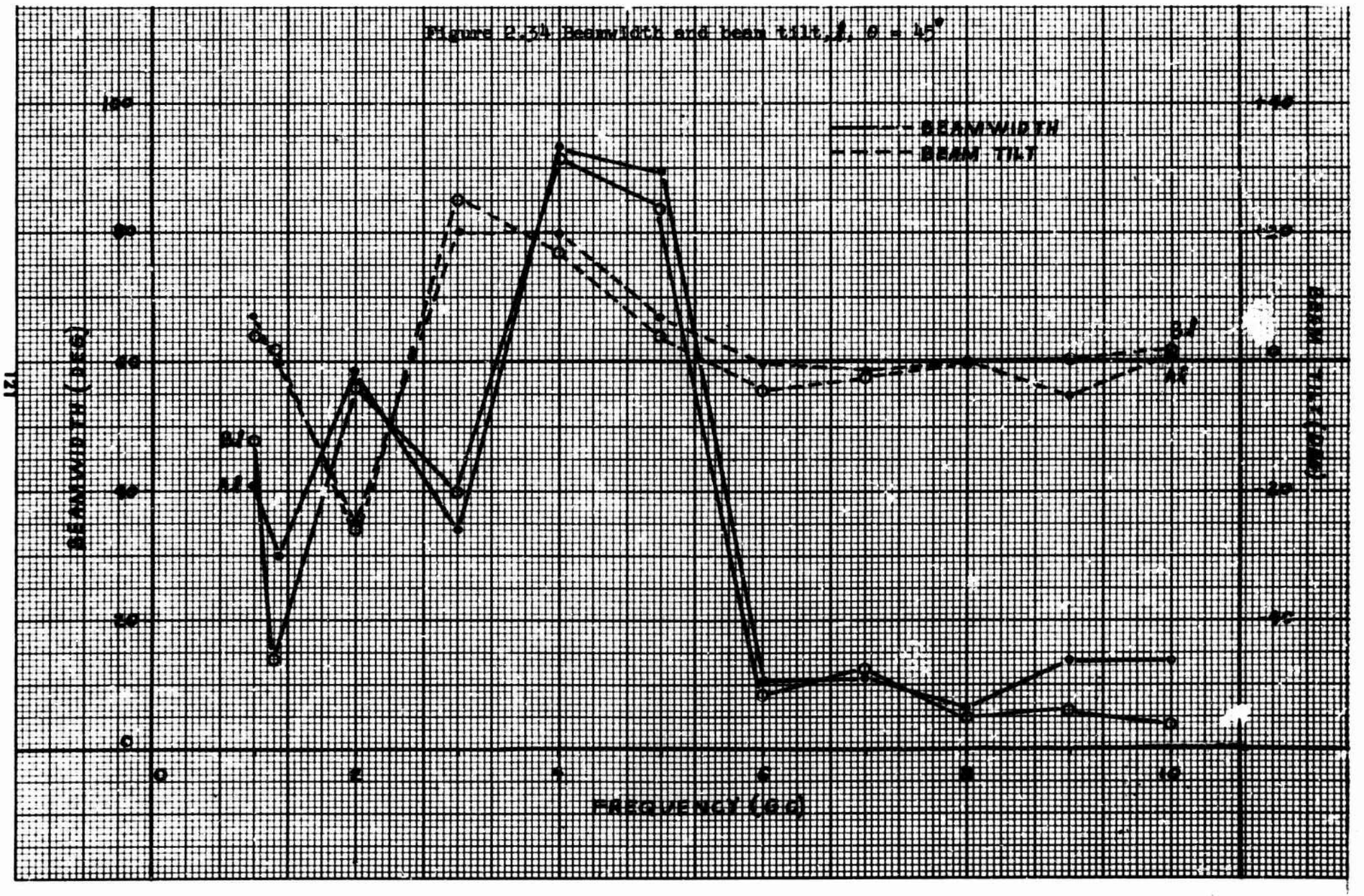
Figure 2.34 Beamwidth and beam tilt, β, θ = 45°
BEAMWIDTH
BEAM TILT
BEAMWIDTH (DEG)
BEAM TILT (DEG)
FREQUENCY (GHz)

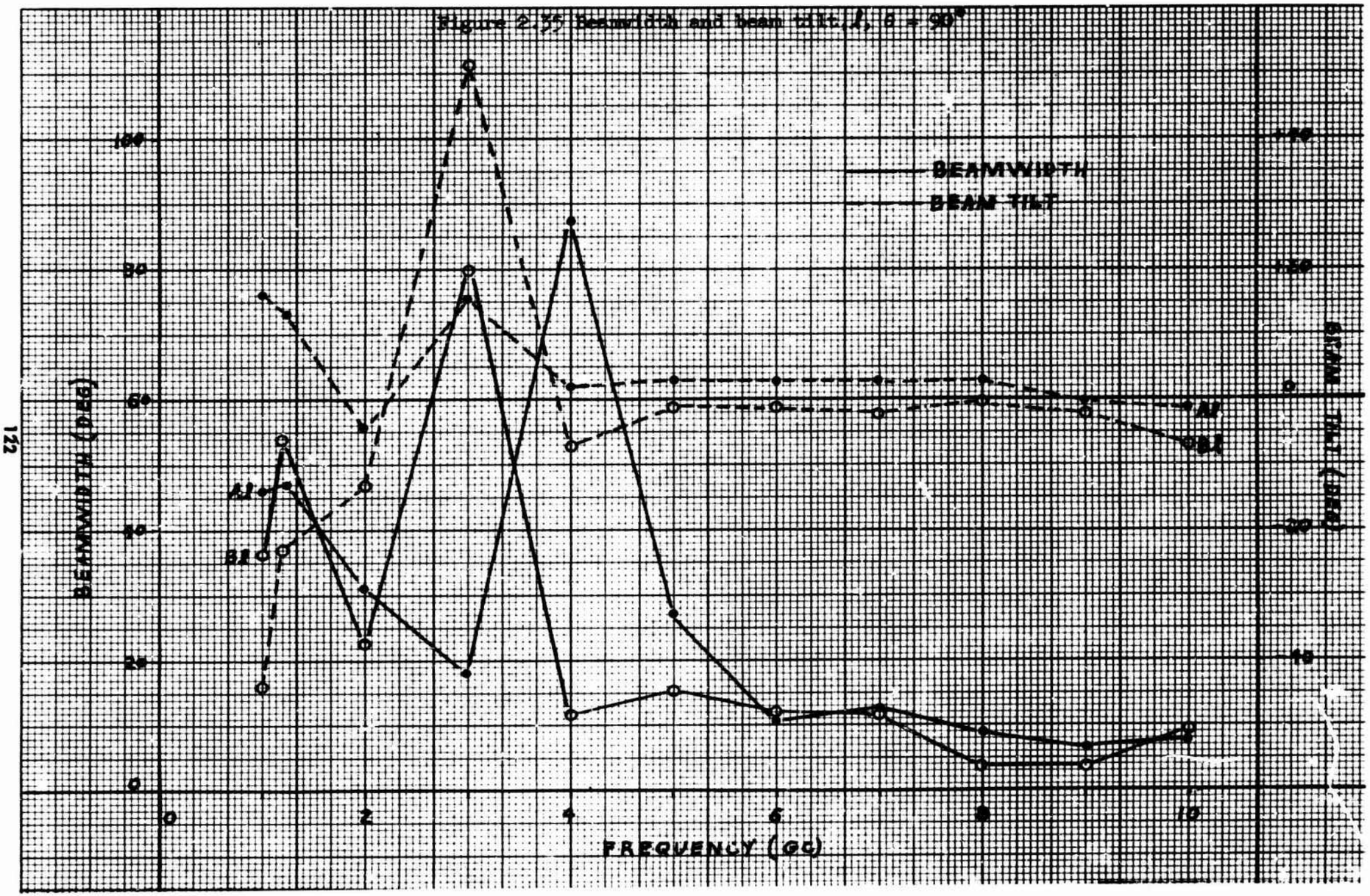
Figure 2.35 Beamwidth and beam tilt, $\theta = 90°$
BEAMWIDTH
BEAM TILT
BEAMWIDTH (DEG)
BEAM TILT (DEG)
FREQUENCY (GC)
100
80
60
40
20
0
-40
-20
0
20
40
0
2
4
6
8
10
A1
B1
A2
B2

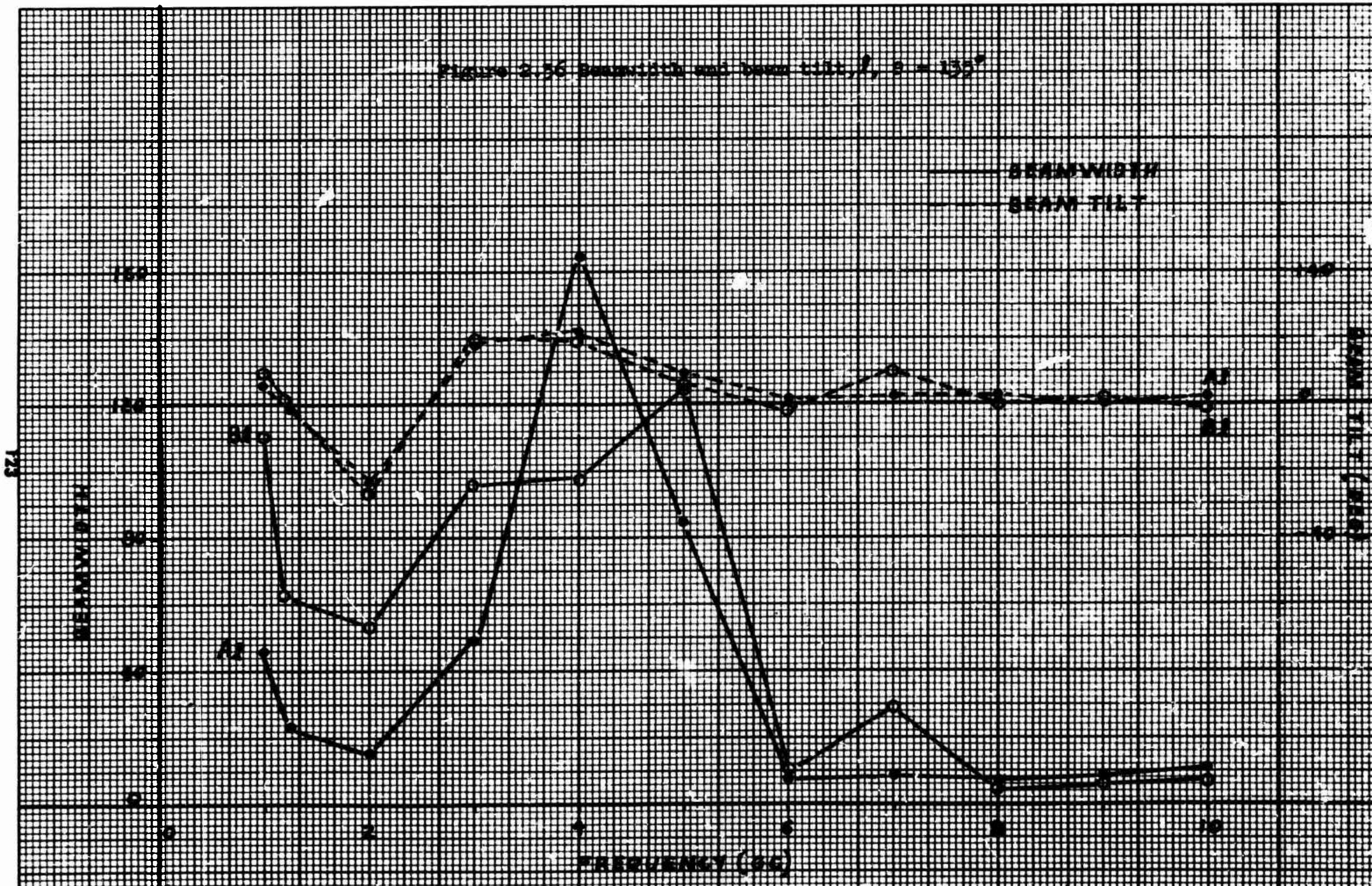

Figure 2.56 Beamwidth and beam tilt, ℓ, θ = 135°

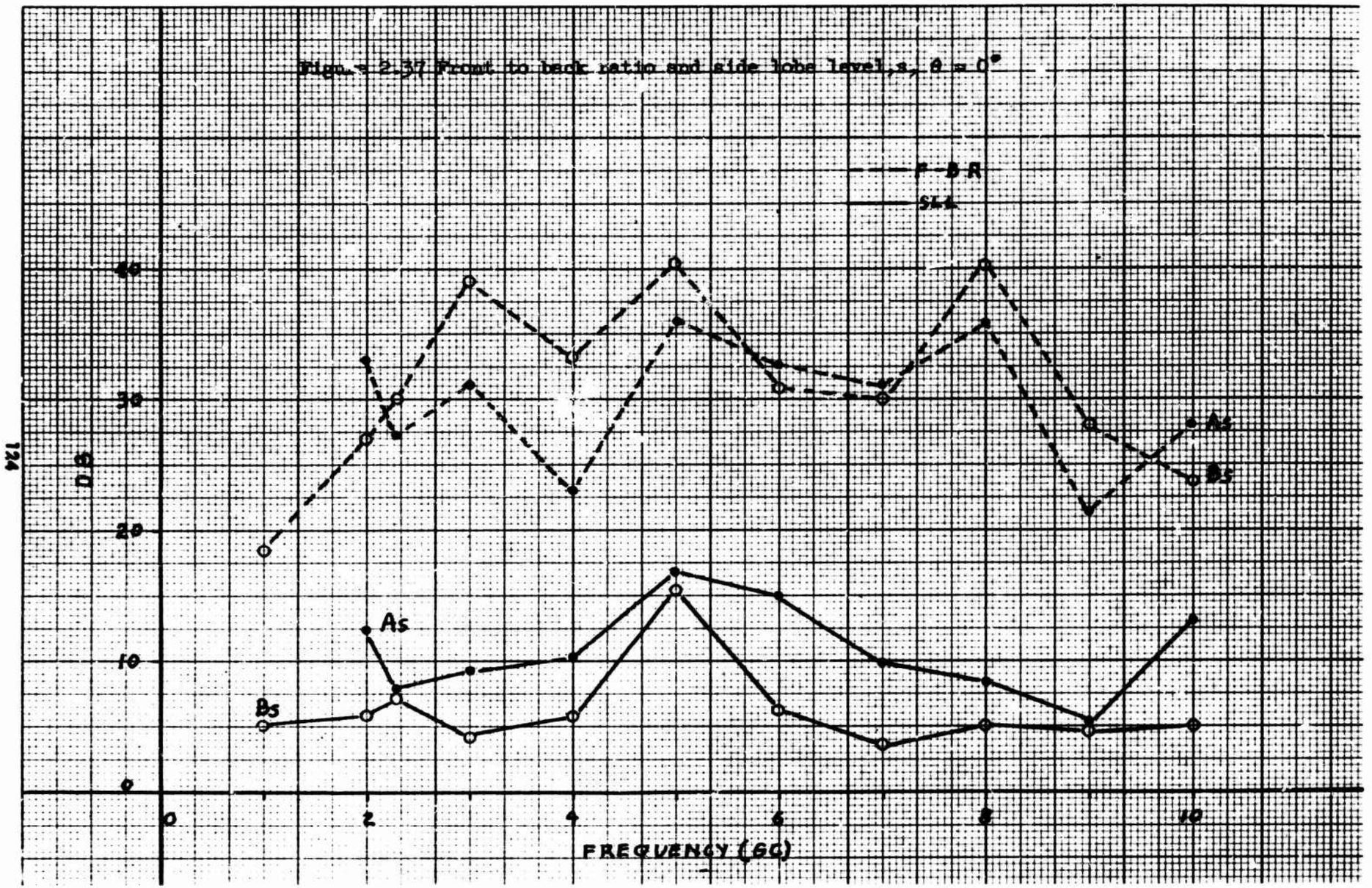
Fig. 2.37 Front to back ratio and side lobe level, $\theta = 0°$
F - B R
SLL
40
30
20
10
0
DB
124
As
Bs
0
2
4
6
8
10
FREQUENCY (GC)

Figure 2.38 Front to back ratio and side lobe level, s, $\theta = 45^{\circ}$

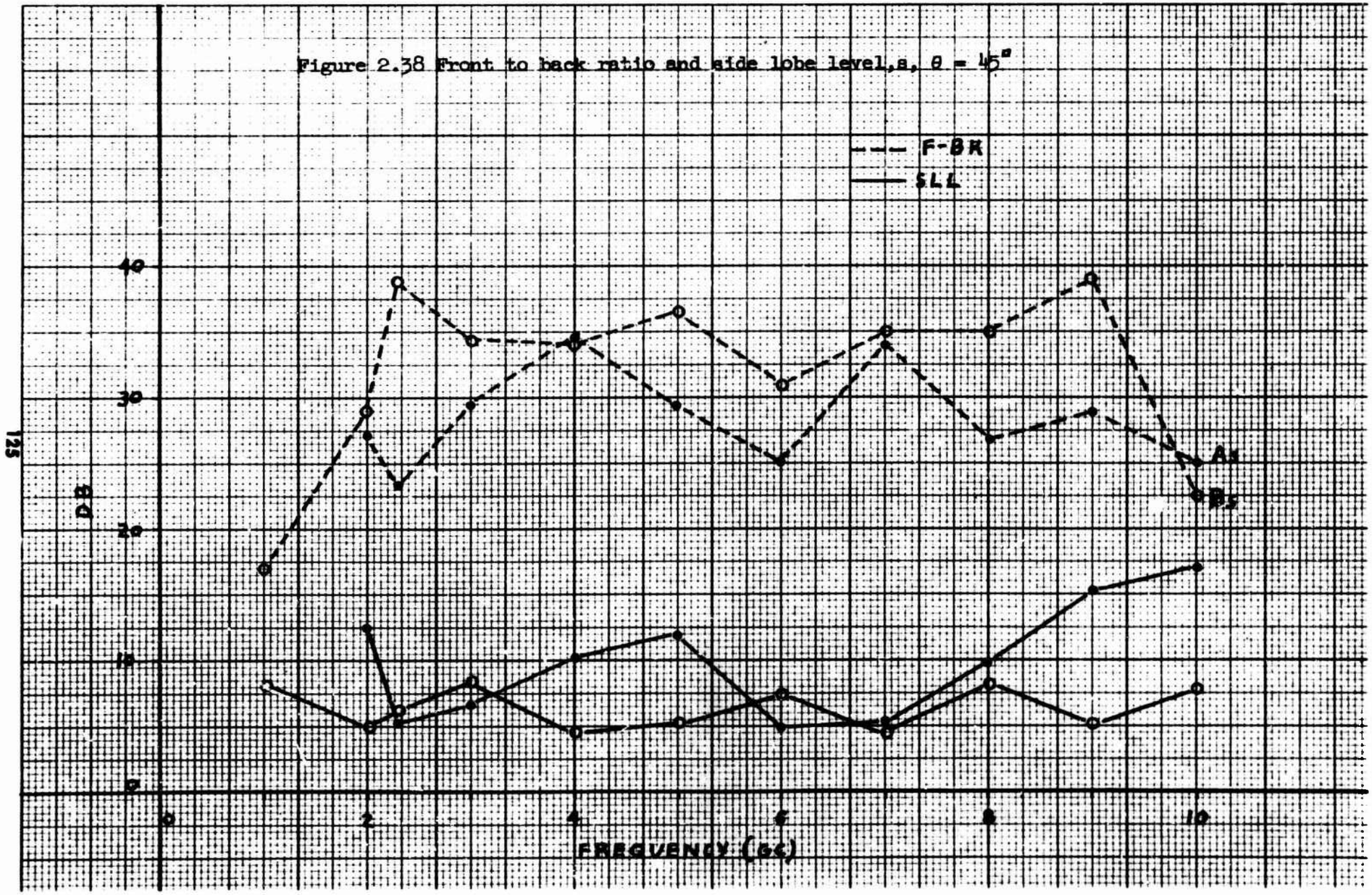

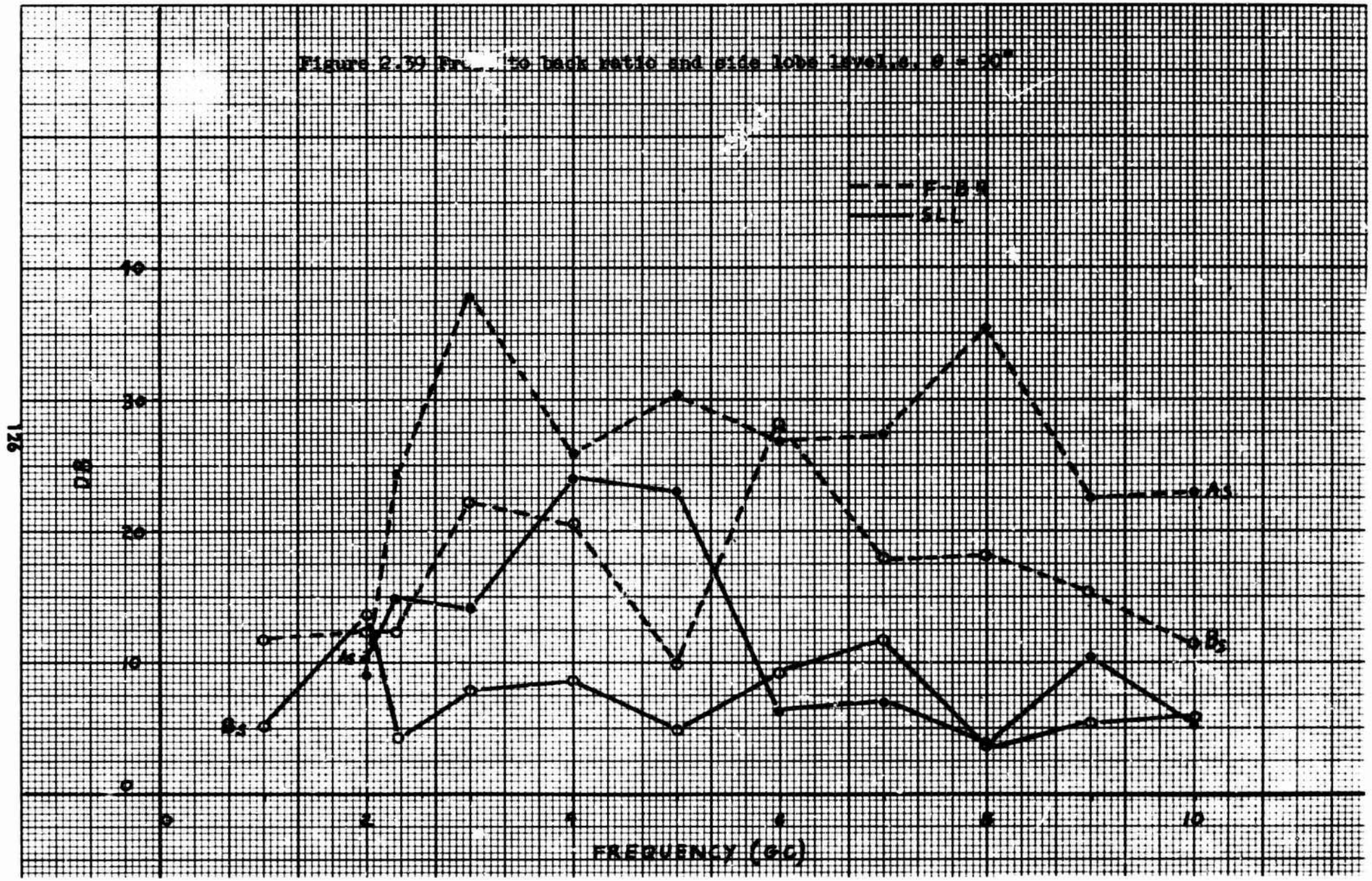
Figure 2.39 Fr... to back ratio and side lobe levels, θ = 90°
F-B
SLL
40
30
20
10
0
dB
126
0
2
4
6
8
10
FREQUENCY (GC)
A5
B5
B4

Figure 8.30 Front to back ratio and side lobe level, s, $\theta = 135°$

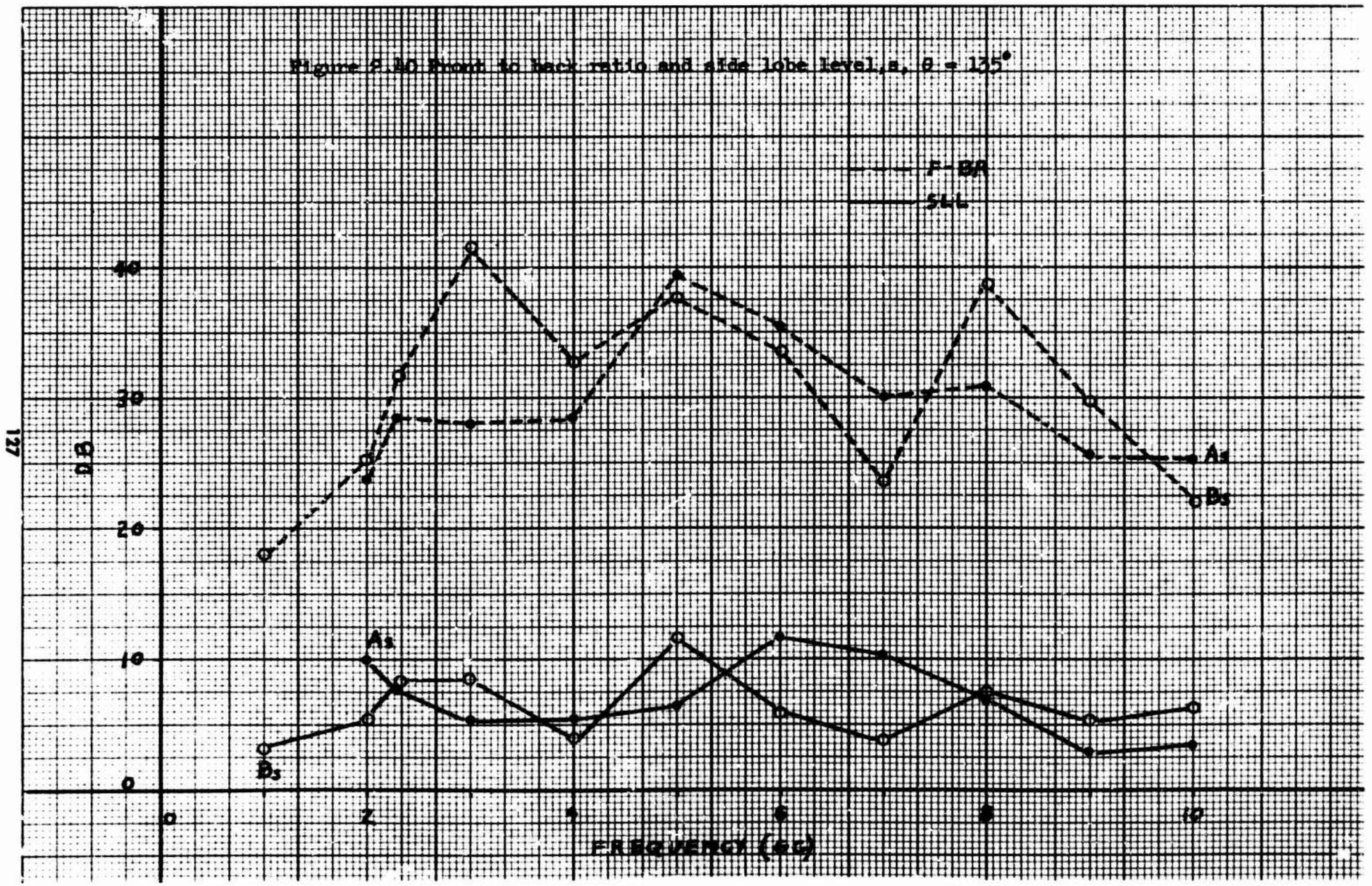

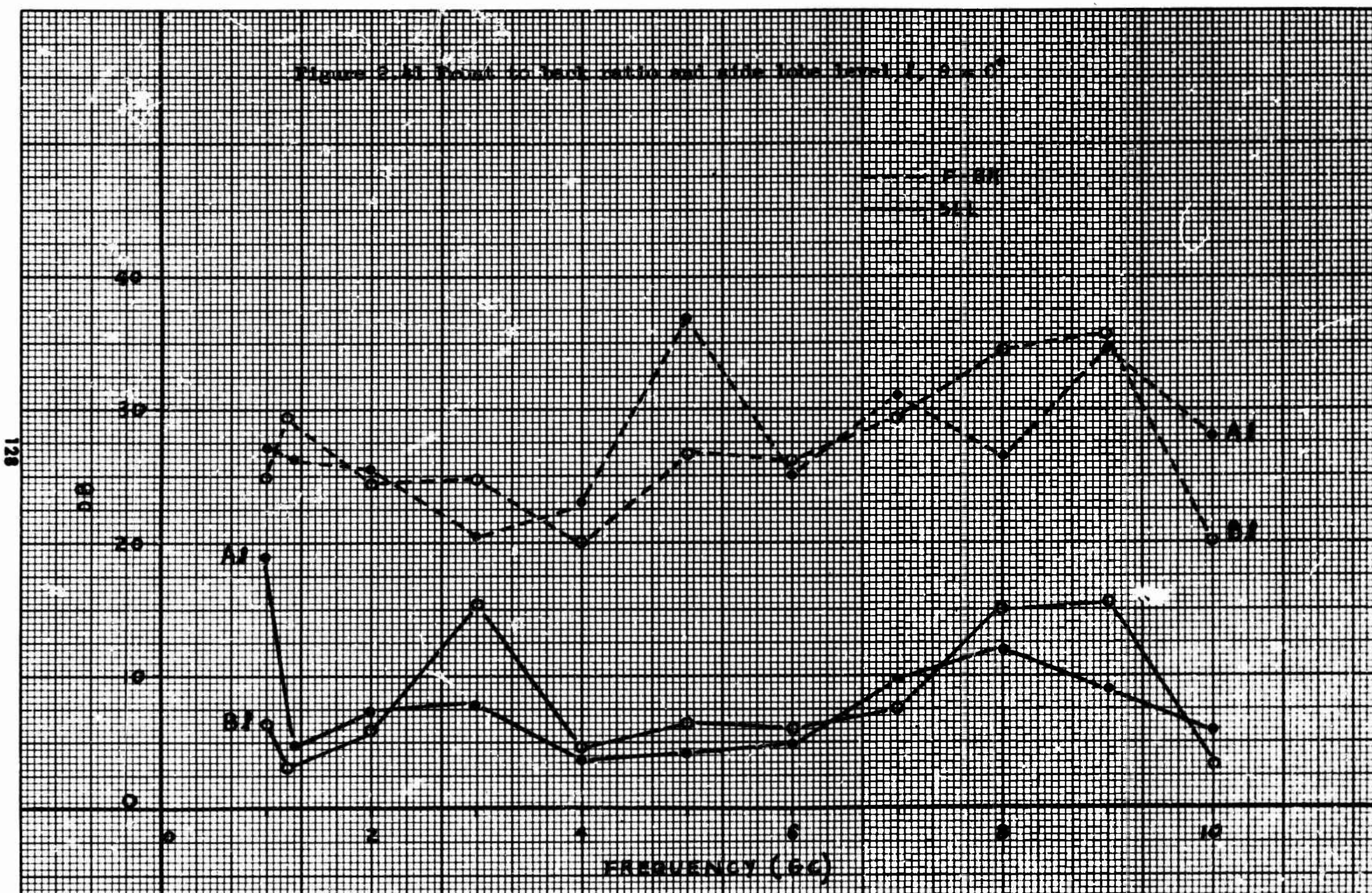

Figure 2.41 Front to back ratio and side lobe level, θ = 0°

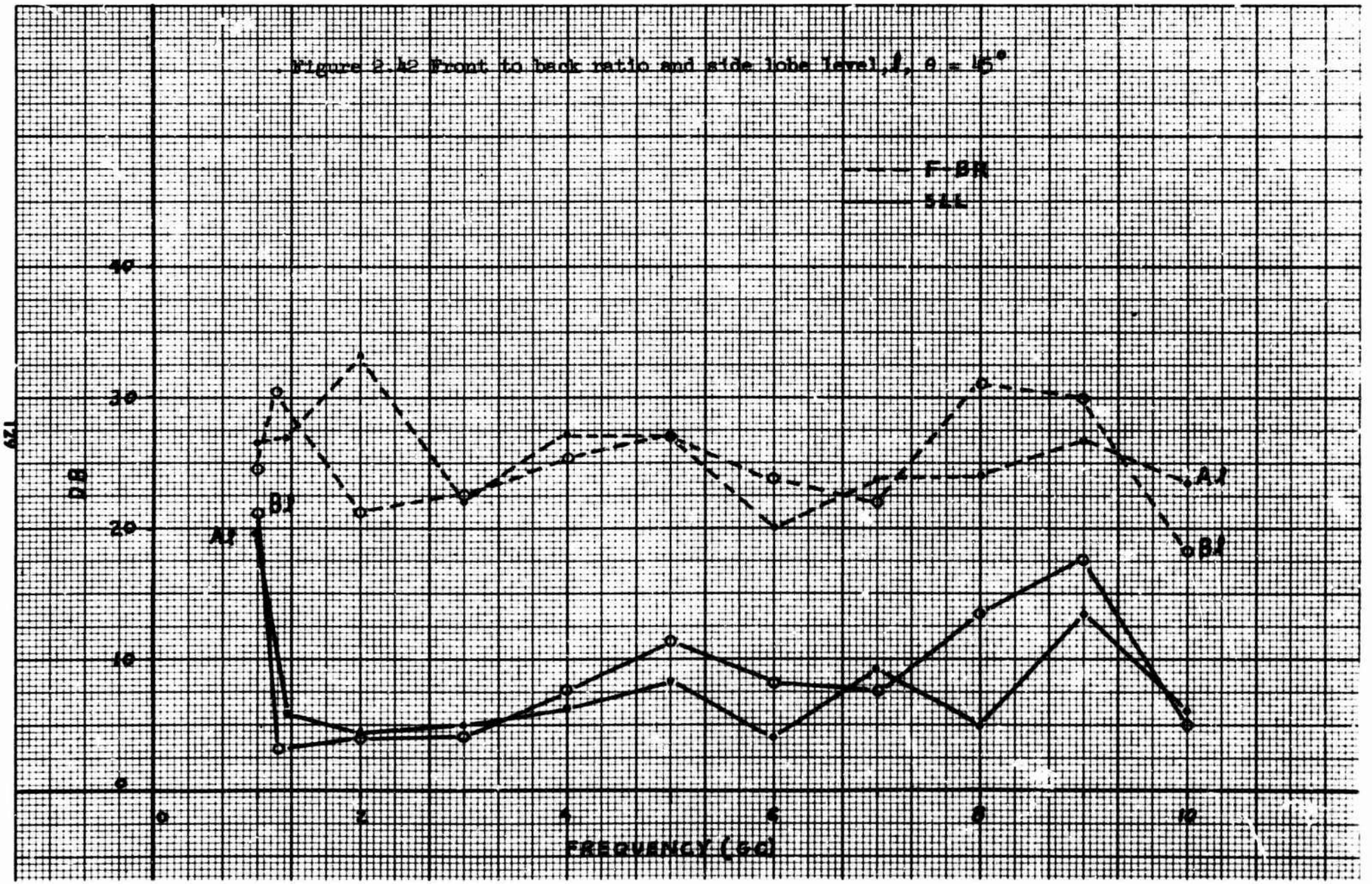

Figure 2.42 Front to back ratio and side lobe level, ℓ, $\theta = 45°$

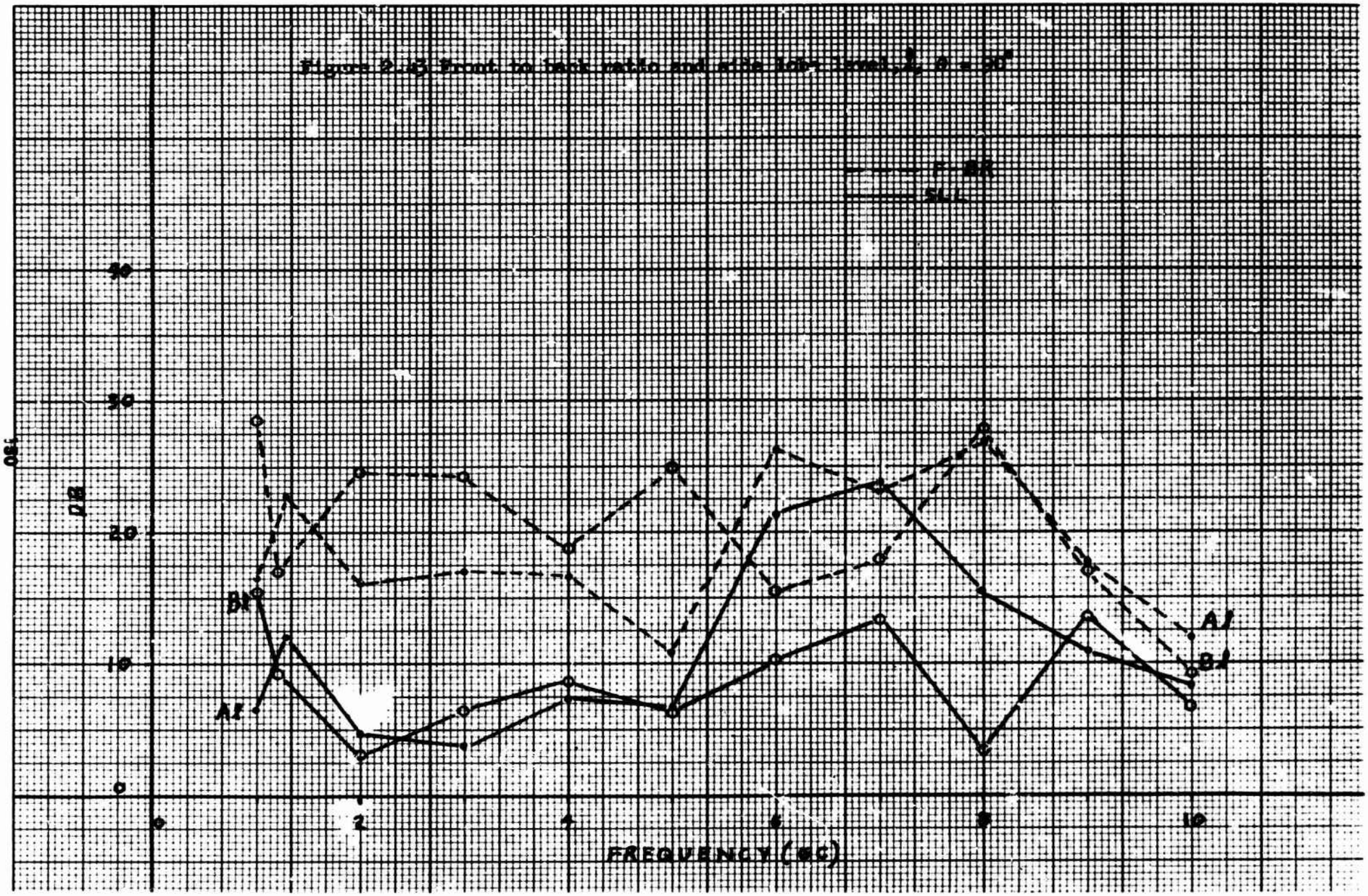
Figure 2.43 Front to back ratio and side lobe level, θ = 90°
SLL
FR
30
20
10
0
dB
2
4
6
8
10
FREQUENCY (KC)
A1
B1
A2
B2

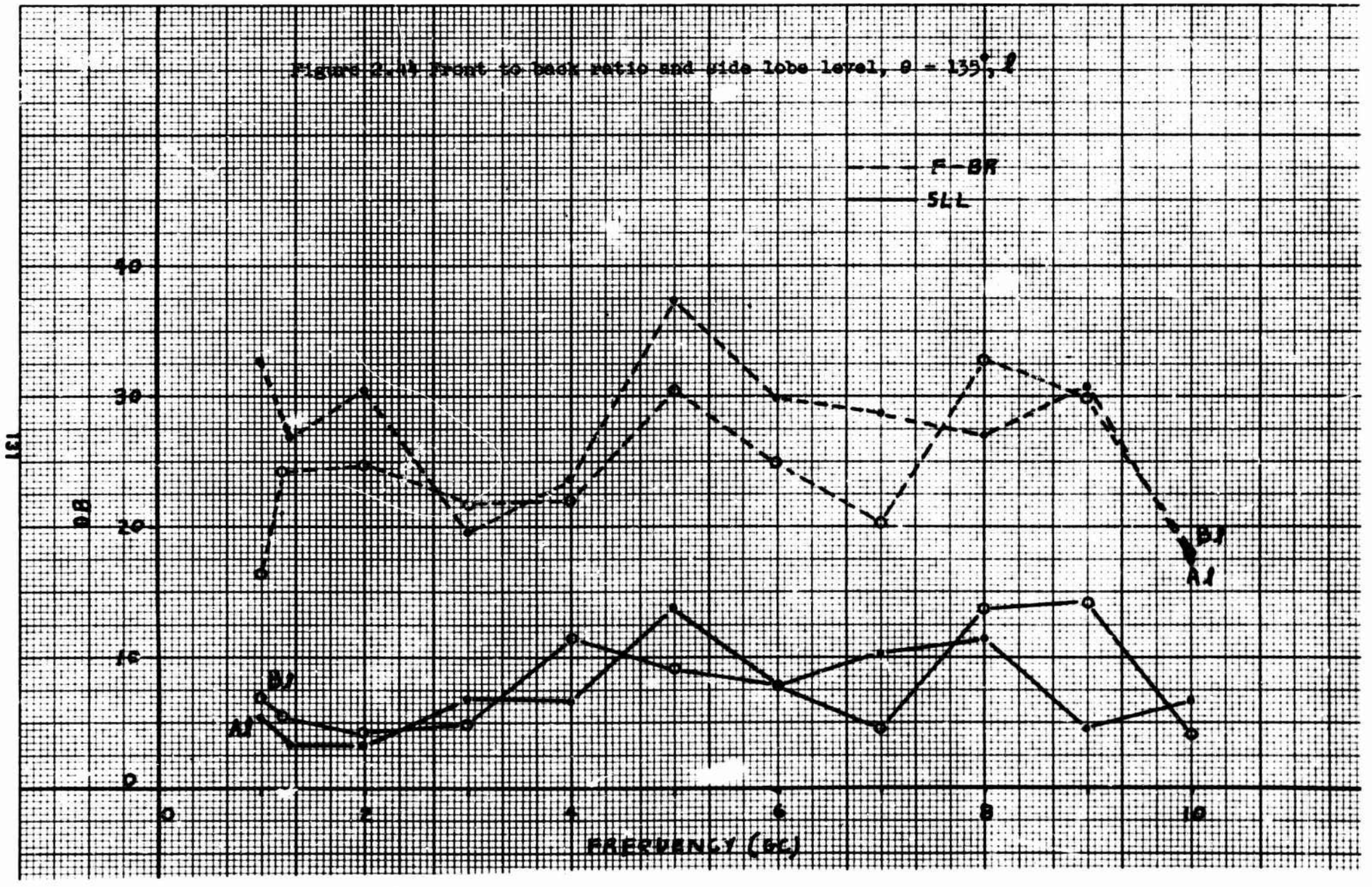

Figure 2.44 Front to back ratio and side lobe level, $\theta = 139^\circ$, ℓ

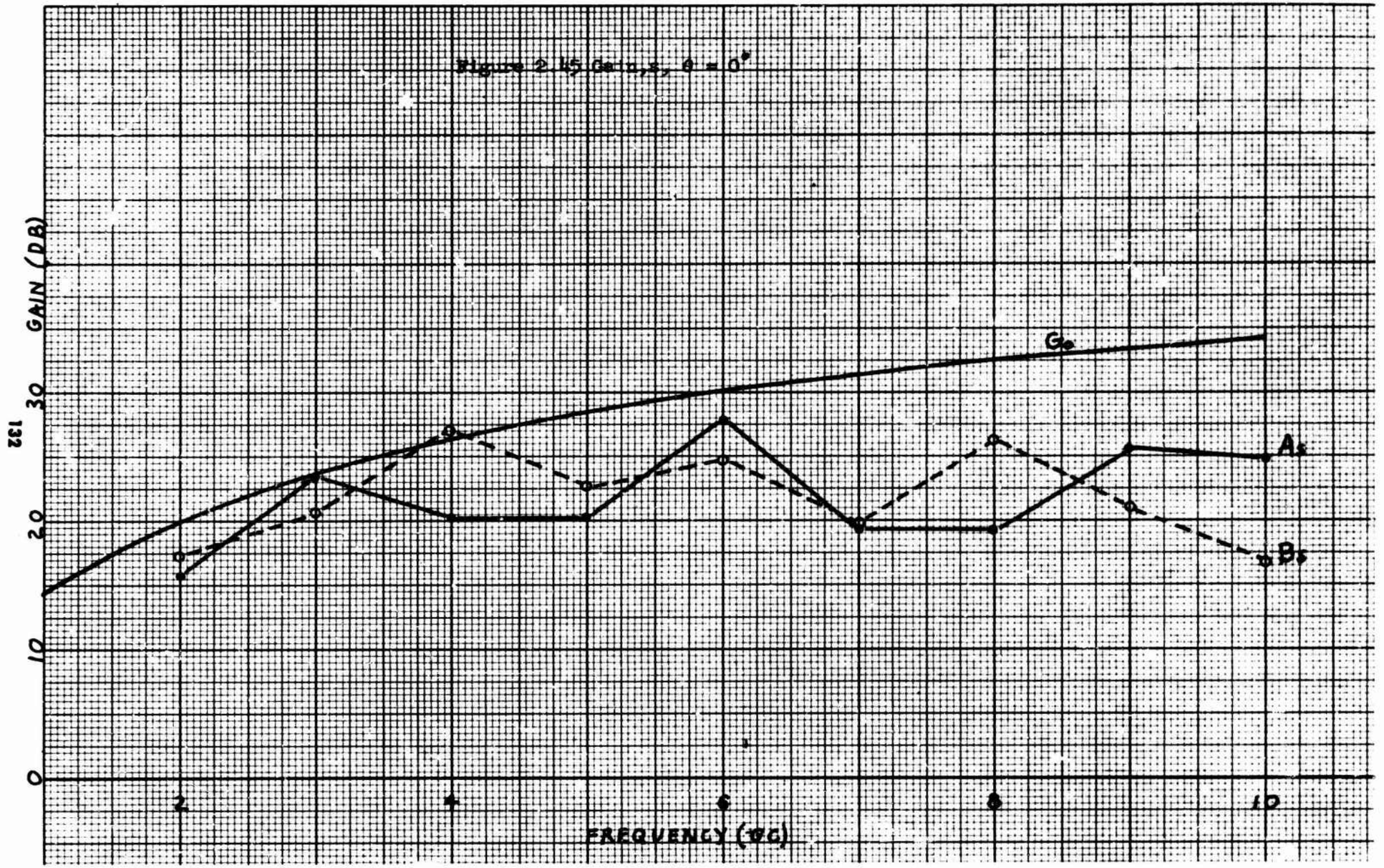

Figure 2.45 Gains, $\theta = 0°$

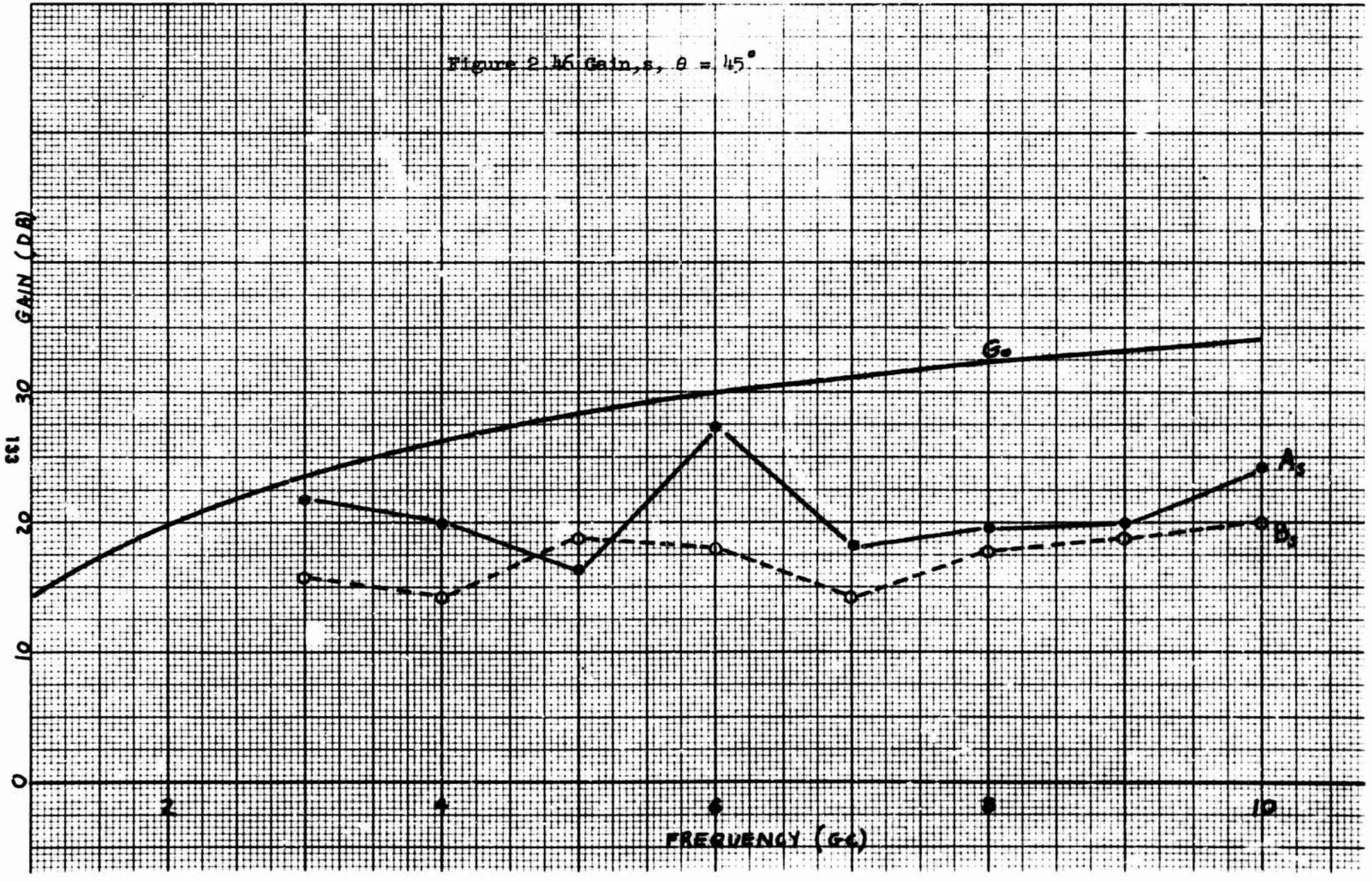

Figure 2.46 Gain, s, $\theta = 45°$

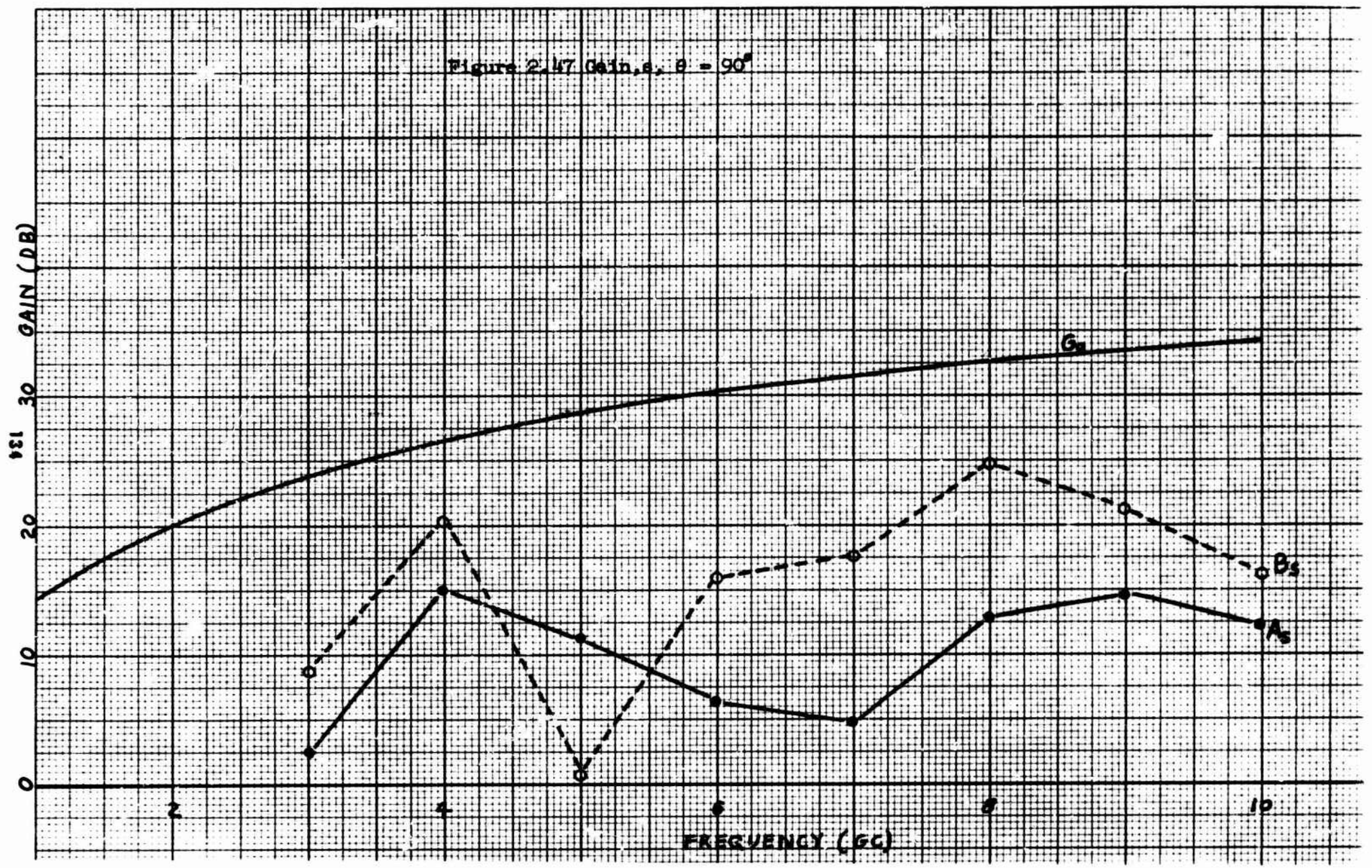

Figure 2.47 Gain, e, $\theta = 90°$

As
Bs
10
FREQUENCY (GC)
Figure 6.30 Beam A, θ = 135°
GAIN (DB)
0
10
20
30

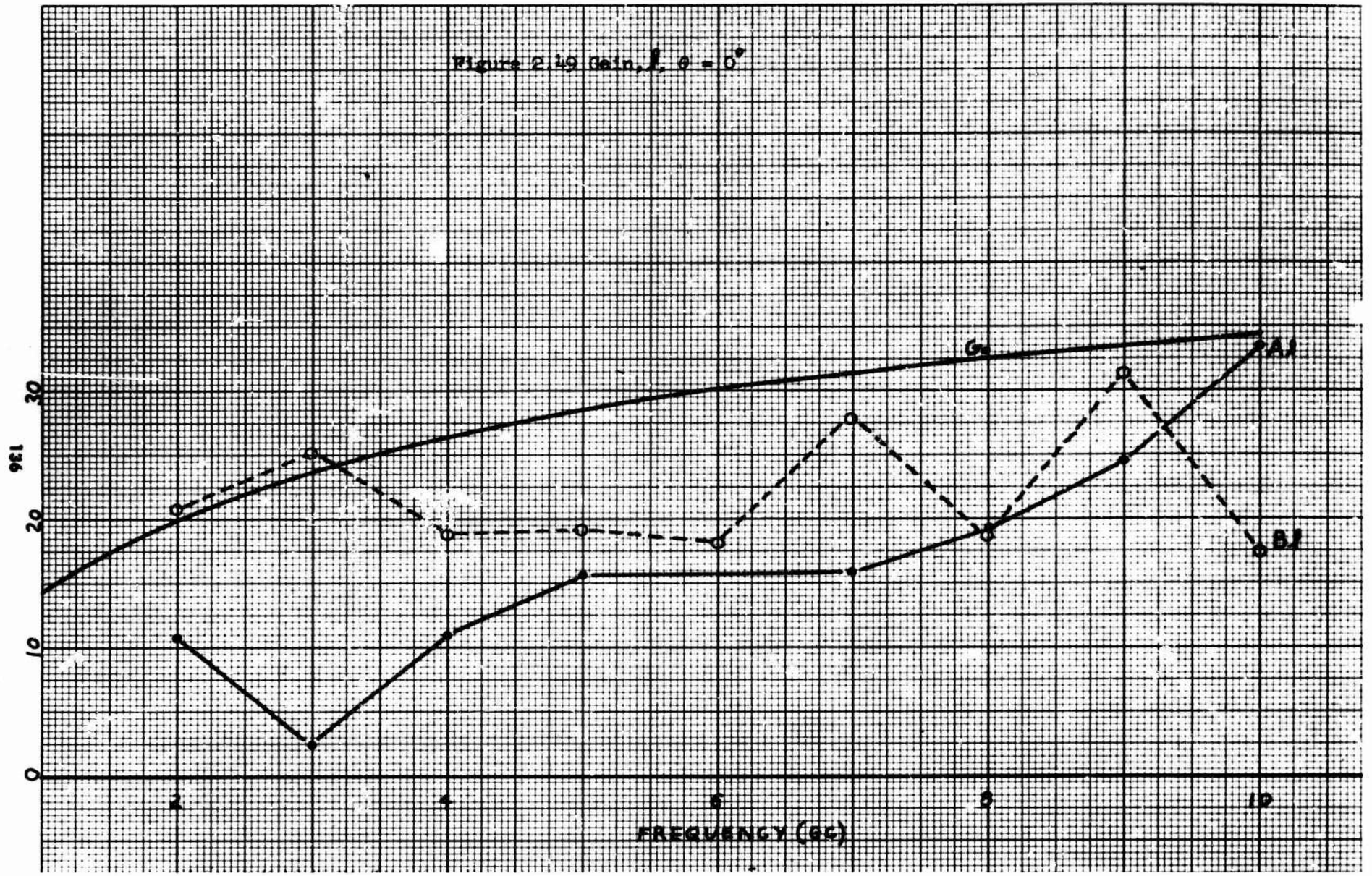
Figure 2.49 Gain, θ = 0°
GAIN (DB)
0
10
20
30
2
4
6
8
10
FREQUENCY (GC)
G
A
B

Figure 2.50 Gain, ℓ, $\theta = 45°$

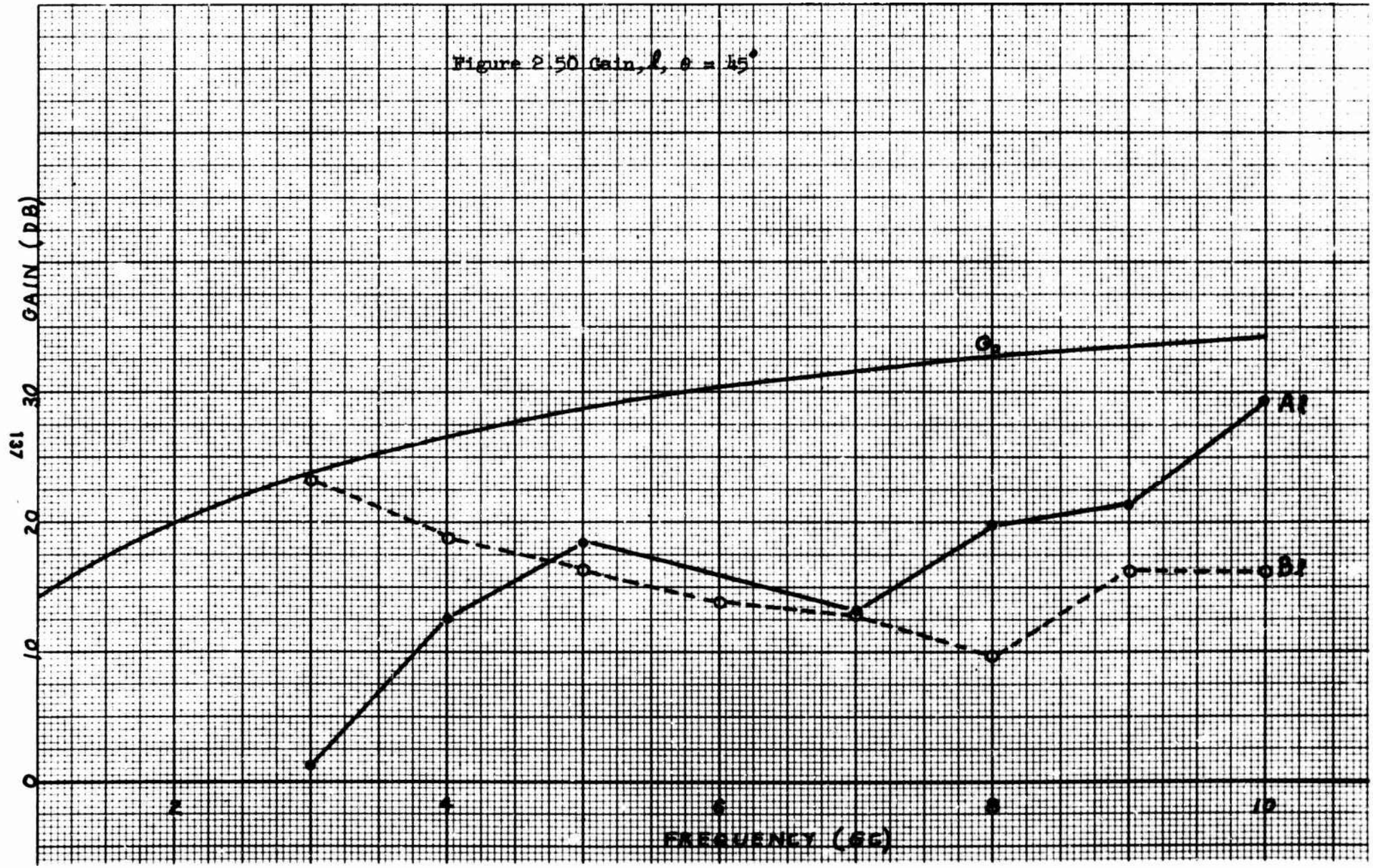

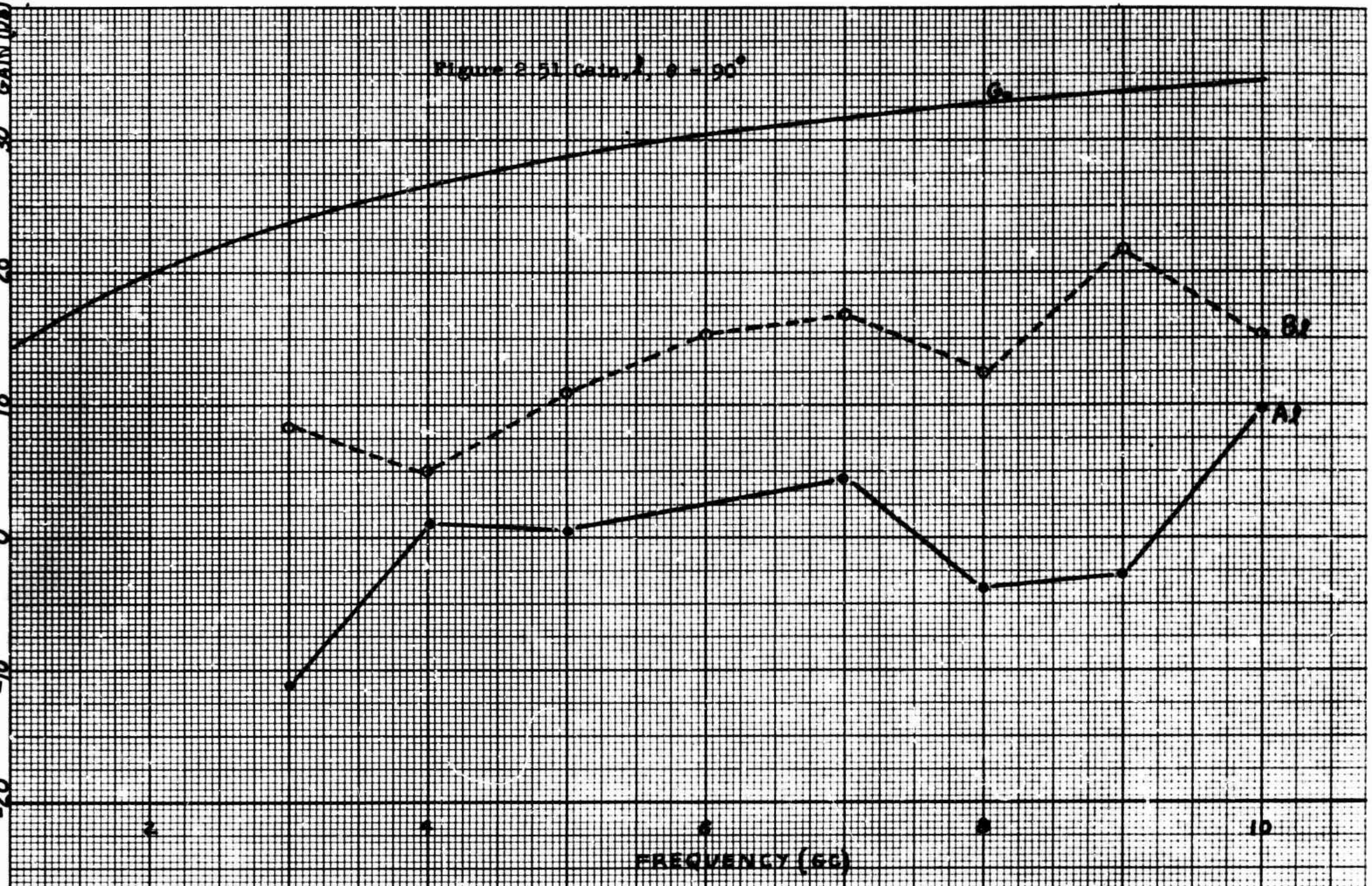

Figure 2.51 Gain, λ, θ = 90°

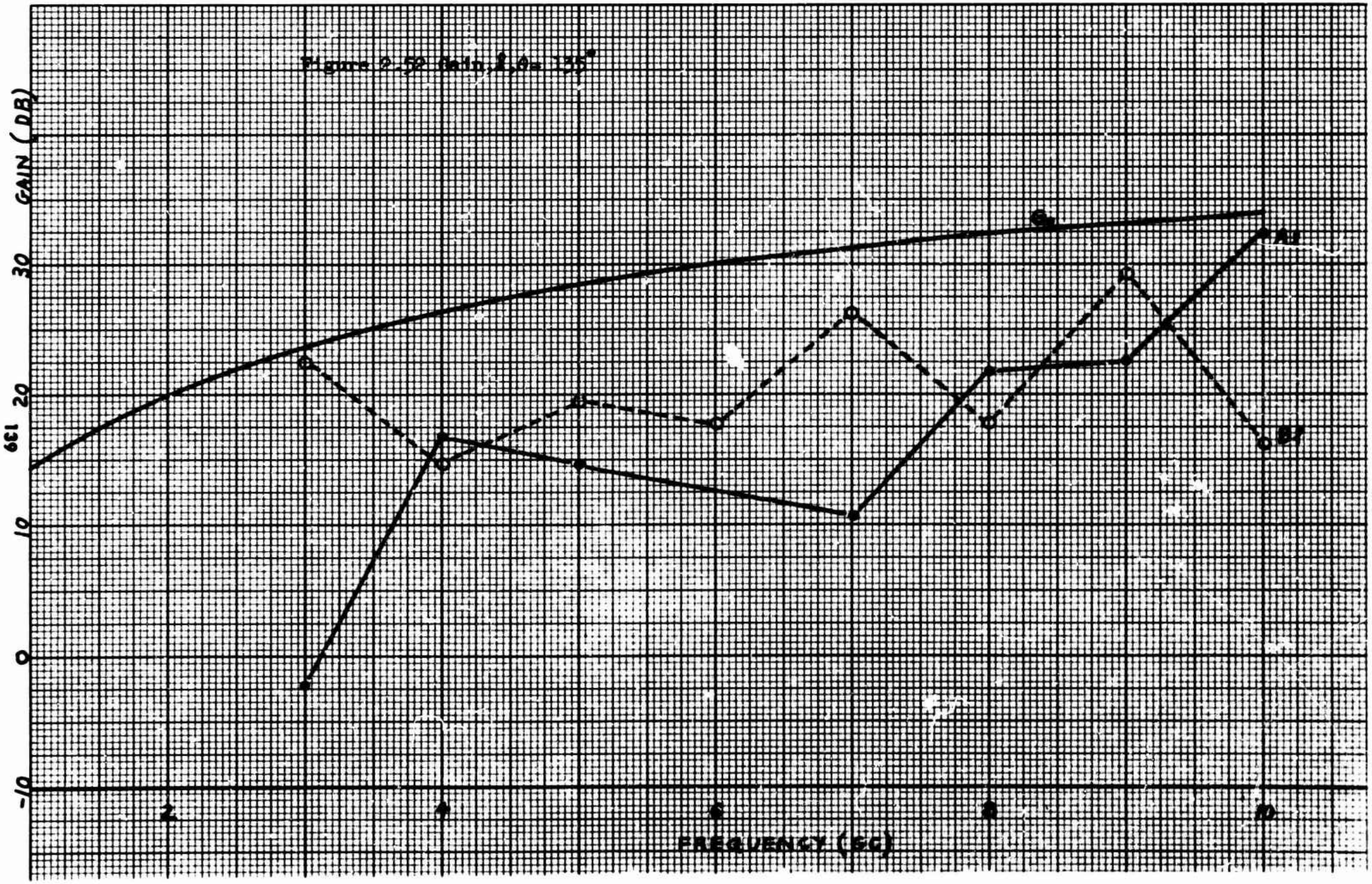

Figure 2.52 Gain, ℓ, $\theta = 135°$

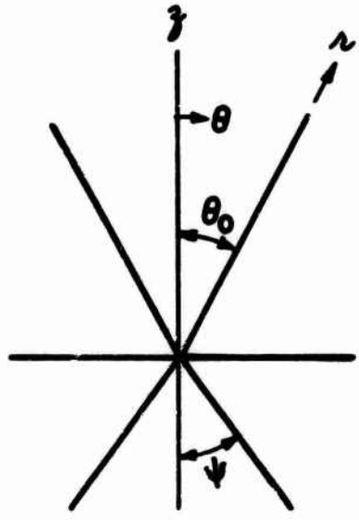

a) BICONICAL ANTENNA OR BICONICAL TRANSMISSION LINE

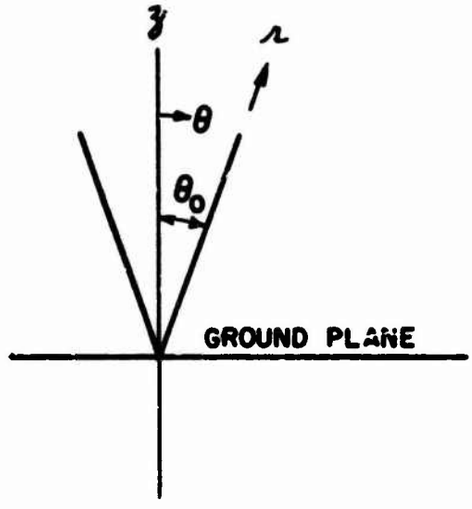

b) DISC-CONE ANTENNA OR SINGLE CONE TRANSMISSION LINE ABOVE AN INFINITE GROUND PLANE

FIGURE 3.1 BICONICAL STRUCTURES

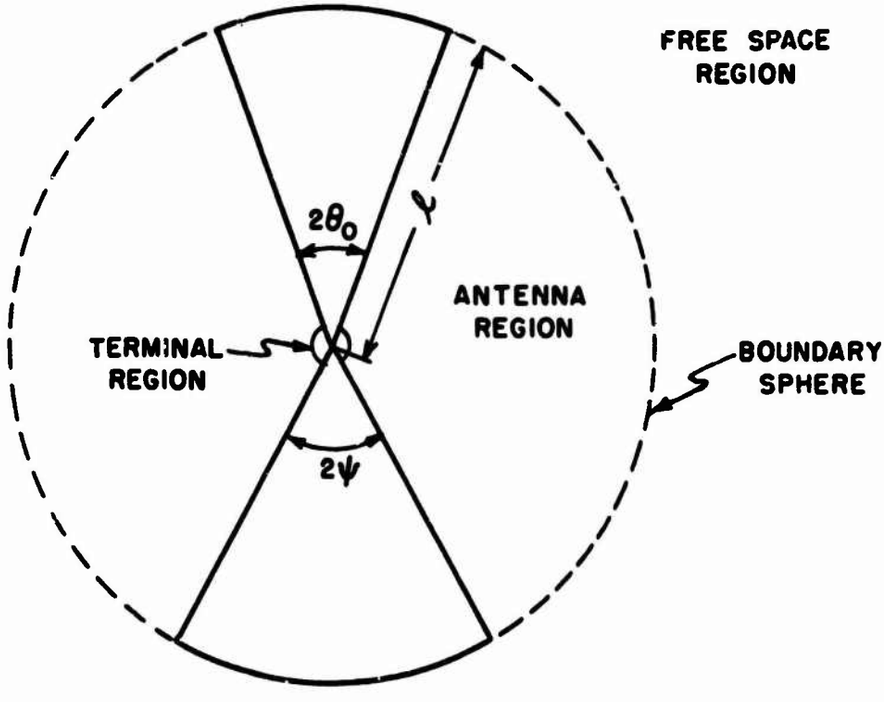

FIGURE 3.2 BICONICAL ANTENNA

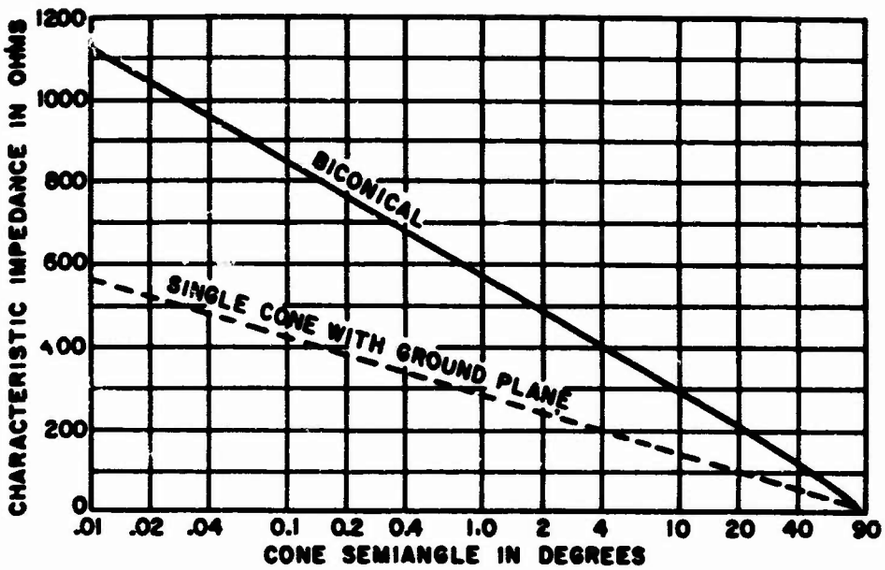

FIGURE 3.3 CHARACTERISTIC IMPEDANCE OF BICONICAL TRANSMISSION LINES

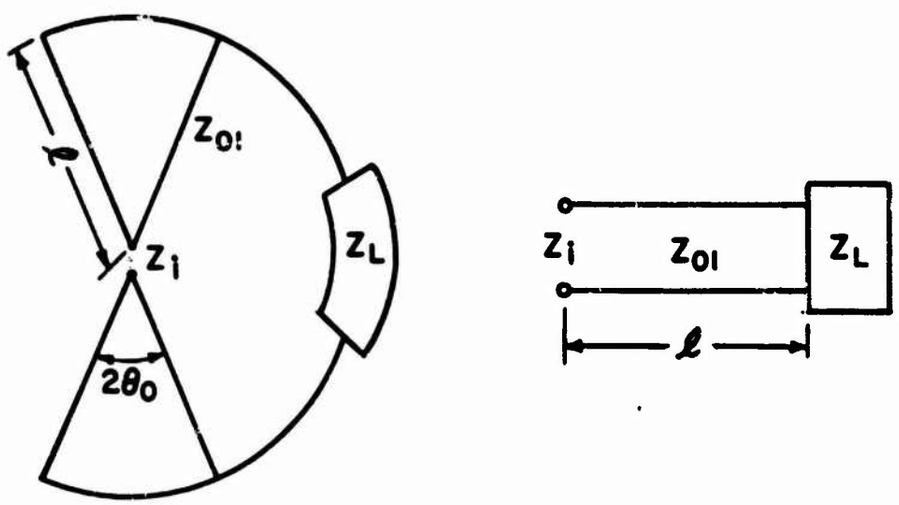

FIGURE 3.4 BICONICAL ANTENNA AND EQUIVALENT TRANSMISSION LINES

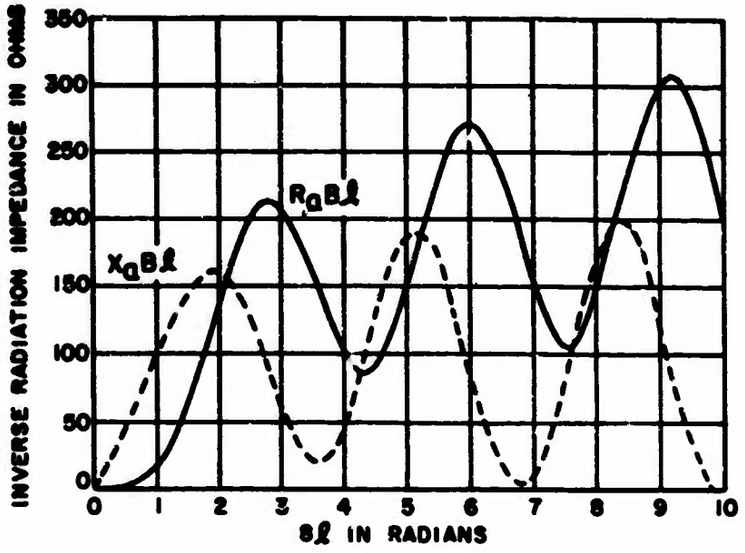

FIGURE 3.5 CURVES FOR THE RESISTIVE AND REACTIVE COMPONENTS OF THE INVERSE RADIATION IMPEDANCE OF AN ANTENNA

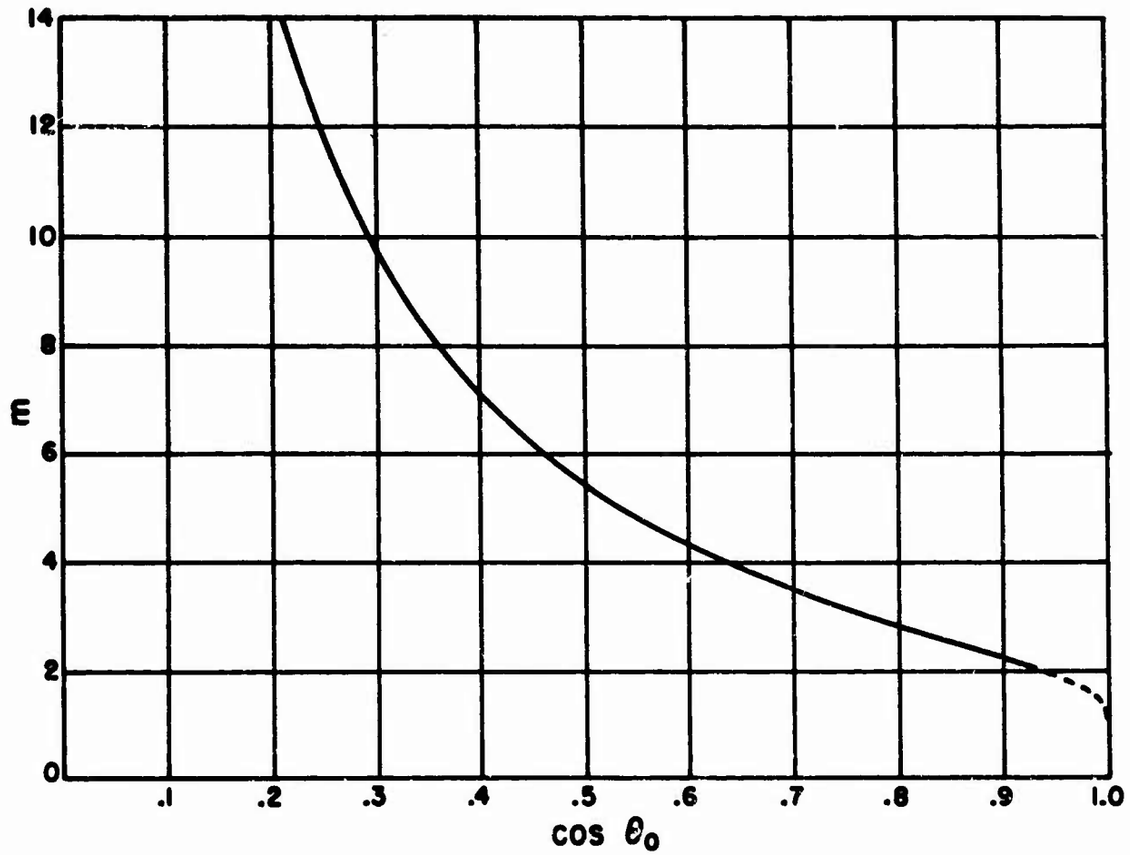

FIGURE 3.6 m VS. COS θ_0

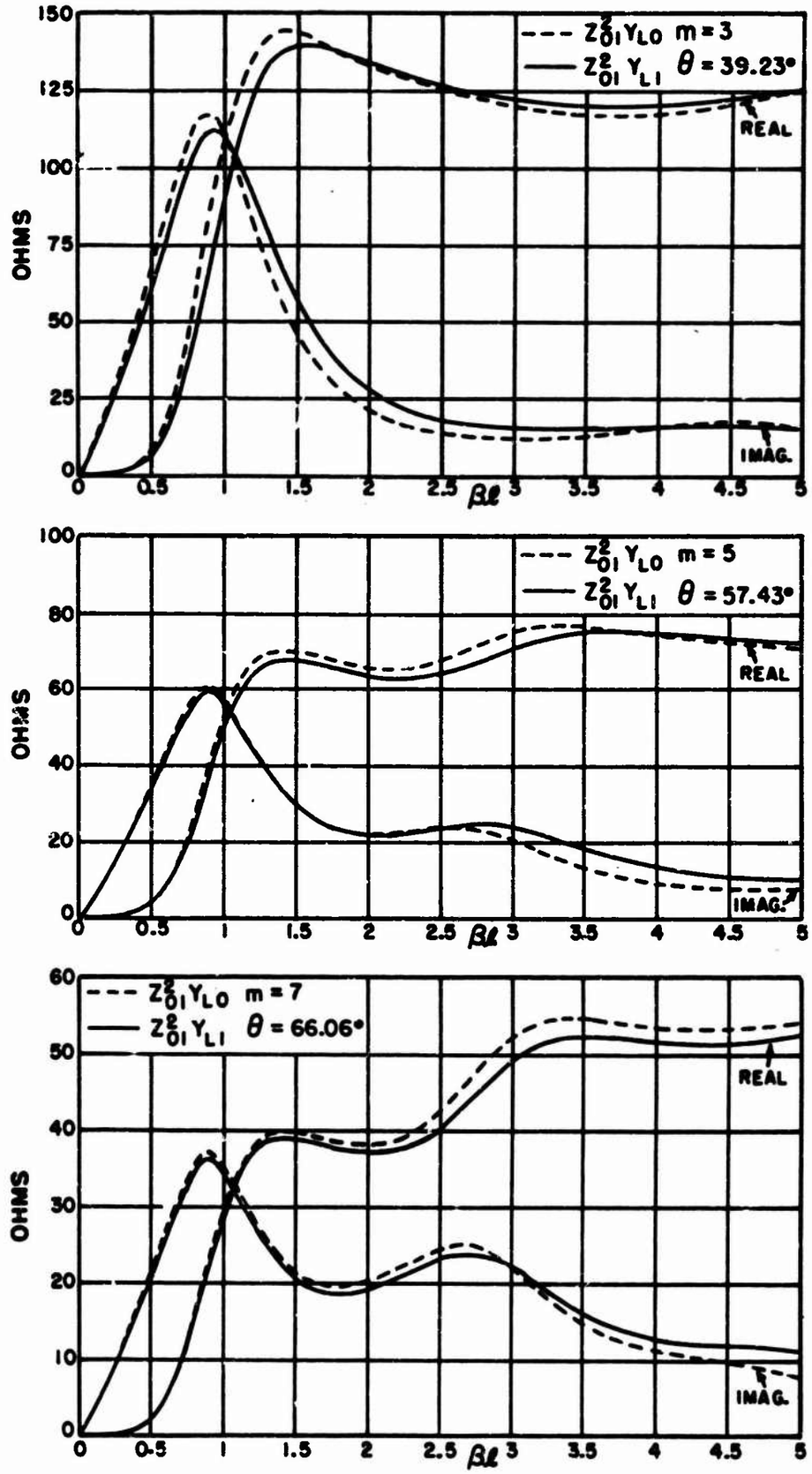

FIGURE 3.7 ZEROTH-ORDER AND FIRST-ORDER SOLUTIONS FOR WIDE-ANGLE CONES.

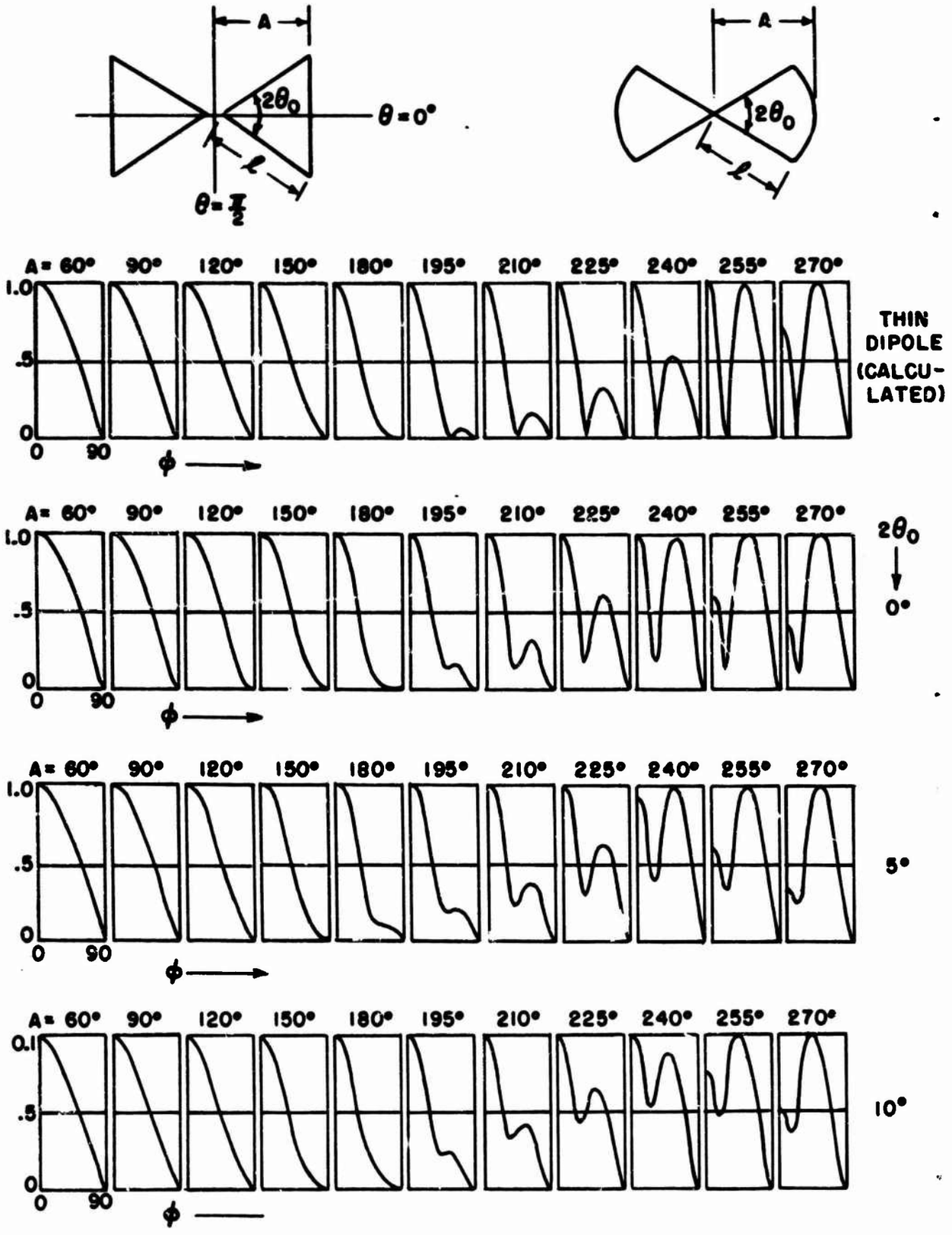

FIGURE 3.8a MEASURED FIELD PATTERNS OF A BICONICAL ANTENNA FOR VARIOUS HEIGHTS AND SEMIANGLES

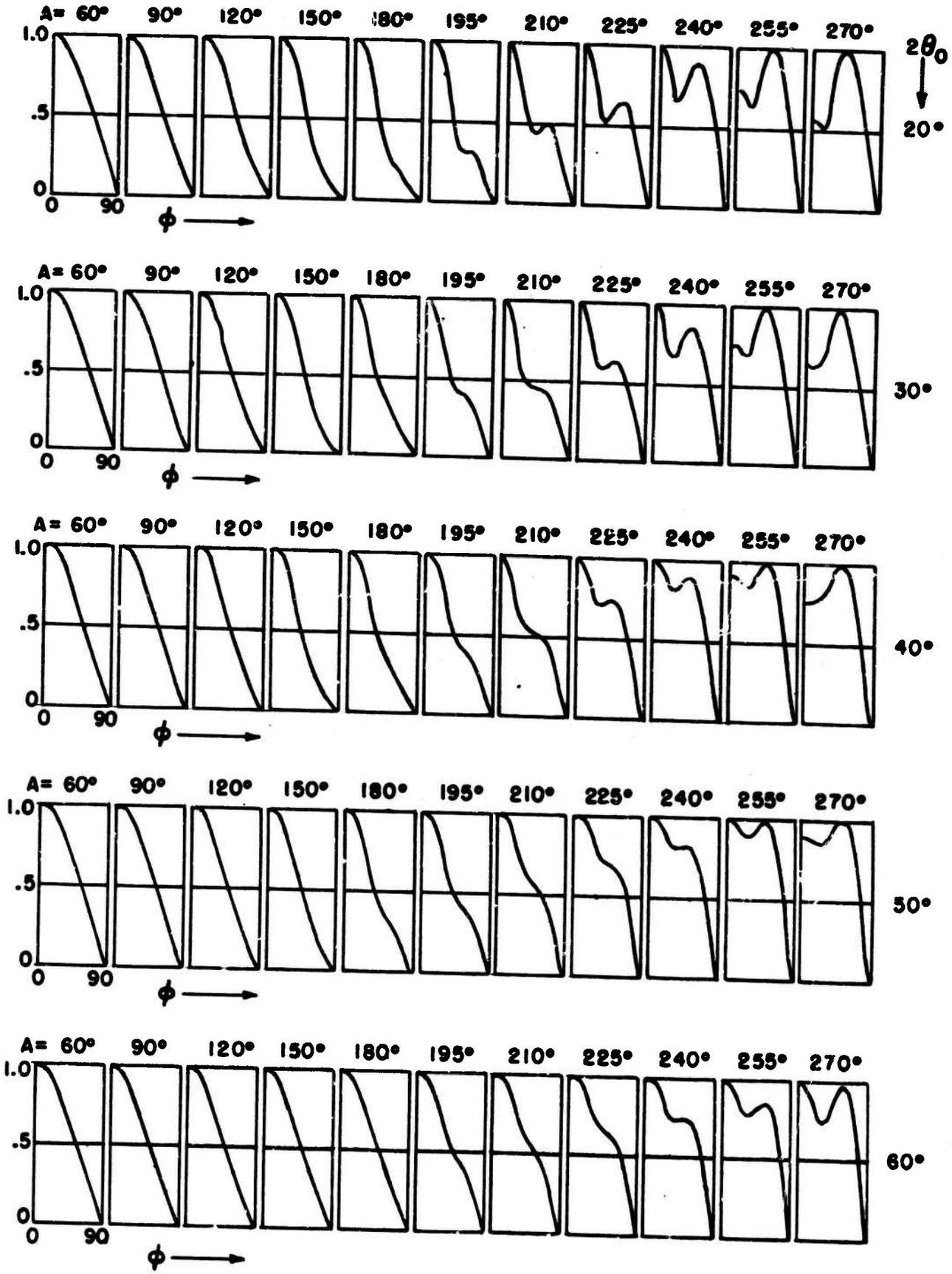

FIGURE 3.8b MEASURED FIELD PATTERNS OF A BICONICAL ANTENNA FOR VARIOUS HEIGHTS AND SEMIANGLES

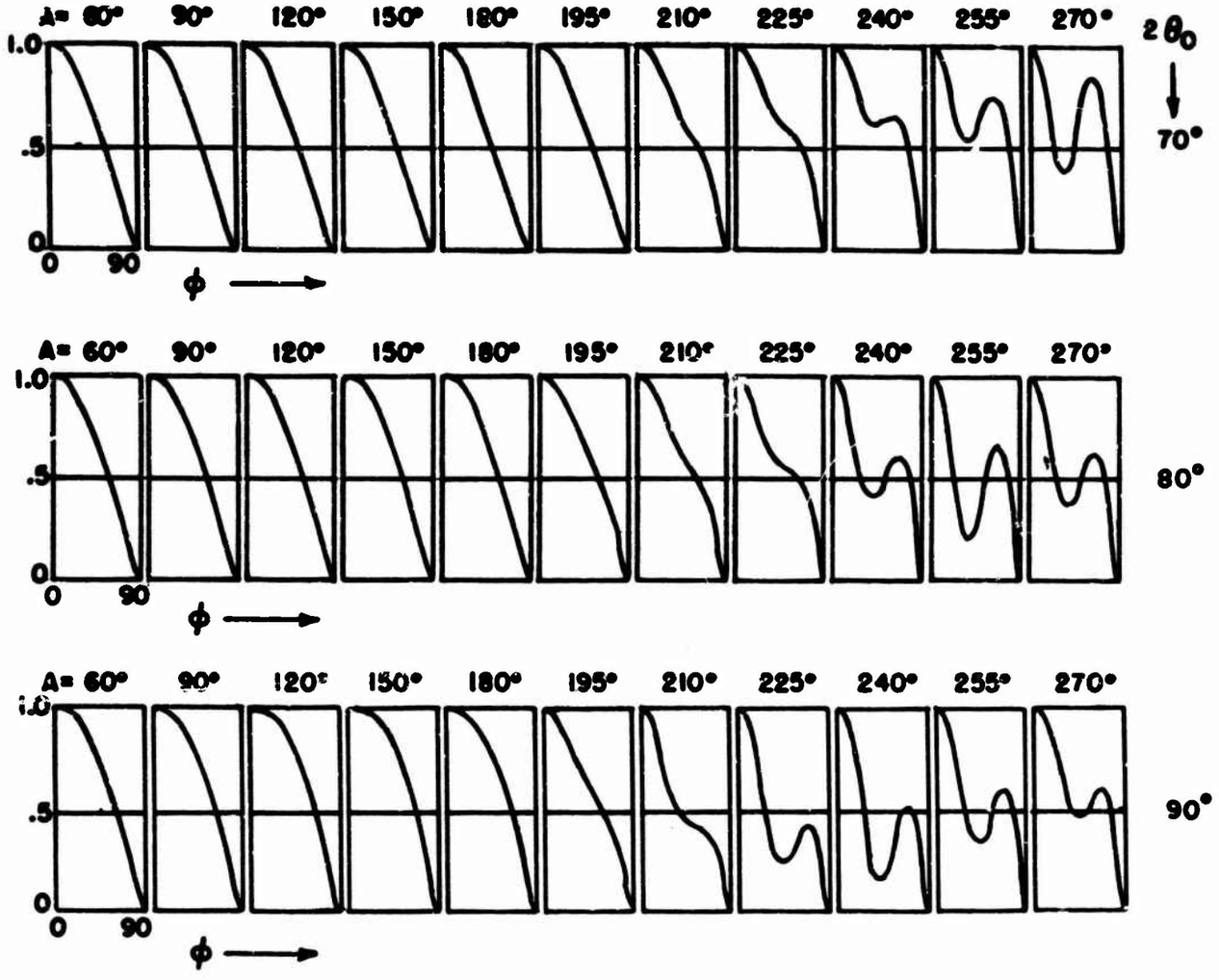

FIGURE 3.8c MEASURED FIELD PATTERNS OF A BICONICAL ANTENNA FOR VARIOUS HEIGHTS AND SEMIANGLES.

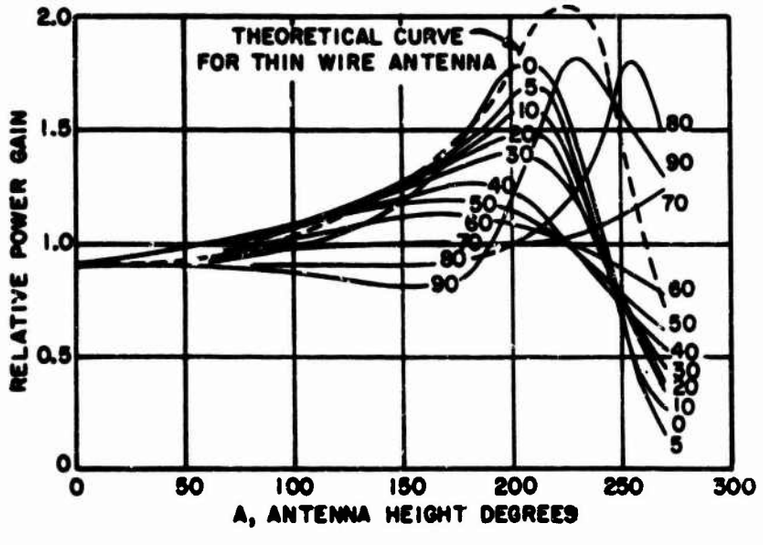

FIGURE 3.9 GAIN OF A BICONICAL ANTENNA CALCULATED FROM MEASURED PATTERNS FOR VARIOUS VALUES OF $2\theta_0$

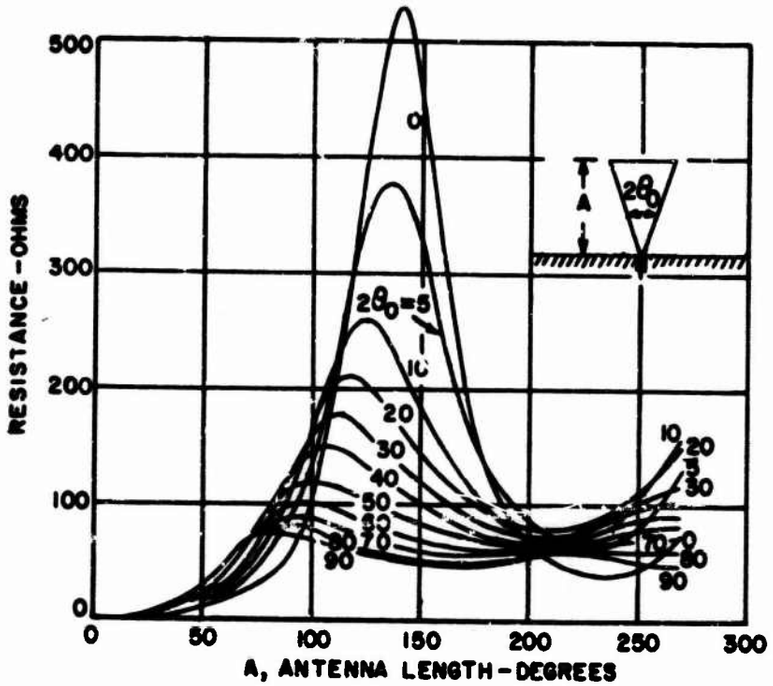

FIGURE 3.10 MEASURED RESISTANCE CURVES OF THE DISC-CONE VS. LENGTH IN ELECTRICAL DEGREES FOR VARIOUS FLARE ANGLES.

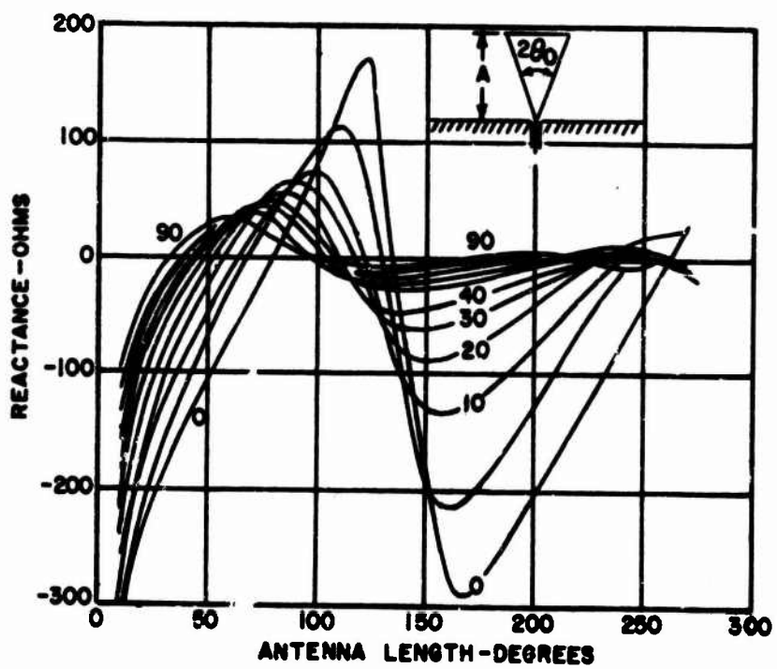

FIGURE 3.11 MEASURED REACTANCE CURVES OF THE DISC-CONE VS. LENGTH IN ELECTRICAL DEGREES FOR VARIOUS FLARE ANGLES.

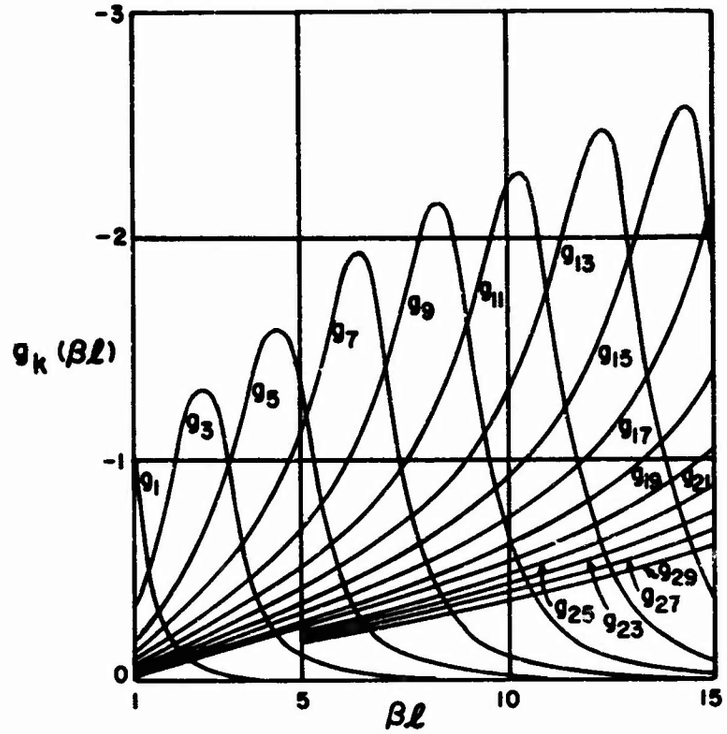

FIG. 3.12 REAL PART OF THE ZETA FUNCTION.

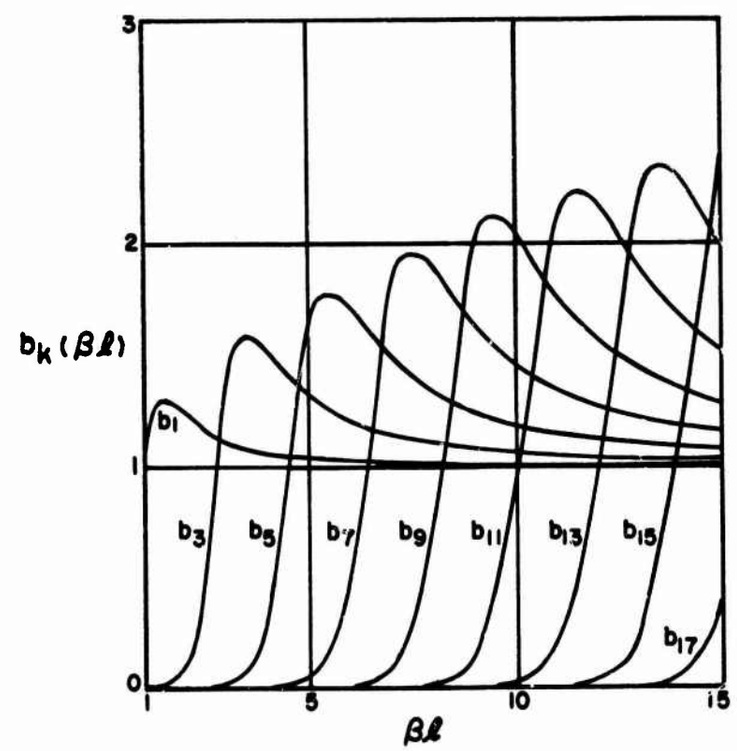

FIG. 3.13 IMAGINARY PART OF THE ZETA FUNCTION.

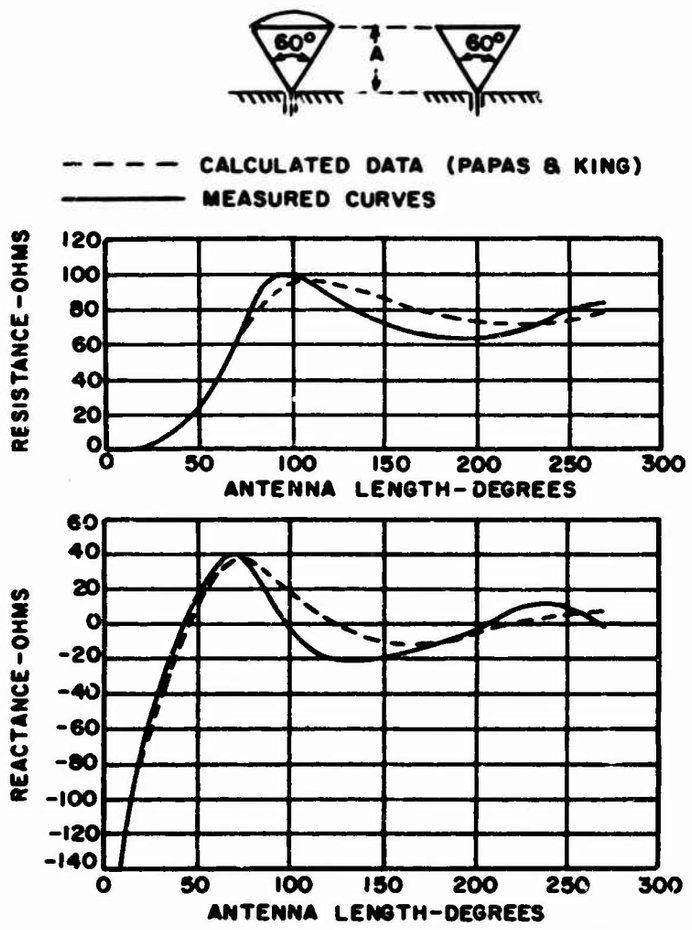

FIG. 3.14 COMPARISON OF CALCULATED AND MEASURED IMPEDANCE CURVES FOR A 30° SEMIANGLE DISC-CONE.

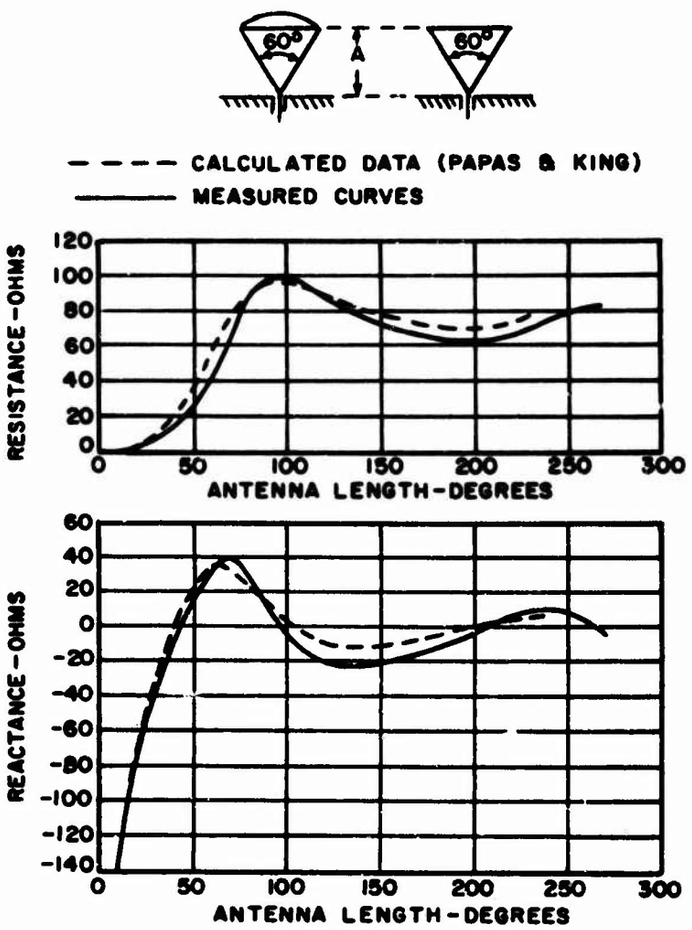

FIG. 3.15 COMPARISON OF CALCULATED AND MEASURED IMPEDANCE CURVES FOR A 30° SEMIANGLE DISC-CONE.

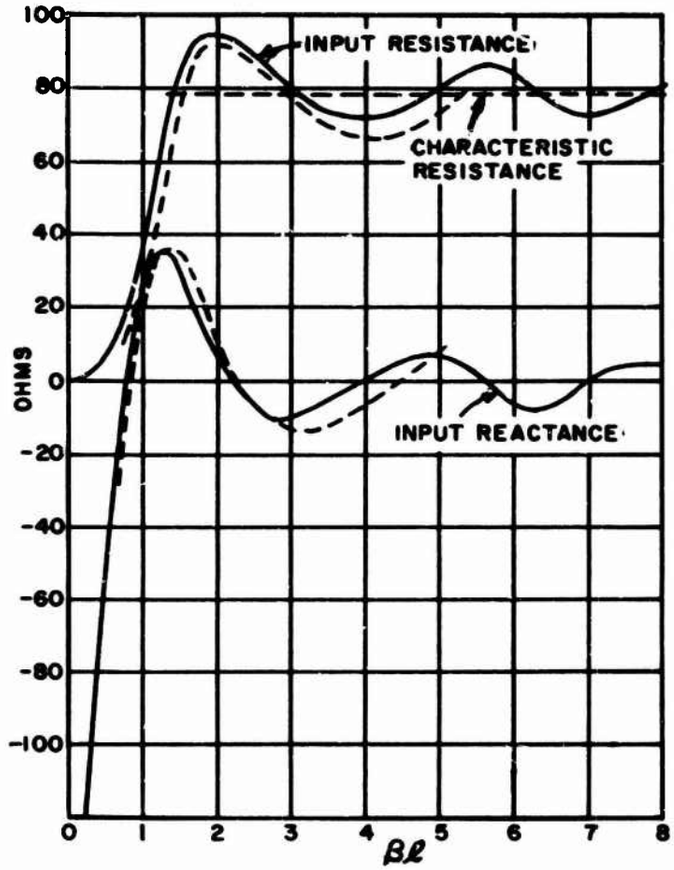

FIG. 3.16 INPUT RESISTANCE AND REACTANCE VERSUS THE PARAMETER $\beta\ell$ FOR $\theta_0 = 30°$. SOLID LINE INDICATES CALCULATED VALUES; BROKEN LINE, MEASURED VALUES.

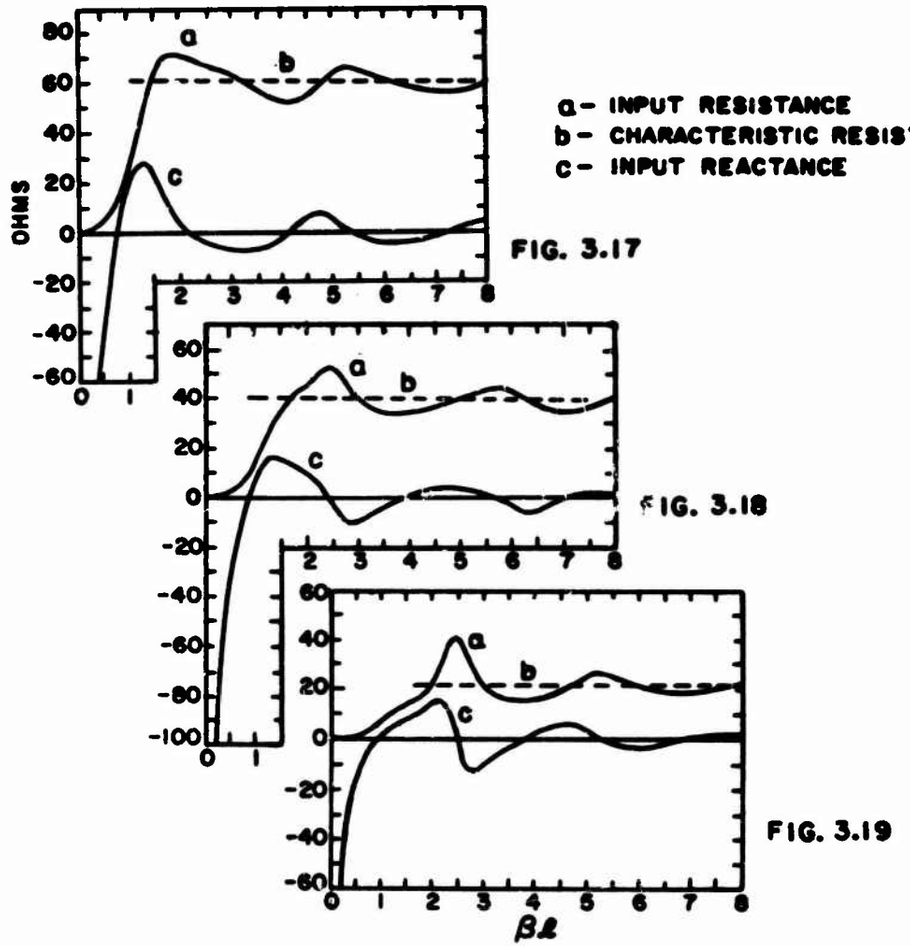

a – INPUT RESISTANCE
b – CHARACTERISTIC RESISTANCE
c – INPUT REACTANCE

FIG. 3.17 INPUT RESISTANCE AND REACTANCE VERSUS $\beta\ell$ FOR $\theta_0 = 40°$.

FIG. 3.18 INPUT RESISTANCE AND REACTANCE VERSUS $\beta\ell$ FOR $\theta_0 = 55°$.

FIG. 3.19 INPUT RESISTANCE AND REACTANCE VERSUS $\beta\ell$ FOR $\theta_0 = 70°$.

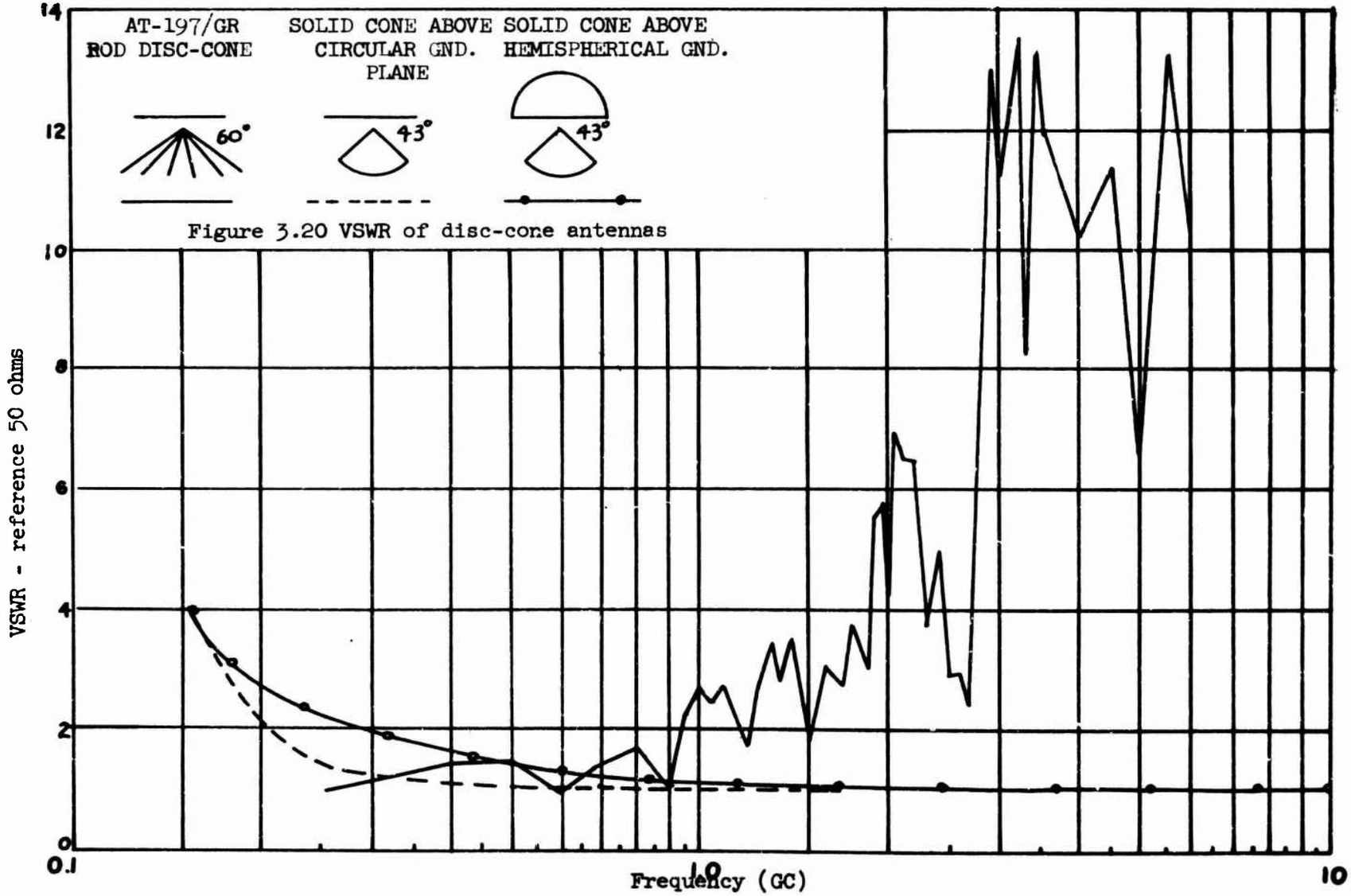

Figure 3.20 VSWR of disc-cone antennas

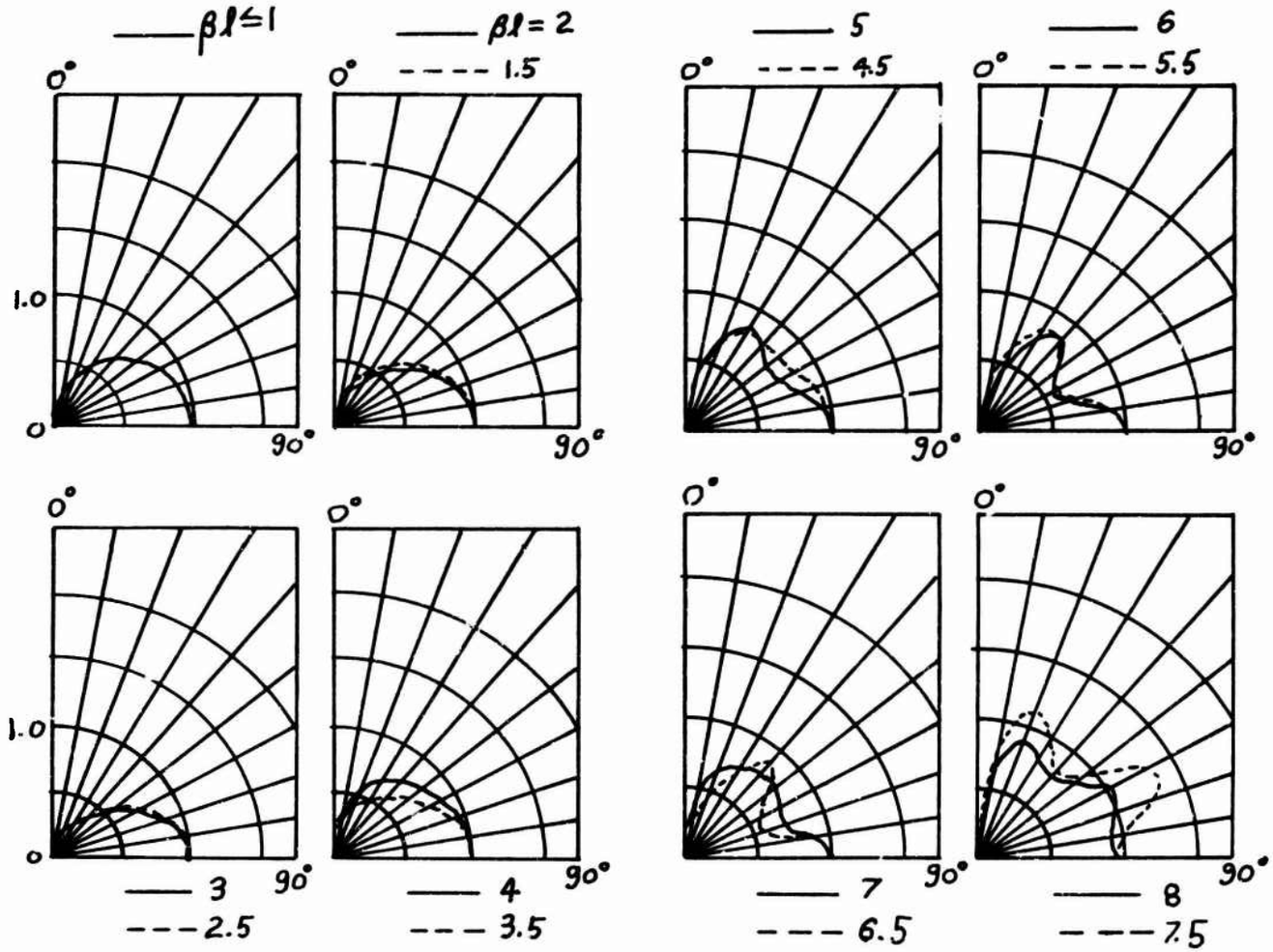

Figure 3.21 Plots of the magnitude of the far-zone electric field for various values of $\beta\ell$

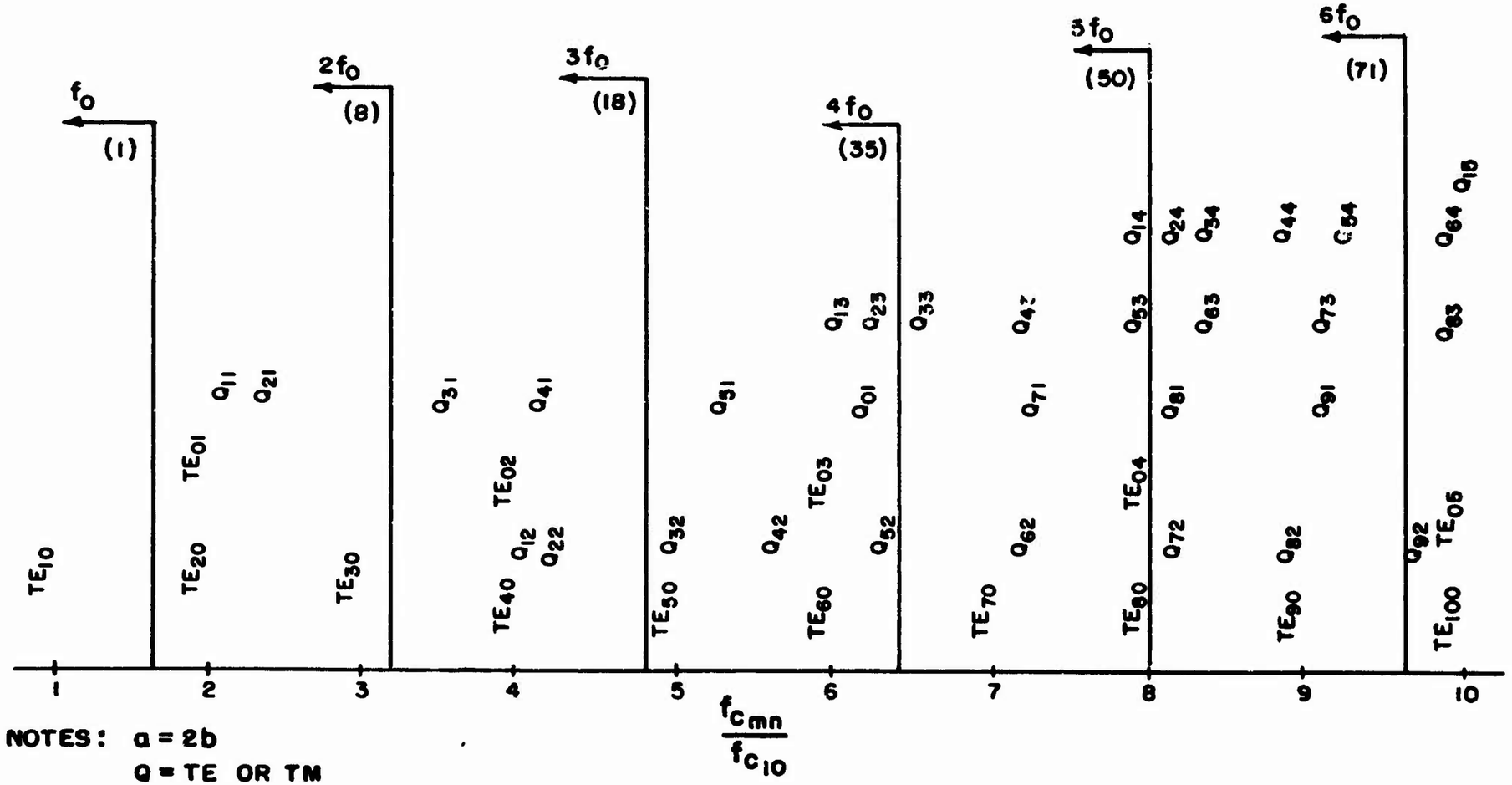

Figure 4.1 Relative cutoff frequencies of various modes for 2:1 rectangular waveguide

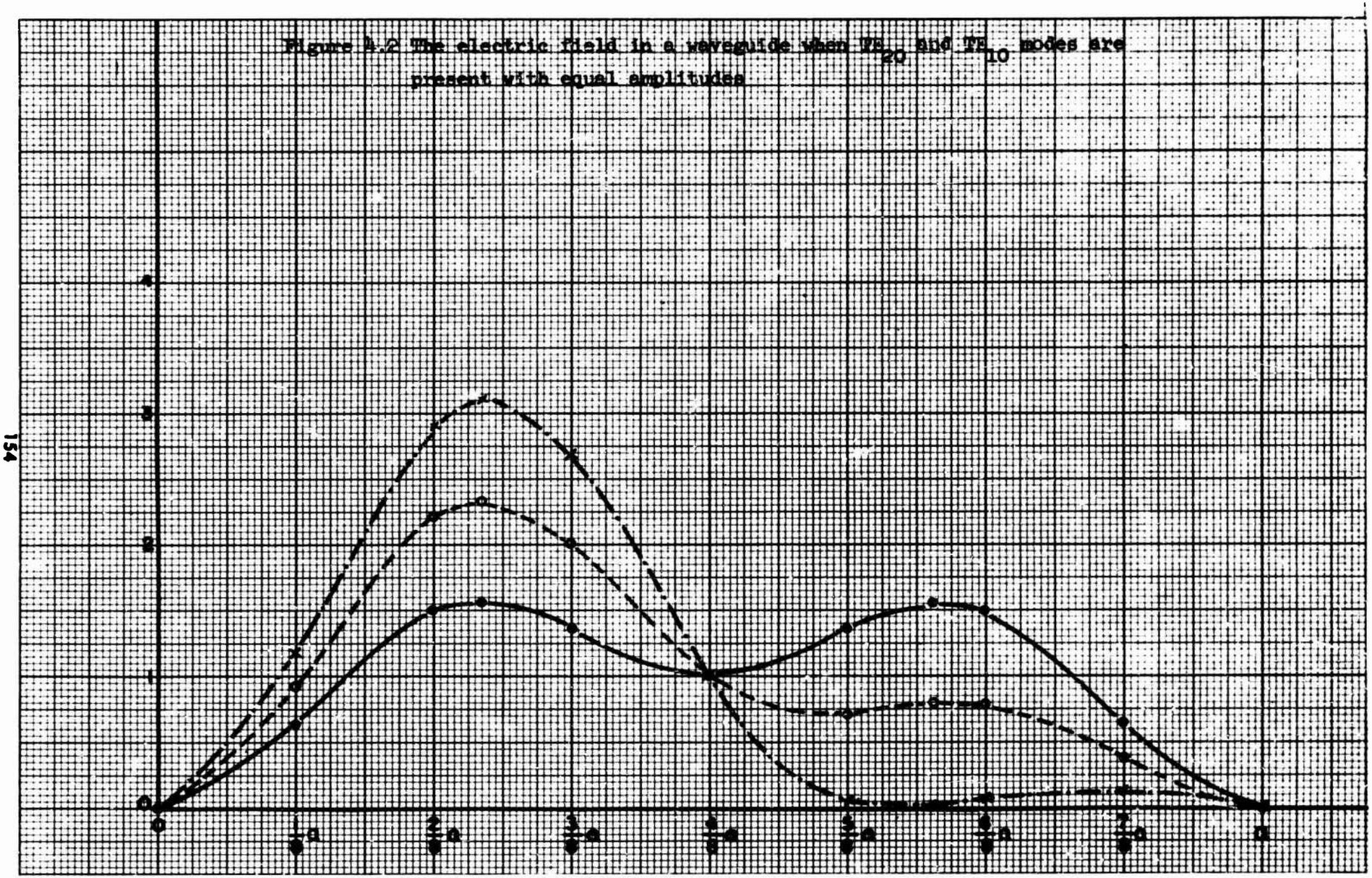

Figure 4.2 The electric field in a waveguide when TE_{20} and TE_{10} modes are present with equal amplitudes

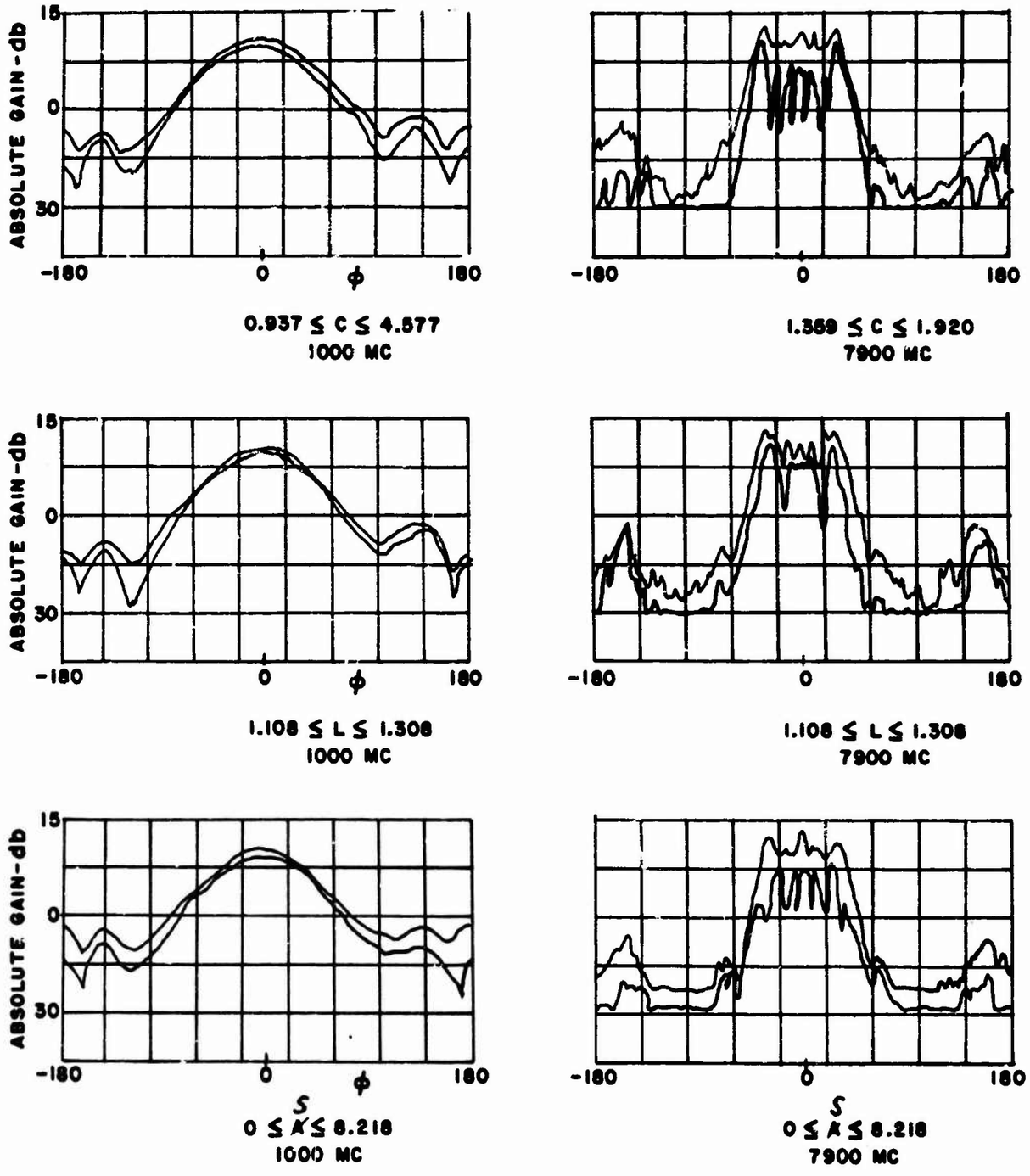

Figure 4.3 Pattern variations of an L-band horn due to variations of critical parameters

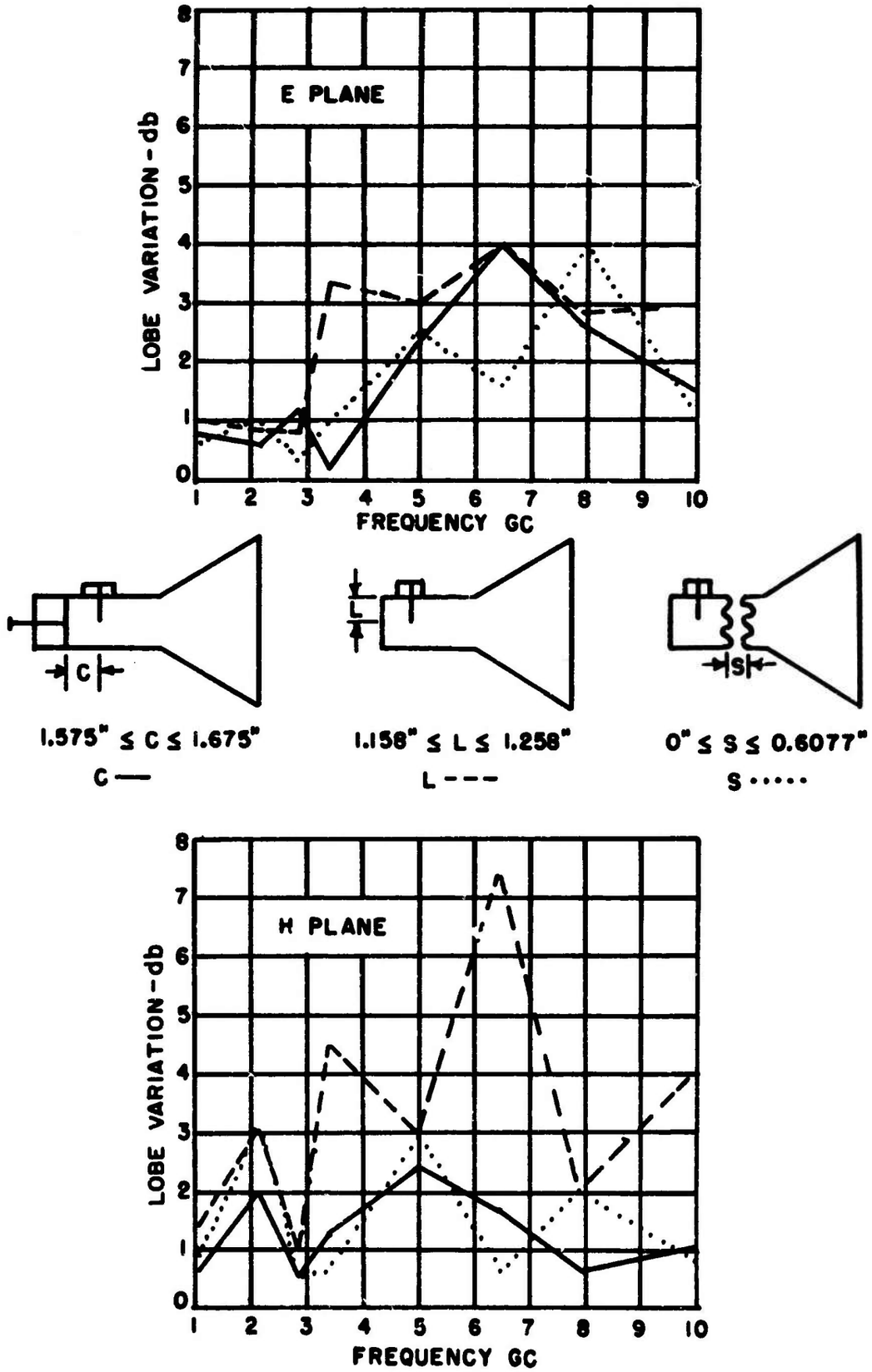

Figure 4.4 Major lobe variations resulting from parameter changes

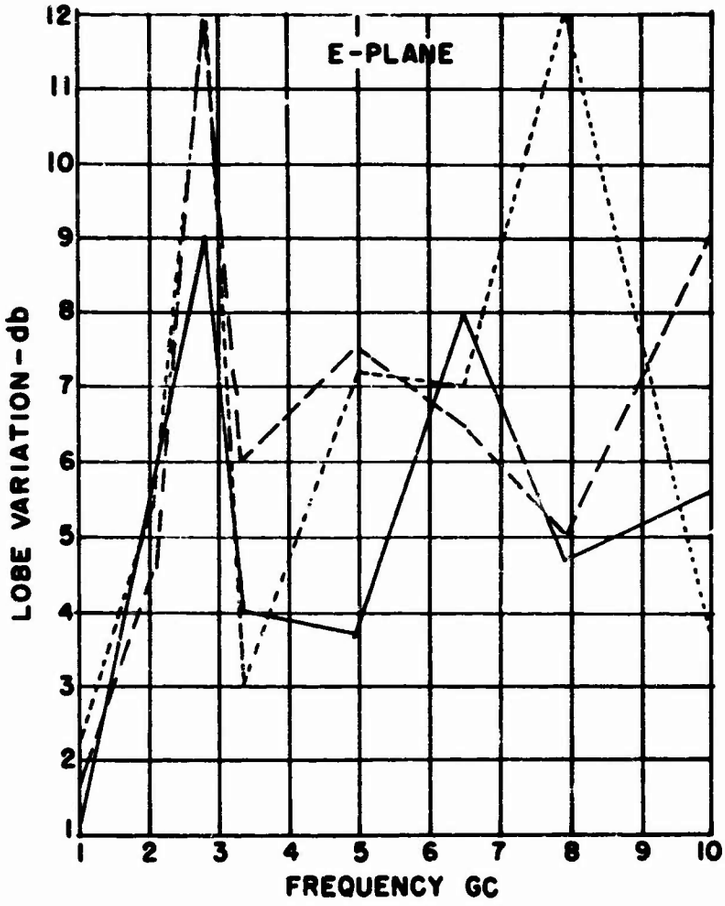

Figure 4.5 Minor lobe variations resulting from parameter changes

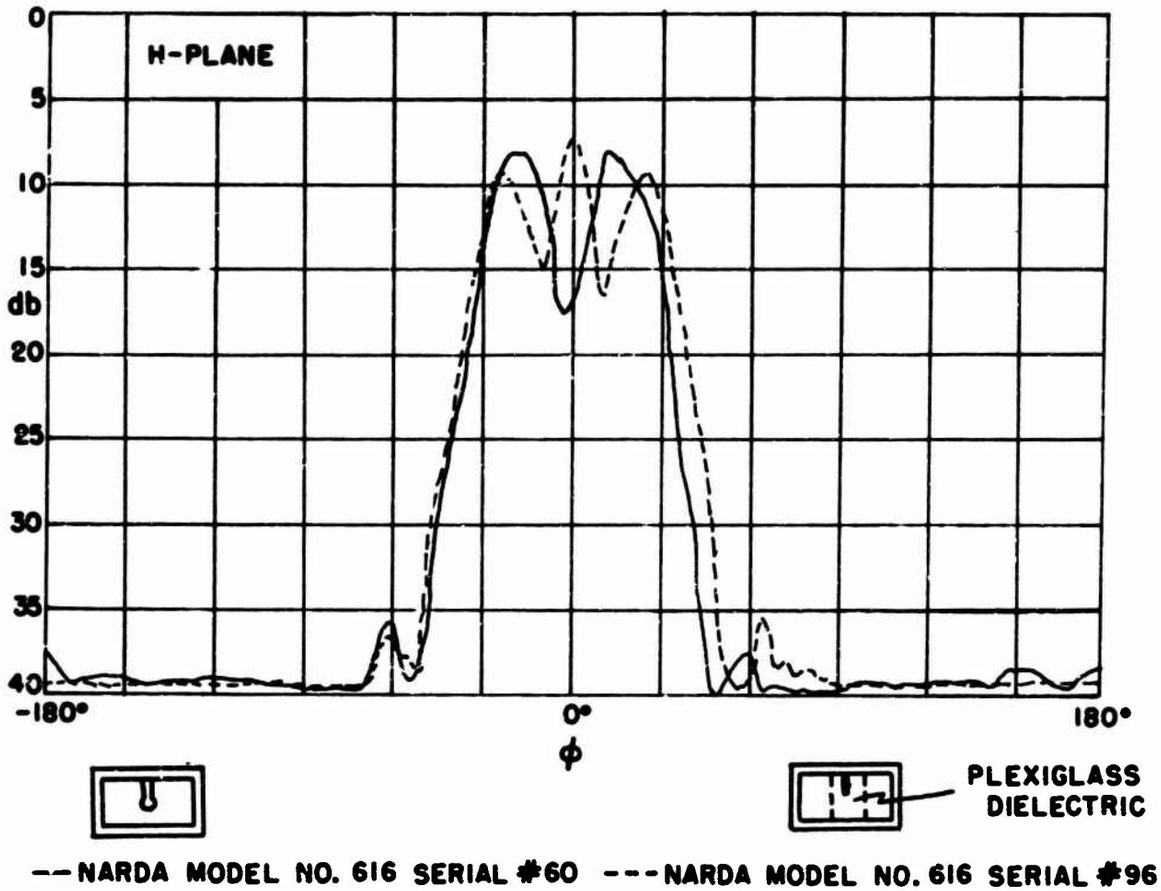

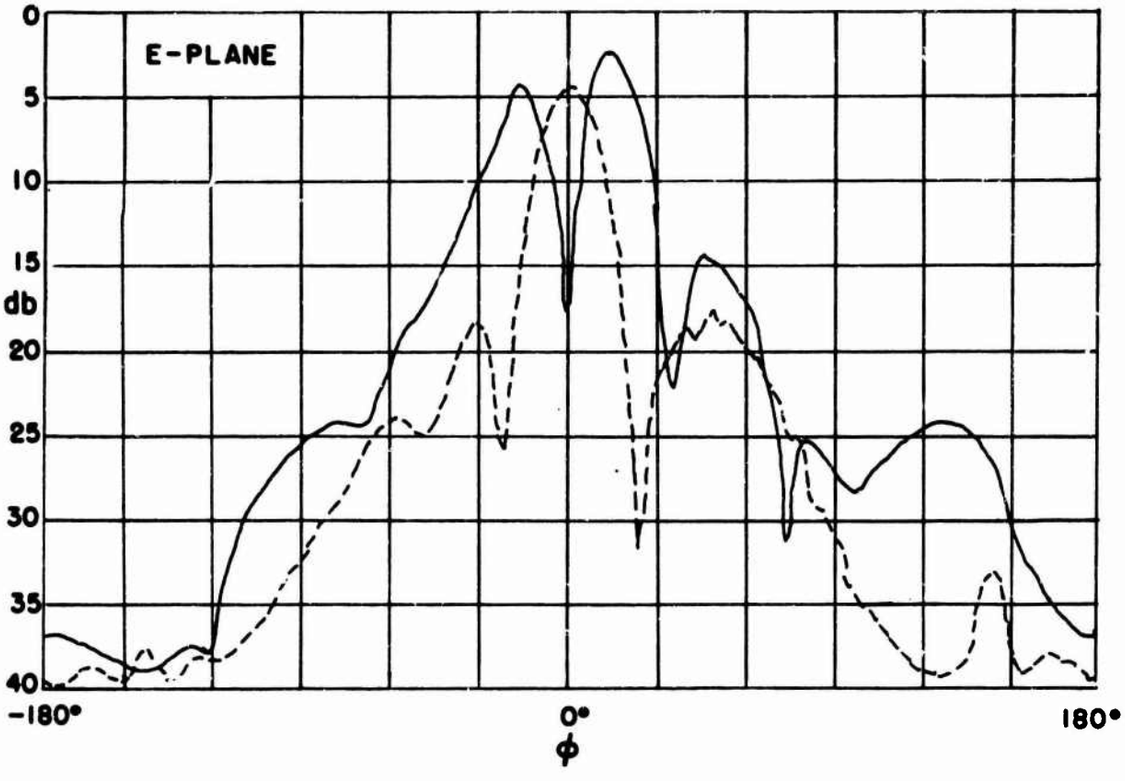

Figure 4.6 Waveguide to coaxial line transducer effect on AN/FPS-8 horn patterns

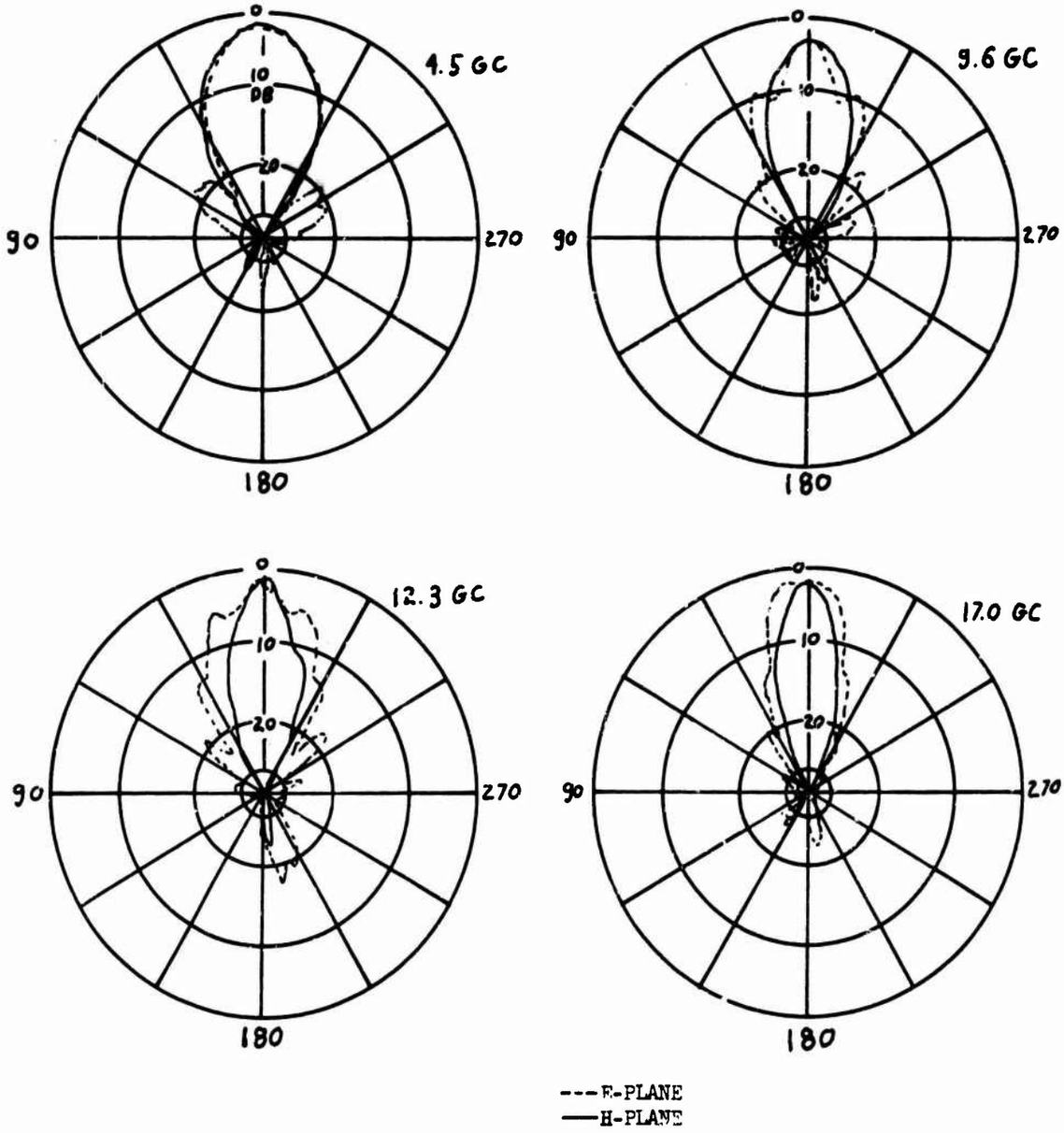

Figure 4.7 Radiation patterns of a linearly polarized S-band sectorial horn for TE_{10} mode propagation

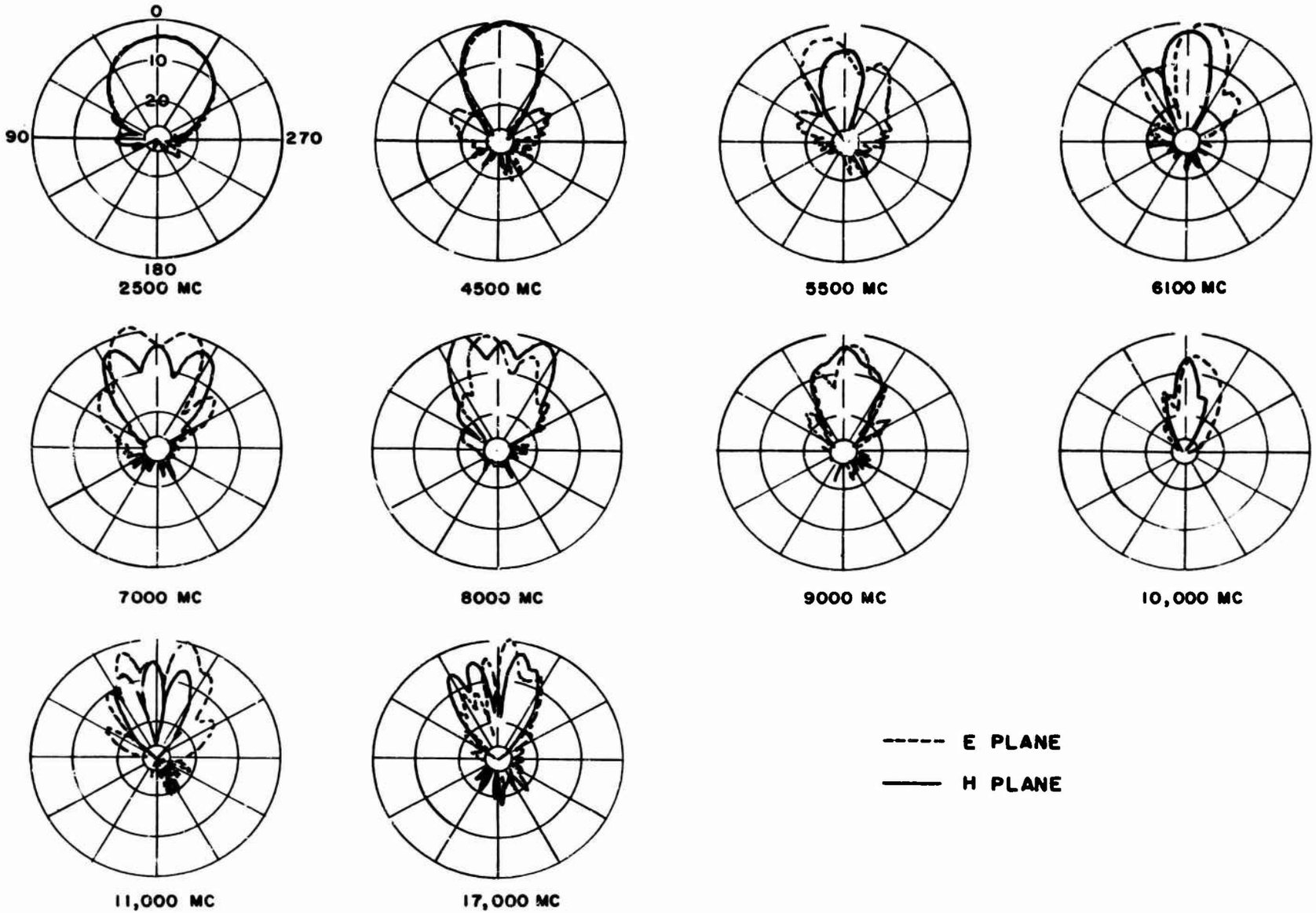

Figure 4.8 Radiation patterns of an S-band linearly polarized horn with higher order modes

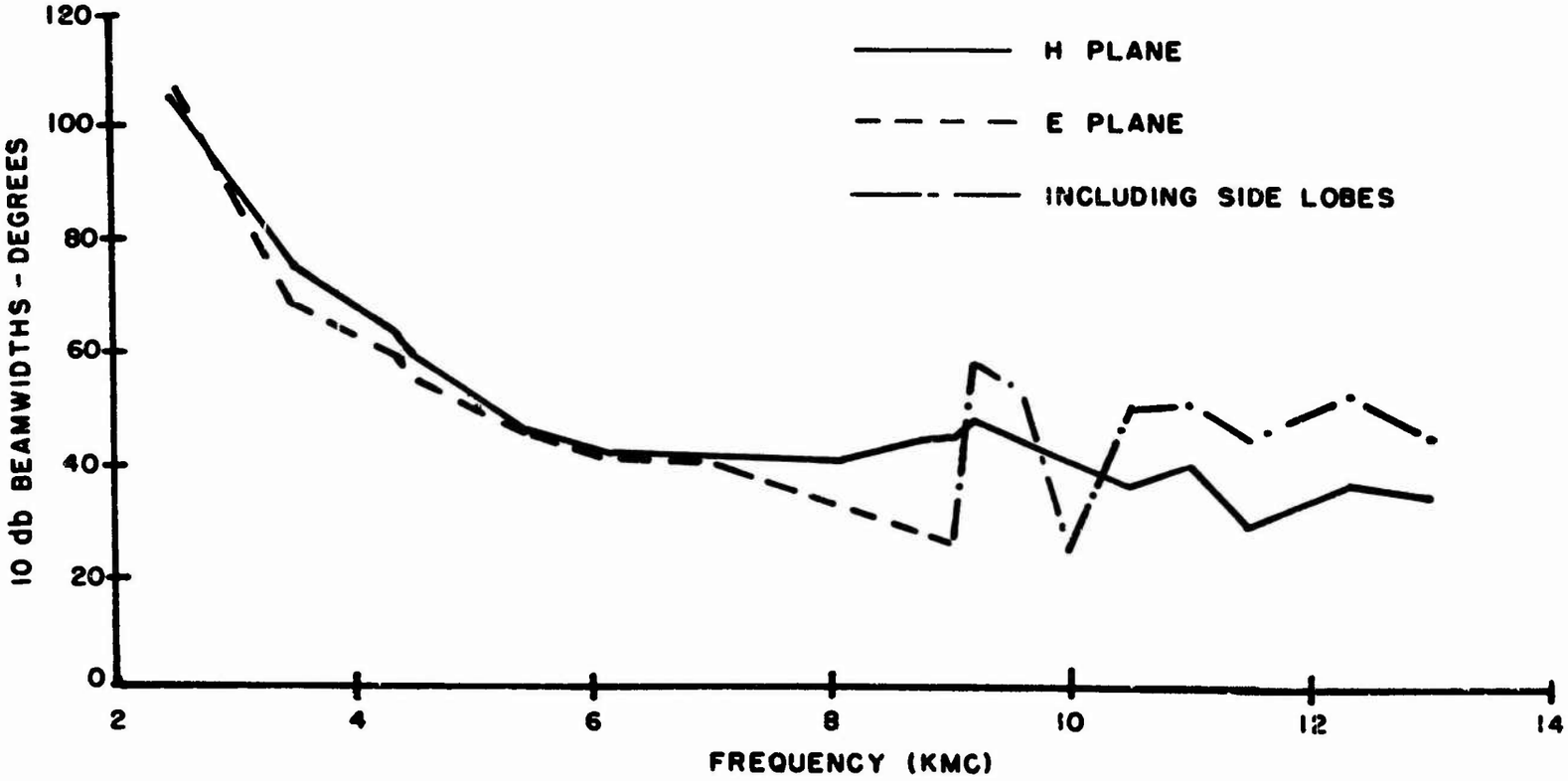

Figure 4.9 Beamwidth vs. frequency for an S-band linearly polarized horn, TE_{10} mode only

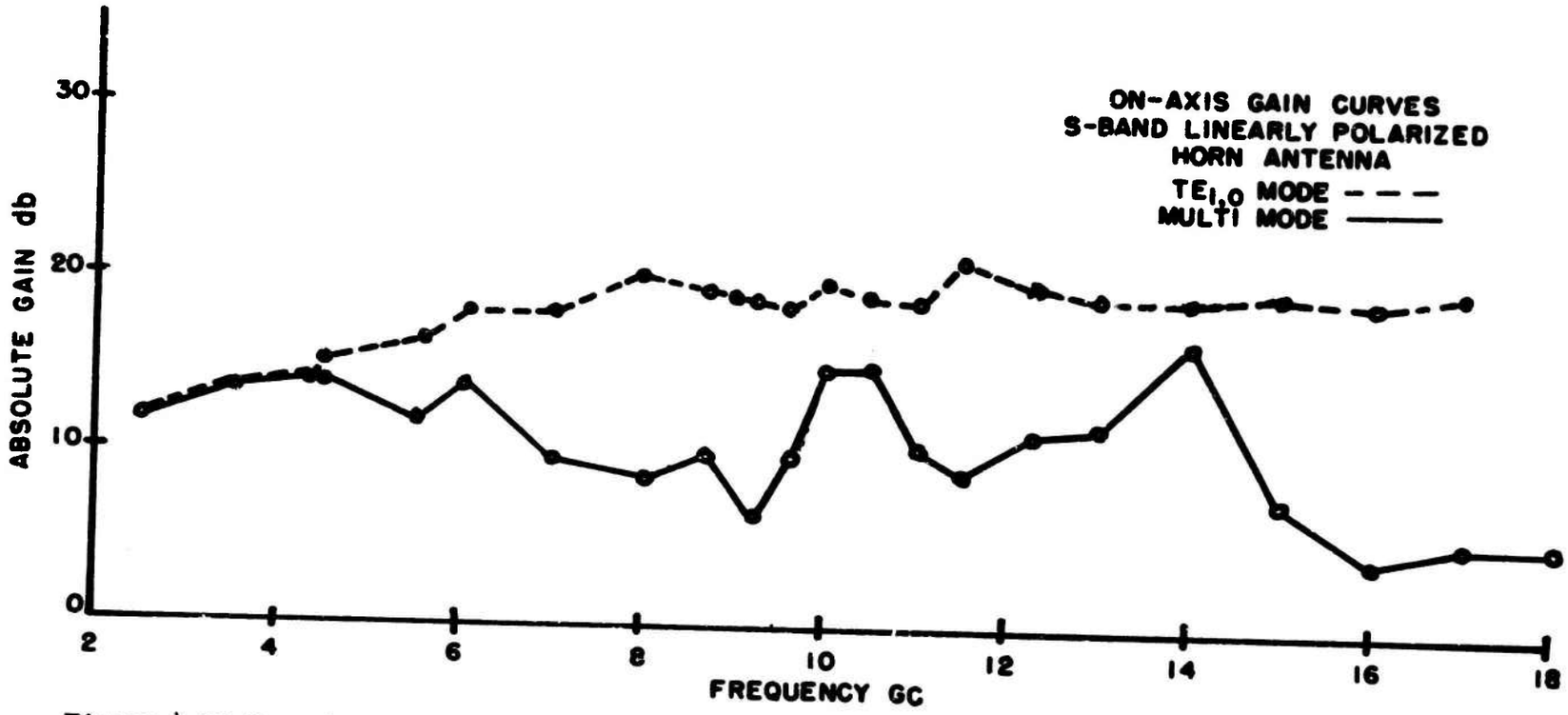

Figure 4.10 On axis gain curves of multi-mode and TE_{10} mode horns

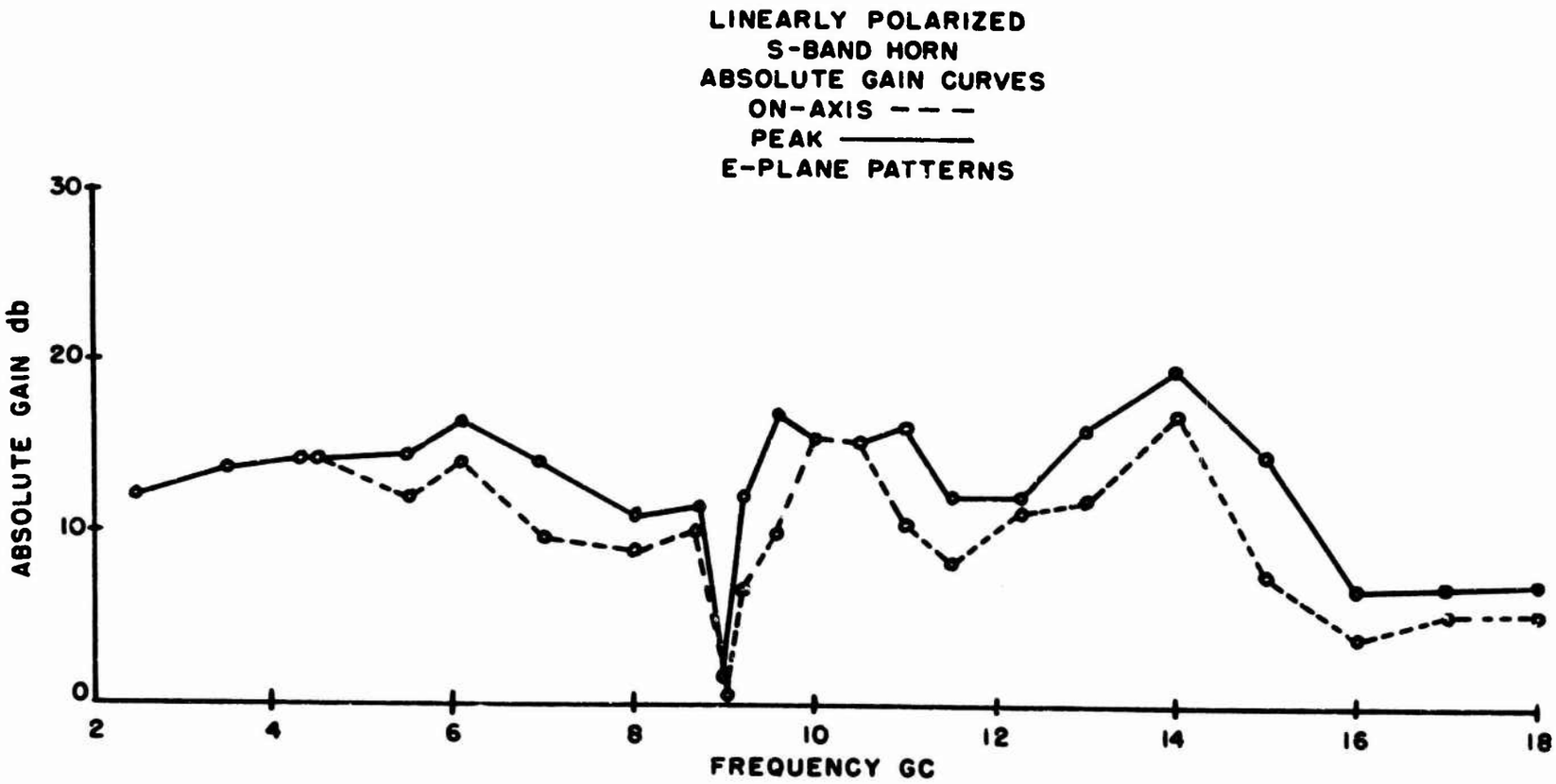

Figure 4.11 On axis and peak gain curves for S-band multi-mode horn(E-plane)

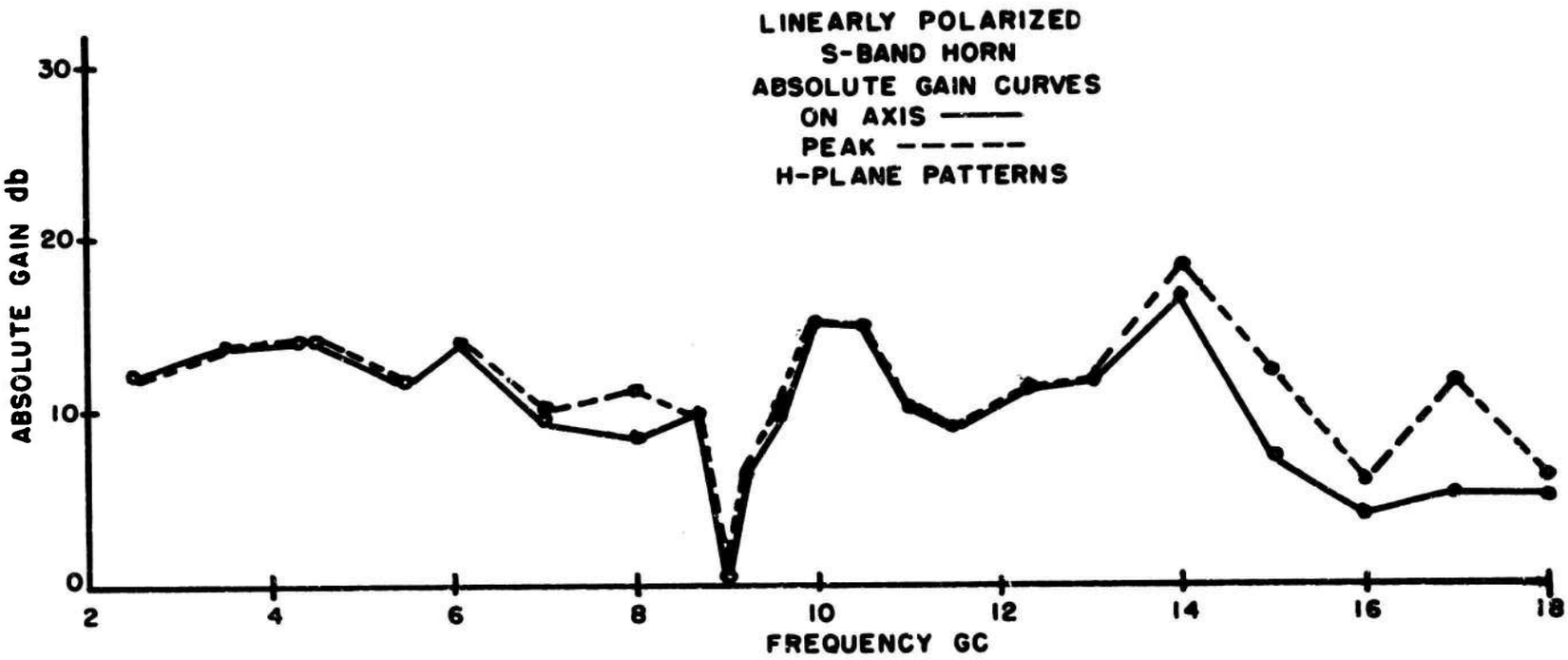

Figure 4.12 On axis and peak gain curves for S-band multi-mode horn(H-plane)

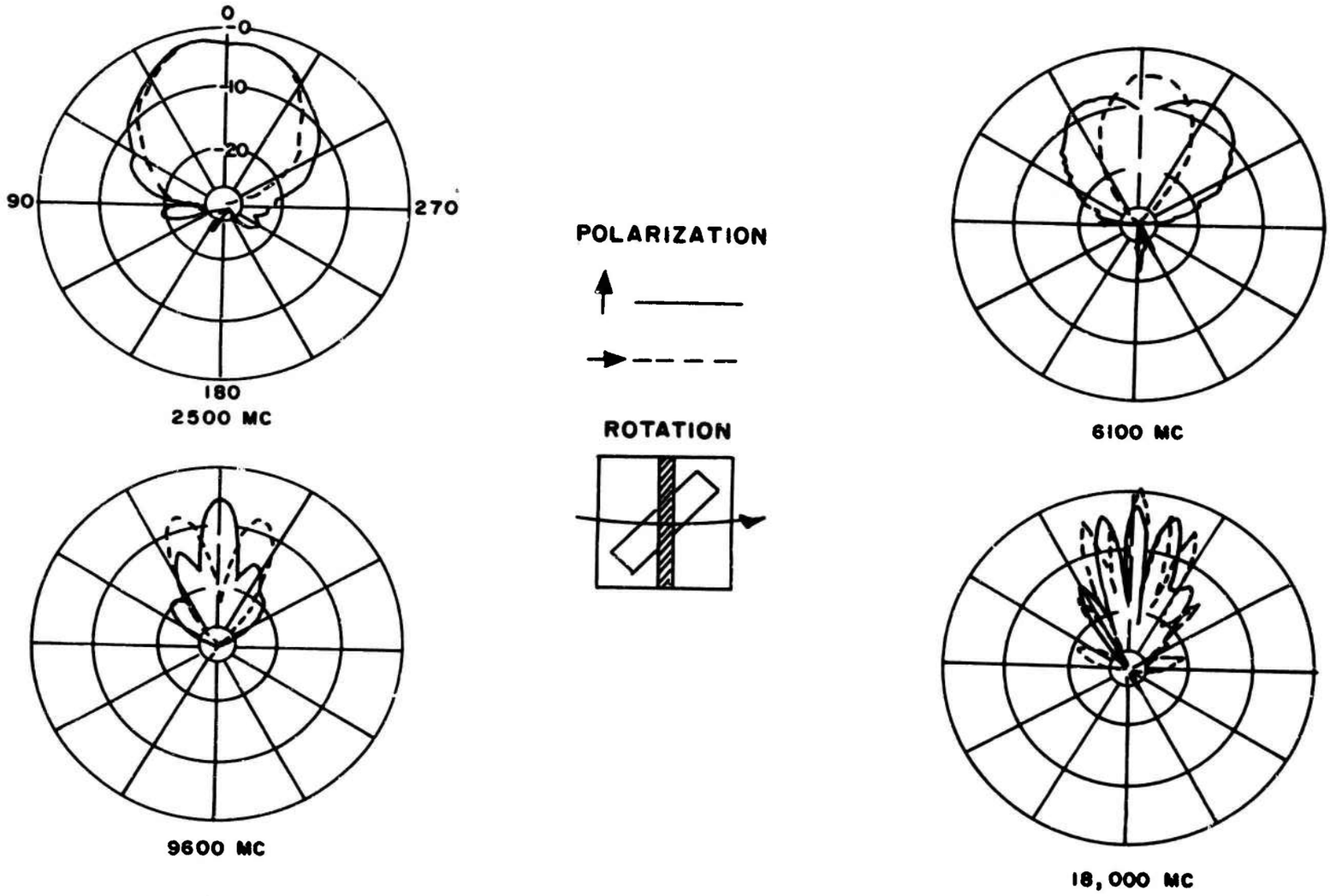

Figure 4.13 Typical radiation patterns of the S-band circularly polarized horn (TE_{10} mode excited in rectangular waveguide section)

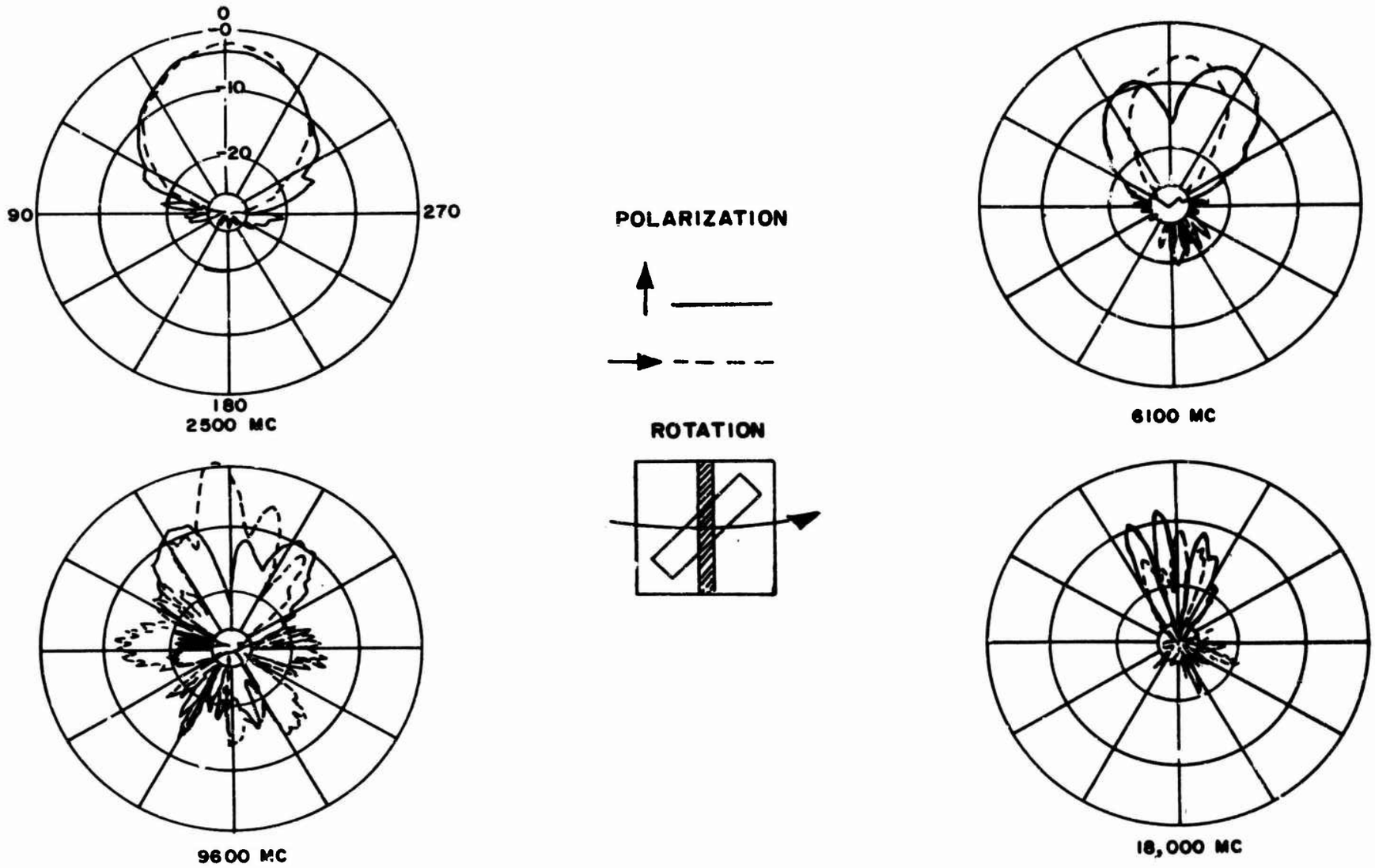

Figure 4.14 Typical radiation patterns of the S-band circularly polarized horn(higher order modes)

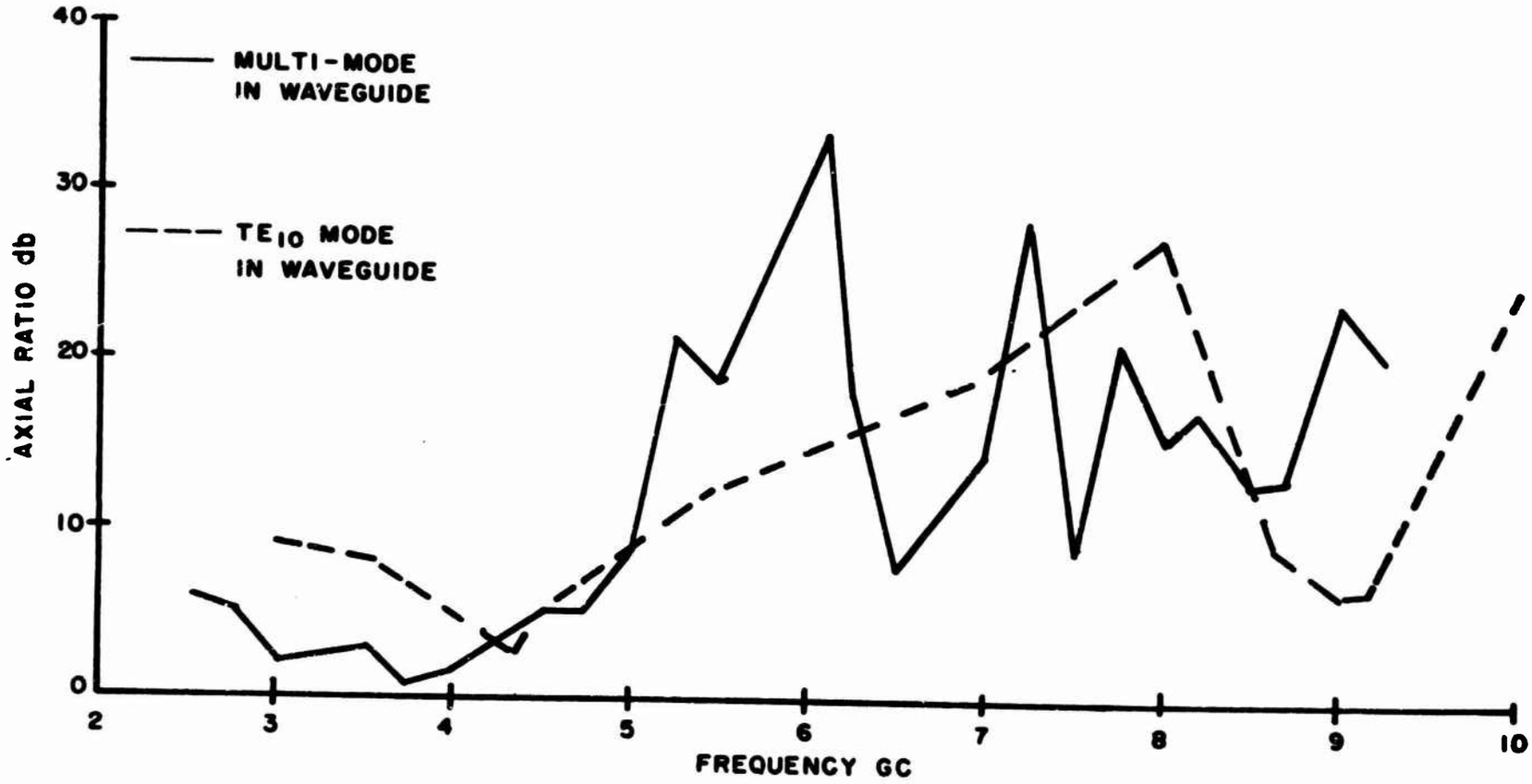

FIGURE 4.15 Axial Ratio Measurements of the Circularly Polarized Horn

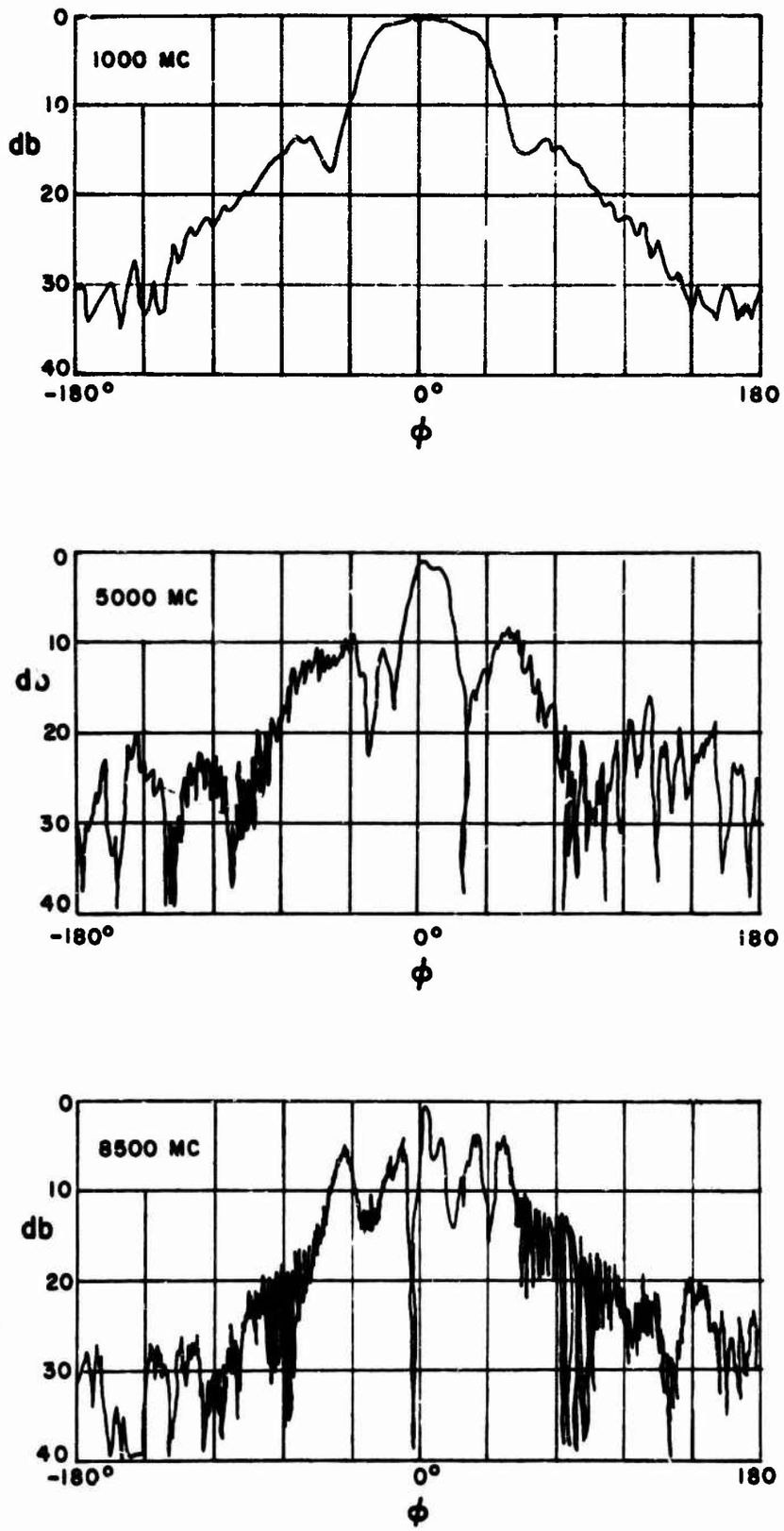

FIGURE 4.16 Primary Radiation Patterns of the AN/FPS-8 Antenna (E-Plane)

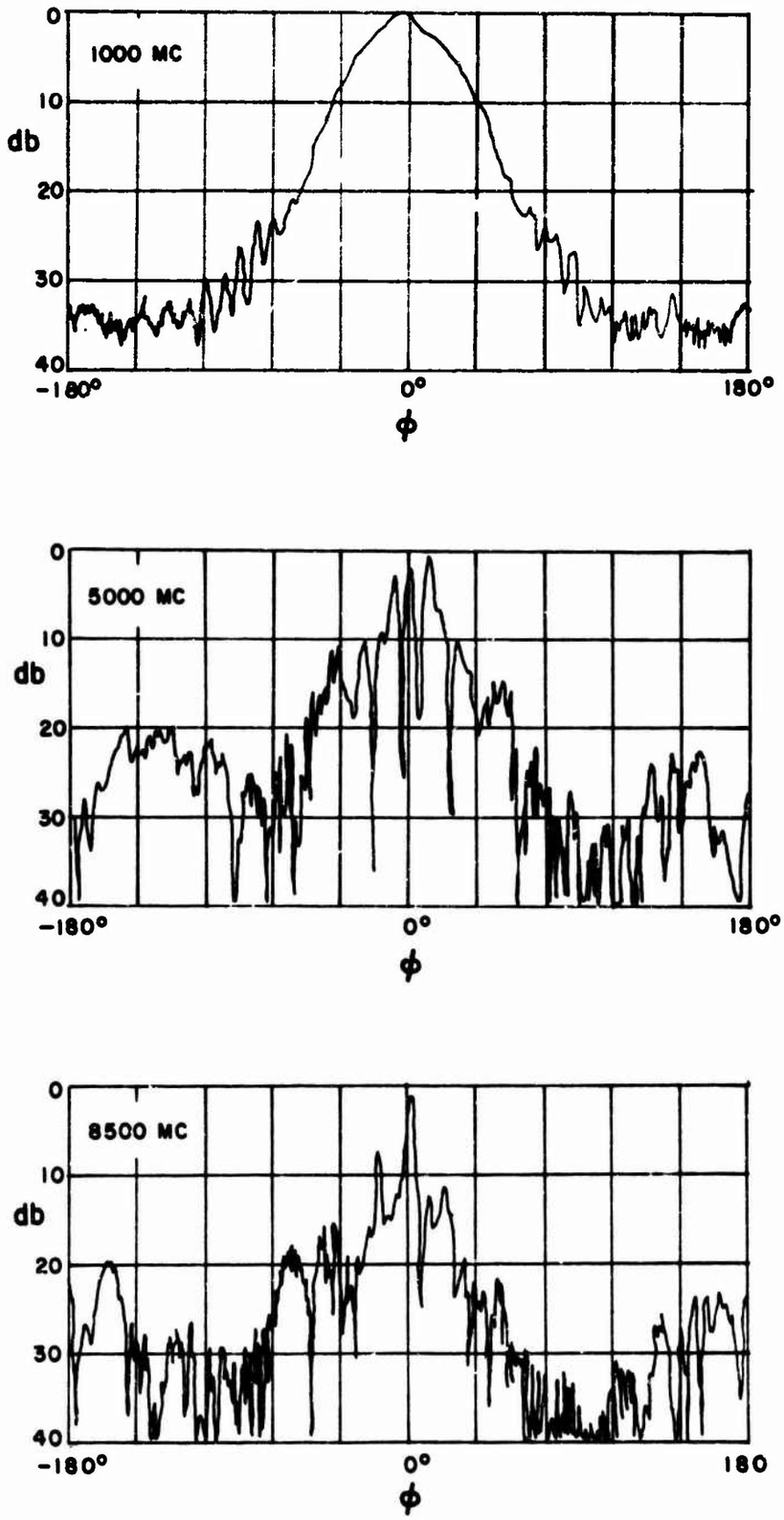

FIGURE 4.17 Primary Radiation Patterns of the AN/FPS-8 Antenna (H-Plane)

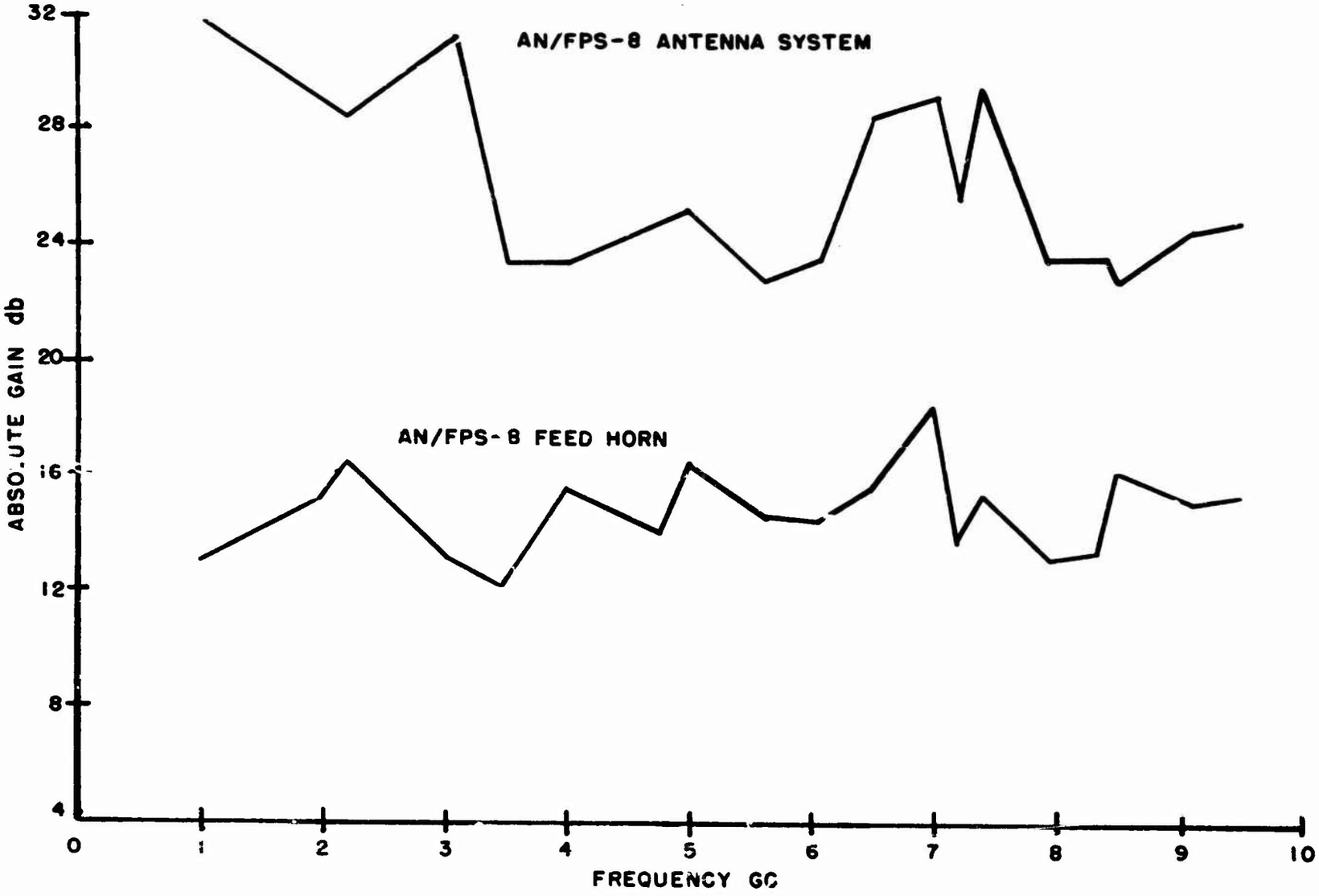

FIGURE 4.18a Gain Comparison of AN/FPS-8 Feed Horn and AN/FPS-8 Antenna System

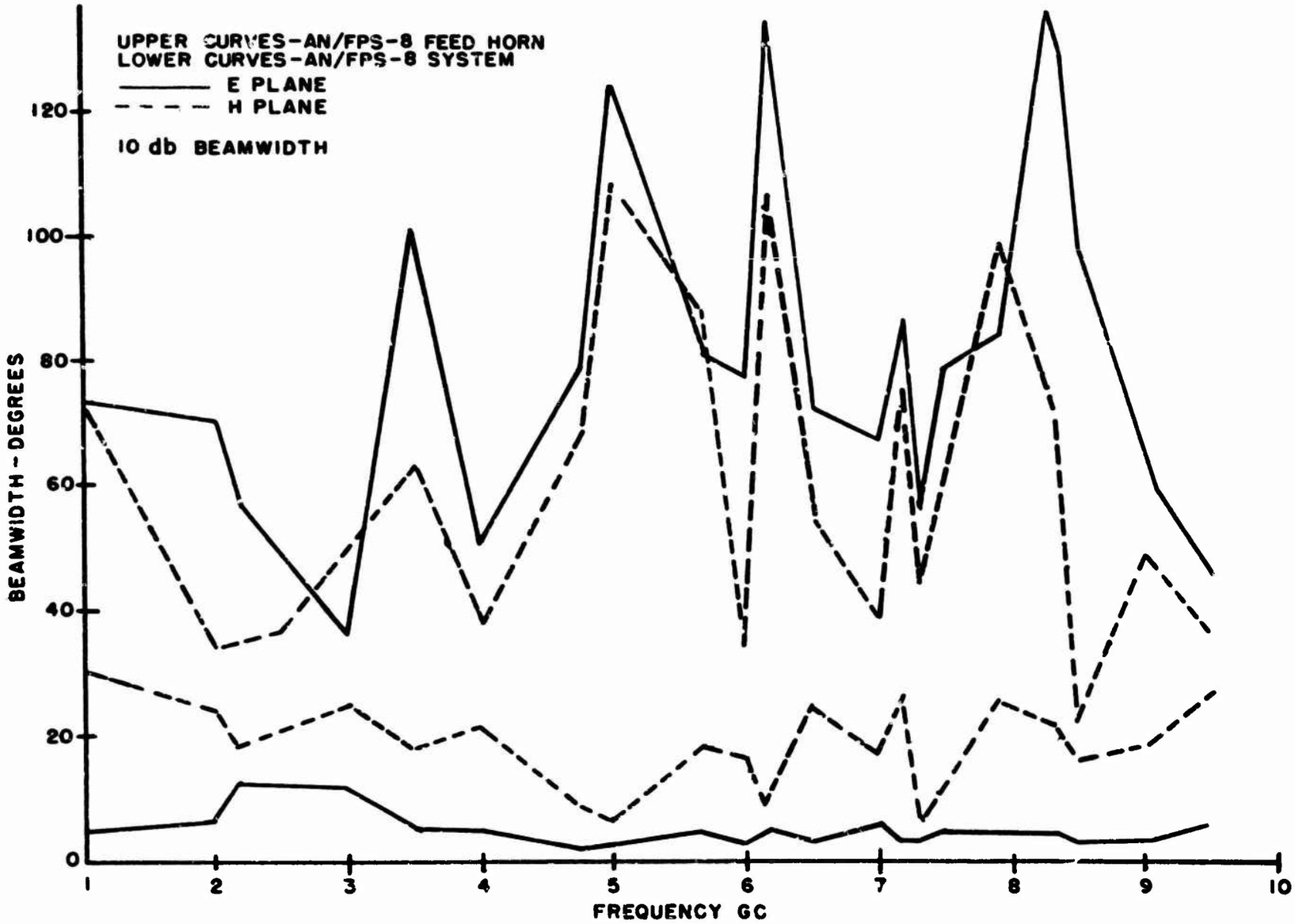

FIGURE 4.18b Beamwidth Comparison of AN/FPS-8 Feed Horn and AN/FPS-8 System at the 10-DB Level

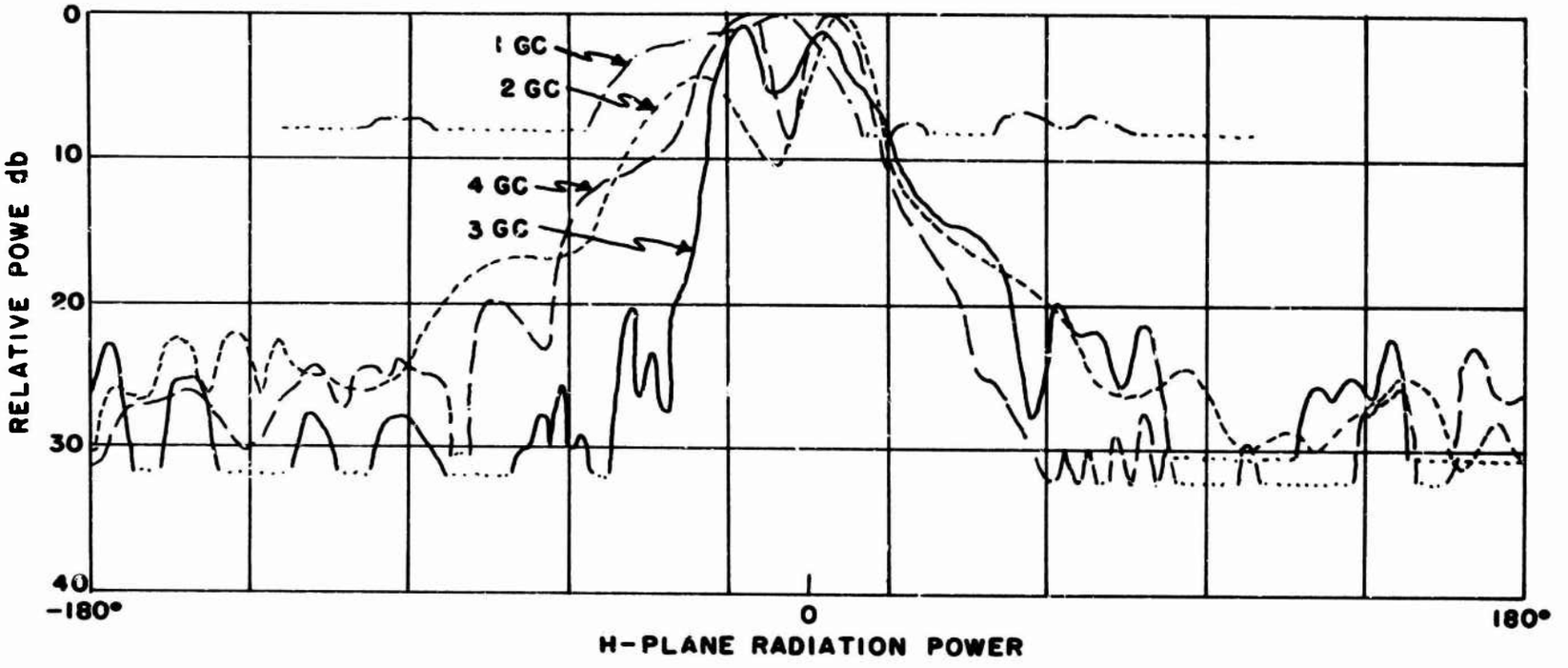

FIGURE 4.19 EXPONENTIAL HORN AT-316, H-Plane Radiation Power Patterns, Horizontal Polarization with UG-953/U Transducer

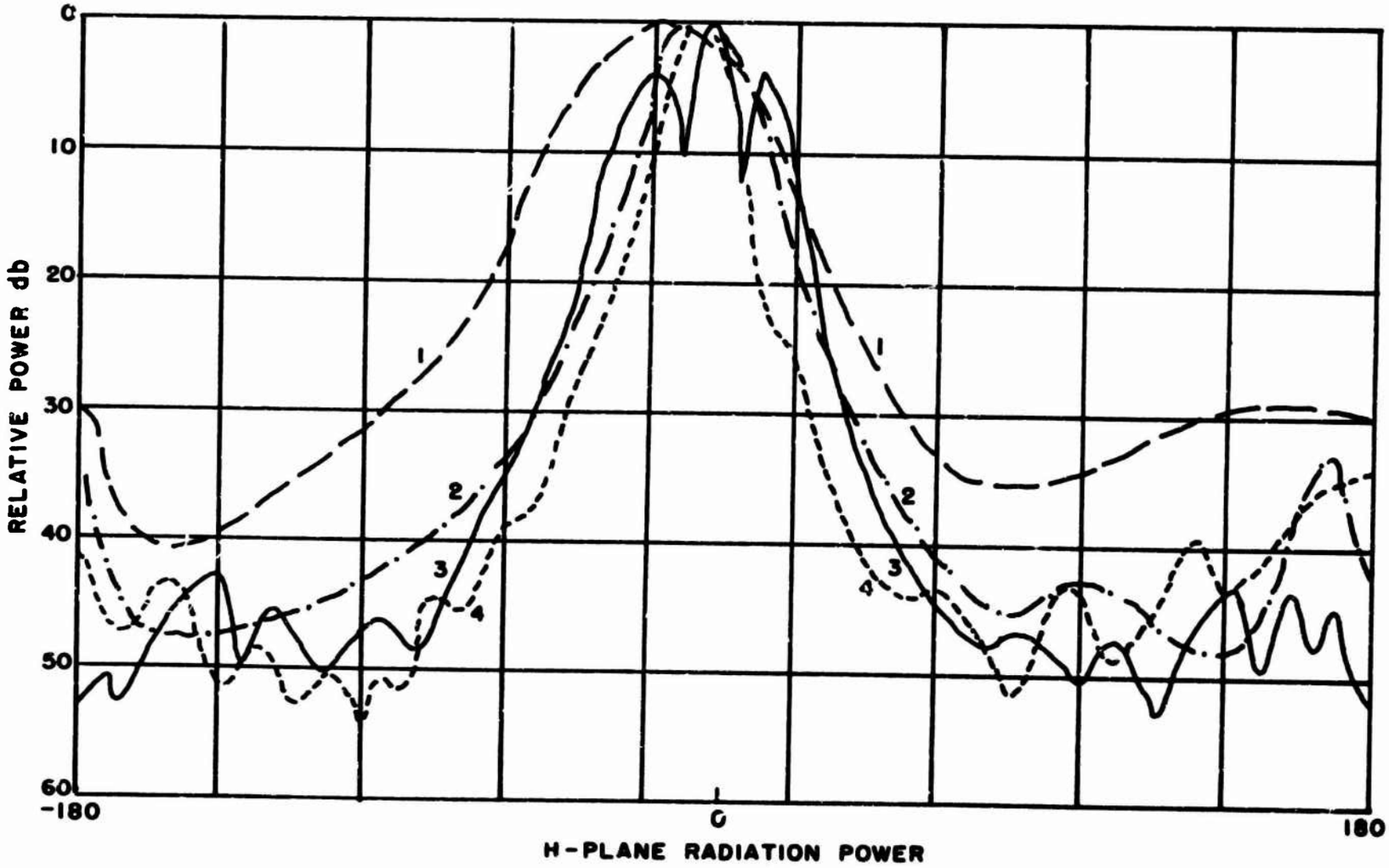

FIGURE 4.20 Exponential Horn AT-316, Plane Radiation Power Patterns, Vertical Polarization with UG-953/U Transducer

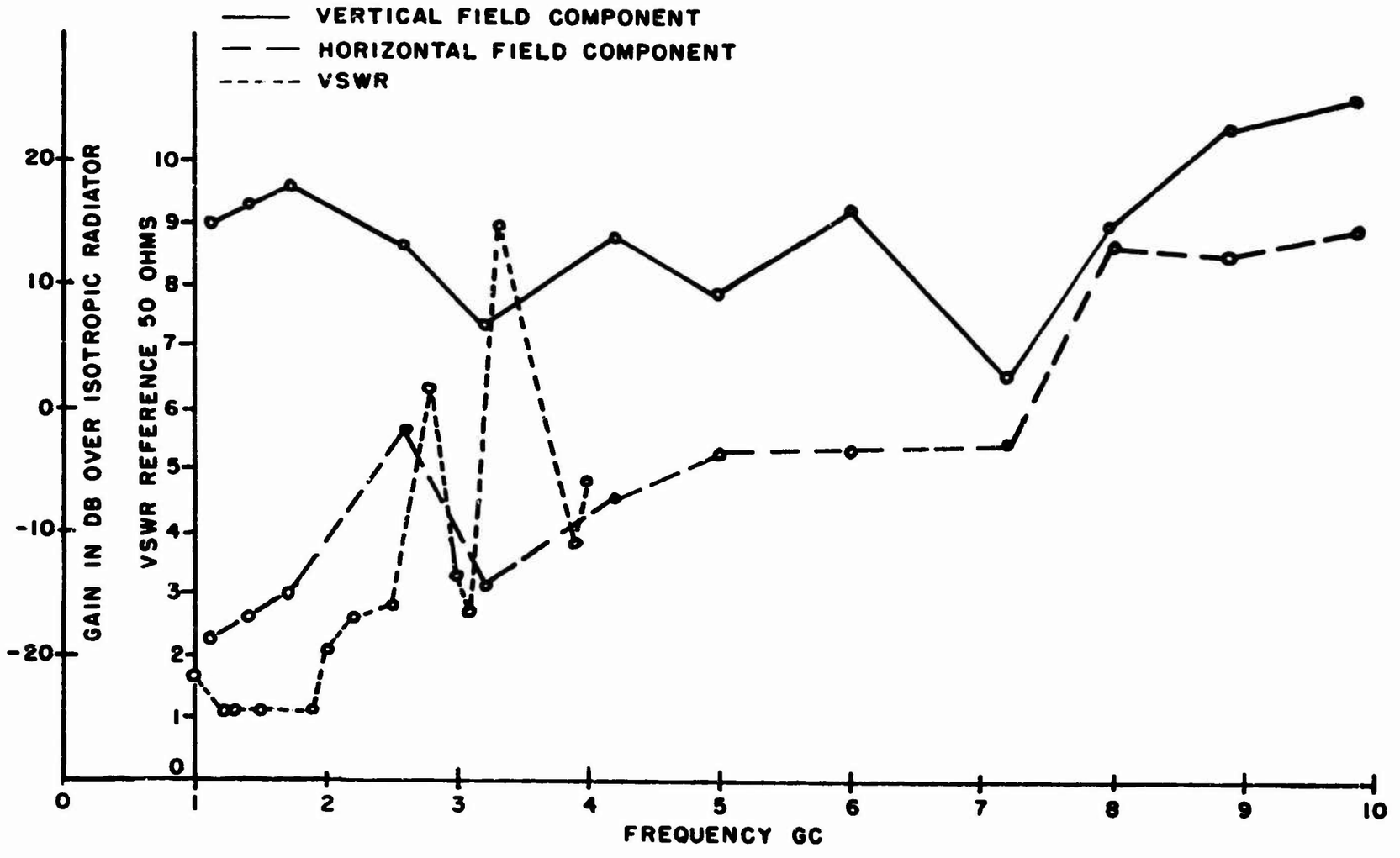

FIGURE 4.21 Gain and VSWR of AT-316 Horn Antenna with UG-953/U Transducer

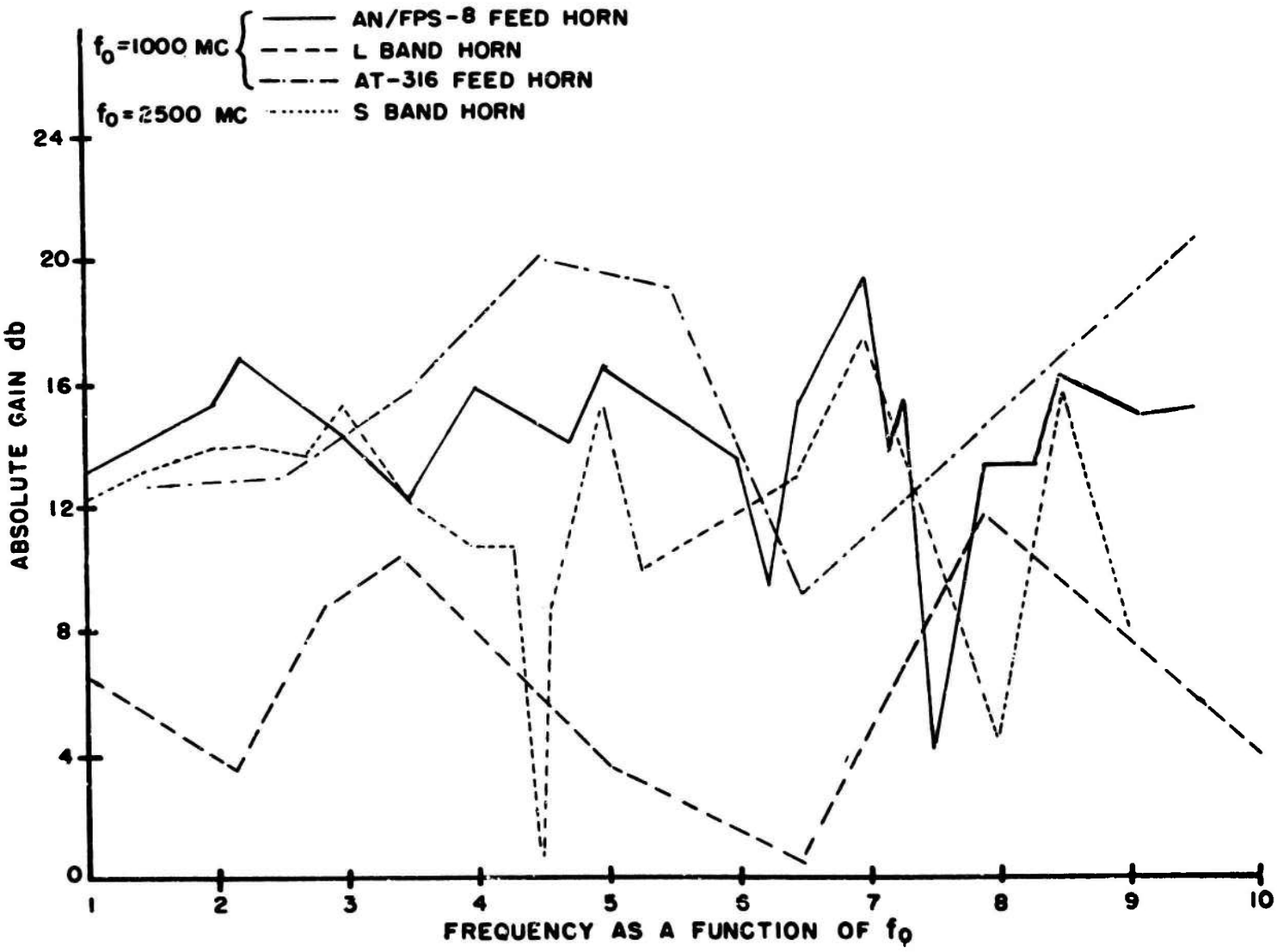

FIGURE 4.22 Comparison of Gain Curves Measured on Several Horn Type Antennas

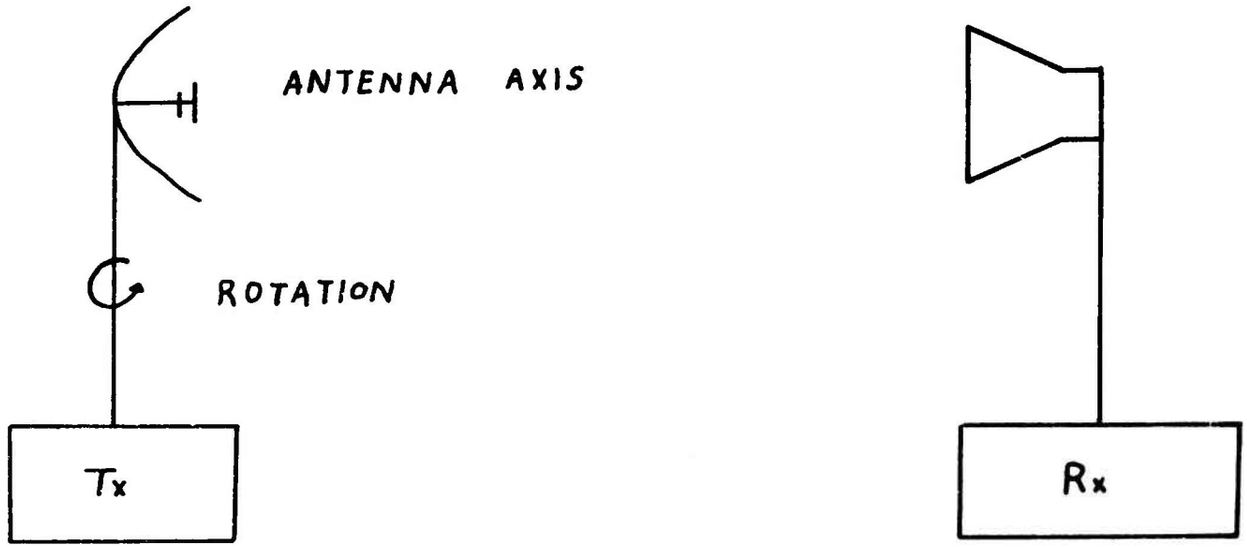

FIGURE 4.23 TYPICAL ANTENNA PATTERN TEST SET-UP

FIGURE 4.24 644 Horn with S281A Transducer

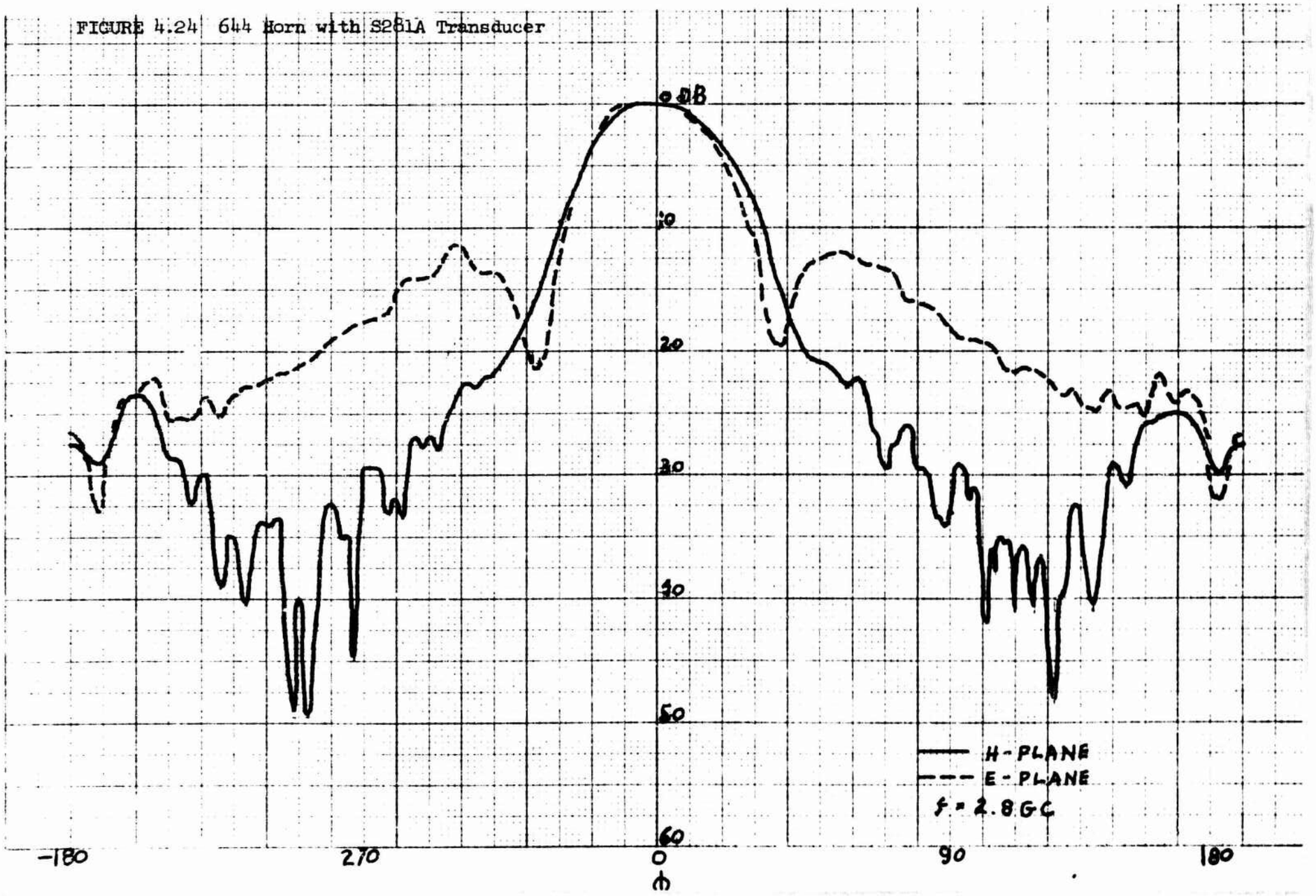

FIGURE 4.25 6dB Horn, SC81A Transducer

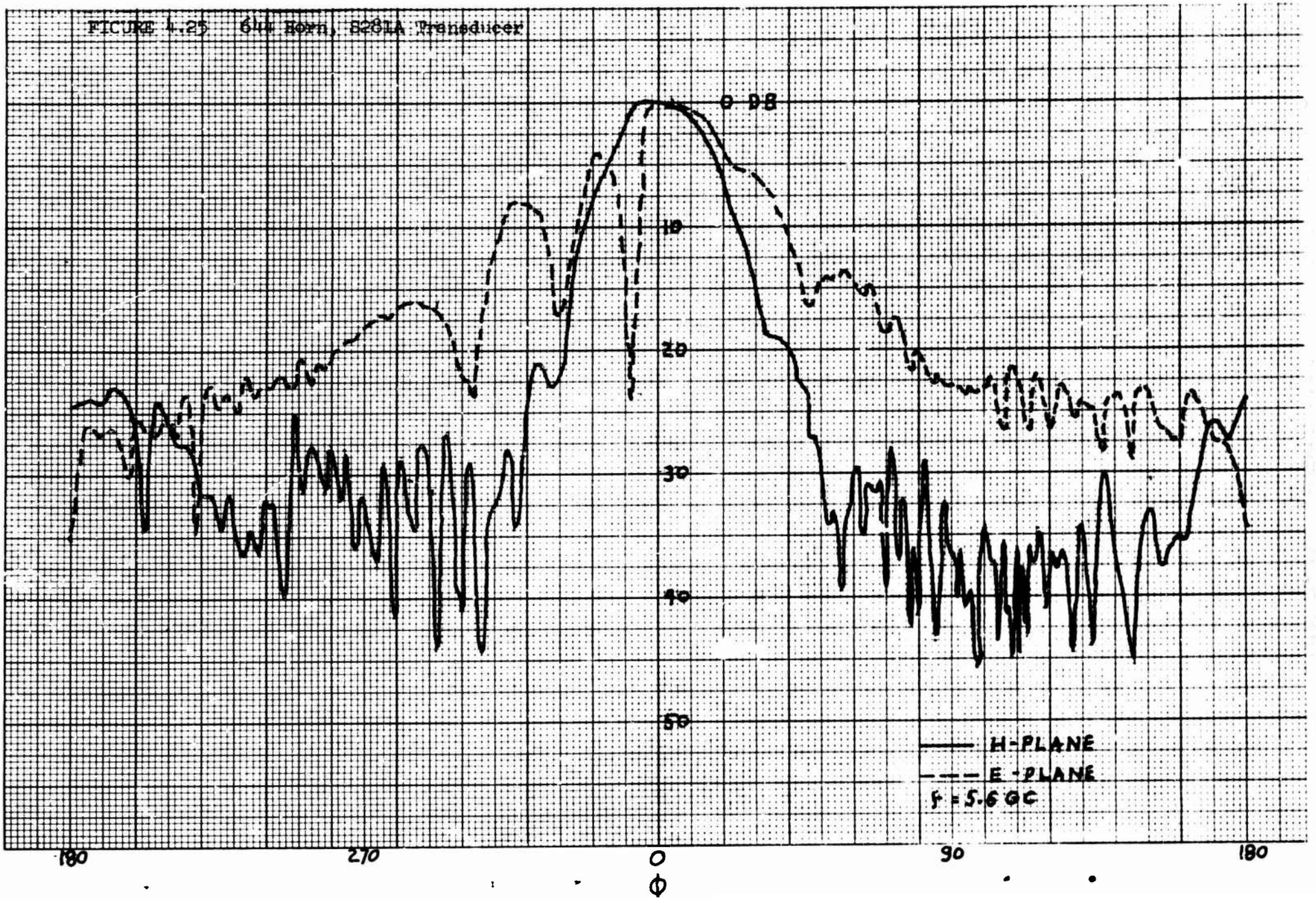

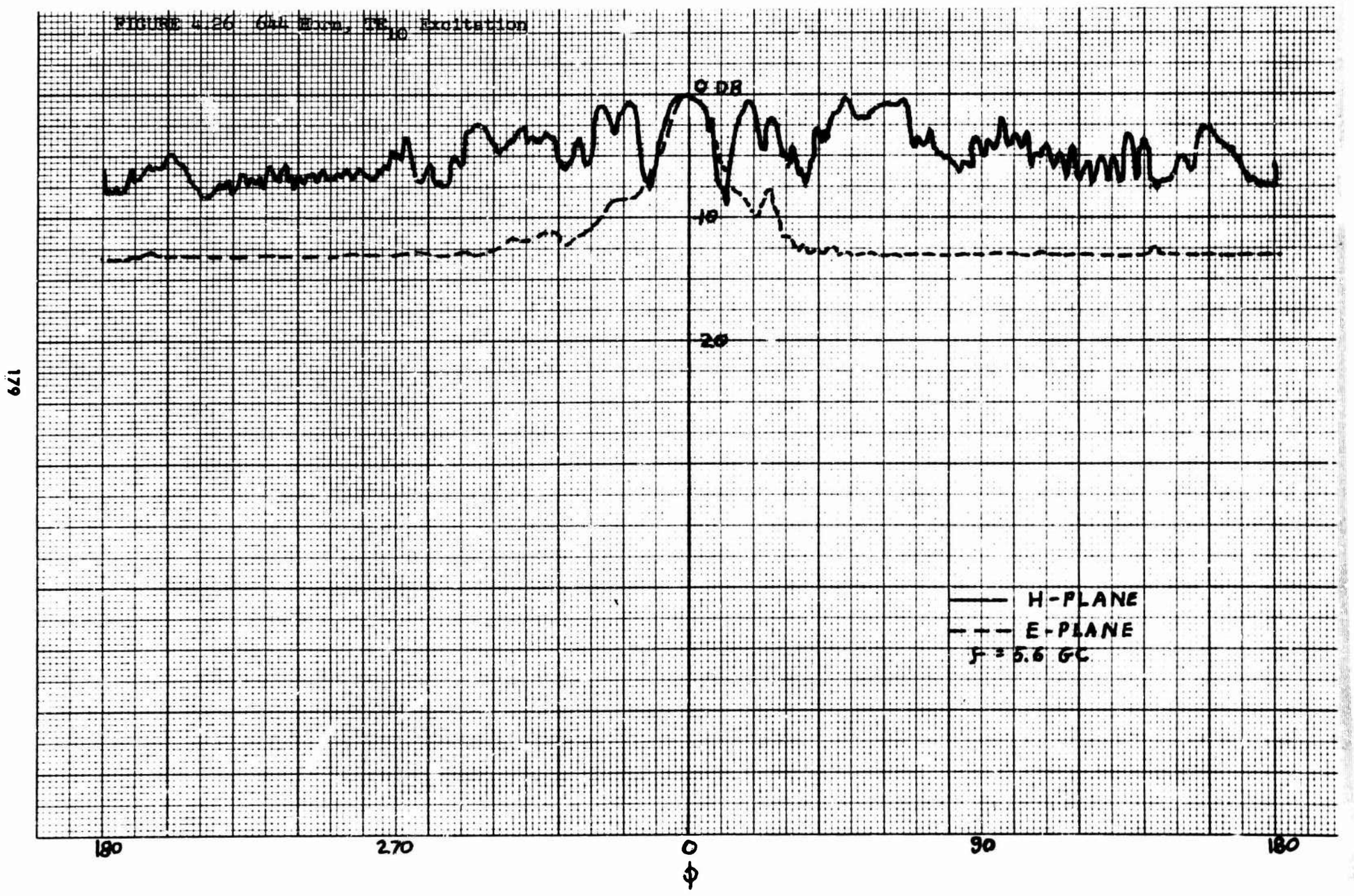
FIGURE 4.26 6.4 cm, TE_{10} Excitation
0 DB
10
20
H-PLANE
E-PLANE
f = 5.6 GC
180
270
0
90
180
φ
φ

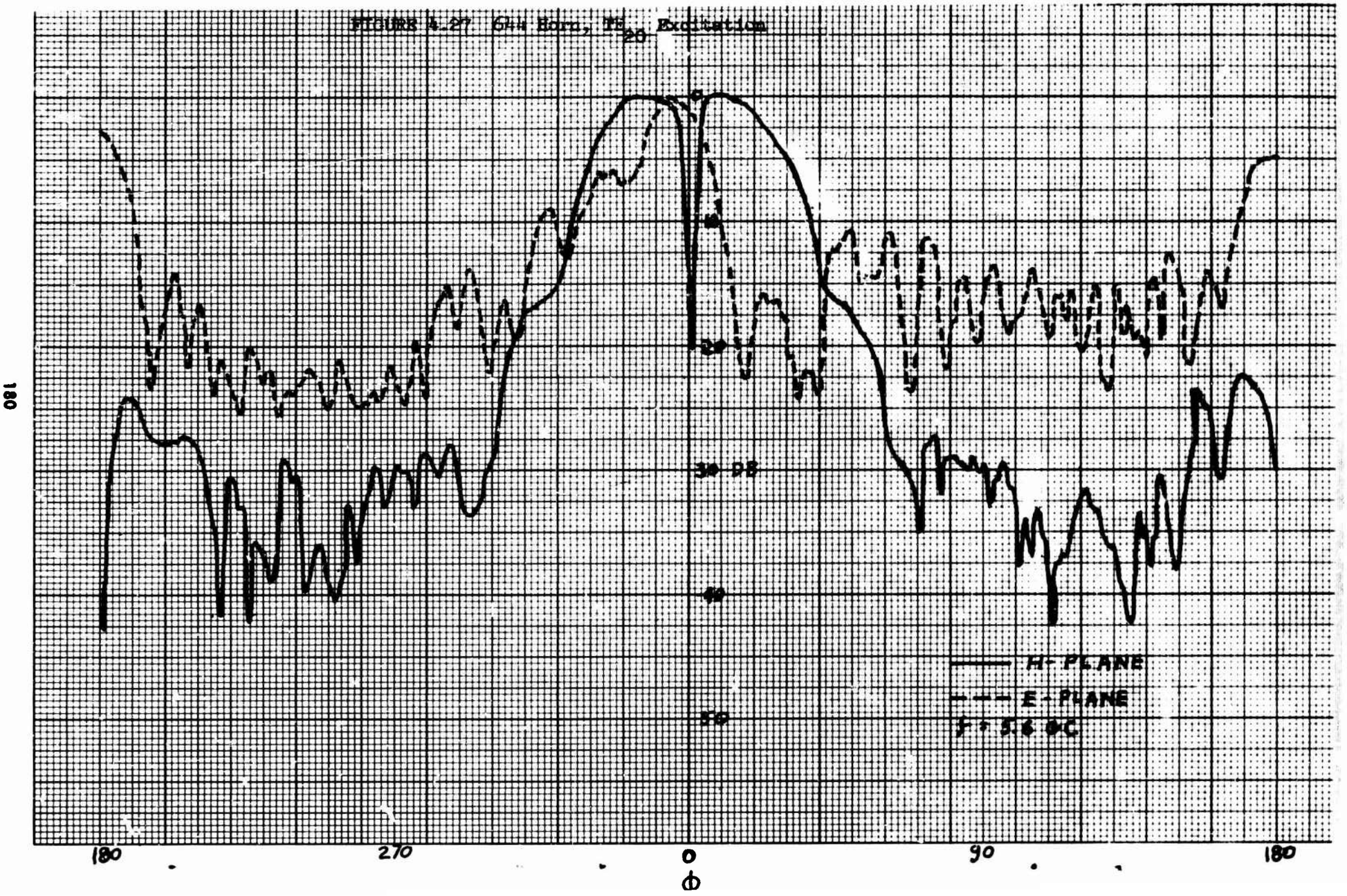
FIGURE 4.27 6λ Horn, TE20 Excitation
180
270
0
90
180
Φ
30 DB
H- PLANE
E- PLANE
f = 5.6 GC

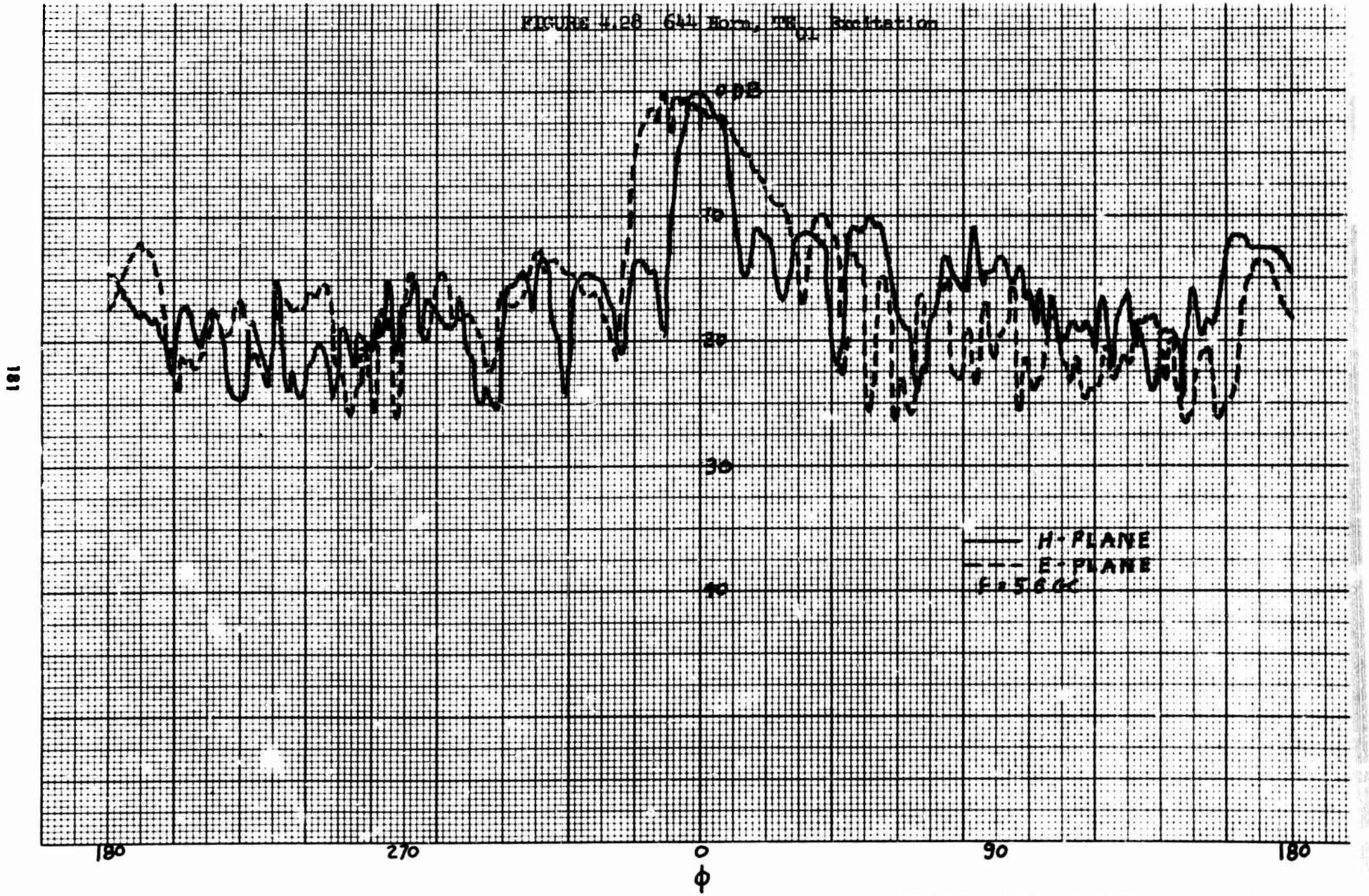
FIGURE 4.28 6dB Horn, TE01 Excitation
0dB
10
20
30
40
H-PLANE
E-PLANE
f=5.6 GC
180
270
0
90
180
φ

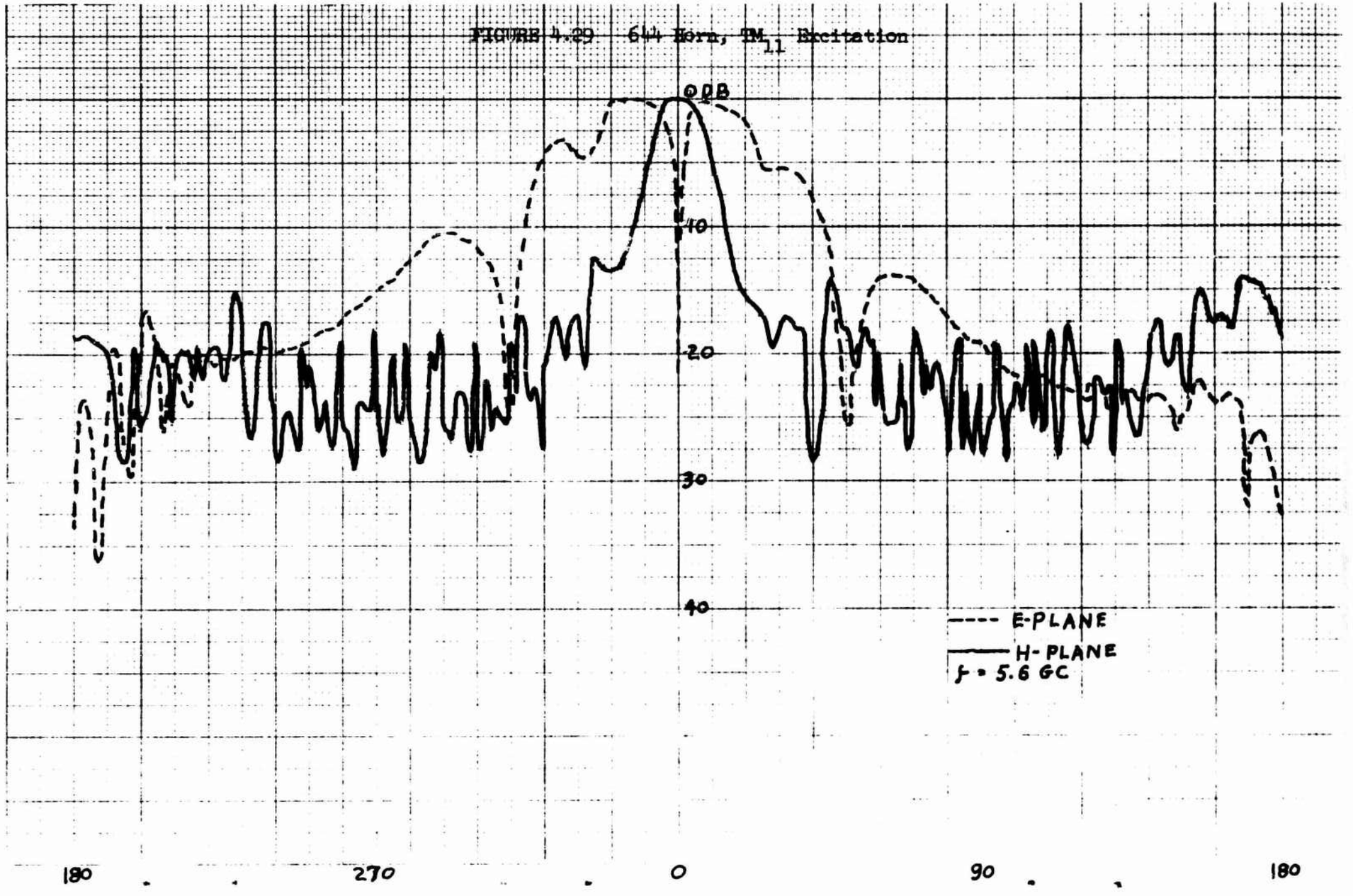

FIGURE 4.29 64 Horn, TM_{11} Excitation

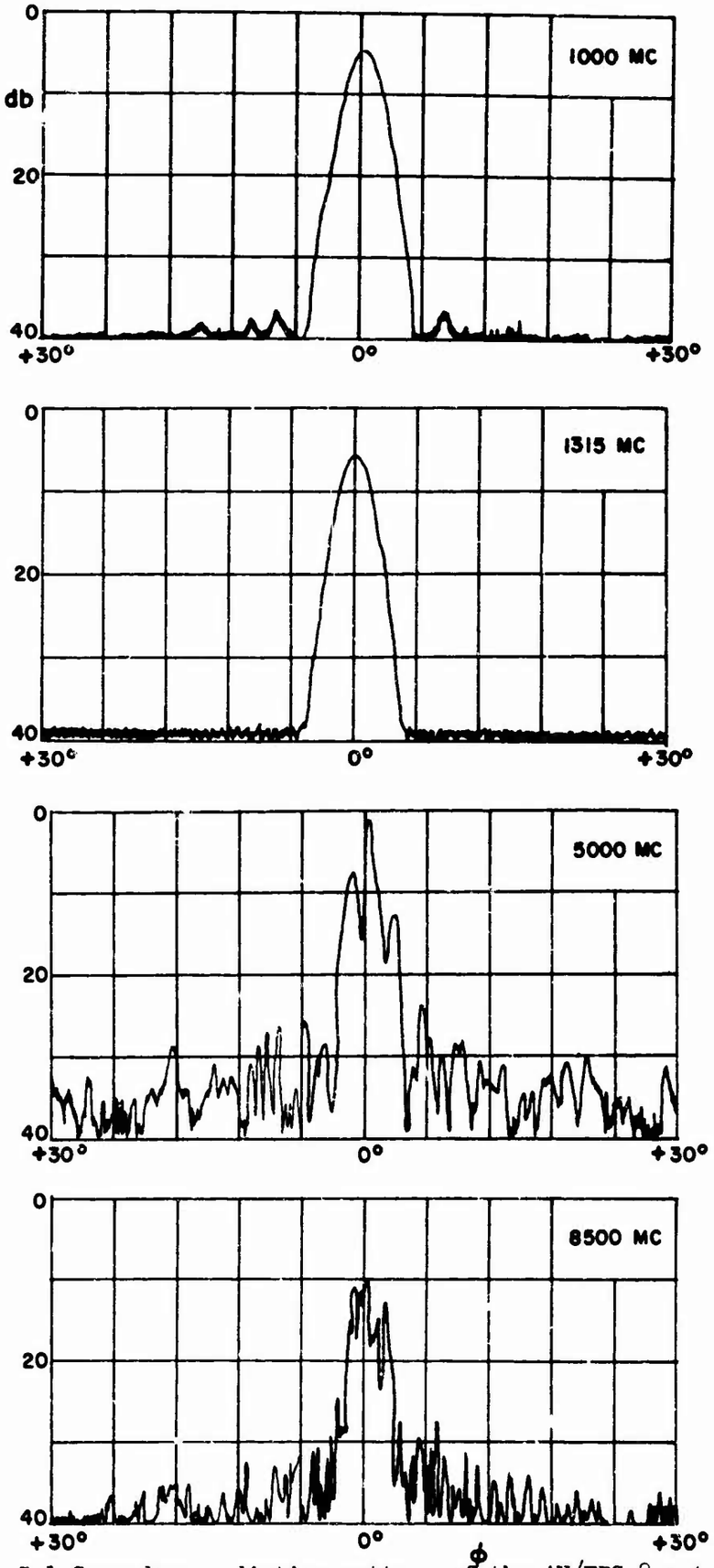

Figure 5.1 Secondary radiation pattern of the AN/FPS-8 antenna(E-plane)

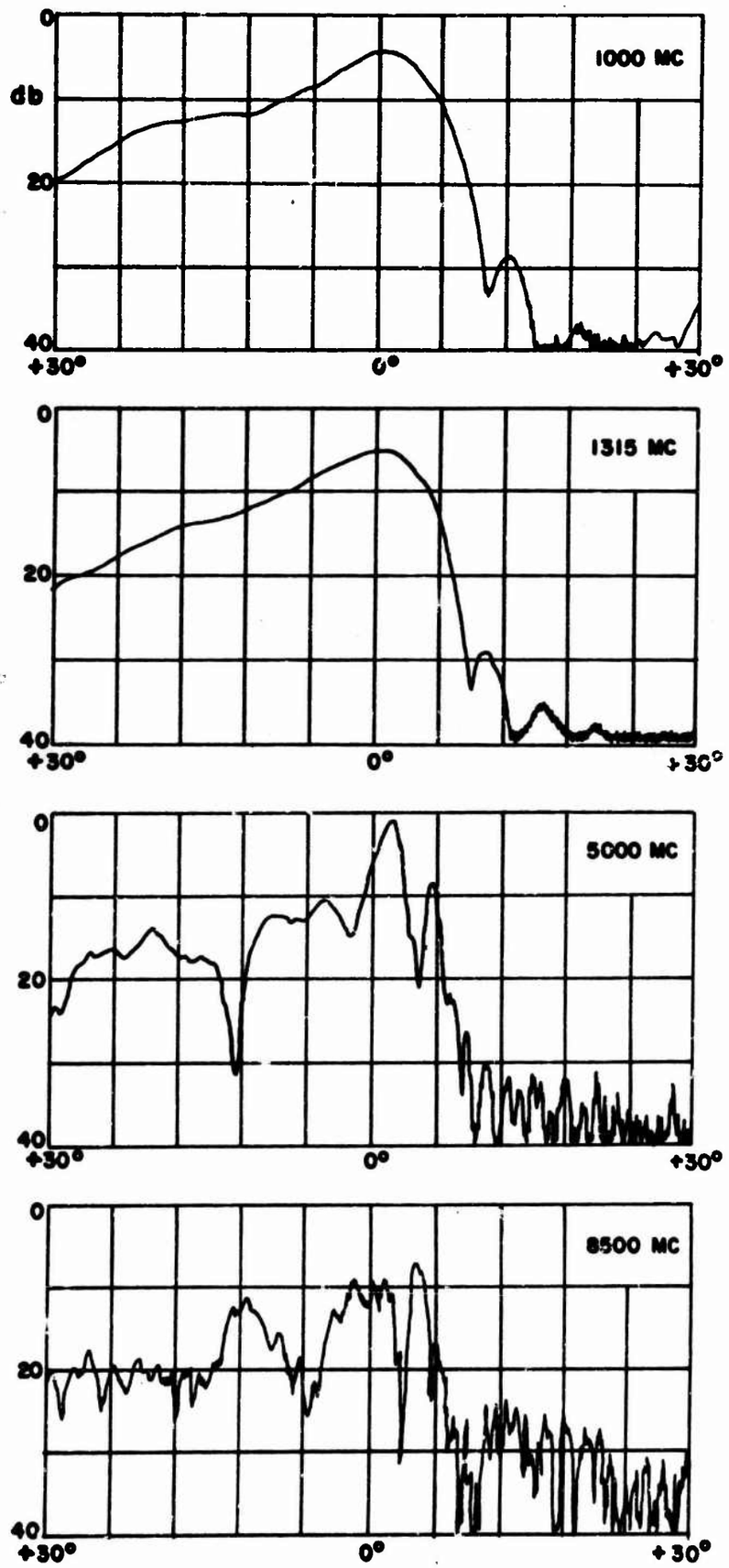

Figure 5.2 Secondary radiation of the AN/FPS-8 antenna(H-plane)

FIG. C.I EXPONENTIAL STANDARD GAIN HORNS.

FIG. C.2 SIX FOOT DIAMETER PARABOLIC REFLECTOR ON THE ANTENNA RANGE.

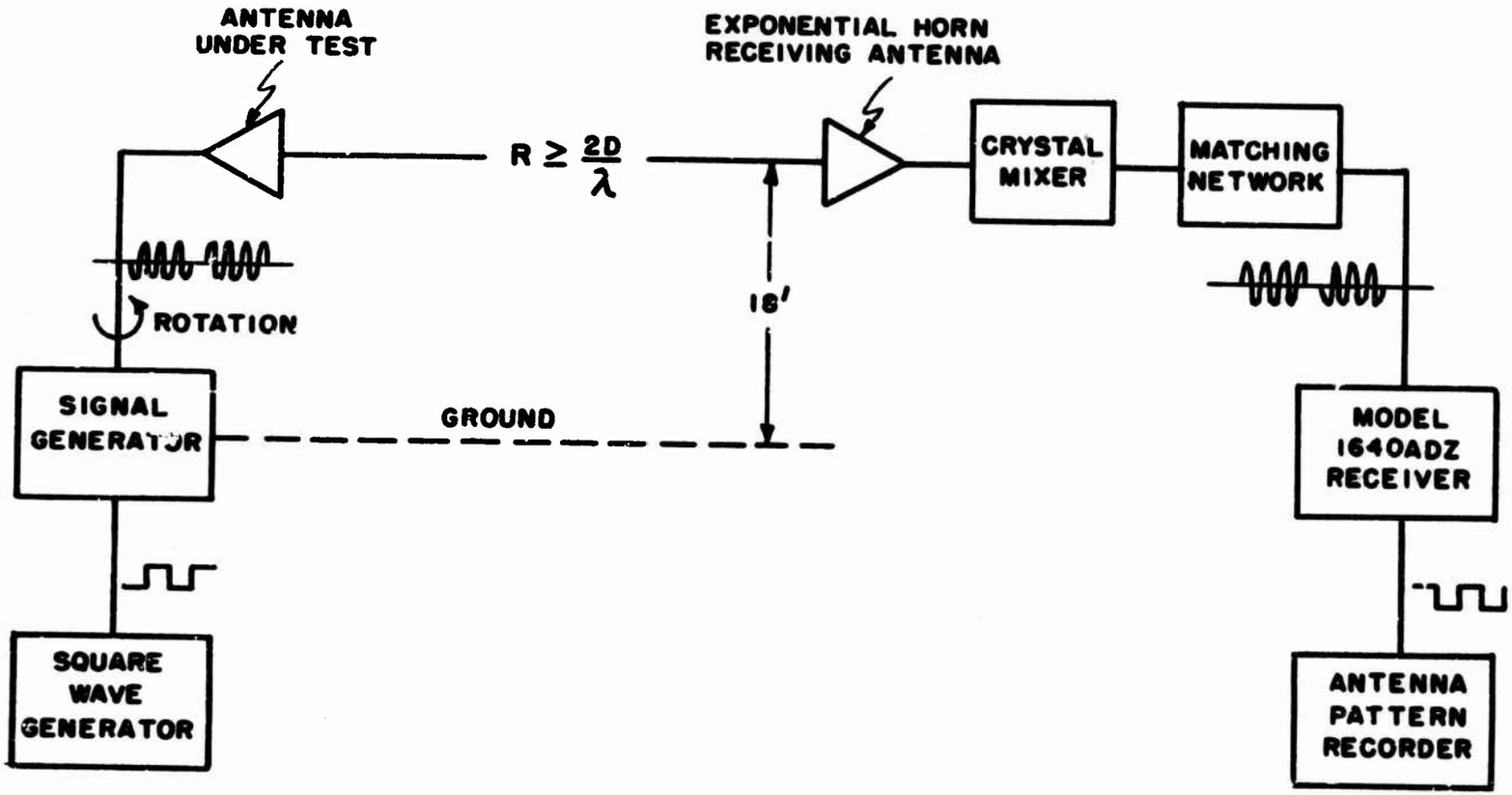

FIG. C.3 RADIATION POWER PATTERN TEST SET-UP.

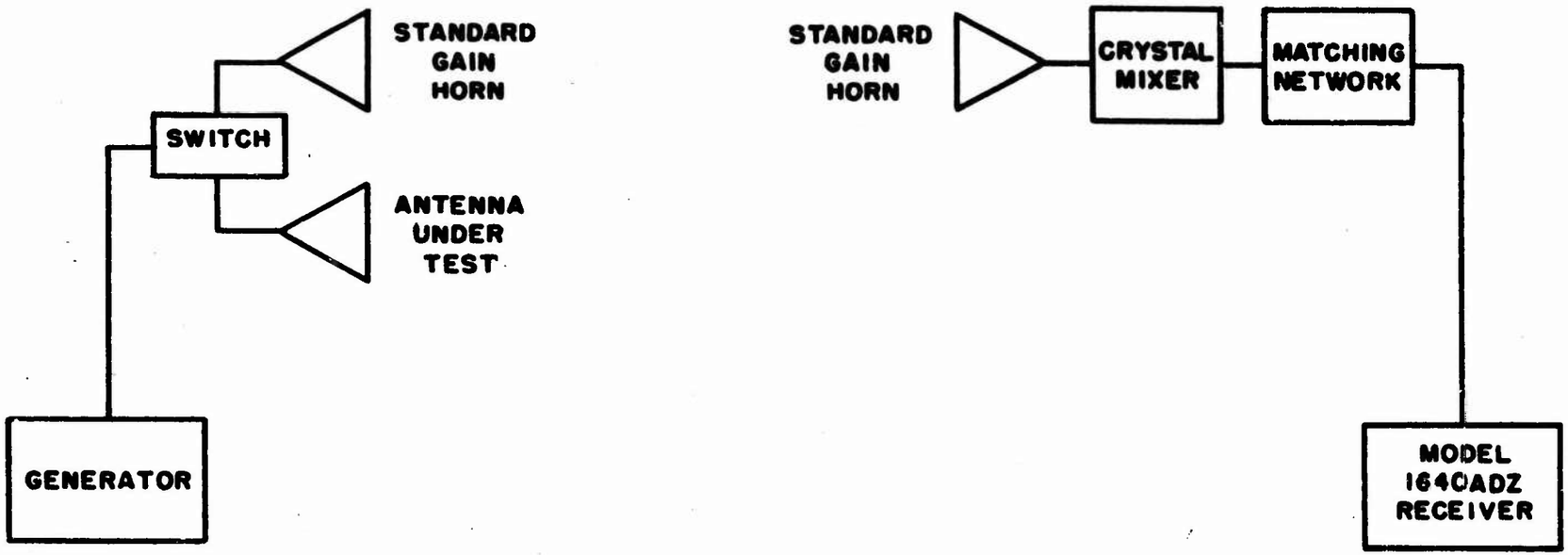

FIG. C.4 GAIN MEASUREMENT TEST SET-UP.

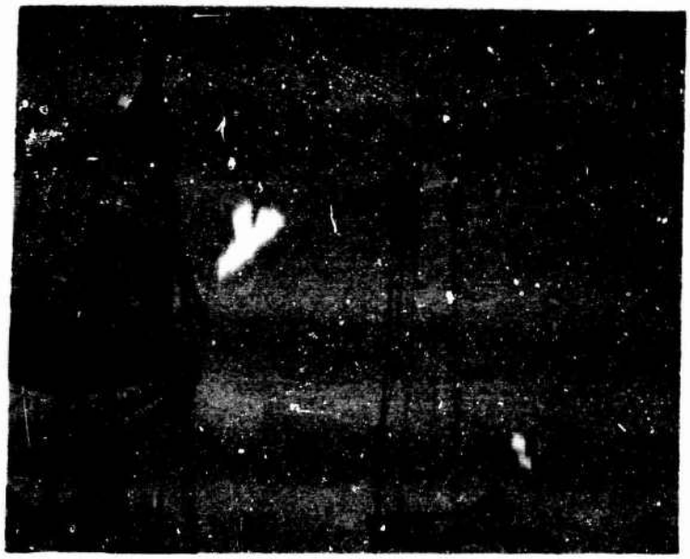

FIG. C.5 TWO FOOT PARABOLIC REFLECTOR IN GAIN MEASUREMENT SET-UP.